

University of Nebraska - Lincoln

DigitalCommons@University of Nebraska - Lincoln

Construction Systems -- Dissertations & Theses

Construction Systems

5-2012

EFFICIENT PRECAST/PRESTRESSED FLOOR SYSTEM FOR BUILDING CONSTRUCTION

Eliya Henin
elijahenin80@gmail.com

Follow this and additional works at: <https://digitalcommons.unl.edu/constructiondiss>



Part of the [Civil Engineering Commons](#), [Construction Engineering and Management Commons](#), and the [Structural Engineering Commons](#)

Henin, Eliya, "EFFICIENT PRECAST/PRESTRESSED FLOOR SYSTEM FOR BUILDING CONSTRUCTION" (2012). *Construction Systems -- Dissertations & Theses*. 8.
<https://digitalcommons.unl.edu/constructiondiss/8>

This Article is brought to you for free and open access by the Construction Systems at DigitalCommons@University of Nebraska - Lincoln. It has been accepted for inclusion in Construction Systems -- Dissertations & Theses by an authorized administrator of DigitalCommons@University of Nebraska - Lincoln.

EFFICIENT PRECAST/PRESTRESSED FLOOR SYSTEM FOR BUILDING
CONSTRUCTION

by

Eliya E. A. Henin

A DISSERTATION

Presented to the Faculty of
The Graduate College at the University of Nebraska
In Partial Fulfillment of Requirements
For the Degree of Doctor of Philosophy

Major: Engineering

Under the Supervision of Professors
George Morcous and Maher K. Tadros

Lincoln, Nebraska

May, 2012

EFFICIENT PRECAST/PRESTRESSED FLOOR SYSTEM FOR BUILDING CONSTRUCTION

Eliya E. A. Henin, Ph.D.

University of Nebraska, 2012

Advisors: George Morcous and Maher K. Tadros

Precast floor systems provide a rapidly constructed solution to multi-story buildings that is economical, high quality, fire-resistant, and with excellent deflection and vibration characteristics. Conventional precast concrete floor system cannot compete with cast-in-place post tensioning flat slab floor systems when high span-to-depth ratio and flat soffit are required. This is due to the significant depth of standard precast beams, and use of column corbels and beam ledges. This research presents the development of a new precast concrete floor system that eliminates the limitations of conventional precast floor system and provides a competitive precast alternative to cast-in-place flat slab floor systems. The main features of the proposed system are: span-to-depth ratio of 30, and flat soffit (no ledges or corbels), and adequate resistance to lateral loads, in addition to economy, consistency with prevailing erection techniques, and speed of construction. The new system is a total precast concrete floor system that consists of continuous columns, prestressed rectangular beams, prestressed hollow-core planks, and cast-in-place composite topping. Fully insulated precast sandwich panels that are alternative to hollow-core planks are also proposed for thermally efficient floor applications. These panels can be easily produced, as they do not require specialized equipment for fabrication, in addition to having comparative weight and capacity to hollow cores.

The dissertation presents the main concepts adopted in the system development as well as the design procedures and construction sequence. Also, full-scale specimens have been erected and tested at the structural laboratory to ensure the structural performance of the proposed system and validated the results of the analytical models.

DEDICATION

I dedicate my dissertation

To The Glory of the LORD, Jesus Christ

I also dedicate this dissertation

To My Parents, My Wife, and My Little Angel, Sara

ACKNOWLEDGMENTS

First of all, and foremost, all thanks to My Lord (Jesus Christ) for the gracious kindness in all the endeavors I have taken up in my life.

I am deeply indebted and grateful to my advisor Dr. George Morcou, Associate Professor, Durham School of Architectural Engineering and Construction, University of Nebraska-Lincoln for his valuable advice, guidance and kind encouragement provided throughout the stages of this study. His ingenious ideas, constructive suggestions and tireless guidance made the completion of this work possible.

I wish to express my great thanks to Dr. Maher K. Tadros, Emeritus professor at the Civil Engineering Department, University of Nebraska-Lincoln for his diligent, guidance, continuous work, serious and numerous useful contributions in various ways to the realization of this study. I also thank my supervisory committee Dr. Christopher Tuan, and Dr. James Goedert.

I am also grateful to Prof. Sires and Dr. Foster for their scientific guidance and help in preparing my dissertation. Thanks are due to the faculty, staff, and collages at the civil engineering and construction-engineering program at the University of Nebraska-Lincoln for their continuous support during my stay in Nebraska.

Last but not least, I owe my family members, my father Ezzat and my mother Mariam a lot for their support to me during my whole life, words are not enough to thank my wife-Dalia-who represents my backbone in life, and my little angel Sara who relief any pain I may suffer by their heavenly smile. May the Lord give me the strength to support them through their lives. Also, I would like to express my deepest thanks to my brothers and my sisters

TABLE OF CONTENTS

Chapter 1	1
INTRODUCTION	1
1.1 Background	1
1.2 Research Objectives.....	3
1.3 Dissertation Organization	3
Chapter 2.....	6
LITERATURE REVIEW	6
2.1 Cast-in-Place Concrete Floor Systems.....	6
2.2 Steel Joist Floor Systems	7
2.3 Precast Concrete Floor Systems.....	9
2.4 Emerging Systems	26
Chapter 3.....	32
SYSTEM DESCRIPTION AND CONSTRUCTION SEQUANCE.....	32
3.1 System Description	32
3.2 Construction Sequence.....	33
Chapter 4.....	42
DESIGN OF FLAT SOFFIT FLOOR SYSTEM UNDER GRAVITY LOAD.....	42
4.1 Introduction.....	42
4.2 Design Example and Procedures	42

4.2.1 Design for Gravity Loads.....	45
4.2.1.1 Floor Panels	45
4.2.1.2 Flat Soffit Beam Design.....	46
4.2.1.3 Column Design	54
4.2.1.4 Design of Temporary and Hidden Corbels	55
4.2.1.5 Design of Beam Hidden Ledges and Temporary Ledges	65
4.3 Flat Soffit Shallow Beam Design aids	72
4.4 Constructability, Cost, and Schedule Analysis	78
Chapter 5.....	83
DESIGN OF FLAT SOFFIT FLOOR SYSTEM UNDER LATERAL LOAD	83
5.1 Introduction.....	83
5.2 Wind Loads.....	84
5.2.1 Low-moderate Wind Zone.....	84
5.2.2 High Wind Zone	88
5.3 Seismic Loads	89
5.3.1 Low-moderate Seismicity Zone.....	90
5.3.1.1 Story Drift	94
5.3.2 High Seismicity Zone	95
5.3.2.1 Story Drift.....	97
5.4 Load Combination for Low Seismicity Zone	99

5.5 Load Combination for High Wind Zone.....	100
5.6 Load Combination High Seismicity Zone	102
Chapter 6.....	105
TESTING OF FLAT SOFFIT FLOOR SYSTEM COMPONENTS AND CONNECTIONS	105
6.1 Introduction.....	105
6.2 Beam-column Connection without Corbel	105
6.2.1 Specimen design	106
6.2.2 Specimen Fabrication and Erection	110
6.2.3 Material Properties.....	111
6.2.4 Test Setup and Procedures	112
6.2.4.1 HC Negative Moment Capacity.....	113
6.2.4.2 Beam Negative Moment Capacity	115
6.2.4.3 Beam Positive Moment Capacity.....	118
6.2.4.4 Beam-Column Connection Shear Capacity	120
6.2.5 Beam-Column Connection without Corbel Application.....	123
6.3 HC-beam Connection without Ledge	126
6.3.1 Specimen Design	127
6.3.2 Specimen Fabrication and Erection	132
6.3.3 Material Properties.....	134

6.3.4 Test Setup and Procedures	136
6.3.4.1 Testing HC-beam Connection.....	136
6.4 Testing the Flat Soffit Beam Flexural Capacity	145
Chapter 7.....	147
PRECAST/PRESTESSED SANDWICH FLOOR PANELS	147
7.1 Introduction.....	147
7.2 Panel Description and Design.....	149
7.3 Thermal Performance.....	151
7.4 Phase I Experimental Investigation	154
7.4.1 Specimens Design.....	155
7.4.2 Specimens Erection.....	158
7.4.3 Material Properties.....	162
7.4.4 Test Setup and Procedures	163
7.4.4.1 First Test (Without Topping)	164
7.4.4.2 Second Test (With Topping).....	166
7.5 Design Optimization and Erection Simplification.....	171
7.6 Phase II Experimental Investigation	175
7.6.1 Specimens Design.....	175
7.6.2 Specimens Erection.....	179
7.6.3 Material Properties.....	181

7.6.4 Test Setup and Procedures	182
7.6.4.1 Flexural Test	182
7.6.4.2 Shear Test.....	194
7.7 Analytical Models.....	202
7.8 Embedment Depth of GFRP Ties	209
7.9 Summary.....	214
Chapter 8.....	215
SUMMARY, CONCLUSIONS AND RECOMMENDATIONS FOR Future WORK	215
8.1 Summary.....	215
8.2 Conclusions.....	216
8.3 Recommendations for Future Works	218
REFERENCES	220
Appendix A.....	A-1
DETAILED DESIGN EXAMPLE FOR SHALLOW FLAT SOFFIT PRECAST CONCRETE FLOOR SYSTEM (BEAM WITH SHEAR KEY).....	.
Appendix B	B-1
FACBRICATION OF BEAM-COLUMN CONNECTION WITHOUT CORBEL COMPONENTS
Appendix C	C-1

ERECTION OF BEAM-COLIMN CONNECTION WITHOUT CORBEL SPECIMEN	
Appendix D.....	D-1
FACBRICATION OF FLAT SOFFIT BEAM.....	
Appendix E.....	E-1
ERECTION OF HC-BEAM CONNECTION WITHOUT LEDGE SPECIMEN.....	
Appendix F.....	F-1
SANDWICH FLOOR PANEL FABRICATION.....	
Appendix G.....	G-1
NU FLOOR DESIGN EXAMPLE (PANEL WITH GFRP TIES).....	

TABLE OF FIGURE

Figure 2.1: Construction of post-tensioned cast-in-place concrete slab (http://www.yde.co.il/Post-Tensioned-Buildings.aspx).....	7
Figure 2.2: Construction of open-web steel joist floor system (http://steeljoist.org/steel_joist_projects/gsa_trade_shop).....	8
Figure 2.3: Construction of steel joist girder floor system	8
(http://steel-girders.rolledsteels.com/steel-girders/)	8
Figure 2.4: Low proposed system (above right), Plan details (top left), and section details (bottom). (Thompson and Pessiki, 2004).....	10
Figure 2.5: Perspective view (top), Cross-section of the beam at mid-span and Cross- section of the beam at end (bottom & middle). (Tadros and Low, 1996).....	11
Figure 2.6: An exploded view illustrating the system elements (top) and plan view of an assembled joint (bottom). (Simanjuntak, 1998).....	12
Figure 2.7: Section view through the side wall and the floor (top), and Section view along the line 2-2 (bottom). (Reay, 1997)	14
Figure 2.8: Cross section elevation view (top) and cross-section elevation view taken along line 2-2 (bottom). (Compton, (1990)	15
Figure 2.9: perspective view of the system (top), and plan view and elevation view taken on line B - B and A - A (bottom). (Wise and Meade, 1978)	17
Figure 2.10: Cross-sectional view (top), and Plan view of the flooring system (bottom). (Rahimzadeh, 2003).....	18
Figure 2.11: precast slab showing the longitudinal extending trusses (left) and perspective view of the special splicing (right). (Wise, 1973).....	19

Figure 2.12: Perspective view showing an example of building framing (top), and cross-section shows the invented system (bottom).(Hanlon, 2008)	22
Figure 2.13: Elevation and Plan show the components of the described system	23
Figure 2.14: Composite Dycore structural floor system. (Composite Dycore Office Structures, 1992)	24
Figure 2.15: Column temporary corbel and cross section of the beam. (Fawzy, 2088) ...	25
Figure 2.16: HC-beam connection under ultimate design load and failure of HC-beam connection. (Morcous and Tadros, 2010)	26
Figure 2.17: European practices in designing hollow core supporting beams. (fib steering committee, 1999)	27
Figure 2.18: D-BEAM™, by Girder-Slab Technologies LLC, Cherry Hill, NJ (2002). 27	
Figure 2.19: Construction using Girder-Slab system of Girder-Slab Technologies LLC Cherry Hill, NJ (2002)	28
Figure 2.20: Filling the Deltabeam with self-consolidating concrete. (http://www.peikko.ca/Default.aspx?id=625741).....	28
Figure 2.21: Construction of Deltabeam floor system. (http://www.peikko.ca/Default.aspx?id=625741).....	29
Figure 2.22: Filigree precast slab with light steel truss. (Pessiki et. al. 1995).....	30
Figure 2.23: The NEW Flooring System components. (Rafael and Orid , 2010).....	31
Figure 3.1: System Components	33
Figure 3.2: Placing temporary corbels	34
Figure 3.4: Welding the top angles to beam and column	35
Figure 3.5: temporary beam ledges.....	36

Figure 3.6: Hollow core planks on temporary beam ledges	37
Figure 3.7: Continuity reinforcement and HC-beam hat and loop bars.....	38
Figure 3.8: Grouting the H.C keys and beam pocket with SCC.....	38
Figure 3.9: Beam continuity reinforcement	39
Figure 3.10: Placing the topping reinforcement	40
Figure 3.11: Pouring and finishing the topping concrete.....	40
Figure 3.12: Removing the temporary corbels and ledges	41
Figure 4.1: Plan, elevation, and side views of the example building.....	44
Figure 4.2: Composite HC End-Span Section	46
Figure 4.3: Dimensions of Standard FS beam with shear key (top) and FS beam with hidden corbel (bottom).....	47
Figure 4.4: Plan and section views of the beam with shear key ledge and temporary steel angles	52
Figure 4.5: Plan and section views of the beam with shear key ledge and coil inserts	53
Figure 4.6: Plan and section views of the beam with ledge and temporary steel angles ..	53
Figure 4.7: Plan and section views of the beam with ledge and coil inserts.....	54
Figure 4.9: Isometric view shows friction bolts and the temporary corbel	56
Figure 4.10: Stiffened angle used as a temporary corbel.....	56
Figure 4.11: Beam-column connection without reinforcement	59
Figure 4.12: Failure mechanisms of beam-column connection	60
Figure 4.13: Recess in the four side of the column.....	61
Figure 4.14: Hidden corbel reinforcement.....	62
Figure 4.15: Cross section of the beam shows the shear connectors	62

Figure 4.16: Beam-column connection.....	65
Figure 4.17: HC-beam connection without reinforcement	66
Figure 4.18: HC-beam connection failure mechanisms.....	67
Figure 4.19: Beam shear key dimension.....	68
Figure 4.20: steel loops were placed in the HC slots.....	68
Figure 4.21: Shape of reinforcement using in the HC-beam connection.....	69
Figure 4.22: HC-beam connection.....	72
Figure 4.23: Design chart for FS 8 (9#8 and 6#6 negative reinforcement)	73
Figure 4.24: Design chart for FS 8 (15#8 negative reinforcement).....	74
Figure 4.25: Design chart for FS 8 (9#9 and 6#8 negative reinforcement)	74
Figure 4.27: Design chart for FS 10 (15#8 negative reinforcement).....	75
Figure 4.28: Design chart for FS 10 (9#9 and 6#8 negative reinforcement)	76
Figure 4.29: Design chart for FS 12 (9#8 and 6#6 negative reinforcement)	76
Figure 4.30: Design chart for FS 12 (15#8 negative reinforcement).....	77
Figure 4.31: Design chart for FS 12 (9#9 and 6#8 negative reinforcement)	77
Table 4.8: A schedule comparison between shallow flat soffit and a typical precast flooring system.....	82
Figure 5.1: Two-dimensional frames adopted for lateral load analysis.....	83
Figure 5.2: Wind load applied to the beam direction.....	85
Figure 5.3: Bending moment due to wind load in the beam direction.....	86
Figure 5.4: Deformed shape due to wind load in the beam direction	86
Figure 5.5: Wind load applied to the HC direction.....	87
Figure 5.6: Bending moment due to wind load in the HC direction.....	87

Figure 5.7: Deformed shape due to wind load in the HC direction	88
Figure 5.8: Seismic load applied to the beam direction.....	91
Figure 5.9: Bending moment due to seismic load in the beam direction.....	92
Figure 5.10: Deformed shape due to seismic load in the beam direction.....	92
Figure 5.11: Seismic load applied to the HC direction.....	93
Figure 5.12: Bending moment due to seismic load in the HC direction.....	93
Figure 5.13: Deformed shape due to seismic load in the hc direction.....	94
Figure 5.14: Beam-Column connection for high-moderate windy zone	101
Figure 5.15: Beam-Column connection for high-moderate seismicity zone	104
Figure 6.1: Plan view of the precast components of test specimen	106
Figure 6.2: Plan View of the Beam End	107
Figure 6.3: Detailing of the precast column.....	108
Figure 6.4: Composite beam and its connection with the column.....	109
Figure 6.5: Concrete strength gain with time.....	112
Figure 6.6: Test setup for evaluating HC negative moment capacity.....	113
Figure 6.7: Load-deflection curve for the HC negative moment capacity test.....	114
Figure 6.8: Cracking of the topping concrete at HC ultimate load.....	115
Figure 6.9: Test setup for evaluating beam negative moment capacity.....	116
Figure 6.11: Cracking of the topping concrete at beam ultimate load.....	117
Figure 6.12: Test setup for evaluating the SIT beam positive moment capacity.....	118
Figure 6.13: Load-deflection curve for SIT beam positive moment capacity test.....	119
Figure 6.14: Cracking of the HC soffit at ultimate load	120
Figure 6.15: Test setup for beam-column connection shear capacity.....	121

Figure 6.16: Load-deflection curve for testing beam-column connection.....	122
Figure 6.17: Failure of beam-column connection.....	122
Figure 6.18: Architectural elevation of the farmer’s mutual building.....	124
Figure 6.19: connection details.....	125
Figure 6.20: Under construction pictures for Farmer’s mutual building.....	126
Figure 6.21: Plan view of the precast components of test specimen	128
Figure 6.22: Dimensions and details of the HC specimen.....	129
Figure 6.23: HC-beam connection reinforcement (Hat and Loops bars).....	130
Figure 6.24: Dimensions and reinforcement details of the beam of the first specimen..	131
Figure 6.25: Details of the tested four HC-beam connections.....	131
Figure 6.26: Blocking the HC openings before erection	132
Figure 6.27: Strain gauges locations.....	134
Figure 6.28: Concrete strength gain with time.....	135
Figure 6.29: Plan view for the test specimens shows the four connections.....	137
Figure 6.30: HC-beam connection setup	138
Figure 6.31: Failure of the HC at the critical section under ultimate loading	139
Figure 6.32: Failure of the HC at the critical section under ultimate loading	140
Figure 6.33: Failure of the HC at the critical section under ultimate loading	140
Figure 6.36: Load-deflection curve of HC-beam connection when tested as cantilever	143
Figure 6.37: Load-strain relationships of HC-beam connection when tested as cantilever	143
Figure 6.38: Flat soffit beam flexural test setup	145
Figure 6.40: Failure mode of the flat soffit beam	146

Figure 7.1: NU Tie.....	150
Figure 7.2: Shear connectors and horizontal shear force.....	150
Figure 7.4: Floor panel B with steel ties.....	154
Figure 7.5: floor panels casting position and nomenclature for the panels	158
Figure 7.6: GFRP and steel ties profile.....	159
Figure 7.7: Hot melt slots into the foam blanks.....	159
Figure 7.8: Insert GFRP tie into the XPS slot and filling the gap with expanding foam insulation.....	160
Figure 7.9: Setup the forms and tension the strands	161
Figure 7.10: Casting the bottom wythe, installing foam panels, and casting the top wythe	161
Figure 7.11: Completing casting the panels.....	162
Figure 7.12: Wet Burlap Curing	162
Figure 7.13: Concrete strength gain with time.....	163
Figure 7.14: Test Setup.....	164
Figure 7.15: Load-deflection relationships for panel A, and B without topping.....	165
Figure 7.16: Built the form for the topping and cast the concrete topping.....	166
Figure 7.17: Second test setup	167
Figure 7.18: Strain Gauges at the top surface	167
Figure 7.19: Load-deflection relationship for the two panels with topping	168
Figure 7.20: Load-strain relationships of top fibers at mid-span.....	169
Figure 7.21: Failure mode of panel A.....	169
Figure 7.22: Failure mode of panel B	170

Figure 7.23: changing ties height in phase I (top) and phase II (bottom).....	171
Figure 7.24: The end of the panels in phase I (top) and phase II (bottom).....	172
Figure 7.25: Topping reinforcement phase I (top) and phase II (bottom).	173
Figure 7.26: Optimize number of strands and number of ties for phase I (top) and phase II (bottom).....	174
Figure 7.27: changes in the cross section for phase I (top) and phase II (bottom).	175
Figure 7.28: Fully insulated floor panels C and D.....	179
Figure 7.29: Insert GFRP tie into the XPS slot and filling the gap with expanding foam insulation.....	180
Figure 7.30: Concrete strength gain with time.....	181
Figure 7.31: Test setup for panel C.....	183
Figure 7.32: Specimen instrumentation	184
Figure 7.33: Measuring the relative movement between the bottom and top wythes	184
Figure 7.34: Load-deflection relationship for the panel C.....	185
Figure 7.35: Load-strain relationship at the top concrete surface.....	186
Figure 7.36: Load-strain relationship for GFRP ties at different locations	187
Figure 7.37: Load-relative movement relationship for connected wytes	187
Figure 7.38: Pull out of GFRP tie at failure.....	188
Figure 7.39: Test setup for panel D	189
Figure 7.40: Specimen instrumentation	190
Figure 7.41: Load-deflection relationships for the panel D.....	191
Figure 7.42: Load-strain relationship at the top concrete surface.....	192

Figure 7.43: Load-strain relationship for GFRP ties at different locations left side (Top) and right side (bottom).....	193
Figure 7.44: Failure mode of panel D.....	194
Figure 7.45: Test 1 setup.....	195
Figure 7.46: Test 1 specimen instrumentation.....	195
Figure 7.47: Load-deflection relationship for test 1	196
Figure 7.48: Load-strain relationship for GFRP ties at left	197
Figure 7.49: Shear failure of test 1.....	197
Figure 7.50: Test 2 setup.....	198
Figure 7.51: Test 2 specimen instrumentation.....	198
Figure 7.52: Load-deflection relationship for test 2&3	199
Figure 7.53: Load-strain relationship of GFRP ties for test 2.....	200
Figure 7.55: Shear failure of test 2 &3	201
Figure 7.56: Truss models of panel A, B, C, and D.....	203
Figure 7.57: 3D FE model of panel A, B, C, and D.....	204
Figure 7.58: Service load deflection of panel A using the truss model and FE model...	205
Figure 7.59: Service load deflection of panel B using the truss model and FE model...	205
Figure 7.60: Service load deflection of panel C using the truss model and FE model...	206
Figure 7.61: Service load deflection of panel D using the truss model and FE model...	207
Figure 7.62: Camber and self-weight deflection of panel C and D	209
Figure 7.63: Plan and Section view of the test specimen	210
Figure 7.64: Test specimen and setup.....	211
Figure 7.65: Pull-out of the tie from the concrete.....	212

Figure 7.66: Rupture of the tie 212

Figure 7.67: Average ultimate load for different tie size and embedment combination 213

Figure 8.1: Proposed Testing Setup and a Preliminary Design of Post-tensioned Hybrid
Connection 219

LIST OF TABLES

Table 4.1: Design parameters	49
Table 4.2: Beam final moments	49
Table 4.3: Reinforcement used in the Designed FS 10.....	50
Table 4.4: Comparison of Demand and Capacity at Critical Sections.	50
Table 4.5: Final shear values	51
Table 4.6: Properties of standard FS beams.....	72
Table 5.1: Wind pressure calculations	85
Table 5.2: Wind pressure calculations	89
Table 5.3: Base shear force calculations.....	90
Table 5.4: Base shear force distribution on each floor	91
Table 5.5: Lateral displacements and interstory drifts due to seismic force in beam direction and HC direction.....	95
Table 5.6: Base shear force calculations.....	96
Table 5.7: Base shear force distribution on each floor	96
Table 5.8: Lateral displacements and inter-story drifts due to seismic force	97
Table 5.9: Lateral displacements and inter-story drifts due to seismic force	98
Table 5.10: Lateral displacements and inter-story drifts due to seismic force	98
Table 5.11: Summary of lateral load analysis results	99
Table 5.12: Comparison of factored lateral load and resistance.....	100
Table 5.13: Summary of lateral load analysis results	100
Table 5.14: Comparison of factored lateral load and resistance.....	101
Table 5.15: Comparison of factored lateral load and resistance for high-moderate windy zone.....	101

Table 5.16: Summary of lateral load analysis results	102
Table 5.17: Comparison of factored lateral load and resistance	102
Table 5.18: Summary of lateral load analysis results	103
Table 5.19: Comparison of factored lateral load and resistance	103
Table 5.20: Comparison of factored lateral load and resistance	104
Table 6.1: Reinforcement used in beam-column connection without corbel	107
Table 6.2: Comparison of Demand and Capacity at Critical Sections.	107
Table 6.3: Summary of Lateral Load Analysis Results	110
Table 6.4: Comparison of Factored Lateral Load and Resistance	110
Table 6.5: Concrete mixes design	111
Table 6.6: Specified and actual concrete compressive strength at testing	112
Table 6.7: Summary of all test results	124
Table 6.8: Concrete mixes design	135
Table 6.9: Specified and actual concrete compressive strength at testing	135
Table 6.10: Summary results for HC-beam connections tests	144
Table 7.1: Comparing the proposed against existing floor systems	148
Table 7.2: R-Values calculations for sandwich panel with concrete solid ends	152
Table 7.3: R-Value calculation for fully insulated sandwich panel	153
Table 7.4: Concrete design mix for precast panel	163
Table 7.5: Comparing the theoretical against measured flexural capacity of phase I test specimens	170
Table 7.6: Comparing the theoretical against measured flexural capacity of phase II test specimens	194

Table 7.7: Comparing the theoretical against measured flexural capacity of phase II test specimens	208
Table 7.8: GFRP-tie size-embedment combinations and test results	211

Chapter 1

INTRODUCTION

1.1 Background

Conventional precast hollow-core (HC) floor systems consist of HC planks supported by inverted-tee (IT) precast prestressed concrete beams, which are, in turn, supported on column corbels or wall ledges. These floor systems provide a rapidly constructed solution to multi-story buildings that is economical, fire-resistant, and with excellent deflection and vibration characteristics. The top surface of HC floor systems can be a thin non-structural cementitious topping, or a 2 in. concrete composite topping that provides a leveled and continuous surface. Despite the advantages of conventional precast HC floor systems, they have four main limitations: a) low span-to-depth ratio, b) presence of floor projections, such as column corbels and beam ledges, c) low thermal insulation; and d) lack of resistance to lateral loads without shear walls.

For a 30 ft span floor, conventional precast HC floor system would require a 28 in. deep IT plus a 2 in. topping, for a total floor depth of 30 in., which results in a span-to-depth ratio of 12. On the other hand, post-tensioned cast-in-place concrete slab floor systems can be built with a span-to-depth ratio of 45, which results in a structural depth of 8 in. If the structural depth of precast floor systems can come close to that of post-tensioned cast-in-place concrete slab system, then precast concrete could be very favorable due to their rapid construction and high product quality. Reducing the structural floor depth lead to reduce floor height, this in turn makes savings in architectural, mechanical and electrical (AME) systems and may allow for additional floors for the same building height. The cost of AME is about 75 to 80% of the total building life cycle cost, and any small

savings in these systems would have a significant impact on the overall project economics.

Although the use of column corbels and beam ledges is the common practice in parking structures and commercial buildings, it is not aesthetically favorable in residential and office buildings, such as hotels. False ceiling are sometimes used in these applications to hide the unattractive floor projections, which results in reduced vertical clearance.

Elimination of floor projections combined with shallow structural depth will improve the building aesthetics and overall economics.

Hollow cores (HC) are considered one of the most common precast floor systems due to their advantages in terms of economy, lightweight, structural capacity, and ease of production and erection. The main limitation of the HC planks is the thermal insulation.

If the HC planks replaced with floor panels have comparative weight and structural capacity while have thermal insulation that will be more efficient combined with shallow structure depth will save much energy, which results in decreasing the live cycle cost.

Shear walls are typically used in conventional precast HC floor systems to resist lateral loads. However, owners and developers prefer the flexibility a beam/column frame offers, as opposed to structural walls that increases construction duration, adds to the cost, and cannot be moved during remodeling. Precast concrete floor systems could gain significant advantages over steel open web joist systems and cast-in-place floor systems if they can be designed and detailed to resist lateral loads and minimize the used of shear walls, especially, if this advantage is combined with the shallow structural depth.

1.2 Research Objectives

The main objective of this project is to develop a flat soffit shallow precast floor system for multi-story residential and office buildings. The developed system will eliminate or minimize the limitations of existing precast floor systems with regard to span-to-depth ratio, floor projections, thermal efficient, and lateral load resistance while maintaining speed of construction, simplicity, and economy. To achieve this general objective, the following specific five goals are identified for the proposed system:

1. Has a span-to-depth ratio of 30 to reduce the floor height and save in architecture, mechanical, and electrical costs.
2. Eliminates the column corbels and beam ledges to provide additional space and flat soffit for residential building, and office buildings.
3. Be continuous for as much of the load as possible to provide adequate structural capacity to resist both gravity and lateral loads, which minimizes the need for shear walls
4. Has a fully insulated floor panel, which results in improving building thermal efficient.
5. Has an easy-to-produce and erect precast/prestressed components with minimal cast-in-place operations to ensure practicality, economy, and speed of construction.

1.3 Dissertation Organization

This dissertation is organized into six chapters as follows:

Chapter 1: This chapter presents background information; research objectives, and dissertation organization.

Chapter 2: This chapter reviews the literature and current practices of different types of floor systems. Four different categories of floor system will be presented: such as cast-in-place concrete floor systems, steel joist floor systems, precast concrete floor systems, and emerging systems. Also the pros and cons of each system will be presented.

Chapter 3: This chapter presents description and construction sequence of proposed system.

Chapter 4: In this chapter a design example of six-story office building will be presented in addition to the design procedures of the building component such as floor panels, flat soffit beam, column, hidden corbels, and hidden ledges under gravity loads.

Chapter 5: This chapter discusses the lateral loads analysis of the proposed flat shallow floor system include the wind and seismic loads for two different regions (high and low) calculated according to ASCE 7-05. These loads were applied to six-story building in both beam and hollow core directions. Also two dimensional frame analysis was performed using SAP 2000 will be presented.

Chapter 6: This chapter shows the experimental investigation which carried out to investigate the structural performance of building component of the proposed systems. Three full-scale specimens will be presented: beam-column connection without corbel, HC-beam connection without ledge and flat soffit beam.

Chapter 7: This chapter presents a new floor panels which is alternative to the hollow core planks with high thermal efficiency. The R-value calculation will be discussed for fully insulated panel and for panels with concrete solid block at each end. Four full-scale panels will be tested under flexural and shear, in addition to analytical models to predict the service load deflection will be presented

Chapter 8: This chapter presents summary of the work, research conclusions, and recommendations for future work.

Chapter 2

LITERATURE REVIEW

The various floor framing systems available in the US market at the meantime can be categorized into four groups: cast-in-place concrete floor systems, open-web steel joist systems, precast concrete floor systems, and emerging systems. The following subsections briefly describe each of these categories and present their advantages and limitations.

2.1 Cast-in-Place Concrete Floor Systems

Cast-in-place concrete slab floor systems are the most flexible floor systems as it provides the designer with the freedom in floor plan designs. These systems include: one-way slab and beam, two-way slab and beam, ribbed slab, flat slab, flat slab with drop panel, flat slab with column capitals, slab with slab band, waffle slab, and waffle slab with drops. Cast-in-place concrete slab can be the shallowest floor system when post-tensioning is applied as it allows a span to depth ratio of up to 45 for two-way slab systems, which results in a 8" thick slab for a typical bay of 30 ft x 30 ft compared to a 12" thick slab for the same bay when no post-tensioning is used. In addition to these advantages, post-tensioned cast-in-place concrete slabs provide a clean flat soffit that is suitable for residential applications. For more information on the different types of post-tensioned floor systems and their span ranges, see Post Tensioning Institute (PTI, 2006)The major drawbacks of the cast-in-place construction, in general, are the cost and duration required for shoring, forming, pouring, and stripping operations. In addition, post-tensioning operations increase the construction cost, duration and complexity as it

requires the involvement of specialty contractors. Figure 2.1 shows an example of the construction of post-tensioned concrete floor.



Figure 2.1: Construction of post-tensioned cast-in-place concrete slab

(<http://www.yde.co.il/Post-Tensioned-Buildings.aspx>)

2.2 Steel Joist Floor Systems

The open web steel joist system is an attractive solution for commercial applications as shown in Figure 2.2. Open web steel joists are light weight and easy to install. A 28 in.-32" deep open web steel joist is typically used for 32 ft span with 4 – 6 ft spacing. Metal decking is generally used to form a 2"-4" thick composite slab. The utilities can pass through the joist openings, saving the height needed for the utilities. However, as steel prices continue to climb, these systems become less attractive. Also, a false ceiling is required to cover the unattractive framing system, resulting in a large total floor height. Several commercial products are currently available in the US market. Steel Joist Institute (SJI, 2007) gives more information about open web steel joist system.

Steel Joist Girders are open web steel trusses used as primary framing members as shown in Figure 2.3. The span of a joist girder shall not exceed 24 times its depth. Joist girders have been designed to allow for a growing need for deeper/longer spans with primary structural members (depths of 20" to 120" and span lengths to 120 feet). For more information about the joist girders see specification guide under Joist Girders, Quincy Joist Company, (2012).



Figure 2.2: Construction of open-web steel joist floor system

(http://steeljoist.org/steel_joist_projects/gsa_trade_shop)



Figure 2.3: Construction of steel joist girder floor system

(<http://steel-girders.rolledsteels.com/steel-girders/>)

2.3 Precast Concrete Floor Systems

Precast concrete floor systems can be made of a wide range of precast concrete products, such as hollow core slabs, solid slabs, double tees, and inverted tee/rectangular/L-shaped beams. These products can be also used in conjunction with steel beam and cast-in-place concrete topping in some applications to satisfy design requirements.

A conventional precast concrete floor system utilizes hollow core slabs supported by precast/prestressed concrete inverted tee beams which are in turn supported on column corbels or wall ledges. It provides an economical and fire-resistant floor system with excellent deflection and vibration characteristics for both residential and commercial applications. The top surface can be prepared for installation of a floor covering by placing thin non-structural cementations leveling topping, or a composite 2-3" concrete composite topping (Precast/Prestressed Concrete Institute, 1998). For a 30 ft span, a 28" deep beam can be used in addition to 2" cast-in-place topping, which results in a total of 30" thick floor. Also, the beam projection below the hollow core planks (ledge) does not allow the utilities to pass through resulting in a reduction in the clear floor height.

Innovative precast floor systems have been developed over the last few decades by researchers and industry experts. Low et al. (1991 and 1996) developed a shallow floor system for single story construction as it uses single-story precast columns as shown in Figure 2.4. The beam weight and the complexity of its design and detailing were discouraging to producers.

Thompson and Pessiki, (2004) developed a floor system of inverted tees and double tees with openings in their stems to pass utility ducts. This solution does not utilize the HC

planks, which are the most dominant and economical product for noni-parking applications

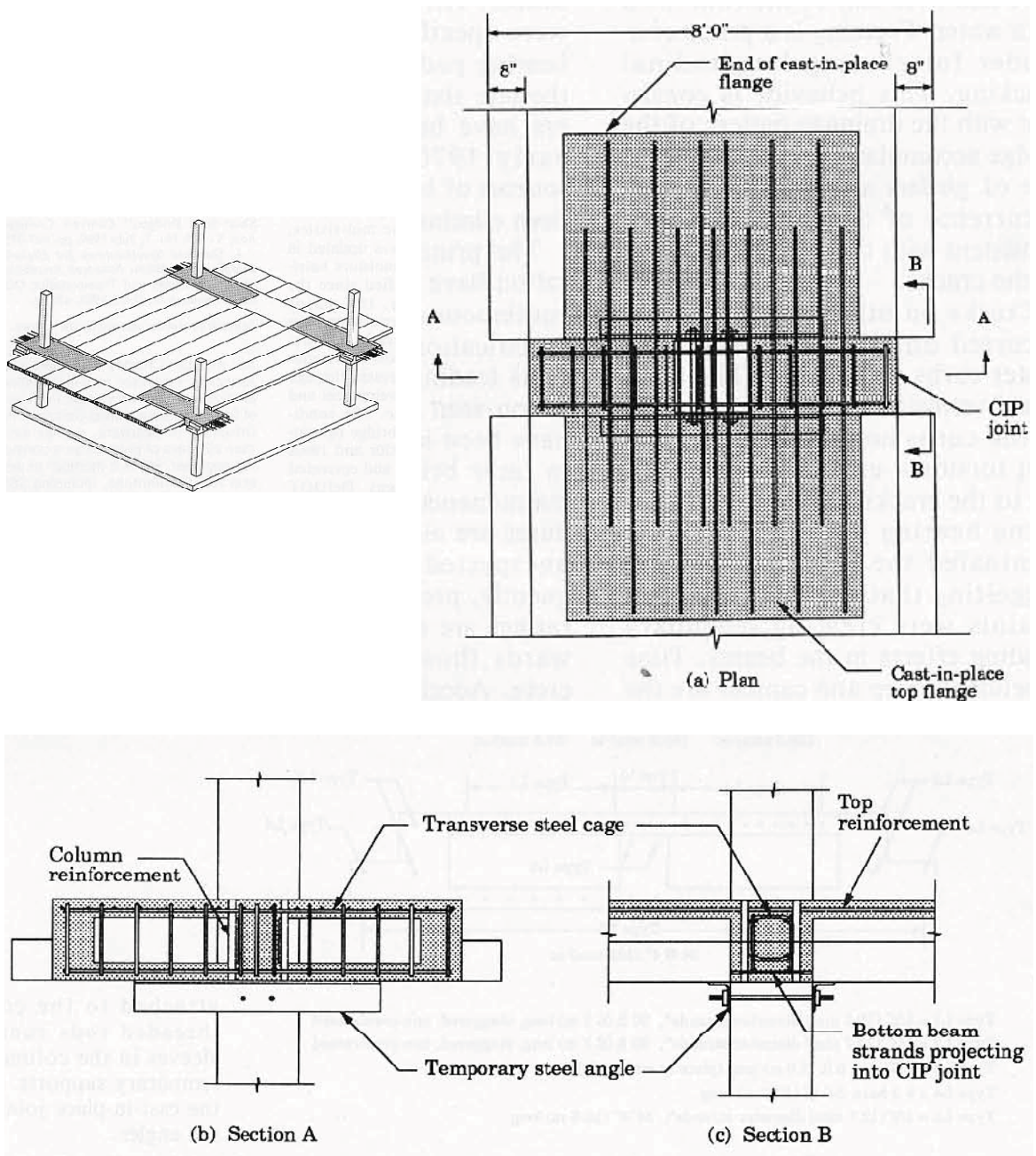


Figure 2.4: Low proposed system (above right), Plan details (top left), and section details (bottom). (Thompson and Pessiki, 2004)

Tadros and Low, (1996) developed a new precast system that consists of precast concrete beams and columns as shown in Figure 2.5 (Patent number US 2002/0062616 A1). The precast columns have voids at the floor level. Two steel angles are attached to the sides of each column at the beam level. These angles are used as temporary supports for the beams. Negative reinforcement is placed at the top of the beam through the column void. Cast-in-place concrete is poured to fill the void between the ends of the beams and column.

Column 14H
 Beam (16L, and 16F)
 Ledges (24E, and 24F)
 Voids (80)
 Steel angles (82A)
 Support frame (84B, and 84A)
 Reinforcing rods (51, 53, and 55)
 Sleeve (57)

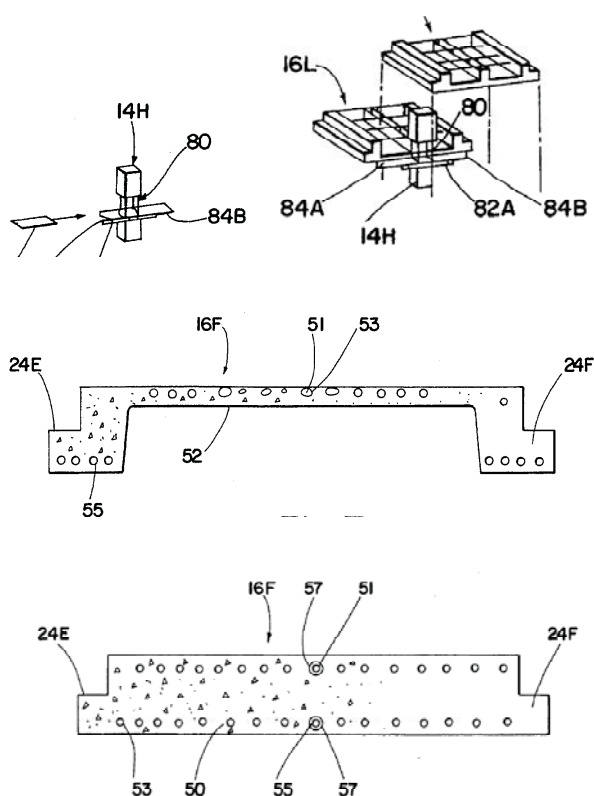


Figure 2.5: Perspective view (top), Cross-section of the beam at mid-span and Cross-section of the beam at end (bottom & middle). (Tadros and Low, 1996)

Simanjuntak, (1998) developed a precast concrete system which consists of columns and slabs joined together as shown in Figure 2.6 (Patent number 5,809,712). Each corner of the slab has a steel pipe. The slab is a panel made from concrete ribs and thin plates,

where the ribs function as beams. Each column in the system has high tensile steel reinforcement strands protruding at the top end to penetrate the steel pipes of the four corners of the four slabs. The four steel pipes of the four slabs corners meeting on one column are tied together with high tensile steel wire rope through three holes drilled horizontally at three places of the pipe length. Special mortar cement is injected to the implanted pipes through each pipe opening on the side surface of the column, in addition to grouting the gaps between the pipes and slabs. The proposed system eliminates the need for column corbels, in addition to using shallow ripped slab. The main drawbacks of that system are: 1) limitations on the distance between the columns, because of the slab dimension, 2) inadequacy of the system under lateral loads due to non-continuity of its connections, 3) consuming more time due to the connections details and need for skilled labor, and 4) need for false ceiling to cover the unattractive slab ribs

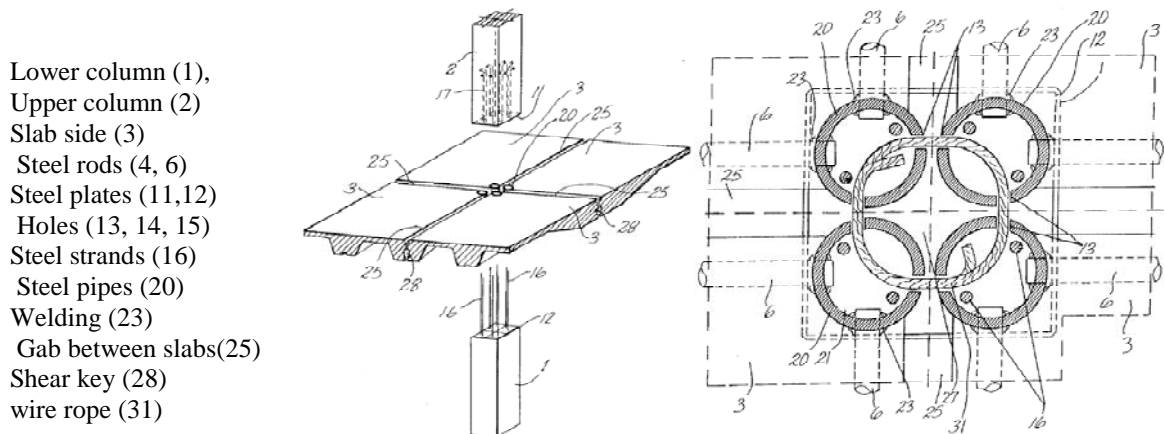


Figure 2.6: An exploded view illustrating the system elements (top) and plan view of an assembled joint (bottom). (Simanjuntak, 1998)

Reay, (1997) developed method of construction of a multi-story building. The system consists of precast slab walls and solid floor slab panels as shown in Figure 2.7 (Patent number 5,660,020). The slab floor has a lower precast concrete floor unit. A concrete

topping will be added to the floor slab after the floor is in position. The wall is precast with a cavity. If so desired, a metal or concrete support can be inserted in the cavity. The floor unit is precast with one or more reinforcing rods, and positioned adjacent the floor unit edge. A metal end cap is positioned at the edge and incorporates a bent metal strap with two ends and a top portion. The ends are welded with the end cap. The end of each of two reinforcing rods is rigidly secured by welding to the strap metal. A solid square, metal bar is dimensioned to slide through the end cap and be precisely located within a metal collar. The collar is of complementary dimensions to the solid square bar, and secured to the top portion of the strap. Once in position and the floor complete the bar acts to transfer loads between the floor and the sidewall. A locating pin (of flat mild steel) is positioned in the unit and it is secured to one or more of the reinforcement. A notch is placed on the underside of the square bar. That system provides flat soffit floor. The drawbacks of that system are: 1) it requires shoring during the construction stage, 2) inadequacy of the system in resisting lateral loads due to discontinuity of slab-column connections, and 2) it should have at least two connections at each panel to transfer the load to the wall which consuming time.

- Slab floor (2)
- Concrete wall (3)
- Lower precast unit (4)
- Concrete topping (5)
- Cavity (6)
- Reinforcing rods (9)
- Floor unit edge (10)
- Metal end cap (11)
- Metal Strap (12)
- End of metal strap (13)
- Solid square metal bar (15)
- Metal collar (16)
- Flat mild steel pin (17)
- End of the pin (18)
- Notch (19)

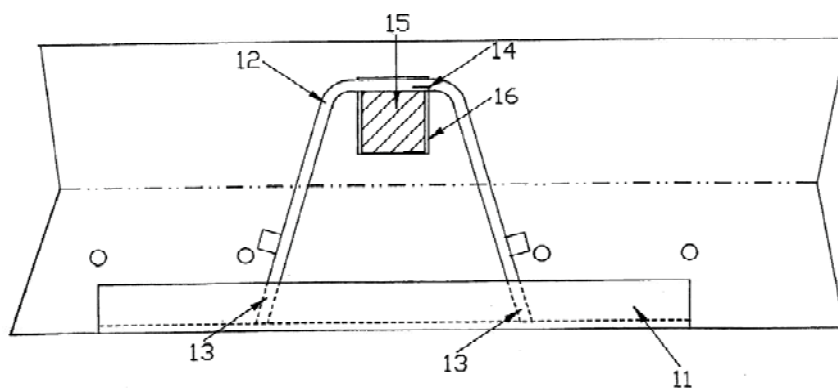
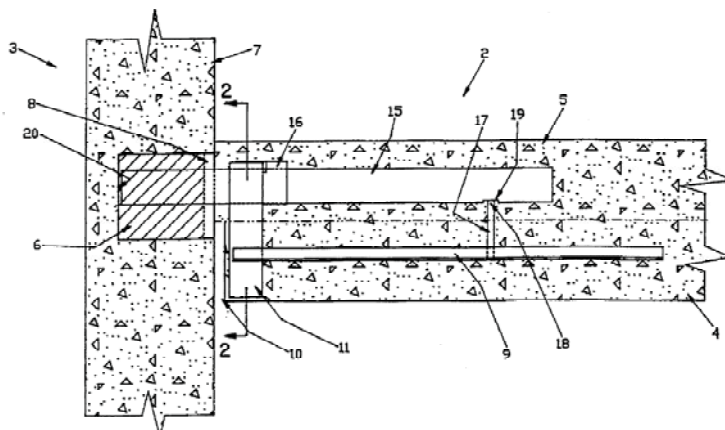


Figure 2.7: Section view through the side wall and the floor (top), and Section view along the line 2-2 (bottom). (Reay, 1997)

Compton, (1990) developed a new precast concrete beam supported at its end by columns using retractable hanger located in cavities at the upper ends of the beam as shown in Figure 2.8 (Patent number 4,903,448). Each hanger extends as cantilever into a recess in

the adjacent column. In its extend position, the hanger has its opposite ends supported on bearing plates in the cavity and in the recess. The drawbacks of that connection are: 1) inadequacy of the system in resisting lateral loads due to discontinuity of beam-column connections; and 2) for precast components it has many details and that required highly skilled labor

Beam (10), Column (11)
 Hunger member (12)
 Hunger eye device (13)
 Load transfer means (17)
 Components of a beam hanger arrangement (15)
 Floor slab (16), Recess (22)
 Beam end surface (18)
 Cavity (19), Beam upper surface (20)
 Column end (30), Beam end (31)
 Projection (32, 33)
 Hunger member top surface (34, 35)
 Wedge portion (36)
 Wedge portion top surface (37)
 Cavity bottom surface (39)
 Cavity upper end (40), Hunger side surface (42)
 Cables (45), Upper return bend portion (47)
 Legs (48), Frame (49)
 Bottom bars (52), Top bars (53)
 U-shaped stirrups (54), L bars (56)
 Prestressing cables (59)

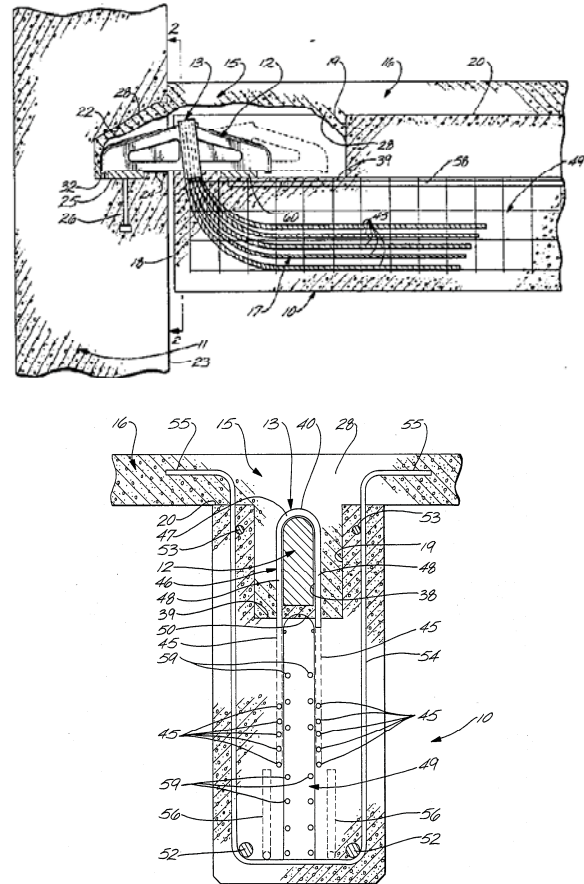


Figure 2.8: Cross section elevation view (top) and cross-section elevation view taken along line 2-2 (bottom). (Compton, (1990)

Wise and Meade, (1978) introduced a new building structure, in which precast columns, beams and deck members are used (Patent number 5,081,935). The basic structure is supported by precast concrete columns. At least one reinforcing rods in each corner was

extending upwardly in the first floor columns. The upper portion of column is hollow and has U-shaped groove as indicated in Figure 2.9. Above the first floor column is the second floor precast column. The upper column is structurally similar to the lower column. The pairs of rods are clamped together by coupling means. Supported in the hollow portion of the bottom column is at least one horizontal beam. Except at corners of the floor, there will be at least two beams supported by a column. The beam is U-shaped having hollow section. The U-shaped solid beams having rods extending from the end thereof into the U-shape hollow column. When the topping layer of concrete is later poured, the beam extended rods serve to lock in the beam into the finished unitary structure. Supported on the upper edges of the beams are deck plates, which are typically precast concrete slabs with length up to 60 ft. or more, widths of 4 to 8 ft. or more.(particularly suitable for this application are those precast concrete slabs sold under the trademark FILIGREE WIDESLAB. Once all mechanical and electrical work is completed on the deck created by beams and deck plate, and the second column are in place, the final step is pouring the concrete topping. Covering large spans is considered the main advantage of that system. The drawbacks of that system are: 1) during the construction, it is often desirable to have the beams supported by shoring; 2) it is hard to align the top column vertically because it will be resting on top of these rods which extend upward from the bottom column so that the top of the rods form a leveled plan; and 3) it requires a false ceiling to cover the unattractive beam drop.

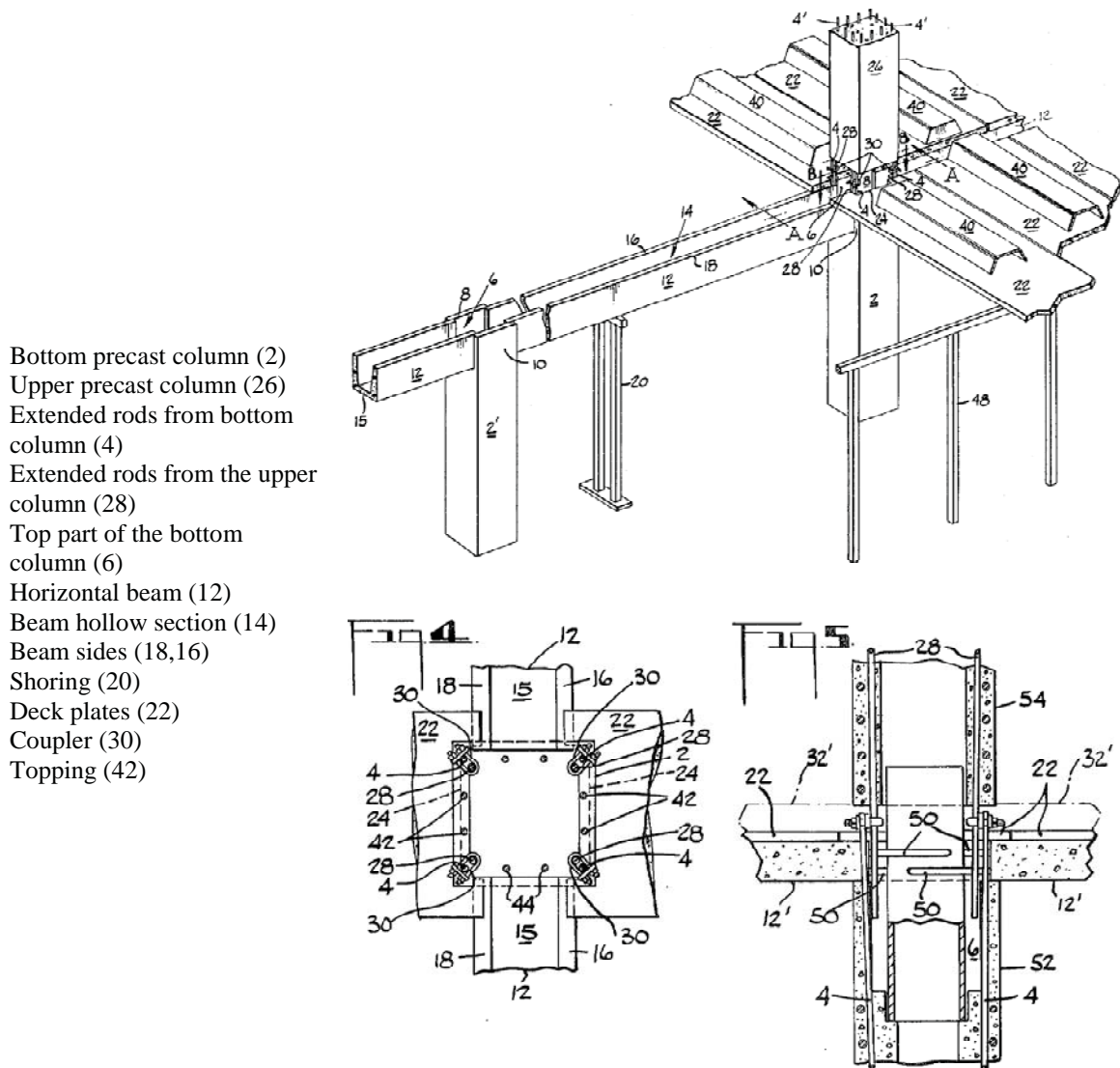


Figure 2.9: perspective view of the system (top), and plan view and elevation view taken on line B - B and A - A (bottom). (Wise and Meade, 1978)

Rahimzadeh, (2003) developed a structural framing system. This system consists of a steel beam that supports flooring sections interconnected using cast-in-place concrete (Patent number US 6,543,165 B2). The system is created by anchoring steel beams to vertical columns as shown in Figure 2.10. The floor sections span between the steel beams. Cast-in-place concrete is poured into the beams to connect the flooring sections. The concrete forms a rigid joint between the steel beam, floor sections, and the columns.

The drawbacks of that system are: 1) inadequate fire resistance; 2) it requires false ceiling to cover the drops of the beams; and 3) inadequacy of the system to resist lateral loads due to simple beam-column connections.

Vertical Column (14)
 Composite beam (16)
 Floor component (12)
 Sheath and solidifying material (24)
 Bottom plate (26)
 Containment sides (28)
 Reinforcement means (30)
 Joining Means (32)
 Support surface (34)
 The upper-most edge (38)
 Reinforcing means (40)
 Saddles (44)

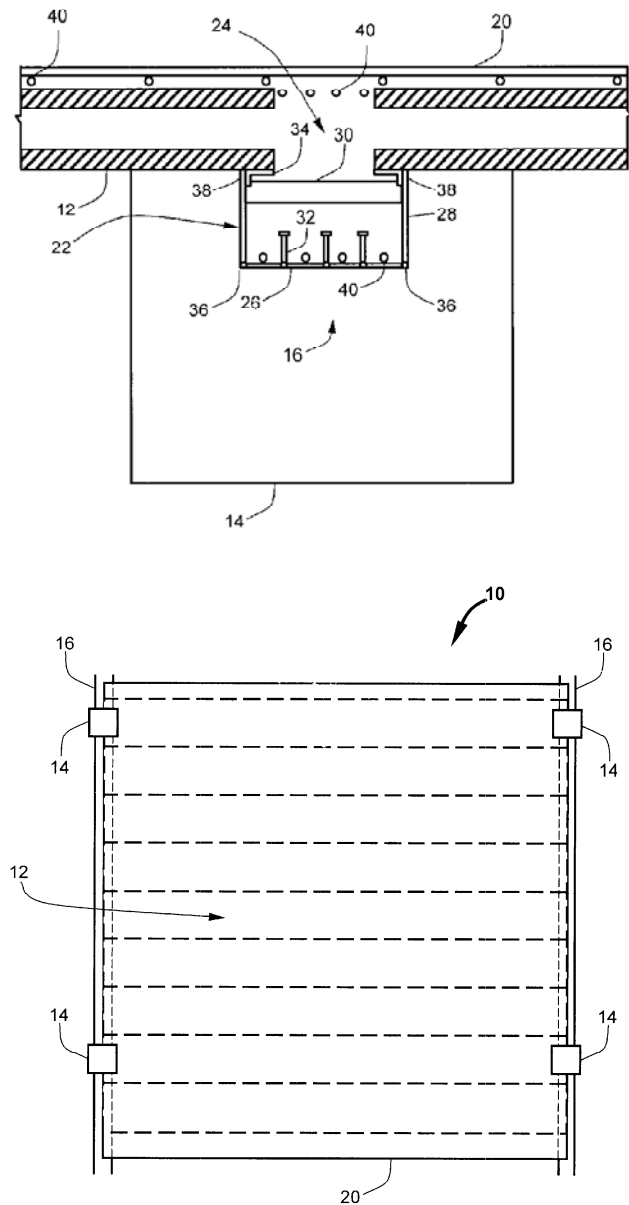


Figure 2.10: Cross-sectional view (top), and Plan view of the flooring system (bottom).

(Rahimzadeh, 2003)

Wise, (1973) introduced a method for building two way slabs, flat slabs, reinforced concrete floors, and roofs employing composite concrete flexural construction with little or no formwork (Patent number 3,763,613). The bottom layer of the composite concrete floor is formed by using thin prefabricated concrete panels laid side by side in place with their ends resting on temporary or permanent supports. The panels are precast with one or more lattice-type girders or trusses extending lengthwise from each panel having their bottom chords firmly embedded in the panel and with the webbing and top chords extending above the top surface of the panel as shown in Figure 2.11(left). Transverse reinforcing of the panel is achieved by embedding reinforcing bars in the precast panels. The ends of these bars take the shape of hooks, which extend above the upper surface of the panel along the marginal edges. These hooks are joined by special splicing means to offer transverse reinforcement from panel to panel as shown in Figure 2.11 (right). The splice is completed and the transverse reinforcement is achieved when the concrete topping is applied on the site to form the composite concrete floor slab. The main drawback of that system is the need for shoring in construction stage, in addition to the limitation in the dimensions of the panels.

Composite concrete floor (10)
 Special hooks (18)
 Transverse reinforcing bars (19)
 Splicing elements (20)

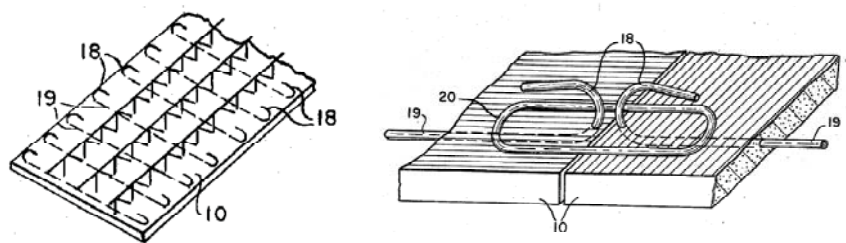


Figure 2.11: precast slab showing the longitudinal extending trusses (left) and perspective view of the special splicing (right). (Wise, 1973)

Hanlon, (2008) introduced a building system using modular precast concrete components that include a series of columns with wide integral capitals (Patent number US2008/0060293 A1). Wide beam slabs are suspended between adjacent column capitals by hangers. Joist slabs can be suspended between the beam slabs and column capitals to provide a floor surface as shown in Figure 2.12. After the columns have been erected, beam slabs are suspended between adjacent column capitals. Hangers extending from the ends on the top surface of the beam slabs allow the beam slabs to be dropped into place between adjacent capitals. These hangers are anchored to the upper surface of the column capitals to suspend and support the beam slab. After the insulation of the beam slabs, a number of joist slabs can be dropped into place across the span between adjacent runs of column capitals and beam slabs. Finally, the finished assembly can be covered with a thin concrete topping. This system is a good system for long spans column grids with increasing thickness. The main drawback of that system is the need for heavy construction equipment in erection due to the weight of the precast components.

Columns (10)
 Capitals (20)
 Beam slabs (30)
 Hangers (70)
 Joist slabs (40)

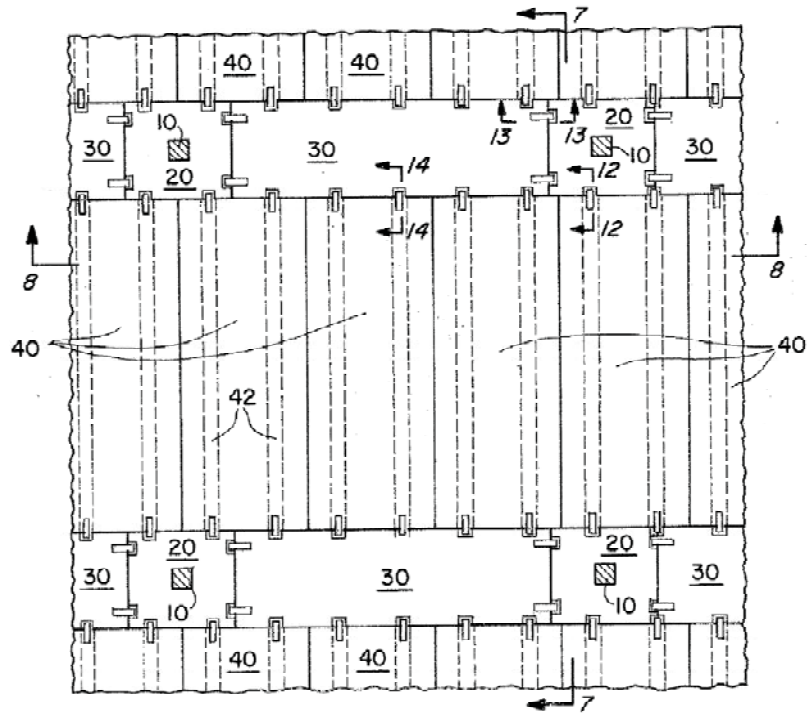
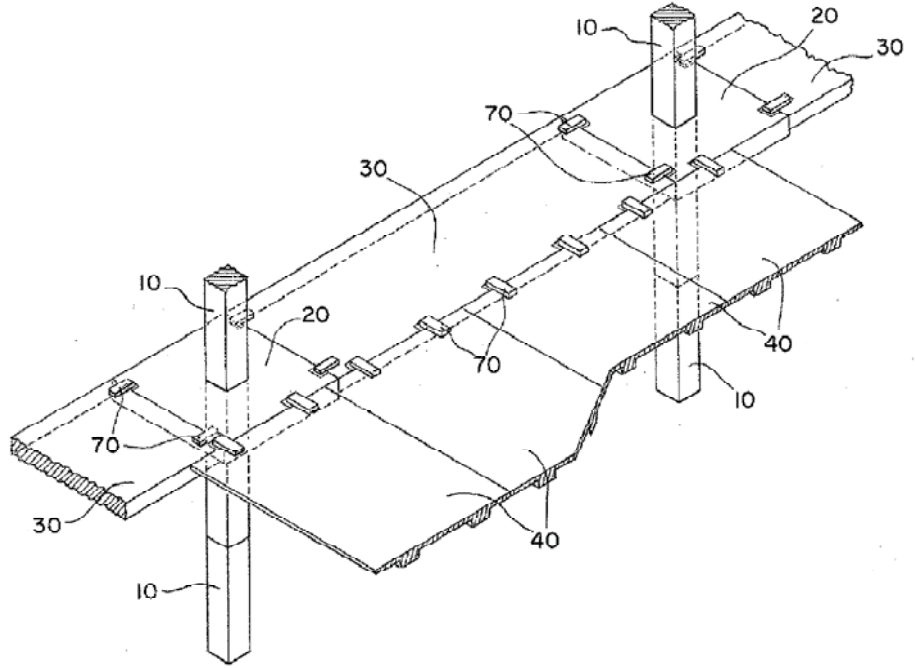


Figure 2.12: Perspective view showing an example of building framing (top), and cross-section shows the invented system (bottom).(Hanlon, 2008)

Hanlon et al. (2009) developed a total precast floor system for the construction of the nine-story flat-slab building in Avon, CO. This system consists of precast concrete stair/elevator cores; 10-in. deep \times 4-ft wide prestressed concrete beam-slab units; 10-in.-deep prestressed concrete rib-slab floor elements; 10-in.-thick variable-width beam slab; and integrated precast concrete columns with column capital as shown in Figure 2.13. The need for special forms to fabricate these components and the need for high capacity crane for erection are the main limitations of this system.



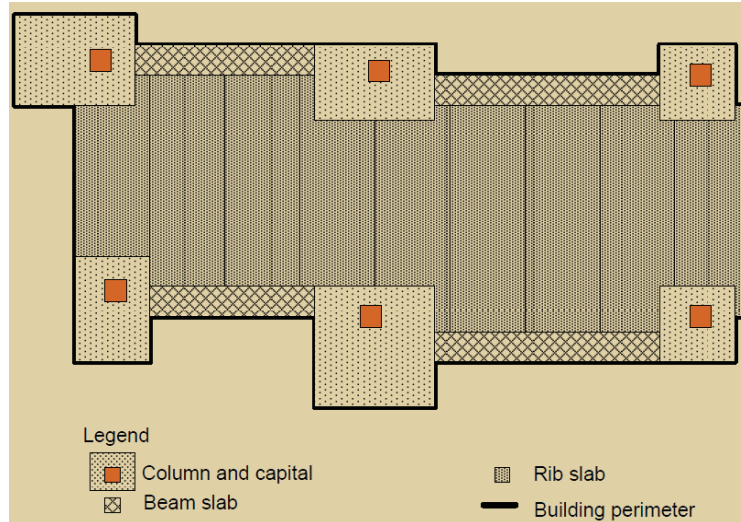


Figure 2.13: Elevation and Plan show the components of the described system. (Hanlon et al. 2009)

Composite Dycore Office Structures (1992) developed the Dycore floor system for office buildings, schools, and parking garages. This system consists of shallow soffit beam, high strength Dycore floor slabs, and continuous cast-in-place/precast columns with blockouts at the beam level as shown in Figure 2.14. In this system, precast beams and floor slabs act primarily as stay-in-place forms for major cast-in-place operations required to complete the floor system.

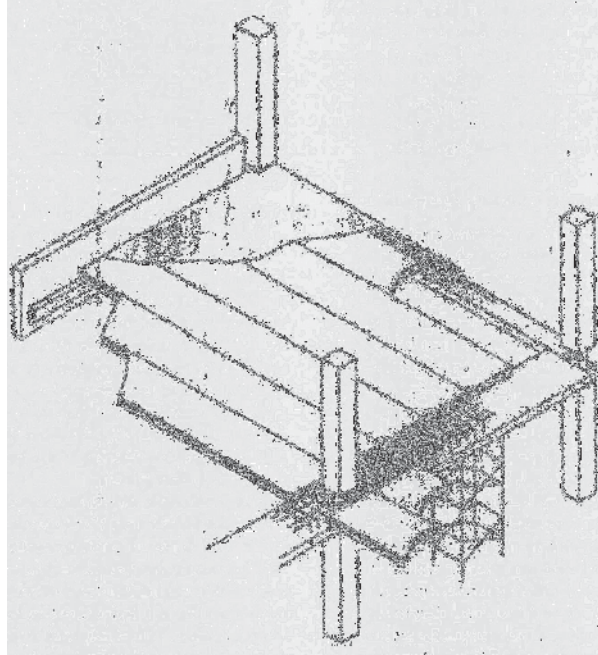


Figure 2.14: Composite Dycore structural floor system (Composite Dycore Office Structures, 1992)

Fawzy, (2088) developed a new continuous precast/prestressed concrete shallow floor system that eliminates the need for column corbels as shown in Figure 2.15 and shear walls which results in reducing floor height. The system consists of continuous precast columns, partially continuous 13 in. deep inverted tee beams, partially continuous 8 in. hollow-core planks, and minimum of 2 in. thick composite topping. Experimentally investigate was done to check the constructability and structural capacity of the system, a full-scale specimen of 20 ft x 20 ft area around an interior column was fabricated . This specimen includes a 14 ft long column, two IT beam segments 11 ft long each, and eight hollow core segments 8 ft long each. Three primary tests were performed on the specimen: a) IT beam continuity test, b) hollow-core continuity test, and c) beam-to-column connection test.

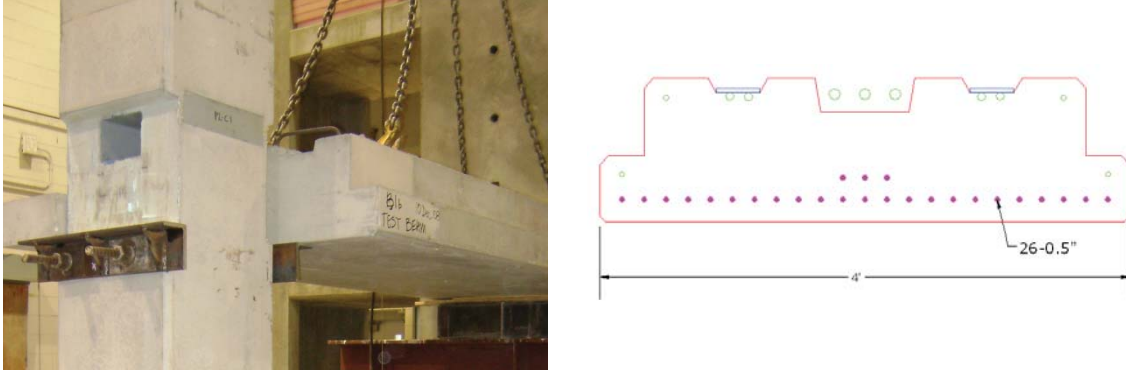


Figure 2.15: Column temporary corbel and cross section of the beam. (Fawzy, 2009)

Morcous and Tadros, (2010) developed a new HC-beam connection without ledge. They tested a full-scale specimen. The test specimen consisted of 15 ft long rectangular beam that is 10 in. thick, 48 in. wide, and four 8 ft long HC planks that are 10 in. thick and 48 in. wide each. The beam was supported by two roller supports that are 14 ft apart. Temporary supports for HC planks were erected using two alternatives: 1) $\frac{3}{4}$ in. inserts embedded in the beam to connect, the threaded rods holding HSS 5 ft long 4 in. 4 in. x $\frac{1}{8}$ in., and; 2) #5-inverted U bar on top of the beam. That has $\frac{1}{2}$ in. threads along the last 4 in. at each end to hang two angles back to back. HC planks were supported on the temporary supports and concrete blocks. During the test, the connection failed at the shear key as shown in Figure 2.16, which resulted in the separation of the hollow core from the topping and the cracking of the topping slab.

This dissertation is an evolution of the system developed by Fawzy (2009) and the connection developed by Morcous and Tadros (2010).



Figure 2.16: HC-beam connection under ultimate design load and failure of HC-beam connection. (Morcou and Tadros, 2010)

2.4 Emerging Systems

Several efforts have been made to minimize the depth of flooring systems by combining steel and precast concrete products. Figure 2.17 shows steel beam shapes used in Europe to support hollow core planks by their bottom flanges and the composite topping by their top flange. The first two shapes are plate girder (built up) sections, and the third is a rolled steel section (Board of Federation International Du Beton (fib) steering committee, 1999). These systems provide a high span-to-depth ratio, however, they are limited to about 20 ft spans, which is reasonable for apartment/hotel buildings, but considerably less

than the spans generally required for office building applications. These systems may merit further investigation if the fire protection issues of the underside of the beam can be satisfactorily resolved and if the cost of fabrication is comparable to the equivalent prestressed concrete beam.

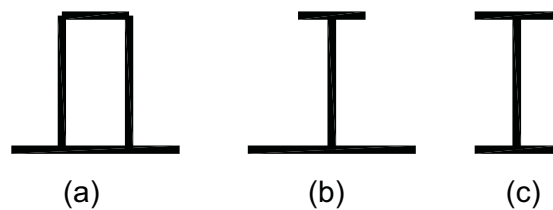


Figure 2.17: European practices in designing hollow core supporting beams. (fib steering committee, 1999)

In the United States, the steel beam shape shown in Figure 2.18 and Figure 2.19 has been developed by Girder-Slab Technologies LLC of Cherry Hill, NJ, (2002), Cross. (2003), Veitas (2002), and Peter A. N., (2001) Similar to the European practices, the precast planks are supported on the bottom flange of the steel beam. The D-BEAM™ steel girder is a proprietary shallow beam that spans usually 16 feet, which would not suit typical office framing spans. Longer spans require extra manufacturing and shipping cost.

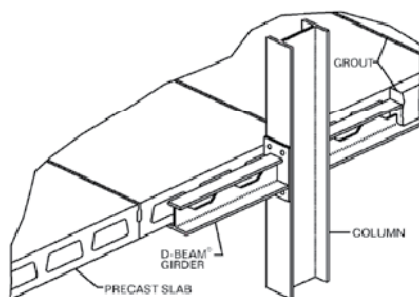


Figure 2.18: D-BEAM™, by Girder-Slab Technologies LLC, Cherry Hill, NJ (2002).



Figure 2.19: Construction using Girder-Slab system of Girder-Slab Technologies LLC
Cherry Hill, NJ (2002)

The Deltabeam, a product of the Peikko Group, Peikko News (2010) is an example of these products. The Deltabeam a hollow steel-concrete composite beam made from welded steel plates with holes in the sides. It is completely filled with concrete after installation in site as shown in Figure 2.20. Deltabeam acts as a composite beam with hollow-core, thin shell slabs, and in-situ casting. Deltabeam can have a fire class rating as high as R120 without additional fire protection.



Figure 2.20: Filling the Deltabeam with self-consolidating concrete.

(<http://www.peikko.ca/Default.aspx?id=625741>)

The Deltabeam height varies based on the required span. For a 32 ft span, the Deltabeam can be as shallow as 23" (21" deep beam + 2" topping). Although Deltabeam is shallower than the corresponding precast/prestressed concrete inverted tee as shown in Figure 2.21, it requires shoring for erection, adding shims to the base plate to raise up hollow core to match the level of the top plate, and additional fire protection operations if higher ratings are required. All of these operations result in a significant increase to the construction cost and duration. In addition, Deltabeam can be erected only as a simple beam with continuous column, continuous beam with discontinuous column, or simple beam with discontinuous column. Deltabeam cannot be used as a continuous beam with continuous columns, which reduces the system's ability to resist lateral loads due to wind or earthquake and increases construction complexity.



Figure 2.21: Construction of Deltabeam floor system.

(<http://www.peikko.ca/Default.aspx?id=625741>)

The use of built-up steel sections in precast concrete construction in the US would require that steel sections be purchased from a steel fabricator, which is not a desirable approach for US precasters. Most US precasters have limited welding capabilities, as they are not equipped to perform continuous welding for plate girders. Therefore, solutions that require limited use of structural steel are more desirable.

Filigree Wideslap System was originally developed in Great Britain and is presently used under the name of OMNIDEC (Mid-State filigree Systems, Inc. 1992). “It consists of reinforced precast floor panels that serve as permanent formwork. The panels are composite with cast-in-place concrete and contain the reinforcement required in the bottom portion of the slab. They also contain a steel lattice truss, which projects from the top of the precast unit as shown in Figure 2.22. The steel truss ensures composite behavior between precast and cast-in-place concrete and provides the unit with stiffness during erection. The typical thickness of the prefabricated unit is 2.25 in. The units are made in lengths up to 70 ft, and typical widths of 8 ft or less. Slab units can be pretensioned: when reinforcing steel and concrete are field-placed, the resulting floor is camber free. One of the main advantages for this system is a flat soft floor which does not require a false ceiling. However, this system has poor thermal insulation, and requires extensive techniques to produce” (Pessiki et. al. 1995)

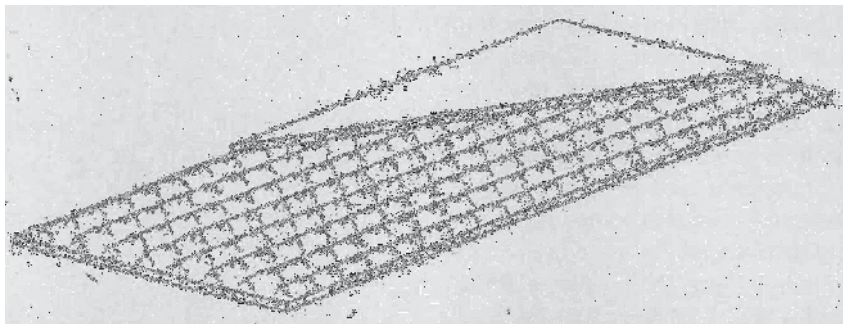


Figure 2.22: Filigree precast slab with light steel truss. (Pessiki et. al. 1995)

Rafael and Orid (2010) developed a new flooring system which consists of a structural grid of concrete beams with expanded polystyrene (EPS) foams in between as shown in Figure 2.23. The concrete beams have cross section of 4 x 12 in and the forms are 1.2 in higher. The grid has beams in two directions every 32 in. The floor is finished with a light paving system on top and a light ceiling system underneath. When finished, it weights 41 psf, in buildings with columns separated by 23.3 ft and with a structure slab thickness of 11.8 in. The production of these slabs is simple and usually is carried out in a factory. First the EPS 4 x 8 ft forms are put together on a flat surface. If the final slab size is not a multiple of 4 x 8 ft, then the EPS must be cut. After that the reinforcing steel and the embedded connections are situated in the beam forms. Then, the concrete fills the grid of beams. Finally, the precast pieces can be carried to the construction site or they can be finished, including all the pipes, the floor and ceiling surface in the factory. This system has many advantages, such as lightweight, flat soffit, and thermal insulation. However, some of its disadvantages include the floor thickness, unique fabrication process of EPS forms due to the special connections required.

- 1- Pavement.
- 2- EPS formwork.
- 3- Precast slab beams.
- 4- Connections.
- 5- Services.
- 6- Ceiling.

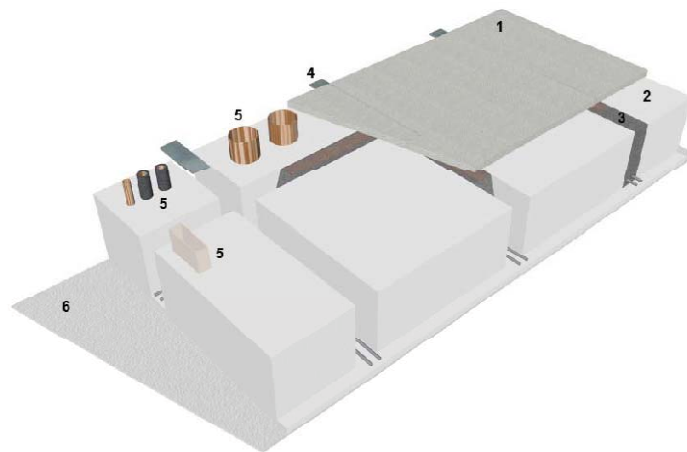


Figure 2.23: The NEW Flooring System components (Rafael and Orid, 2010)

Chapter 3

SYSTEM DESCRIPTION AND CONSTRUCTION SEQUENCE

3.1 System Description

The proposed floor system consists of the following components:

- Precast concrete columns
- Precast beams
- Precast floor panels
- Cast-in-place composite topping

The main challenges faced in this proposed system were:

- **Minimizing the depth of the beams:** This was achieved by making the beam wide to have the most amount of strands in a fewer number of rows, which lower the centroid of prestressing force for higher flexural capacity. In addition, reducing the beam depth was achieved by making it continuous for topping weight and live loads.
- **Eliminating corbels:** This was achieved by using temporary supports in place of column corbels during construction. The beam-column connection was made using shear keys and reinforcing bars to transfer the vertical shear from the beam to column under ultimate loads after the removal of the temporary support. Full scale testing was carried out to evaluate the adequacy of the connection
- **Eliminating ledges:** This was achieved by using temporary supports in place of beam ledges during construction. The HC-beam connection was made using shear keys or hidden corbels and reinforcing bars to transfer the vertical shear from the HC planks and beam under ultimate loads after the removal of the temporary

support. Full scale testing was carried out to evaluate the adequacy shear capacity of the HC- beam connection.

- **Providing continuity for lateral load resistance:** A composite reinforced concrete topping was used to make both beams and HC planks continuous for live load. This continuity created adequate negative moment capacity to suppress the positive moments generated by lateral loads.

3.2 Construction Sequence

Step 1) precast of building components (beams, columns, and HC planks) as shown in Figure 3.1

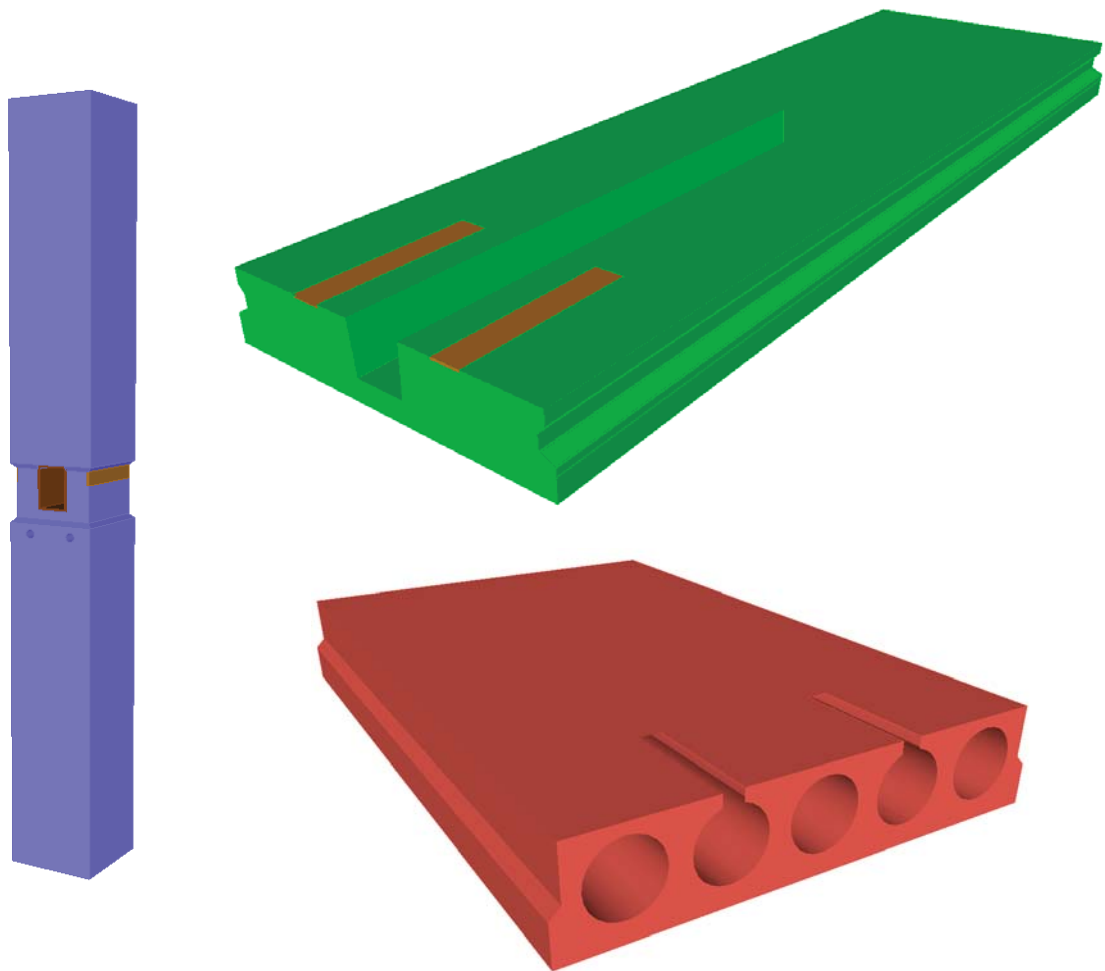


Figure 3.1: System Components

Step 2) The precast columns are bolted to the foundation and temporary corbels are installed beneath the beam lines. These corbels consist of two angles. The angles were bolted to the column using two friction bolts through holes in the column as shown in Figure 3.2. These angles are temporary, low cost supports for the precast beam during construction and can be reused several times.

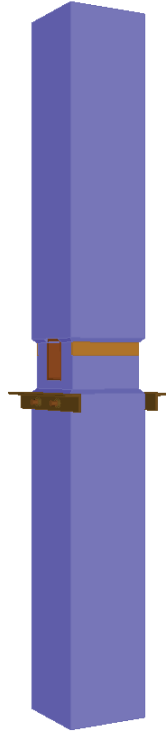


Figure 3.2: Placing temporary corbels

Step 3) Precast/prestressed beams are placed on each side of the column so that the beams align to each other and the beam pockets align to the column opening as shown in Figure 3.3. The beams were placed at a distance of 1 in. from the column face in addition to the 1 in. recess in column sides, which creates a 2 in. wide gap between the column face and beam end to be grouted later and ensure the adequacy of the compression flange to resist negative moment at the support.

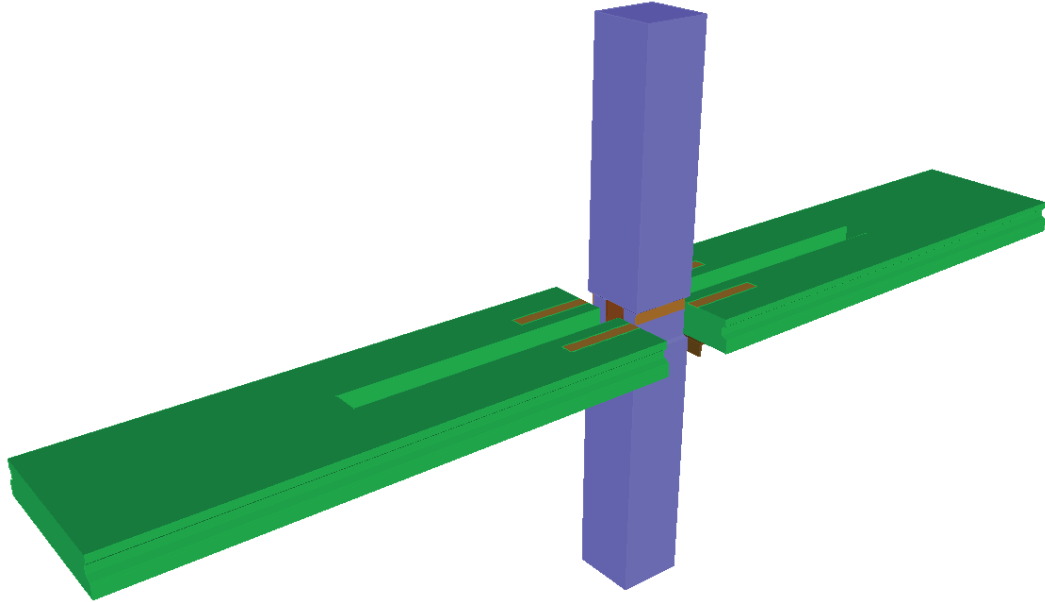


Figure 3.3: the beams on the temporary corbels

Step 4) Two steel angles were welded to the beam end plates and column side plates as shown in Figure 3.4. These angles are required to stabilize the beams during HC erection in addition to its contribution in resisting negative moment.

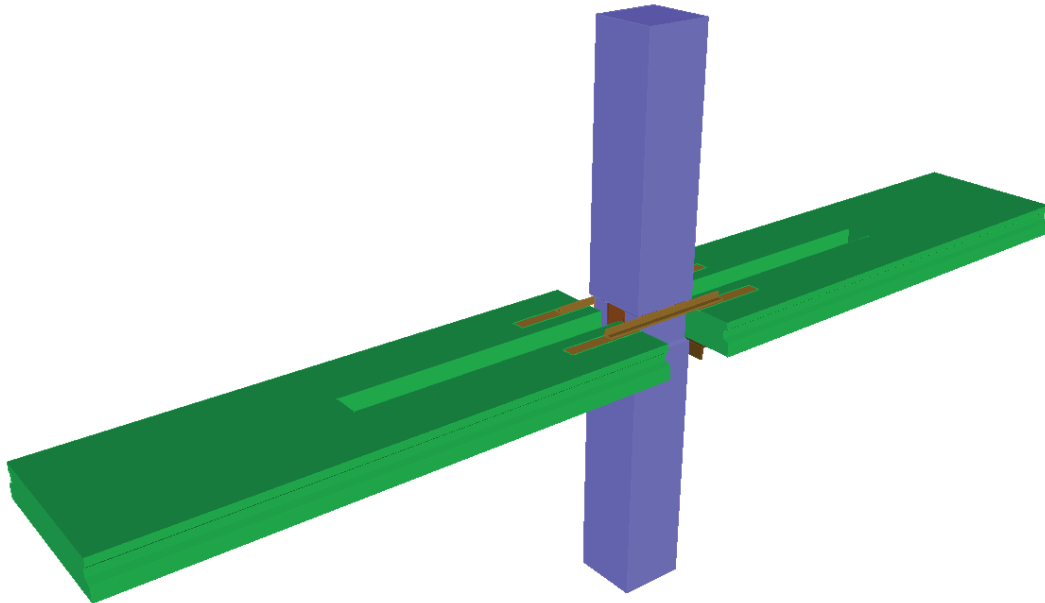


Figure 3.4: Welding the top angles to beam and column

Step 5) Steel tubes or steel angles are installed as temporary ledges to support the hollow core planks. The tubes are connected to the bottom of the precast beam using coil inserts and bolts. The steel angles are connected by welded the angle to the plates preinstalled on the beam side as shown in Figure 3.5.

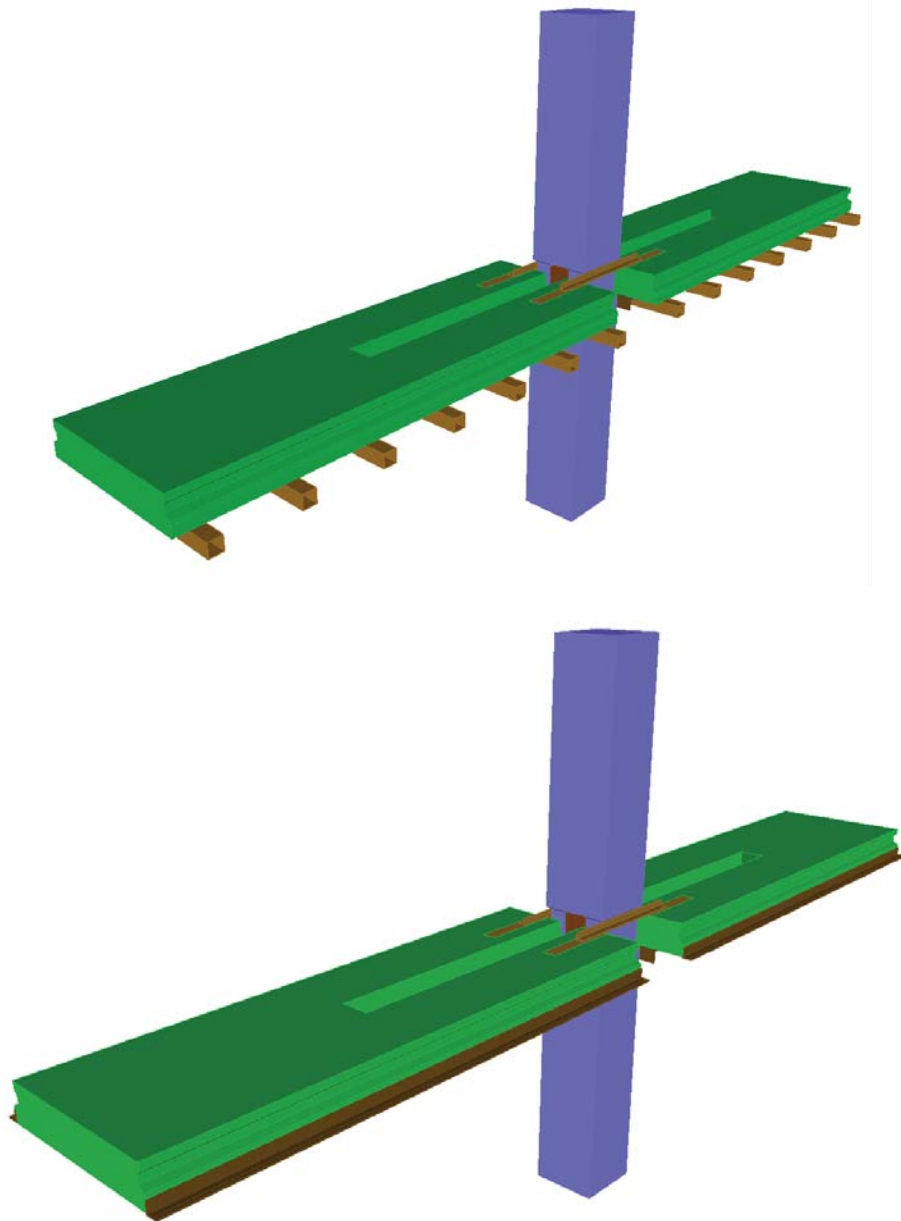


Figure 3.5: temporary beam ledges

Step 6) HC planks are placed on the temporary beam ledges on each side of the beam as shown in Figure 3.6.

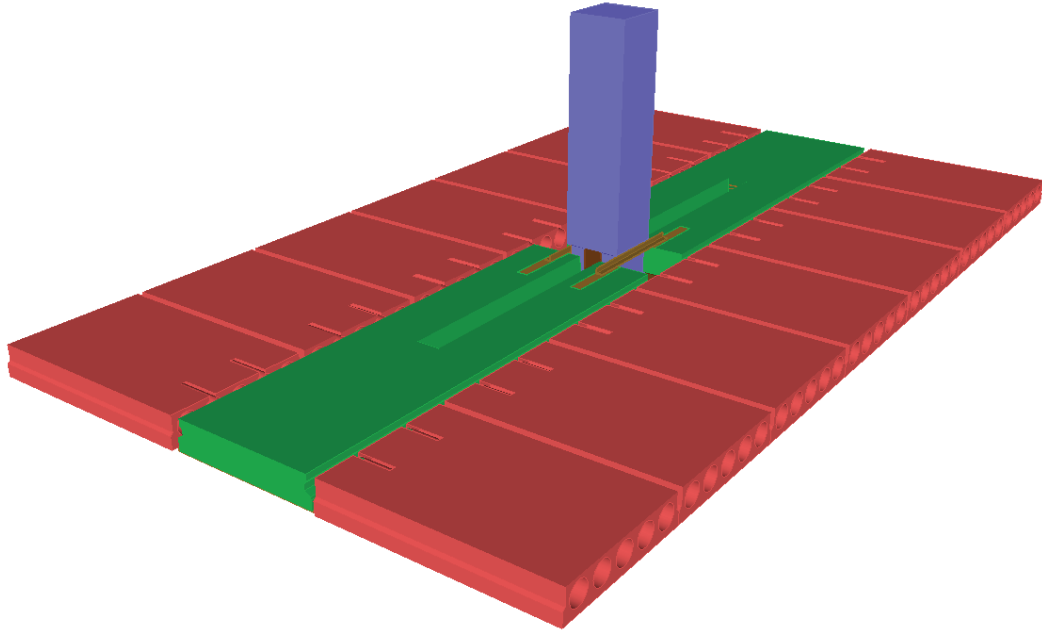


Figure 3.6: Hollow core planks on temporary beam ledges

Step 7) Continuity reinforcement is placed in the beam pockets and through the column opening. This reinforcement includes the hidden corbel reinforcement needed for the beam-column connection and the hat and loop bars connecting the HC planks to the beam placed over the beam at the HC keyways and slots in the HC opening as shown in Figure 3.7.

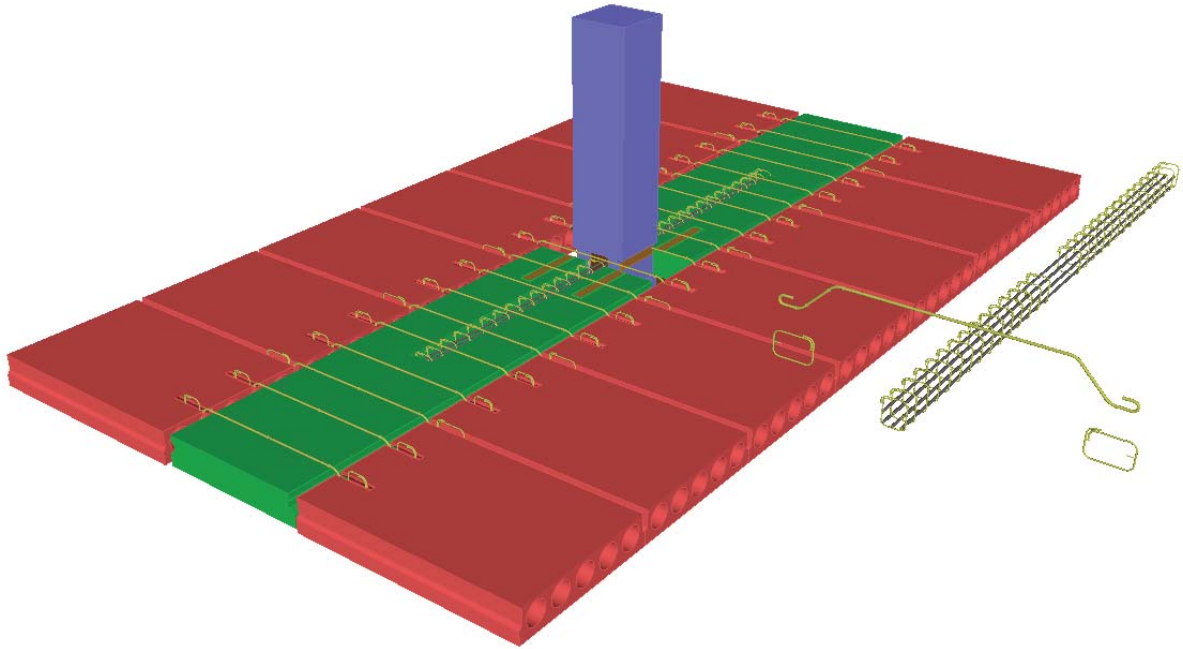


Figure 3.7: Continuity reinforcement and HC-beam hat and loop bars

Step 8) The HC keyways, beam pockets, and column opening were grouted using flowable concrete as shown in Figure 3.8.

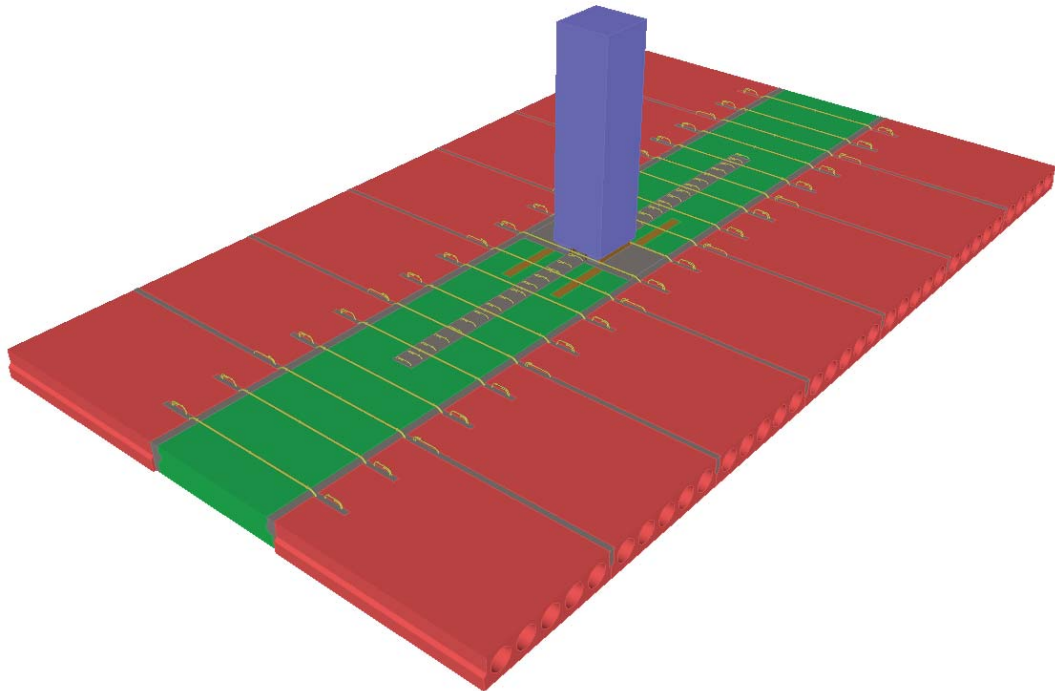


Figure 3.8: Grouting the H.C keys and beam pocket with SCC

Step 9) Second layer of continuity reinforcement is placed over the beam, as shown in Figure 3.9

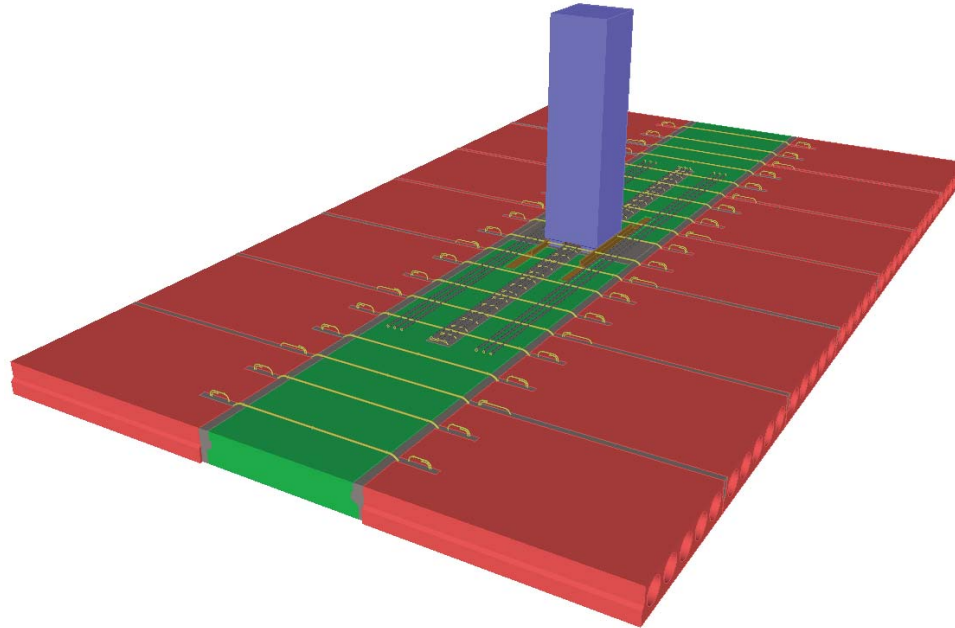


Figure 3.9: Beam continuity reinforcement

Step 10) Welded wire reinforcement is placed over the HC planks to reinforce the composite topping as shown in Figure 3.10.

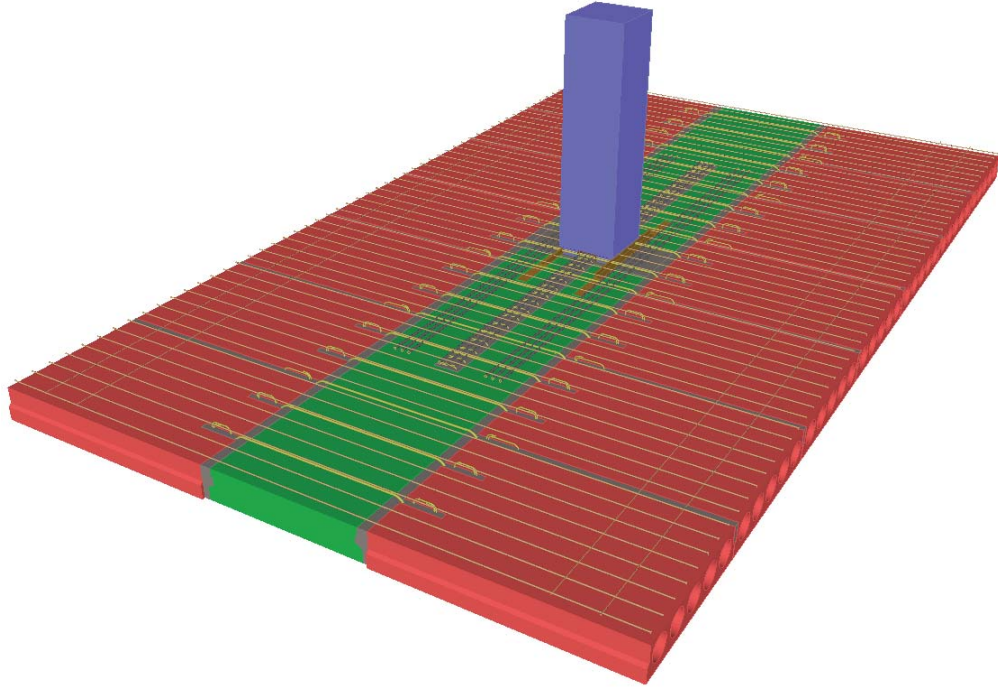


Figure 3.10: Placing the topping reinforcement

Step 11) Topping concrete is poured using medium slump 3.5 ksi concrete as shown in Figure 3.11.

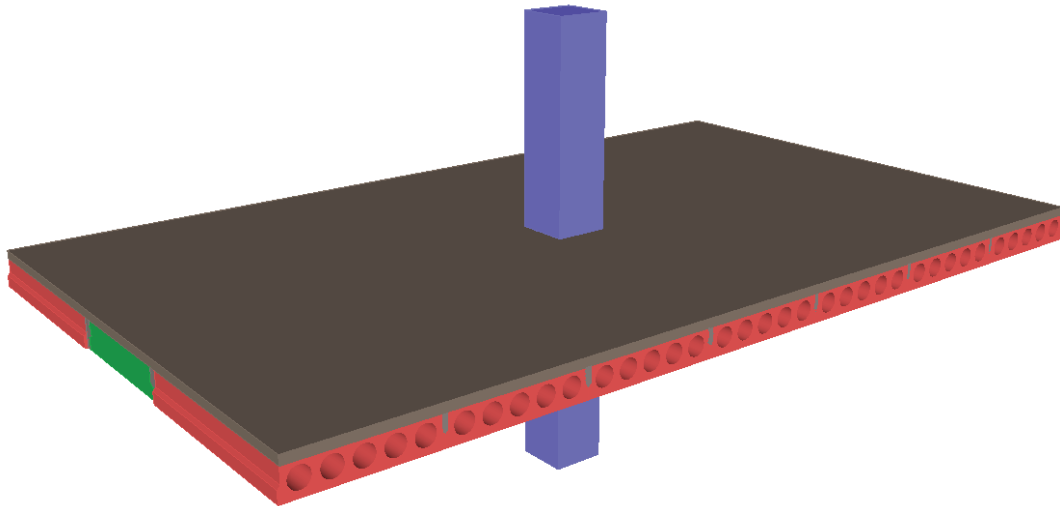


Figure 3.11: Pouring and finishing the topping concrete

Step 12) Finally, the temporary corbels and ledges are removed after topping concrete reaches the required compressive strength to provide a flat soffit as shown in Figure 3.12.

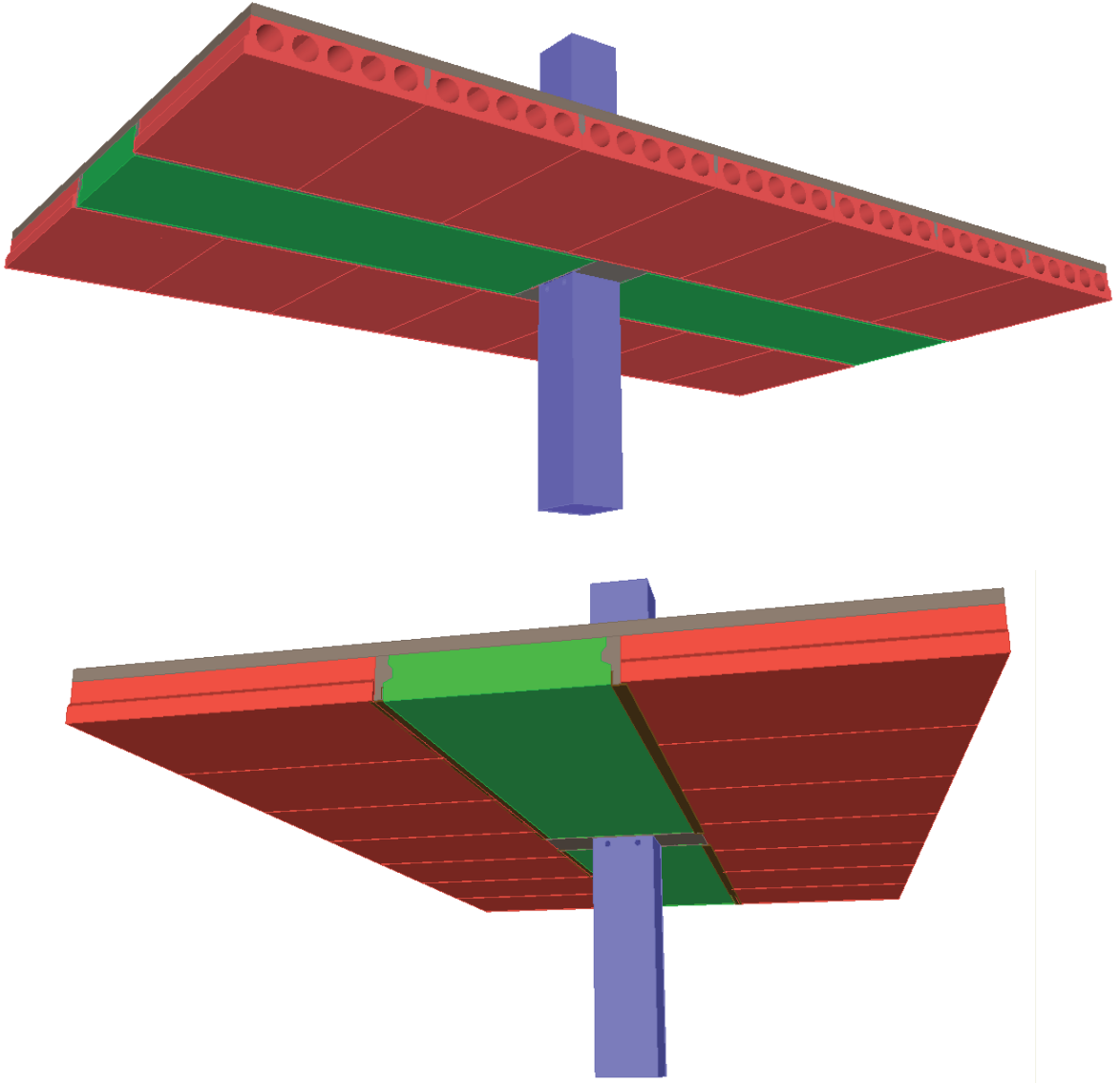


Figure 3.12: Removing the temporary corbels and ledges

Chapter 4

DESIGN OF FLAT SOFFIT FLOOR SYSTEM UNDER GRAVITY LOAD

4.1 Introduction

The purpose of the design procedures shown in this chapter is to present the steps for designing the flat soffit shallow precast concrete floor system in sufficient detail to allow a knowledgeable engineer to replicate the design on actual projects. The next sections discuss design concepts and Appendix A presents the design calculations in details. Design procedures were entirely performed according to the provisions of the following design codes, standards, and manuals:

- American Concrete Institute (ACI) “*Building Code Requirements for Structural Concrete (ACI 318-08) and Commentary*”
- American Institute of Steel Construction, (AISC, (2008). “*Steel Construction Manual*”, Thirteenth Edition.
- American Society of Civil Engineering, (ASCE. (2005)) “*ASCE 7-05 Minimum Design Loads for Buildings and Other Structure*”
- Precast/Prestressed Concrete Institute (PCI. (2004)) “*PCI Design Handbook*”, 6th Edition

4.2 Design Example and Procedures

In order to explain the main design criteria that apply to the proposed flat soffit shallow hollow core floor system, an example building is used. Figure 4.1 shows the general plan, elevation, and side views of a six-story office building. The proposed floor system consists of continuous precast columns and partially continuous 10 in. deep rectangular beams, partially continuous 10 in. deep HC planks, and minimum of 2 in. composite

concrete topping. This system benefits the precast/prestressed industry by utilizing typical components that are easy to produce, handle, and erect. The 10 in. thick and 48 in. wide, HC planks are the most affordable precast product due to their lightweight and use in several applications. In addition, the 48 in. wide and 10 in. thick rectangular beams are simple in fabrication, handling and shipping. All the connections in the new system are greatly simplified for the precaster and contractor to speed up fabrication and erection operations, which will result in the quick and wide use of this system. Two key methods can be used to achieve the structural capacity of the proposed shallow floor system under gravity and lateral loads: a) increasing the beam width up to 48 in. to accommodate 19-0.6 in. diameter prestressing strands, and b) making the beam continuous for topping weight and live loads. This continuity necessitates having openings through the continuous column and pockets in the beam to allow the negative moment reinforcement of the beam to go through the column. This will also provide adequate support for the beam, so that the temporary corbels below the beams can be removed. HC planks are also designed with partial continuity to provide adequate resistance to lateral load in other direction.

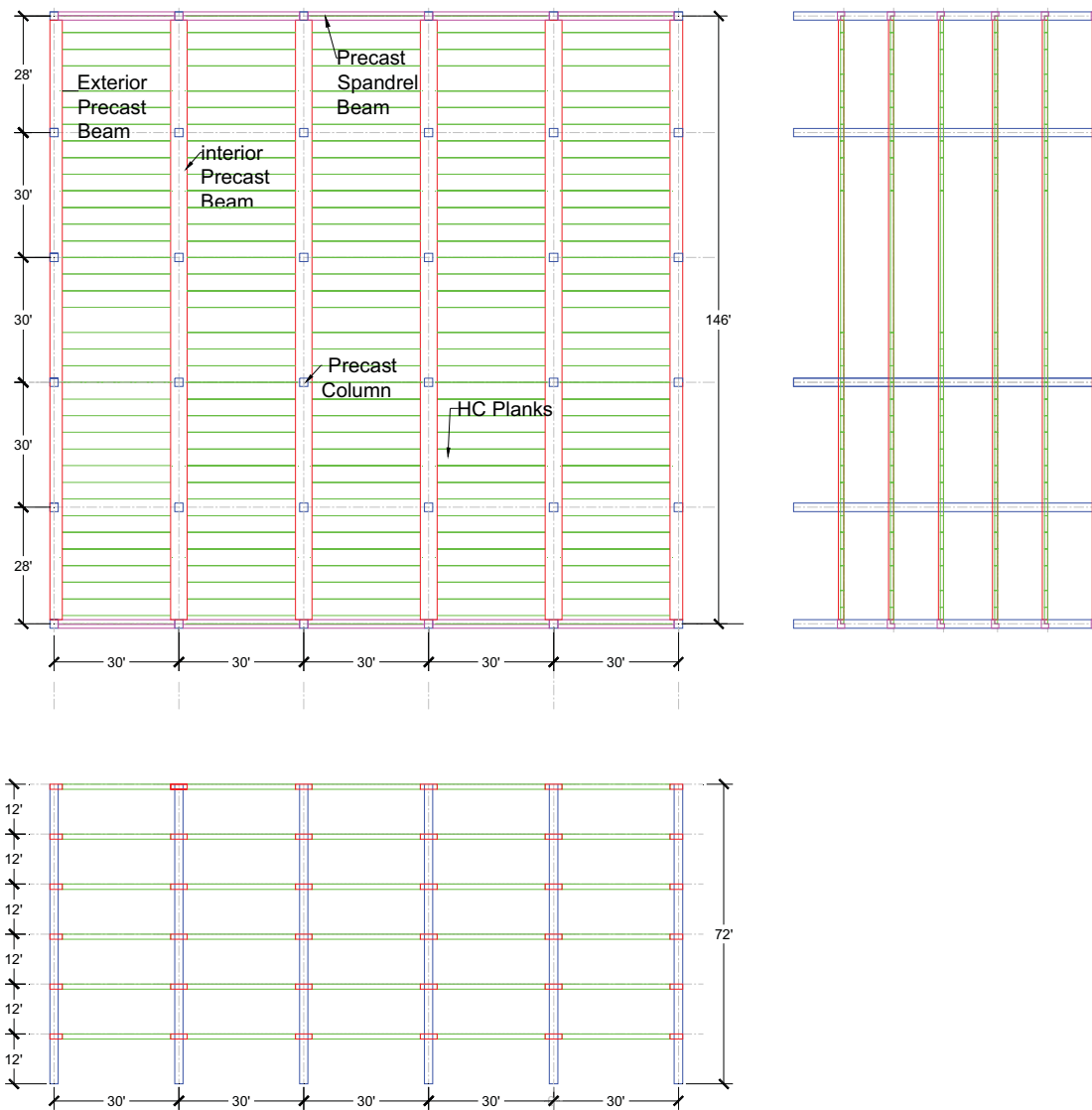


Figure 4.1: Plan, elevation, and side views of the example building

Figure 4.1 shows the plan, elevation, and side views of an example building that will be used in presenting design procedures. This building is a six-story office building that is 150 ft long, 146 ft wide, and 72 ft high designed for a 100 psf live load. The average floor height is 12 ft (from centerline to centerline) and interior bays are 30 ft in the long direction and 30 ft in the short direction, while exterior bays are 30 ft in the long direction and 28 ft in the short direction. It is recommended that the flat soffit beams (FS) be used

along the short direction of the building, while hollow core (HC) planks are used in the long direction of the building. This usually results in a more economical design. Below are the properties of materials used in this design example:

- ▶ Concrete strength of precast components = 6,500 psi at release and 8,000 psi at final
- ▶ Concrete strength of precast Hollow Core 6,000 psi
- ▶ Concrete strength of cast-in-place grout 6,000 psi
- ▶ Concrete strength of cast-in-place topping 4,000 psi
- ▶ Prestressing strands are 0.6 in. diameter Grade 270 low-relaxation
- ▶ Reinforcing steel is Grade 60 deformed bars
- ▶ Welded wire reinforcement (WWR) is Grade 75 deformed wires

4.2.1 Design for Gravity Loads

4.2.1.1 Floor Panels

Two alternative floor panels will be used in this study; a) Hollow core (HC) planks that can be used when there is no need for thermal insulation and b) Sandwich floor panels that can be used when there is a need for the thermal insulation. The following section describes in details the design for both HC only and the sandwich panel will be presented in chapter 7.

Hollow Core (HC) Design

The HC planks used in the proposed system are designed similar to HC planks used in any conventional floor system. Manufacturer tables and design charts are used to determine the maximum span and uniform load that can be carried by a specific type and size of HC planks.

HC planks are designed as simply supported non-composite beams carrying the weight of concrete topping and as simply supported composite beam carrying the live load and superimposed dead loads. Camber and deflection of HC planks are calculated to determine the thickness of the topping at the beam mid-span and end-span sections.

HC planks are made continuous over the interior beams to create a moment resisting frame in the HC direction for resisting lateral loads. Therefore, the negative moment capacity of the composite end-span section of HC, shown in Figure 4.2, is calculated using strain compatibility to determine whether additional reinforcement is needed over the column strip.

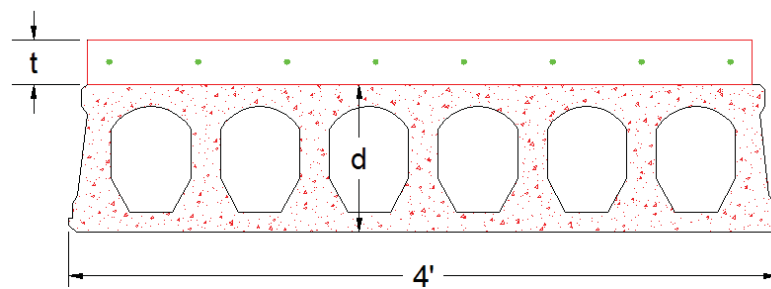


Figure 4.2: Composite HC End-Span Section

4.2.1.2 Flat Soffit Beam Design

Two different cross sections of flat shallow beams were designed to be used in the proposed system; a) beam with shear key and b) beam with hidden corbel. Three standard flat soffit beams (FS) are proposed for each cross section to be used with 8 in. 10 in., and 12 in. thick HC planks to cover a wide range of spans and loading conditions. Figure 4.3 shows the dimensions of the six FS beams (three from each cross section). For the building example presented in this study, FS10 with 10 in. thick HC were selected, which results in an average span-to-depth ratio of 30. The following subsections summarize the

flexure design, and shear design for this beam. Detailed design calculations for the same example are presented in Appendix A.

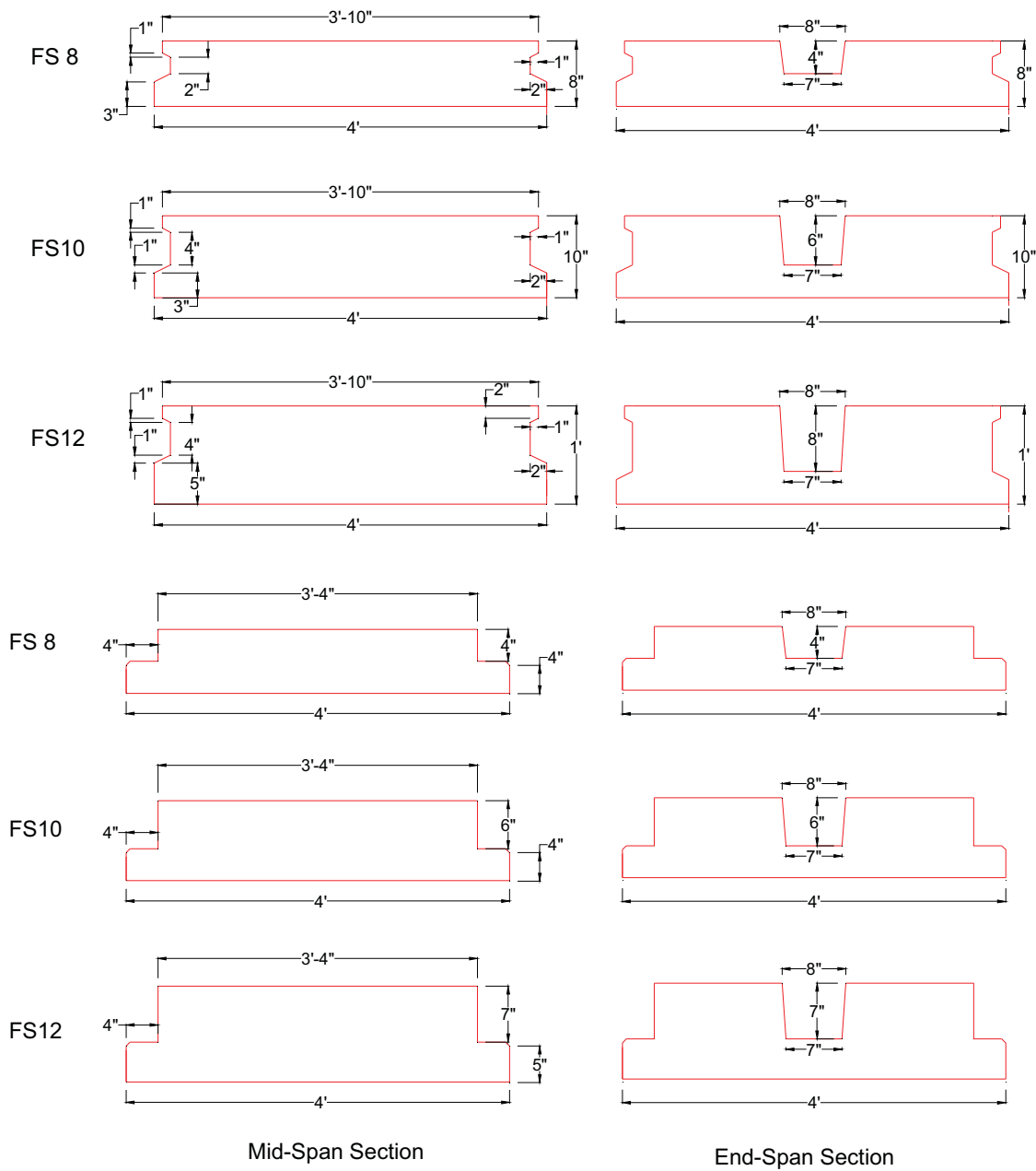


Figure 4.3: Dimensions of Standard FS beam with shear key (top) and FS beam with hidden corbel (bottom)

A. Flexure Design

Making the beam continuous for topping weight, live loads, and superimposed dead loads was achieved in two stages:

- 1) Placing negative moment reinforcement in the pockets at the beam ends and through the column and pouring the pockets to make the non-composite beam continuous for topping weight, and
- 2) Placing negative moment reinforcement in the concrete topping to make the composite beam continuous for superimposed dead and live loads.

Therefore, the flexural capacities of both mid-span and end-span sections are checked for the following three conditions:

- Simply supported non-composite beam subjected to prestressing force and the self-weight of FS beam and HC.
- Continuous non-composite beam subjected to topping weight.
- Continuous composite beam subjected to live load and superimposed dead load.

Four sections from the flat soffit beam need to be checked for their flexural capacity.

Non-composite mid-span and end-span sections are fully prestressed concrete sections and need to be checked under service and ultimate loading conditions, while composite mid-span and end-span sections are reinforced concrete sections and need to be checked under ultimate loading conditions only. Non-composite mid-span and end-span sections are designed as Class U sections to determine the required prestressing. Table 4.1 shows beam design parameters required for this building. Table 4.2 shows the final moments of the flat soffit beam obtained using moment coefficients (ACI Section 8.3).

Table 4.1: Design parameters

Selected Beam Type	FS 10
Column Width (in)	20
Average Topping Thickness (in)	2.25
LL (psf)	100
External Bay Size in Beam Direction (ft)	28
Internal Bay Size in Beam Direction (ft)	30
Bay Size in HC Direction (ft)	30
Beam Concrete Strength at Release (psi)	6500
Beam Concrete Strength at Final (psi)	8000
Grout Concrete Strength (psi)	6000
Topping Concrete strength (psi)	4000

Table 4.2: Beam final moments

Factored Non-Composite Positive Moment (kip.ft)	344
Factored Composite Positive Moment (kip.ft)	565
Factored Non-Composite Negative Moment (kip.ft)	76
Factored Composite Negative Moment (kip.ft)	397

Based on the analysis results, the exterior span of the FS10 was found to be the most critical at both positive and negative moment sections. The design of these sections in terms of the number of prestressing strands, precast top reinforcement, pocket reinforcement, and topping reinforcement is presented in Table 4.3. Table 4.4 compares the positive and negative moment capacities of composite and non-composite sections (ϕM_n), versus the ultimate moments (M_u) obtained from the analysis. Capacities were calculated using strain compatibility as it provides more accurate results than the approximate ACI equation 18-3.

Table 4.3: Reinforcement used in the Designed FS 10

Positive Moment Section Reinforcement	Number	Area (in ²)	Size
Prestressing Strands	19	0.217	0.6
Precast Top Reinforcement	7	0.20	#4
Negative Moment Section Reinforcement	Number	Area (in ²)	Size
Precast Top Reinforcement	4	0.44	#6
Pocket Reinforcement (Bottom)	6	0.44	#6
Pocket Reinforcement (Top)	3	0.79	#8
Topping Reinforcement	6	0.79	#8

Table 4.4: Comparison of Demand and Capacity at Critical Sections.

Section	Capacity (ϕM_n) kip.ft	Demand (M_u) kip.ft	Check
Positive Non-Composite Section	385	344	Ok
Negative Non-Composite Section	140	76	Ok
Positive Composite Section	678	565	Ok
Negative Composite Section	425	397	Ok
Factored Composite Positive Moment at the end-section(kip.ft)	100	Demand will be calculated from the lateral load	

Prestress loss calculations performed according to the PCI Design Handbook six edition method outlined in section 4.7. These calculations show elastic shortening losses of approximately 9.13%, long-term losses of 7.9%, and total losses of 17%. The stresses in the concrete after prestress transfer (before time-dependent losses) and stresses in concrete at service loads after allowance for prestress losses are calculated. The calculations indicates that the tension at the extreme top fibers at release exceed the code limits at mid-span and end section, therefore, 4#4 top bonded reinforcement were provided along the entire beam length in addition to 4#6 at the beam ends to control concrete cracking at release. Since the tension at the extreme bottom fibers at final is high

than modulus of rupture, the FS beam was designed a Class U flexural member, which allows the use of uncracked section properties for deflection calculations. End zone reinforcement of this prestressed beam was also calculated according to the PCI design handbook section 4.2.4, and it was found that 2#4 at 2 in. from the beam end is satisfactory as the required area of bursting reinforcement is 0.18 in².

B. Shear Design

The shear force for FS10 was calculated under the three loading conditions presented earlier. Table 4.5 shows the final shear obtained using the shear coefficients (ACI Section 8.3). The flat soffit beam was designed using the ACI simplified method (Section 11.3.2). Based on shear design, it was decided to use 2#4 @ 12 in. spacing along the entire beam length in addition to the 2#4 provided at 2 in. from beam-ends for end zone cracking

Table 4.5: Final shear values

Factored Non-Composite Shear (kip)	56
Factored Composite Shear (kip)	131

Two alternative solutions will be used to create the beam temporary ledges:

- 1) Two steel angles will be welded to beam side plates, which attached to the beam during casting stage
- 2) Steel section will be attached to coil inserts, which placed in the bottom of the beam during the casting stage.

Dimensions, reinforcement details, and method used to support the HC for the proposed beam cross section are shown in Figure 4.4, Figure 4.5, Figure 4.6, and Figure 4.7.

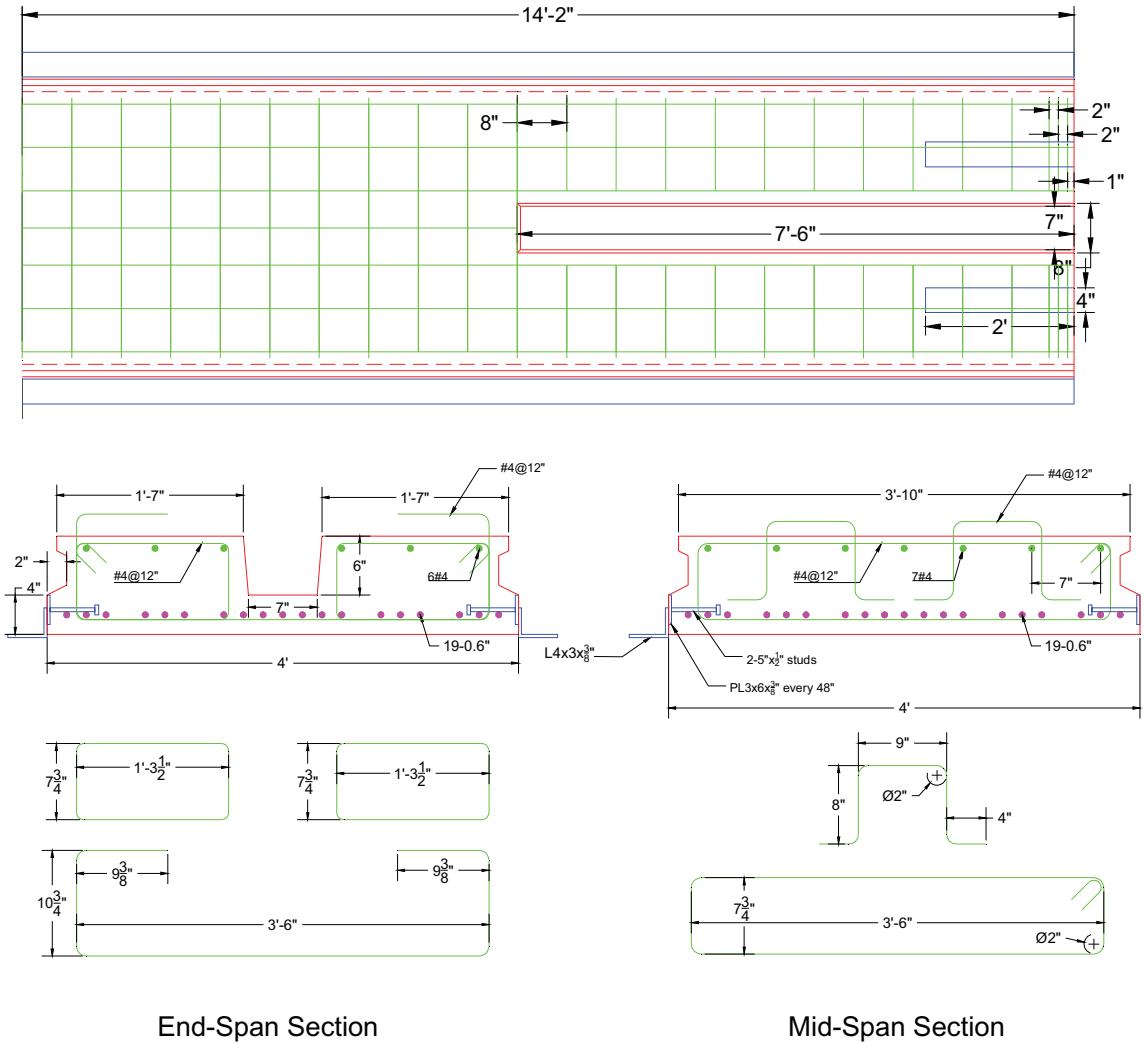
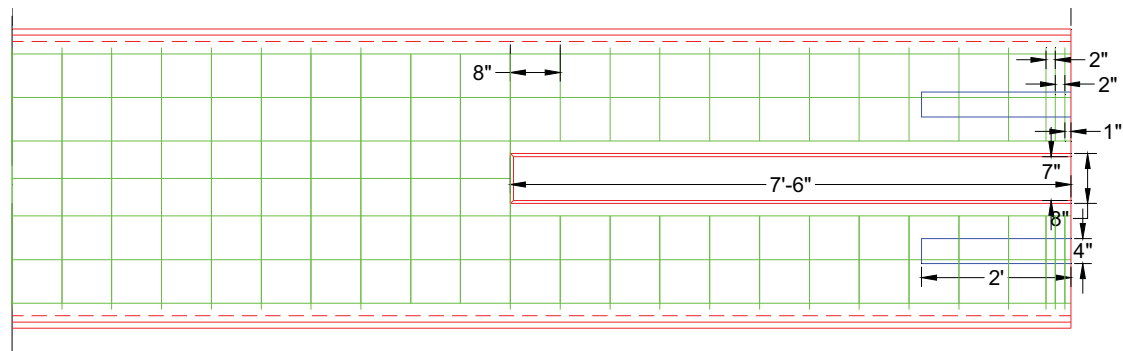


Figure 4.4: Plan and section views of the beam with shear key ledge and temporary steel angles



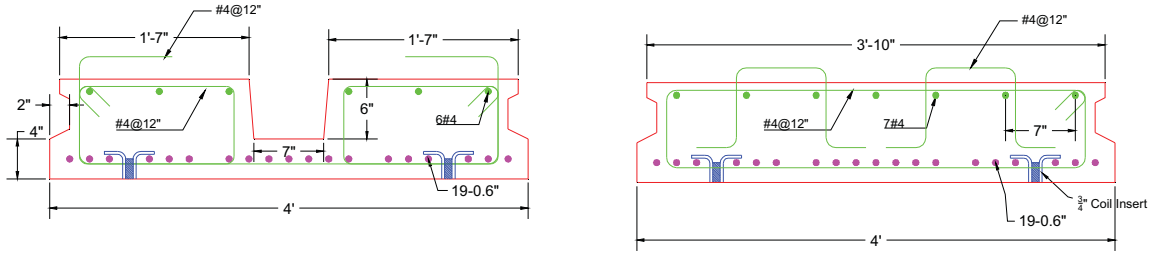
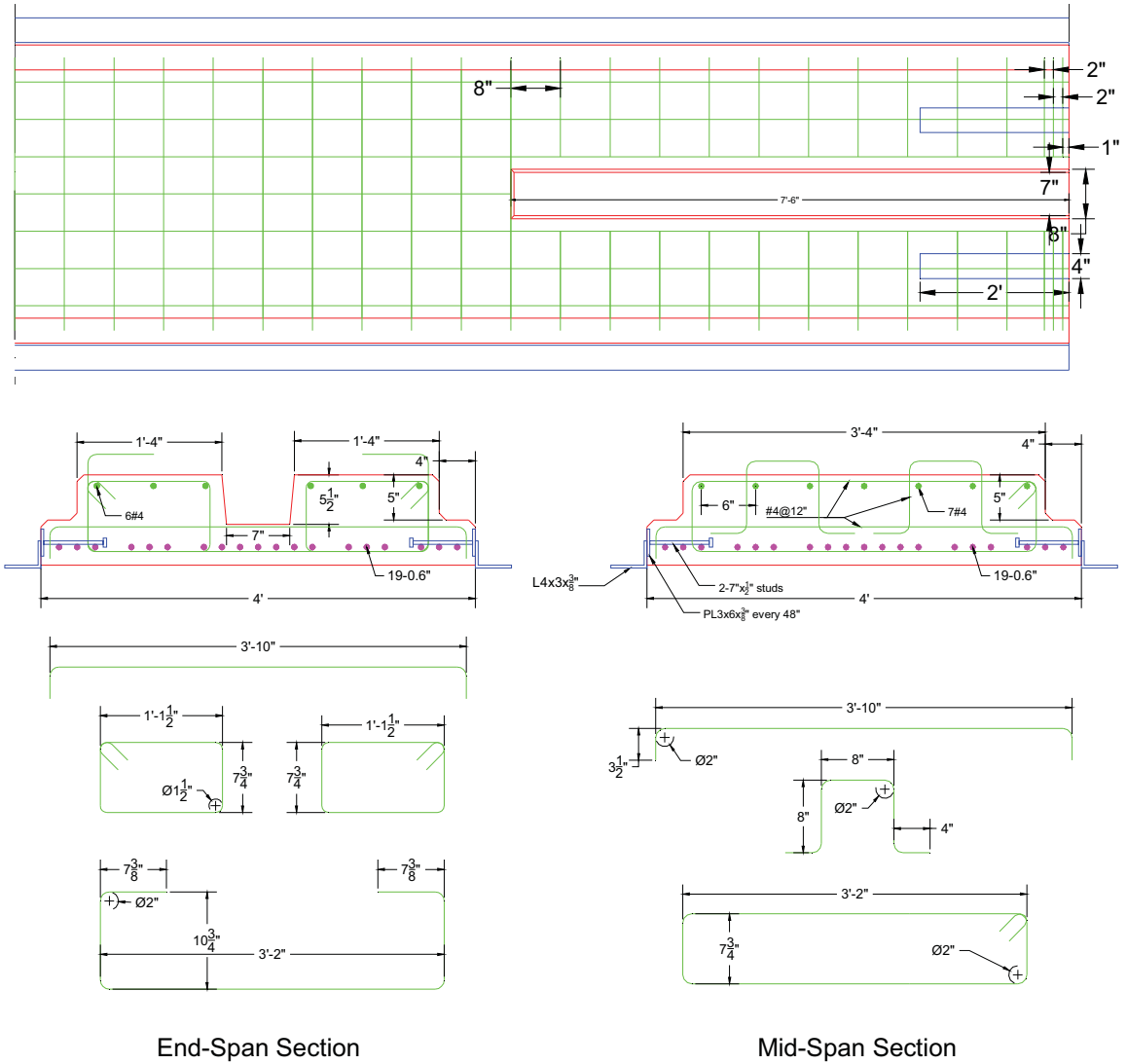


Figure 4.5: Plan and section views of the beam with shear key ledge and coil inserts



End-Span Section

Mid-Span Section

Figure 4.6: Plan and section views of the beam with ledge and temporary steel angles

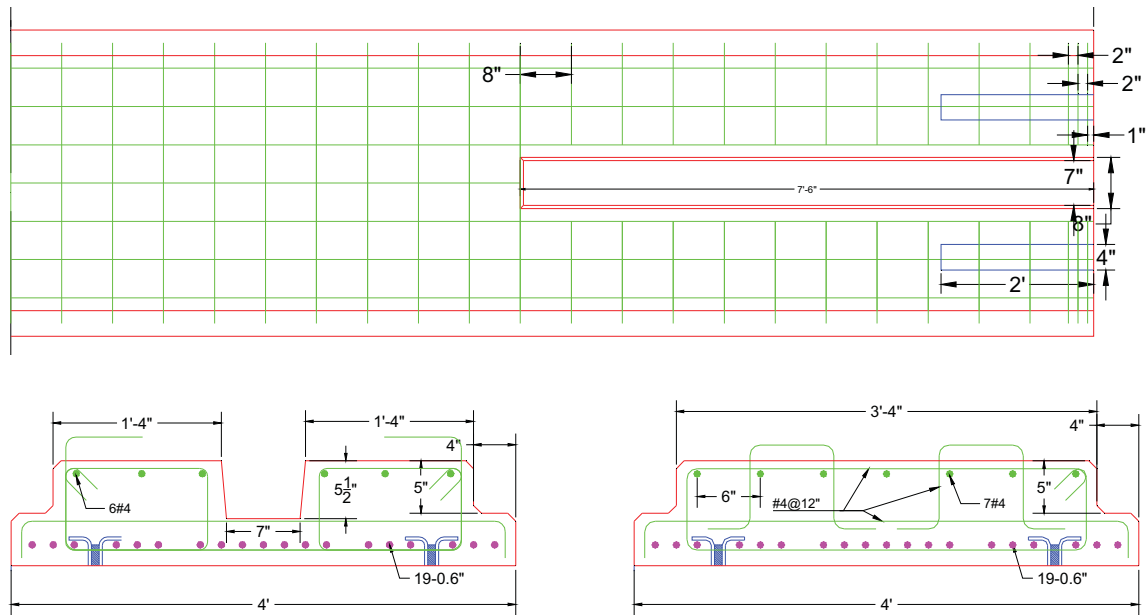


Figure 4.7: Plan and section views of the beam with ledge and coil inserts

C. Torsion Design

The torsion design of FS beam was carried out according PCI Design Handbook 6th Edition section 4.4 and ACI 318-08 section 11.5. The two sections were illustrated that torsion critical section of prestressed members was located at distance $h/2$ from the face of the support. The beam was used to support the HC blanks in construction stage, so the construction stage was considered the critical stage according to torsion design. The maximum torsion moment and torsion load were occurred due to placing the HC planks in one side of the beam. The design proves that #4@12 in. close stirrups are enough to resist the torsion.

4.2.1.3 Column Design

Design of columns for the proposed floor system is similar to the design of column for any conventional floor system. Columns should be designed to resist axial and bending moments according to Section 10.3 of ACI 318-08. Since the column of the proposed

system is continuous precast columns, stresses due to handling, shipping, and erection should be also checked according to Chapter 5 of the 6th edition of the PCI Design Handbook. In order to achieve the continuity of the flat soffit beams and eliminate the need for column corbels, each column has an embedded 18 in. long HSS 10x8x1/2" section and 1 in. recess from all sides at the location of each floor as shown in Figure 4.8. This opening allows the continuity of the beam top reinforcement for resisting the negative moment due to topping weight and live load. Also, when the column opening along with the shear keys on the column sides are filled with concrete they act as a hidden corbel to support the gravity loads of the floor.

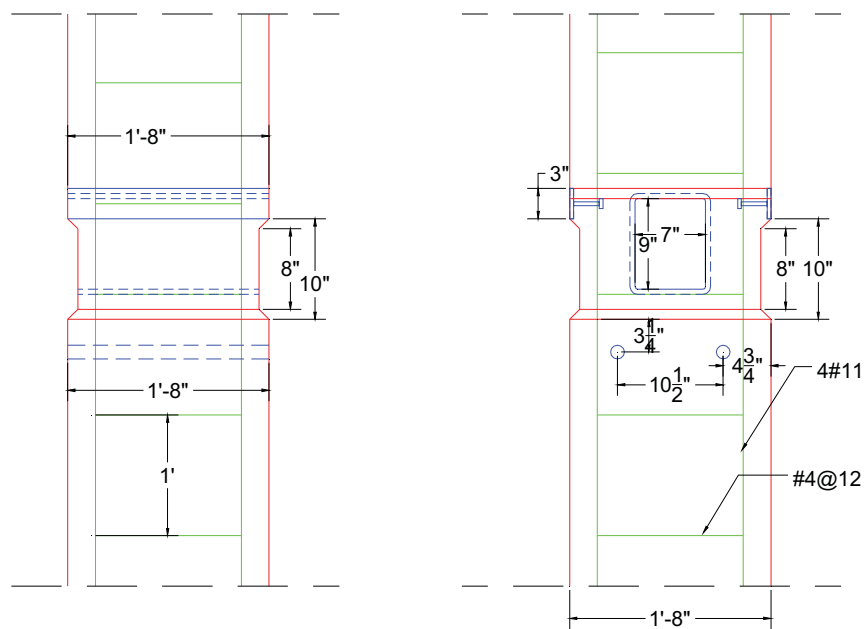


Figure 4.8: Dimensions and reinforcement details of the column at the floor level.

4.2.1.4 Design of Temporary and Hidden Corbels

Temporary Corbels

The design of the temporary corbels is carried out according to the shear-friction design method of ACI Section 11.6.4. Grade 150 threaded rods (TR) are used to attach the

temporary corbels to the two column sides through the holes shown in Figure 4.8. These rods will be tightened to the specified torque that creates a sufficient axial force to transfer the load to the column through friction. The coefficient of friction between the column and the steel temporary corbels is assumed to be 0.7 (ACI 11.6.4.3). Angles or channel sections can be used as temporary corbels along with stiffener plates to support

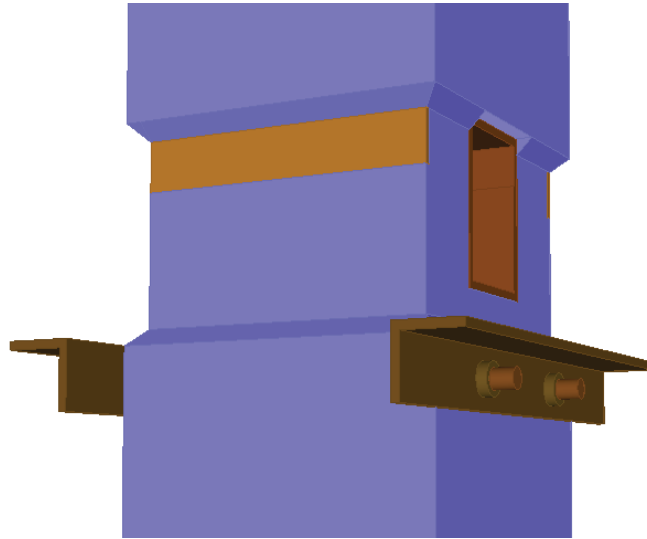


Figure 4.9: Isometric view shows friction bolts and the temporary corbel

Figure 4.10 shows the bearing flange against bending. Also, the size of the angle or channel section is determined so that the bearing flange is at least 4 in. wide and the web height can provide a contact area with the column so that the bearing stress on the concrete is not more than the smaller of 800 psi or $0.2f'_c$.

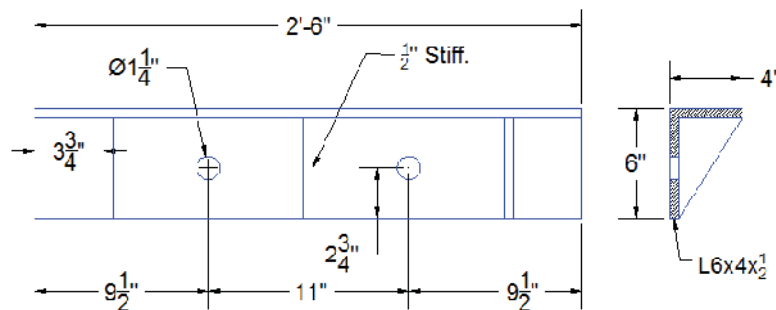


Figure 4.10: Stiffened angle used as a temporary corbel.

The following subsection presents the calculations performed to determine the required diameter of the TR, size angle or channel section, and thickness of stiffeners

Design of Temporary Corbels

Loads

$$h_c = 12 \cdot \text{in}$$

$$W_{\text{beam}} = 0.5 \cdot \frac{\text{kip}}{\text{ft}}$$

$$\text{Inter}_{\text{beam.span}} = 30 \cdot \text{ft}$$

$$\text{Exter}_{\text{beam.span}} = 28 \cdot \text{ft}$$

$$\text{HC}_{\text{weight.sq.ft}} = 0.08 \cdot \frac{\text{kip}}{\text{ft}^2}$$

$$\text{Aver}_{\text{gthickness.top}} = 2.5 \cdot \text{in}$$

$$\text{Span}_{\text{HC.direction}} = 30 \cdot \text{ft}$$

$$\text{Construction}_{\text{L.L}} := 0.015 \frac{\text{kip}}{\text{ft}^2}$$

$$V_{\text{D.from.beam}} := W_{\text{beam}} \cdot \frac{\text{Inter}_{\text{beam.span}}}{2} = 7.5 \cdot \text{kip}$$

$$V_{\text{D.from.HC}} := \text{HC}_{\text{weight.sq.ft}} \cdot L_{\text{HC}} \cdot \frac{\text{Inter}_{\text{beam.span}}}{2} = 29.25 \cdot \text{kip}$$

$$V_{\text{D.from.top}} := \text{Aver}_{\text{gthickness.top}} \cdot \gamma_c \cdot \text{HC}_{\text{span}} \cdot \frac{\text{Inter}_{\text{beam.span}}}{2} = 14.06 \cdot \text{kip}$$

$$V_{\text{Dead.per.corbel}} := V_{\text{D.from.beam}} + V_{\text{D.from.HC}} + V_{\text{D.from.top}} = 50.81 \cdot \text{kip}$$

$$V_{\text{live.per.corbel}} := \text{Construction}_{\text{L.L}} \cdot \text{HC}_{\text{span}} \cdot \frac{\text{Inter}_{\text{beam.span}}}{2} = 6.75 \cdot \text{kip}$$

$$V_{\text{U.per.corbel}} := 1.4 \cdot (V_{\text{Dead.per.corbel}} + V_{\text{live.per.corbel}}) = 80.59 \cdot \text{kip}$$

Resistance

$$A_{\text{net.TR}} := 0.85 \text{in}^2$$

$$\text{Diameter}_{\text{TR}} := 1 \text{in}$$

$$F_{\text{ccolumn}} := 8000 \text{psi}$$

$$\mu := 0.7$$

$$\text{Number}_{\text{TR}} := 2$$

$$\text{Column}_{\text{width}} = 20 \cdot \text{in}$$

$$\phi_{\text{sh}} = 0.75$$

$$f_{\text{uTR}} := 150 \text{ksi}$$

$$f_{yTR} := 120\text{ksi}$$

$$V_n := \mu \cdot \text{Number}_{TR} \cdot f_{yTR} \cdot A_{\text{net},TR} = 142.8 \cdot \text{kip}$$

$$\phi_{sh} \cdot V_n = 107.1 \cdot \text{kip}$$

$$\text{Min}_{\text{Angle.depth}} := \frac{V_{U,\text{per.corbel}}}{\phi_{sh} \cdot \text{Column}_{\text{width}} \cdot 0.2 \cdot F_{\text{ccolumn}}} = 3.36 \cdot \text{in}$$

Stiffener Design

Chosen Angle = L6*4*1/2

$$\text{Stiffner}_{\text{height.a}} := 5.5 \text{ in}$$

$$\text{Stiffner}_{\text{width.b}} := 3.5 \text{ in}$$

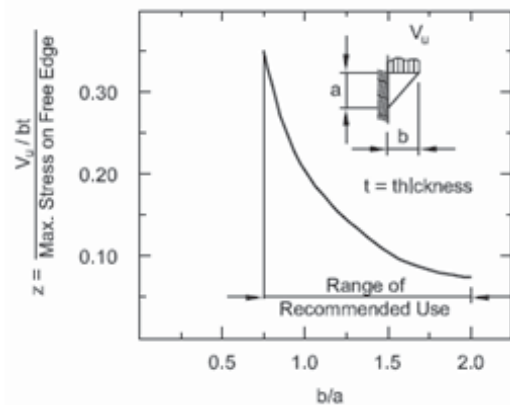
$$a := 5.5 \text{ in}$$

$$b := 3.5 \text{ in}$$

$$\frac{b}{a} = 0.64$$

$$f_{y,\text{stiff}} := 50\text{ksi}$$

$$t := \frac{V_{U,\text{per.corbel}}}{\phi_{SR} \cdot f_{y,\text{stiff}} \cdot b \cdot z} = 1.23 \cdot \text{in}$$



$$z := 0.44$$

$$\phi_{SR} := 0.85$$

Hidden Corbels

Eliminating the column corbel is considered one of the most important features of this research. In this study, the column corbel was replaced by hidden corbel. The shear friction theory was used to design the hidden corbel. Failure mechanisms of the beam-column connection had been studied. In order to understand the failure mechanism, the beam-column connection was drawn without any reinforcement as shown in Figure 4.11

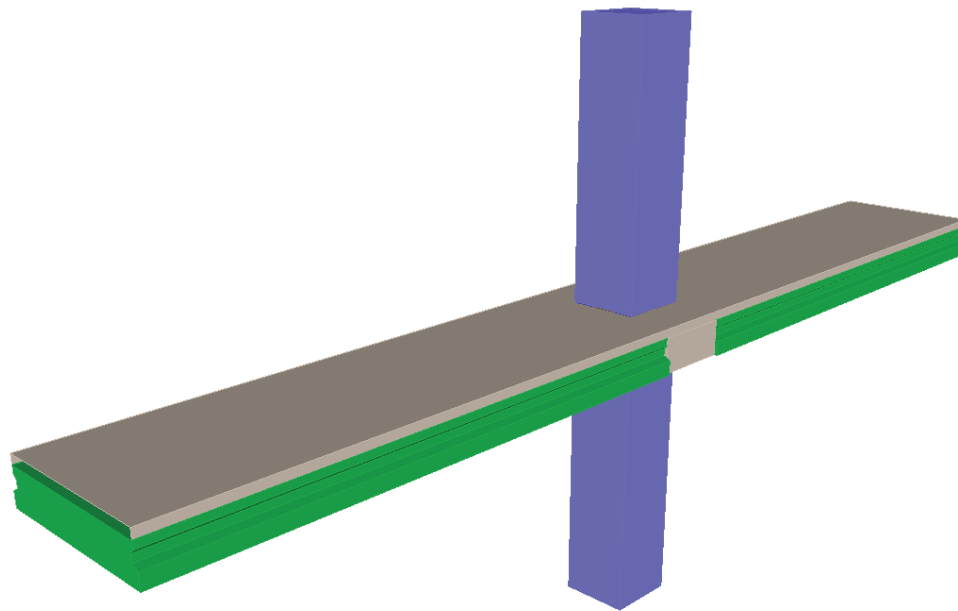
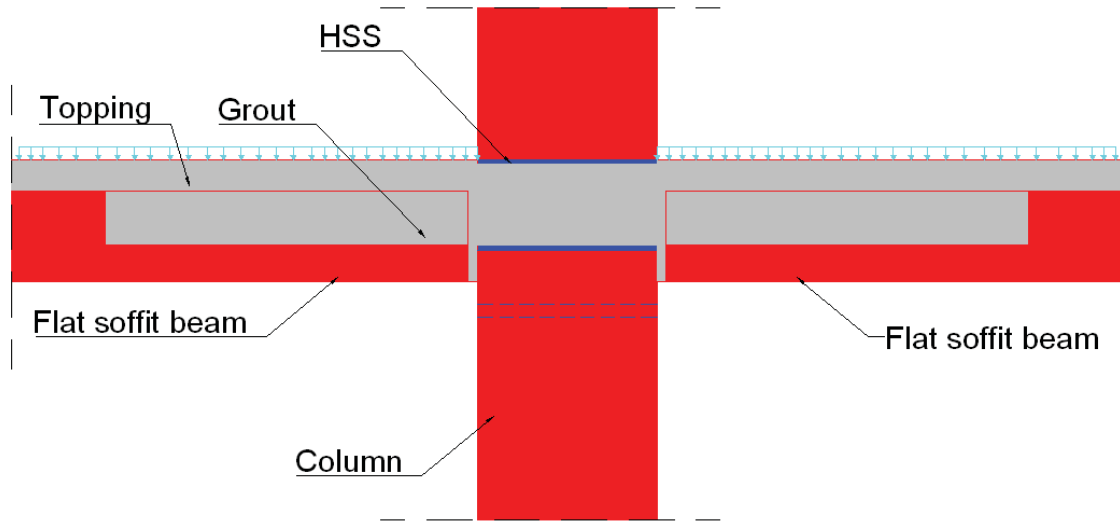
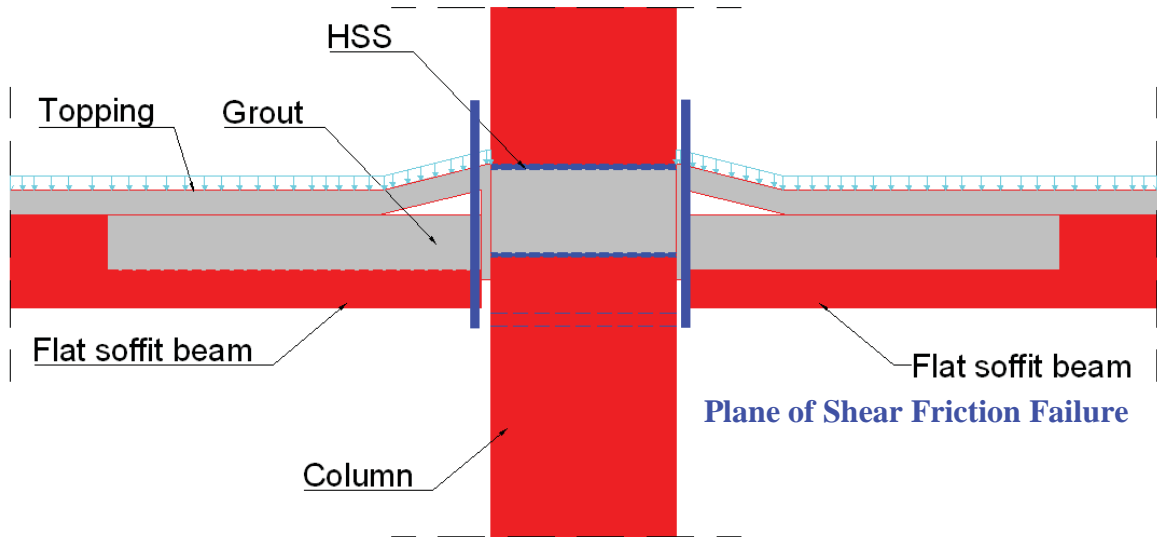
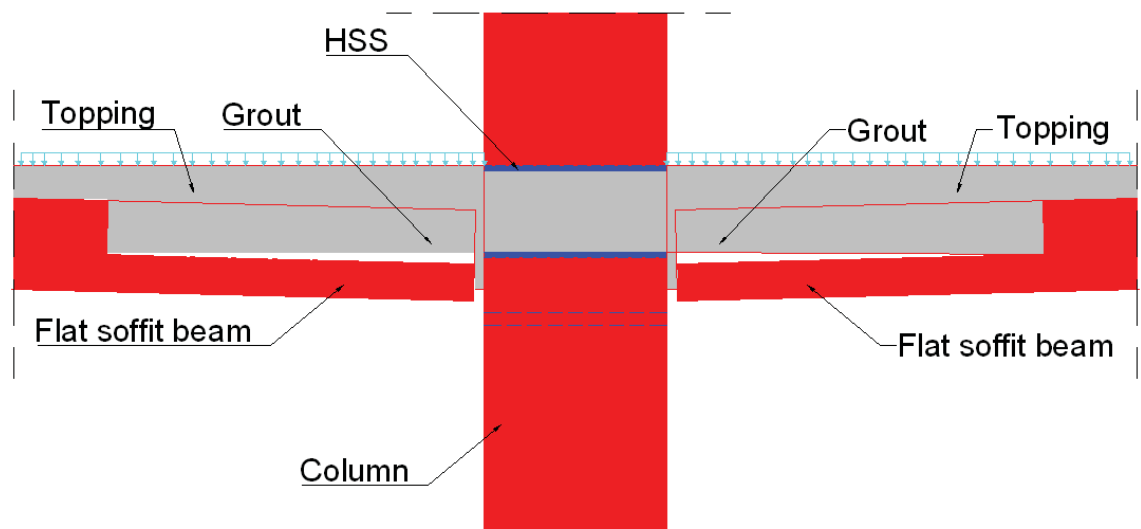


Figure 4.11: Beam-column connection without reinforcement

Figure 4.12 presents the failure mechanisms of the beam-column connection. It is clear that the first mechanism of failure occur due to the interface shear between the beam and the column as shown in Figure 4.12 (a). Figure 4.12 (b) shows the second mechanism of failure which occur losing the bond between the precast beam and the pocket grout



(a) Shear the interface between the beam and the column



(b) Bond failure in the interface between the beam pocket and the grout

Figure 4.12: Failure mechanisms of beam-column connection

Preventing the first failure mechanism was achieved in two stages:

- 1) Make 1 in. recess (shear key) in the four side of the column as shown in

Figure 4.13

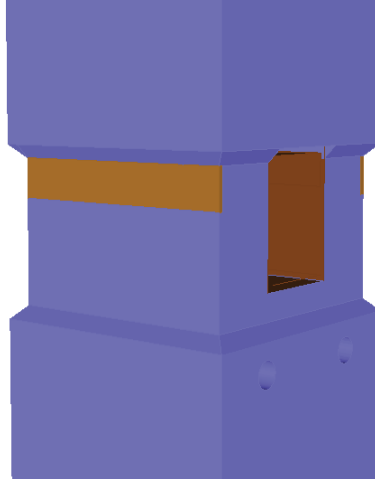
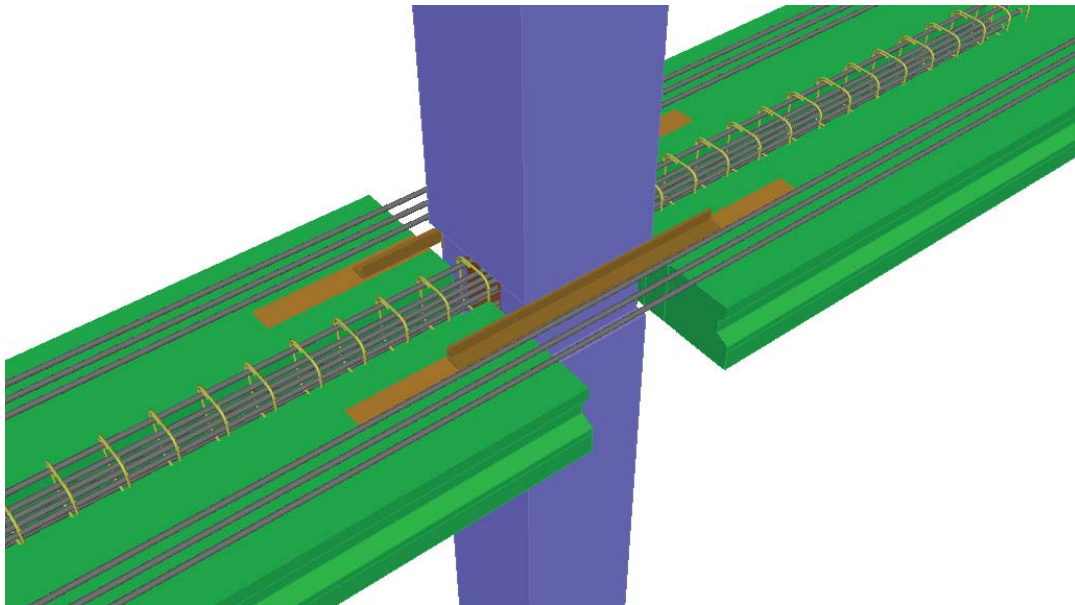


Figure 4.13: Recess in the four side of the column

- 2) Place grade 60 steel bars in beam pockets and through the column opening as shown in Figure 4.14



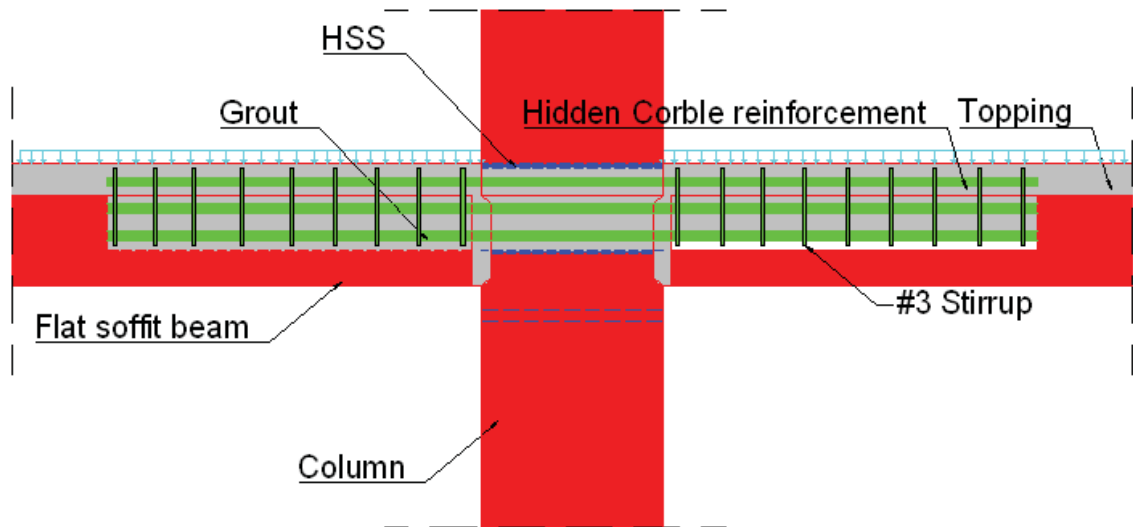


Figure 4.14: Hidden corbel reinforcement

Preventing the second failure mechanism was achieved by making the beam pocket surface roughened, in addition to making the beam composite with the topping by using steel shear connectors as shown in

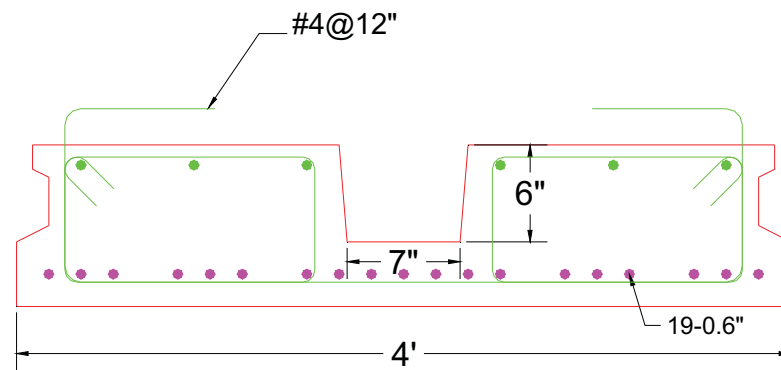


Figure 4.15: Cross section of the beam shows the shear connectors

The design of the hidden corbel is performed according to the shear-friction design method of ACI Section 11.6.4. Grade 60 reinforcing bars provide continuity of the flat soffit beam (i.e. 3#8 and 6#6) that act as shear-transfer reinforcement. According to ACI R11.6.7, no additional reinforcement is required unless the required shear-transfer reinforcement exceeds the provided amount. The coefficient of friction between the FS

beam and column is calculated as the weighted average of 1.4 for the area of hidden corbel (concrete placed monolithically) and 0.6 elsewhere (concrete placed against hardened concrete not intentionally roughened). These two coefficients were averaged based on the ratio of the surface area the monolithically placed concrete to the intentionally roughened hardened concrete. The following section presents factored applied load and factored resistance of the hidden corbel. Figure 4.16 shows the reinforcement details of beam-column connection. It should be noted that the effect of the two angles welded to column sides and the top of beams on the shear transfer is ignored.

Loads

$$h_c = 12 \cdot \text{in}$$

$$W_{\text{beam}} = 0.5 \cdot \frac{\text{kip}}{\text{ft}}$$

$$\text{Inter}_{\text{beam.span}} = 30 \cdot \text{ft}$$

$$HC_{\text{weight.sq.ft}} = 0.08 \cdot \frac{\text{kip}}{\text{ft}^2}$$

$$HC_{\text{span}} = 30 \cdot \text{ft}$$

$$L_L = 0.1 \cdot \frac{\text{kip}}{\text{ft}^2}$$

$$\text{Aver}_{\text{thickness.top}} = 2.5 \cdot \text{in}$$

$$V_{\text{Dead.beam}} := W_{\text{beam}} \cdot \text{Inter}_{\text{beam.span}} = 15 \cdot \text{kip}$$

$$V_{\text{Dead.HC}} := HC_{\text{weight.sq.ft}} \cdot \text{Inter}_{\text{beam.span}} \cdot L_{\text{HC}} = 58.5 \cdot \text{kip}$$

$$V_{\text{Dead.Top}} := \text{Aver}_{\text{thickness.top}} \cdot \gamma_c \cdot HC_{\text{span}} \cdot \text{Inter}_{\text{beam.span}} = 28.12 \cdot \text{kip}$$

$$V_{\text{Dead.Load}} := V_{\text{Dead.beam}} + V_{\text{Dead.HC}} + V_{\text{Dead.Top}} = 101.63 \cdot \text{kip}$$

$$V_{\text{Live.Load}} := L_L \cdot HC_{\text{span}} \cdot \text{Inter}_{\text{beam.span}} = 90 \cdot \text{kip}$$

$$V_U := 1.2 \cdot V_{\text{Dead.Load}} + 1.6 \cdot V_{\text{Live.Load}} = 265.95 \cdot \text{kip}$$

Resistance

$$\text{Area}_{\text{steel}} := 0.79\text{in}^2 \cdot 3 + 0.44\text{in}^2 \cdot 6 = 5.01 \cdot \text{in}^2 \quad f_{yb} = 60 \cdot \text{ksi}$$

$$\text{Depth}_{\text{hidden.corbel}} := 9\text{in} \quad \text{Width}_{\text{hidden.corbel}} := 7\text{in}$$

$$\text{Column}_{\text{width}} = 20 \cdot \text{in} \quad \text{Depth}_{\text{beam}} := 12\text{in}$$

$$\mu_{\text{pocket}} := 1.4 \cdot \frac{(\text{Depth}_{\text{hidden.corbel}} \cdot \text{Width}_{\text{hidden.corbel}})}{(\text{Column}_{\text{width}} \cdot \text{Depth}_{\text{beam}})} = 0.37$$

$$\mu_{\text{precast}} := \left[0.6 \cdot \frac{(\text{Column}_{\text{width}} \cdot \text{Depth}_{\text{beam}} - \text{Depth}_{\text{hidden.corbel}} \cdot \text{Width}_{\text{hidden.corbel}})}{(\text{Column}_{\text{width}} \cdot \text{Depth}_{\text{beam}})} \right]$$

$$\mu_{\text{precast}} = 0.44$$

$$\mu_{\text{avg}} := \mu_{\text{pocket}} + \mu_{\text{precast}} = 0.81 \quad f_{\text{ctop}} = 4 \times 10^3 \cdot \text{psi}$$

$$V_{n1} := (\text{Area}_{\text{steel}} \cdot f_{yb} \cdot \mu_{\text{avg}}) \cdot 2 = 486.97 \cdot \text{kip}$$

$$V_{n2} := (0.2 \cdot f_{\text{ctop}} \cdot \text{Column}_{\text{width}} \cdot \text{Depth}_{\text{beam}}) \cdot 2 = 384 \cdot \text{kip}$$

$$V_{n3} := (480 \cdot \text{psi} + 0.08 f_{\text{ctop}}) \cdot (\text{Column}_{\text{width}} \cdot \text{Depth}_{\text{beam}}) \cdot 2 = 384 \cdot \text{kip}$$

$$V_{n.\text{min}} := \begin{cases} V_{n2} & \text{if } V_{n2} \leq V_{n3} \\ V_{n3} & \text{otherwise} \end{cases}$$

$$V_{n.\text{min}} = 384 \cdot \text{kip}$$

$$V_{n.\text{final}} := \begin{cases} V_{n1} & \text{if } V_{n1} < V_{n.\text{min}} \\ V_{n.\text{min}} & \text{otherwise} \end{cases}$$

$$V_{n.\text{final}} = 384 \cdot \text{kip}$$

$$\phi_{sh} \cdot V_{n.\text{final}} = 288 \cdot \text{kip}$$

$$V_U = 265.95 \cdot \text{kip}$$

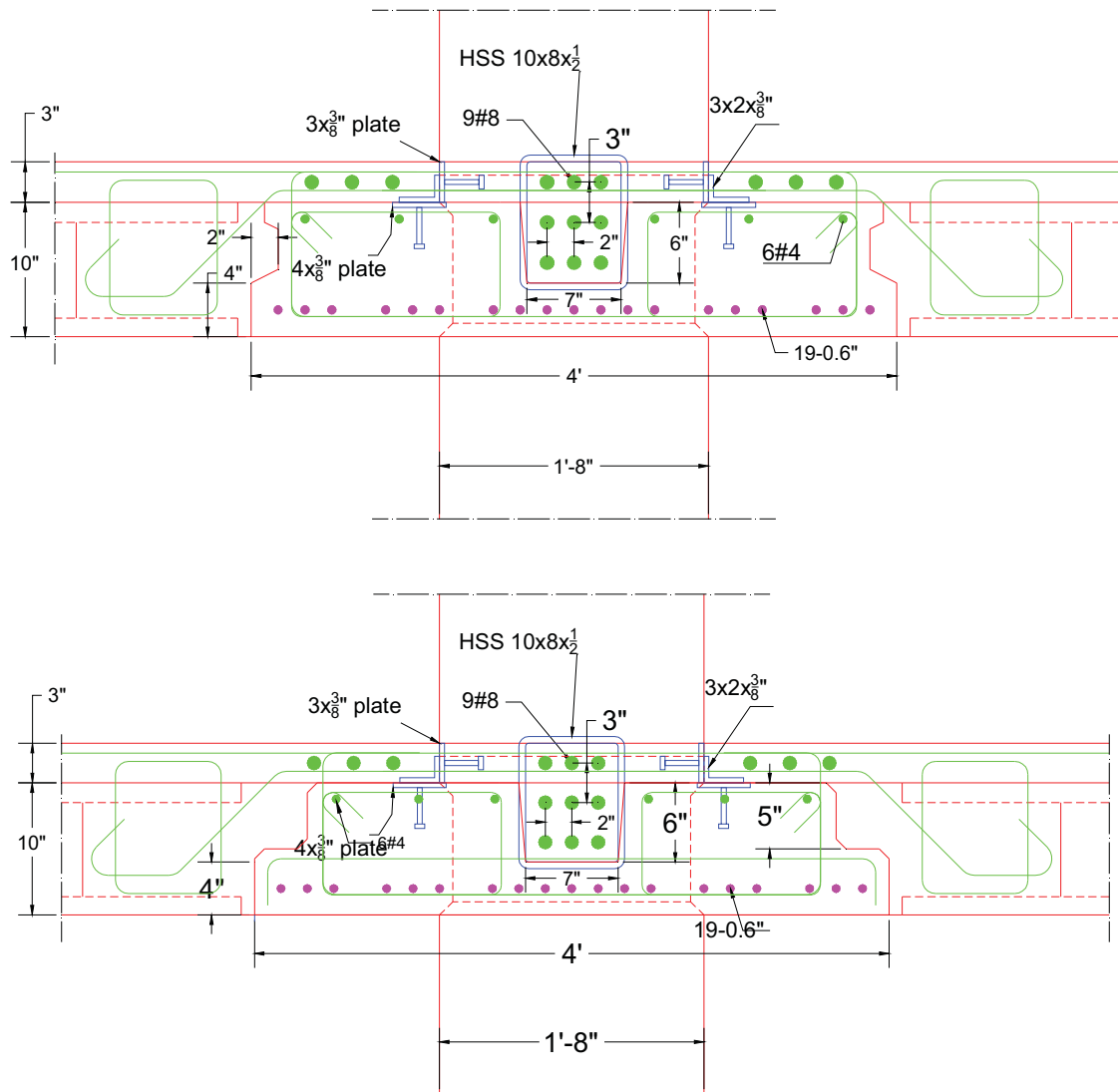


Figure 4.16: Beam-column connection

4.2.1.5 Design of Beam Hidden Ledges and Temporary Ledges

Eliminating the beam ledges is considered one of the most important features of this research. In this study, the beam ledges were replaced by hidden ledges. The shear friction theory was used to design the hidden ledge. Failure mechanisms of the HC-beam connection had been studied. In order to understand the failure mechanism, the HC-beam connection was drawn without any reinforcement as shown in Figure 4.17. Three common failure mechanisms in the HC-beam connection were shown in Figure 4.18.

The first failure mechanism was the collapse of the beam's shear key due to vertical shear load. After that failure, the HC will separate from the concrete topping as shown in Figure 4.18 (a). The second failure mechanism was the interface shear failure in the cast in place concrete between the HC and the beam. This failure will cause the separation of the HC from the Topping as shown in Figure 4.18 (b). The third failure mechanism was the collapse of the HC due to the incline shear plan as shown in Figure 4.18 (c).

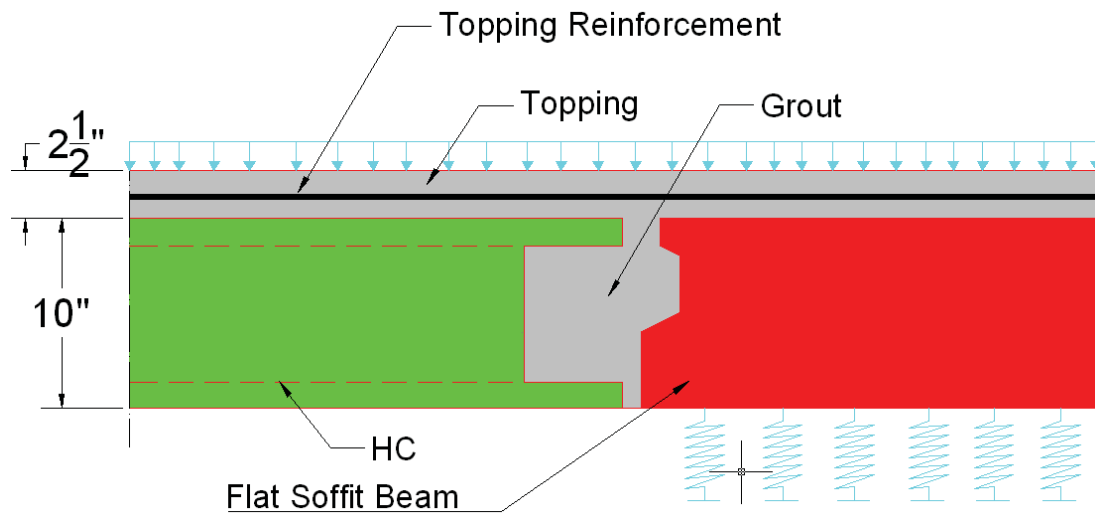
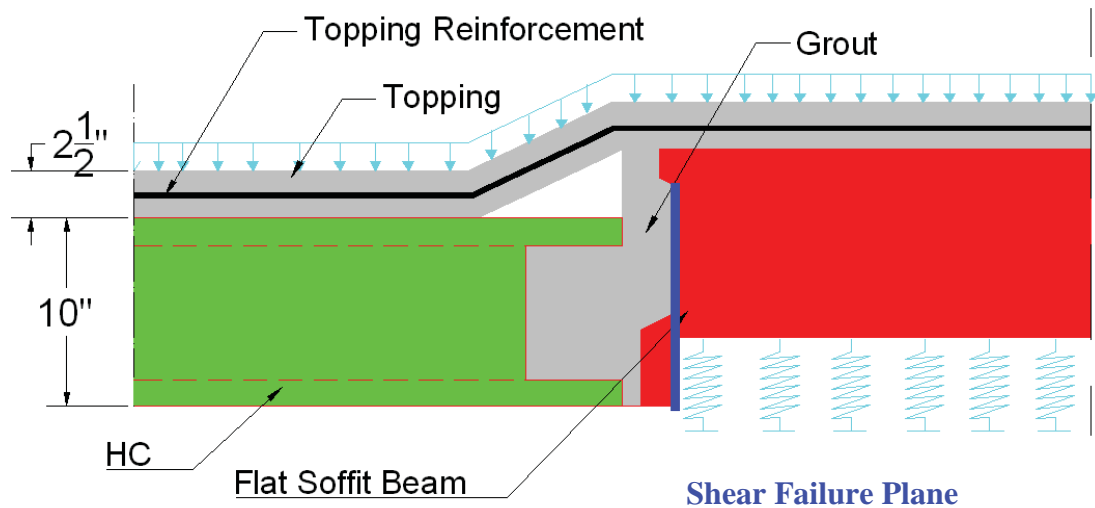
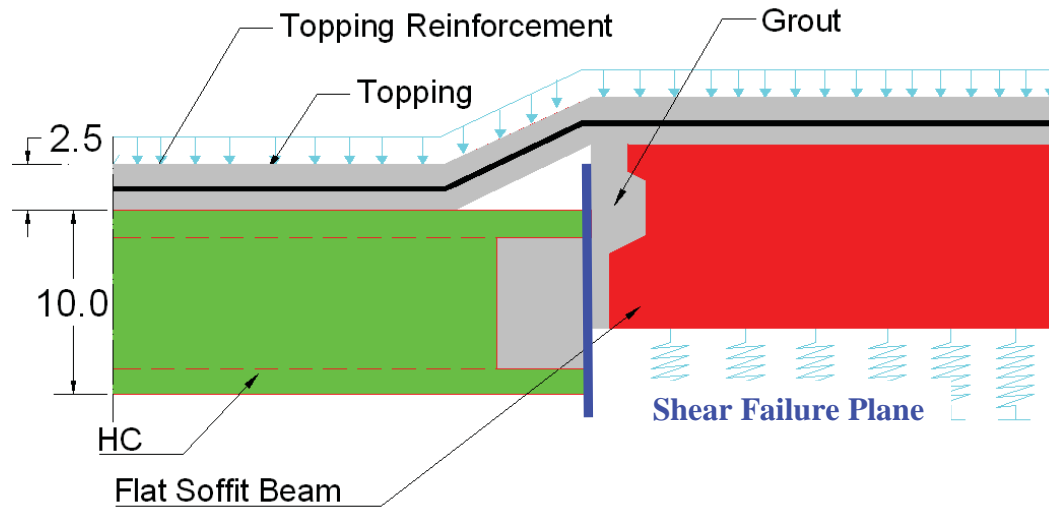


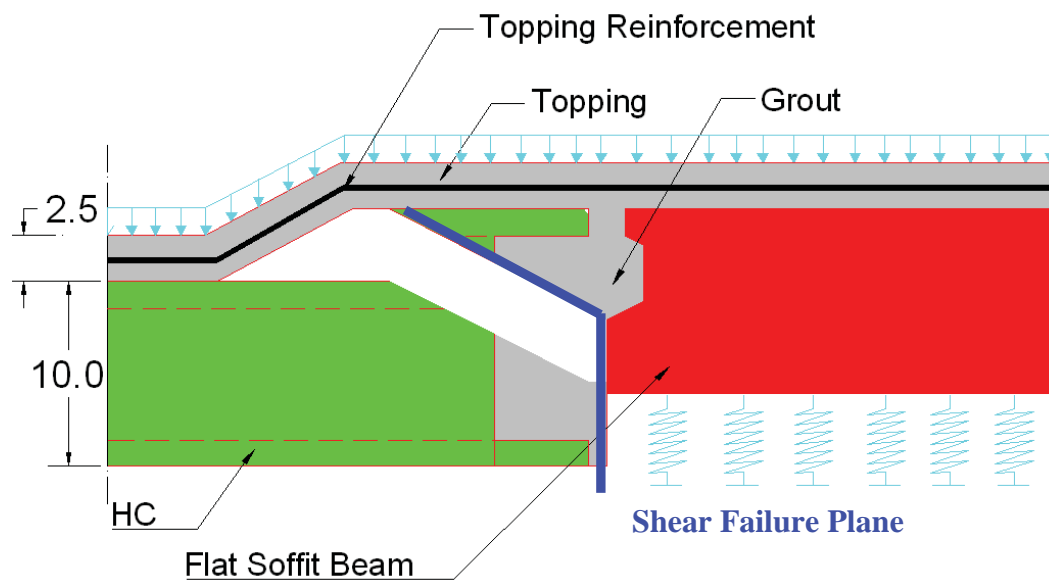
Figure 4.17: HC-beam connection without reinforcement



(a) Shear Failure in the beam shear key



(b) Shear Failure in cast-in-place concrete between the HC and the beam



(c) Shear Failure in the HC

Figure 4.18: HC-beam connection failure mechanisms

To prevent the collapse of beam shear key, the beam shear key was designed according to ACI-308 section 11.6.5. The nominal vertical shear shall not exceed the smallest of $0.2 F_c A_c$, $(480 + 0.08 F_c) A_c$, and $1600 A_c$, where A_c is the area of concrete section resisting shear transfer. According to the previous three equations, the beam shear key

To prevent any failure mechanism steel reinforcement was used in the connection. The connection reinforcement was bent with 45 degrees as shown in Figure 4.21. The reinforcement was bent to resist any vertical or incline shear plan. The following subsection presents how the shear friction theory used in the hidden ledge design.

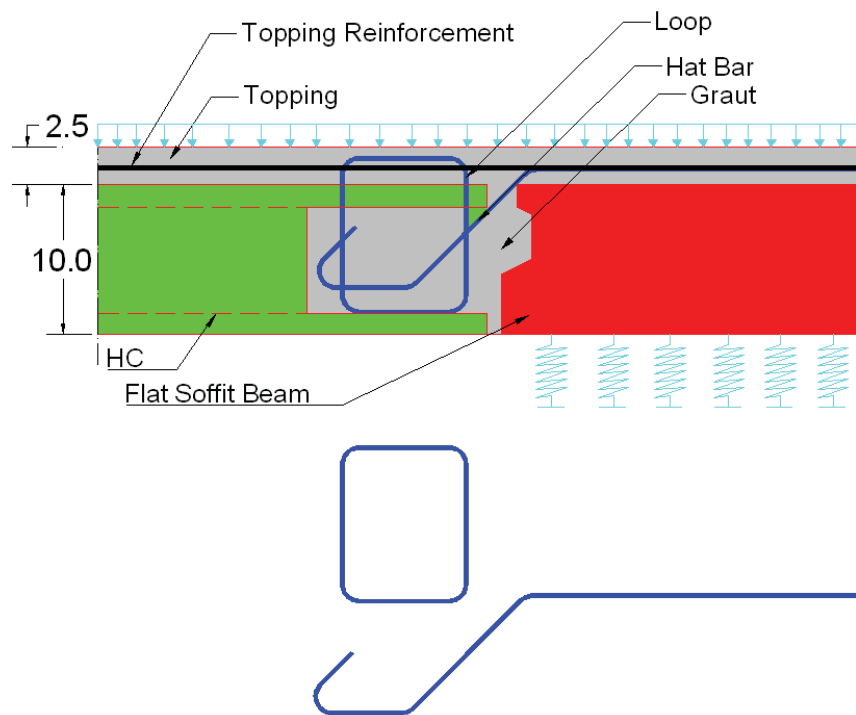


Figure 4.21: Shape of reinforcement using in the HC-beam connection

Hidden ledge design

The design of the beam-hidden ledge is performed according to the shear-friction design method of ACI 318-08 Section 11.6.4. Grade 60 reinforcing bars used to provide a support of the HC act as shear-transfer reinforcement. The coefficient of friction between the beam and HC is calculated as 1 (concrete placed against hardened concrete with surface intentionally roughened).

Loads

$$h_c = 12 \cdot \text{in}$$

$$W_{\text{beam}} = 0.5 \cdot \frac{\text{kip}}{\text{ft}}$$

$$\text{Inter}_{\text{beam.span}} = 30 \cdot \text{ft}$$

$$\text{HC}_{\text{weight.sq.ft}} = 0.08 \cdot \frac{\text{kip}}{\text{ft}^2}$$

$$\text{HC}_{\text{span}} = 30 \cdot \text{ft}$$

$$L_L = 0.1 \cdot \frac{\text{kip}}{\text{ft}^2}$$

$$\text{Aver}_{\text{thickness.top}} = 2.5 \cdot \text{in}$$

$$L_{\text{HC}} = 26 \text{ft}$$

$$V_{\text{Dead.HC.}} := \text{HC}_{\text{weight.sq.ft}} \cdot \frac{L_{\text{HC}}}{2} \cdot \text{HC}_{\text{width}} = 3.9 \cdot \text{kip} \quad \text{Per HC}$$

$$V_{\text{Dead.Top.}} := \text{Aver}_{\text{thickness.top}} \cdot c \cdot \frac{\text{HC}_{\text{span}}}{2} \cdot \text{HC}_{\text{width}} = 1.87 \cdot \text{kip}$$

$$V_{\text{Dead.Load.}} := V_{\text{Dead.HC.}} + V_{\text{Dead.Top.}} = 5.77 \cdot \text{kip}$$

$$V_{\text{Live.Load.}} := L_L \cdot \frac{\text{HC}_{\text{span}}}{2} \cdot \text{HC}_{\text{width}} = 6 \cdot \text{kip}$$

$$V_U := 1.2 \cdot V_{\text{Dead.Load.}} + 1.6 \cdot V_{\text{Live.Load.}} = 16.53 \cdot \text{kip}$$

Resistance

Use # 5 bars

Each Hc has 2.5 hat bars

$$A_{\text{bar}} := 0.31 \text{in}^2$$

$$\text{Area}_{\text{steel.}} := 2.5 \cdot A_{\text{bar}} = 0.78 \text{in}^2$$

$$f_{\text{yb}} = 60 \cdot \text{ksi}$$

$$\mu := 1$$

$$f_{\text{ctop}} = 4 \times 10^3 \cdot \text{psi}$$

$$V_{\text{n1.}} := (\text{Area}_{\text{steel.}} \cdot f_{\text{yb}} \cdot \mu) = 46.5 \cdot \text{kip}$$

$$\text{HC}_{\text{width}} = 4 \text{ft}$$

$$\text{Depth}_{\text{beam}} = 1 \text{ft}$$

$$V_{\text{n2.}} := (0.2 \cdot f_{\text{ctop}} \cdot \text{HC}_{\text{width}} \cdot \text{Depth}_{\text{beam}}) = 460.8 \cdot \text{kip}$$

$$V_{\text{n3.}} := (480 \text{psi} + 0.08 f_{\text{ctop}}) \cdot (\text{HC}_{\text{width}} \cdot \text{Depth}_{\text{beam}}) = 460.8 \cdot \text{kip}$$

$$V_{n.min.} := \begin{cases} V_{n2.} & \text{if } V_{n2.} \leq V_{n3.} \\ V_{n3.} & \text{otherwise} \end{cases}$$

$$V_{n.min.} = 460.8 \cdot \text{kip}$$

$$V_{n.final.} := \begin{cases} V_{n1.} & \text{if } V_{n1.} < V_{n.min.} \\ V_{n.min.} & \text{otherwise} \end{cases}$$

$$V_{n.final.} = 46.5 \cdot \text{kip}$$

$$\phi_{sh} \cdot V_{n.final.} = 34.88 \cdot \text{kip}$$

$$V_{U.} = 16.53 \cdot \text{kip}$$

From the calculation, it was clear that one HC-beam connection can carry 34.88 kips, which was 2.1 times the ultimate shear due to the dead and live loads. Figure 4.22 shows complete reinforcement details for HC-beam connection.

The design of temporary ledges is performed according to beam design of American institute of steel construction (AISC, 2008). It acts like a beam with double cantilever subjected to point load at the cantilevers ends. The point load was calculated from the self-weight of the HC, topping, and the construction load. The temporary ledge subjected to factored moment 3kip.ft approximately. Table 3-13 of AISC manual thirteenth edition illustrates that HSS4x4x1/8 section has enough capacity to carry that moment.

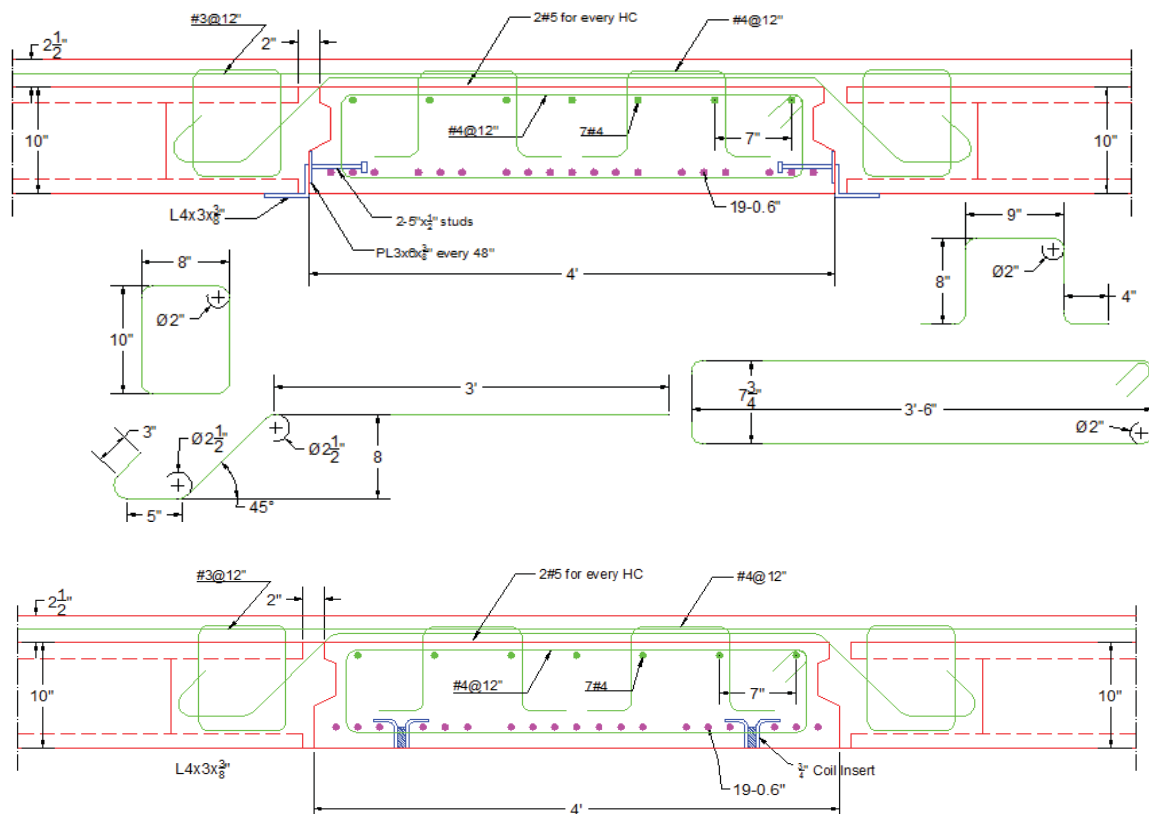


Figure 4.22: HC-beam connection

4.3 Flat Soffit Shallow Beam Design aids

Three standard flat soffit shallow (FS) beams are proposed to an example for the three HC thicknesses (8 in, 10 in, and 12 in) in order to cover a wide range of spans and loading conditions. Table 4.6 lists the properties of the standard FS beams (beam with shear key). Figure 4.3 shows the dimensions of FS beam sections.

Table 4.6: Properties of standard FS beams

Flat Soffit System	Depth (in)	Width (in)	Area (in ²)	Weight (kip/ft)	Y _b (in)	Y _t (in)	I (in ⁴)	HC Thickness (in)	Weight _{H.C.} (psf)
FS8	8	48	384	0.40	4	4	2,048	8	64
FS10	10	48	480	0.50	5	5	4,000	10	72
FS12	12	48	576	0.60	6	6	6,912	12	80

The following charts present the design for three standard flat soffit beam (FS). The vertical axis in the chart presents the value of the live load (psf) and the horizontal axis presents the span of the beam. Every chart has four curves, which defined the HC span direction. All the charts were developed by changing the negative reinforcement, while the positive reinforcement (19-06 in. strand) remaining constant. The design curves for FS 8 were shown in Figure 4.23, Figure 4.24, and Figure 4.25. Figure 4.26, Figure 4.27, and Figure 4.28 show the design charts of FS 10, while Figure 4.29, Figure 4.30, and Figure 4.31 show the design charts of FS 12

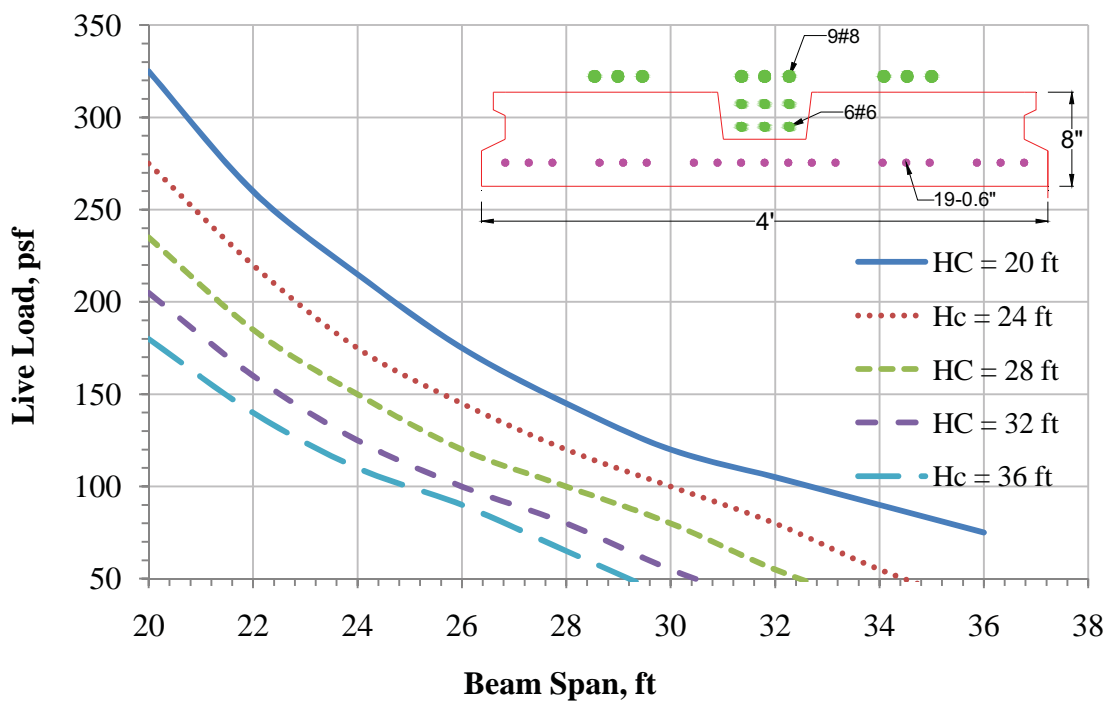


Figure 4.23: Design chart for FS 8 (9#8 and 6#6 negative reinforcement)

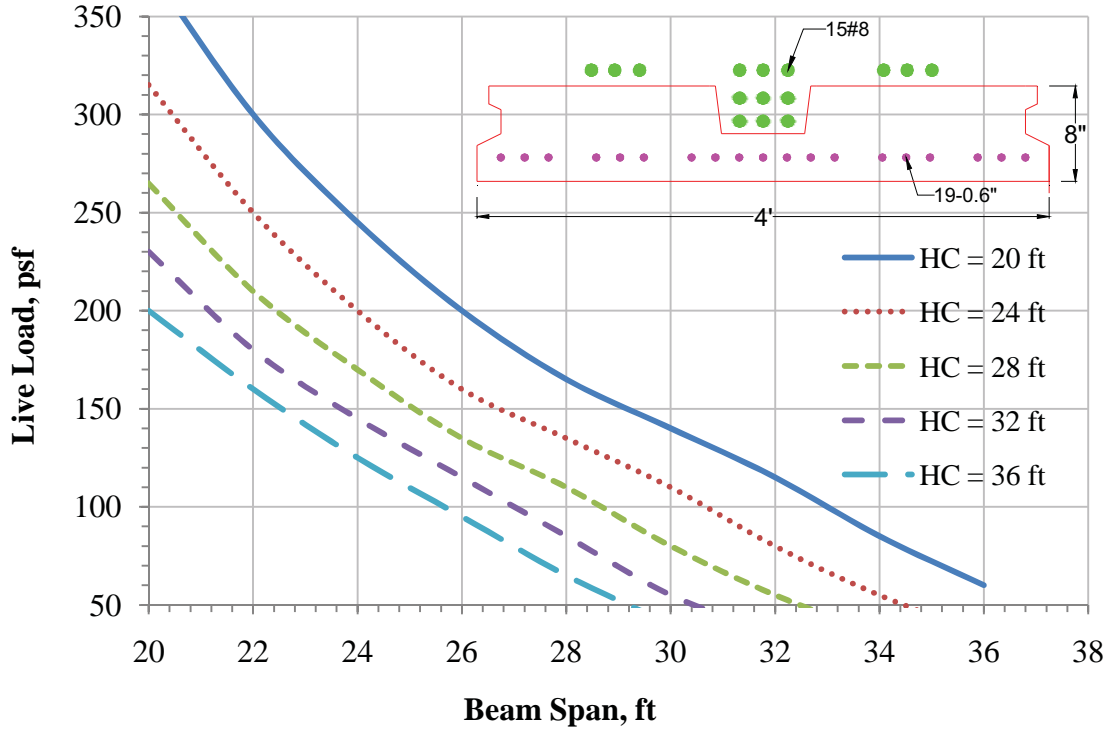


Figure 4.24: Design chart for FS 8 (15#8 negative reinforcement)

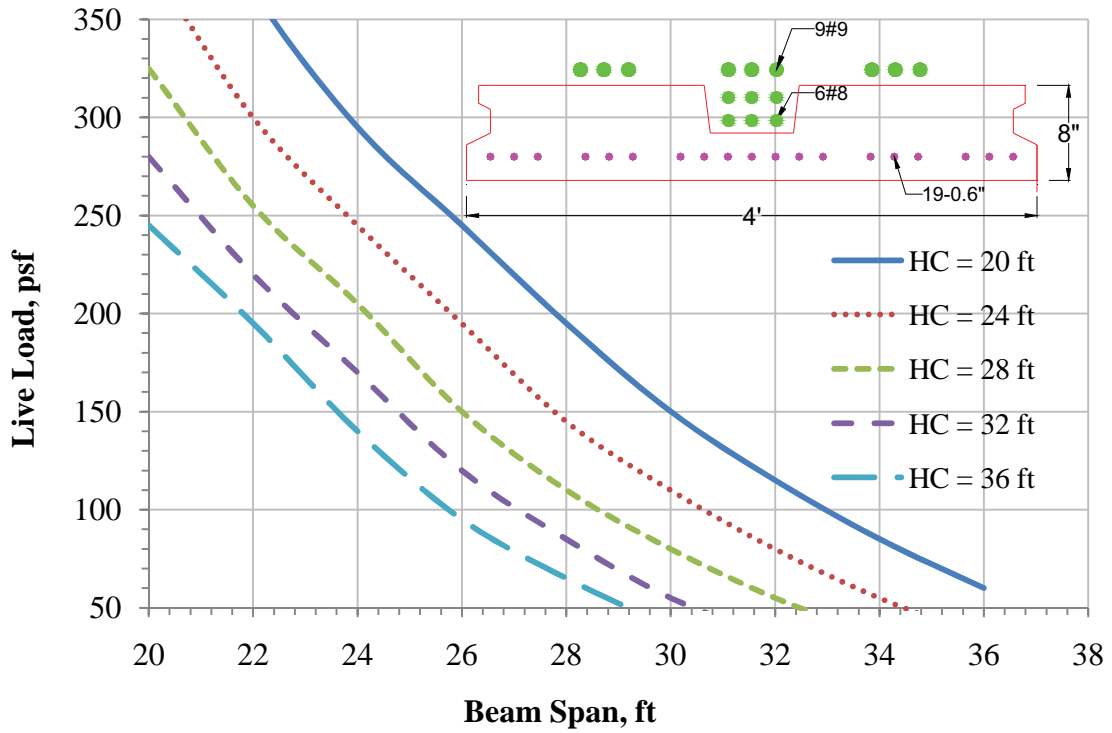


Figure 4.25: Design chart for FS 8 (9#9 and 6#8 negative reinforcement)

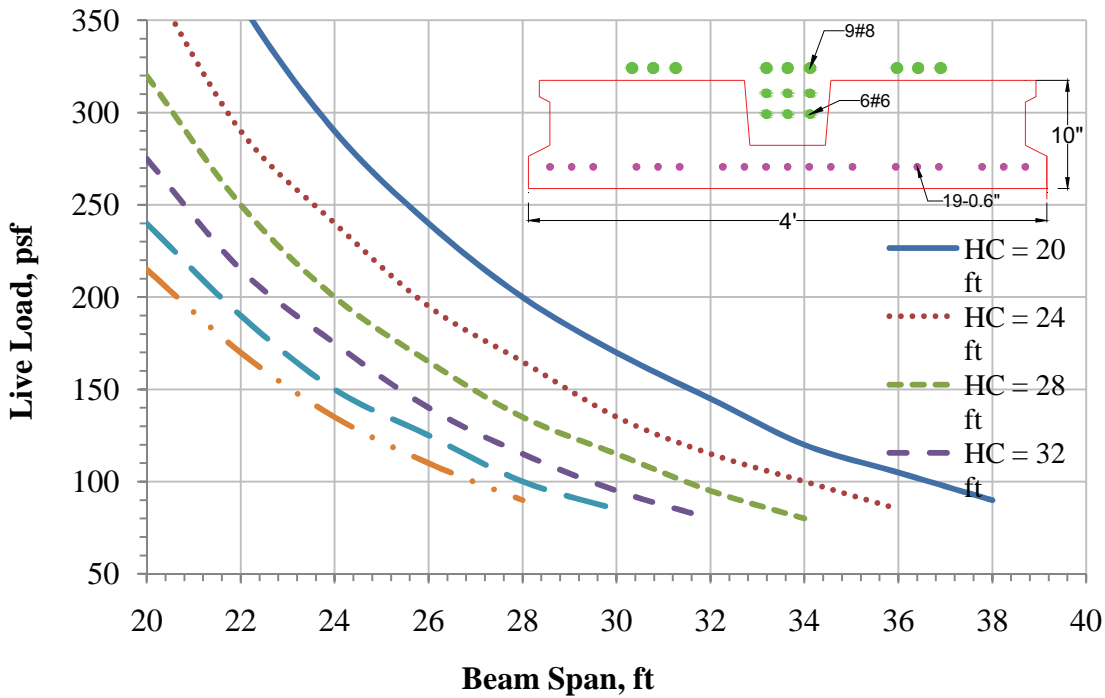


Figure 4.26: Design chart for FS 10 (9#8 and 6#6 negative reinforcement)

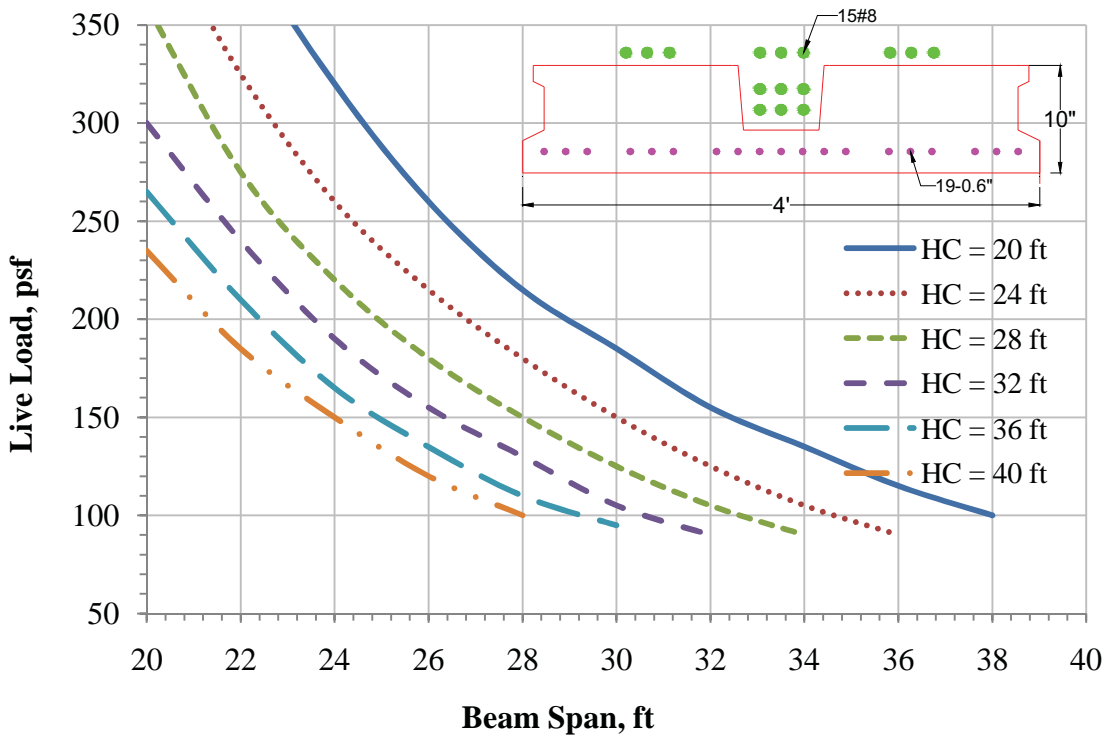


Figure 4.27: Design chart for FS 10 (15#8 negative reinforcement)

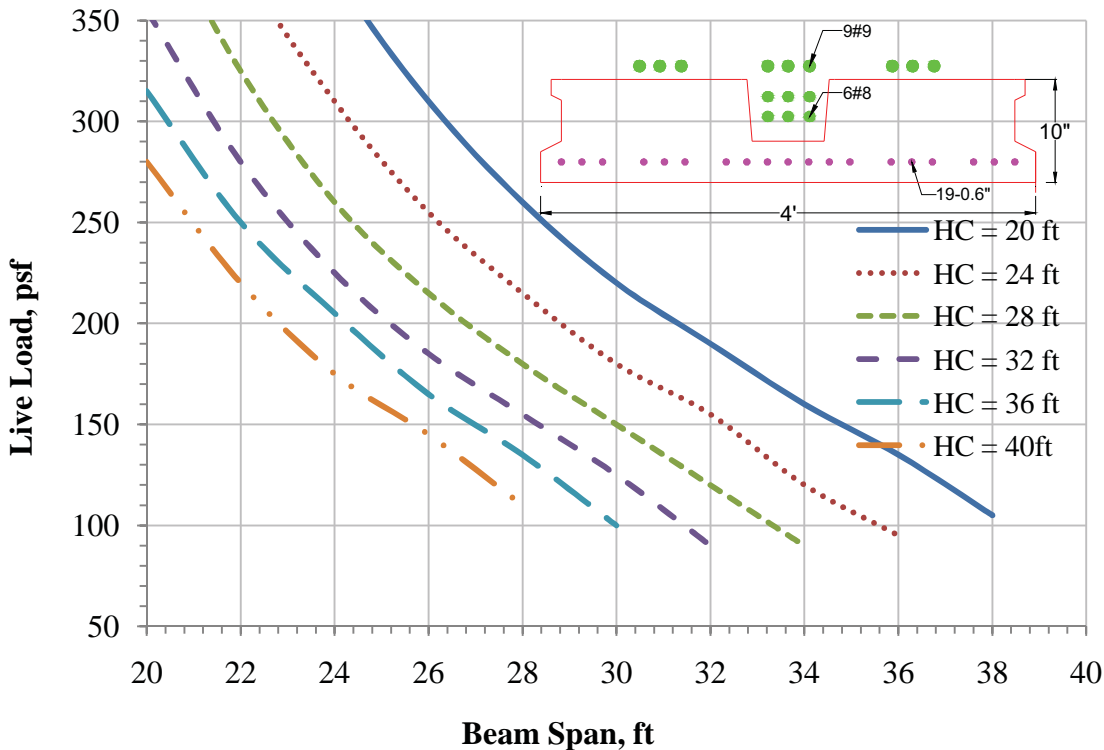


Figure 4.28: Design chart for FS 10 (9#9 and 6#8 negative reinforcement)

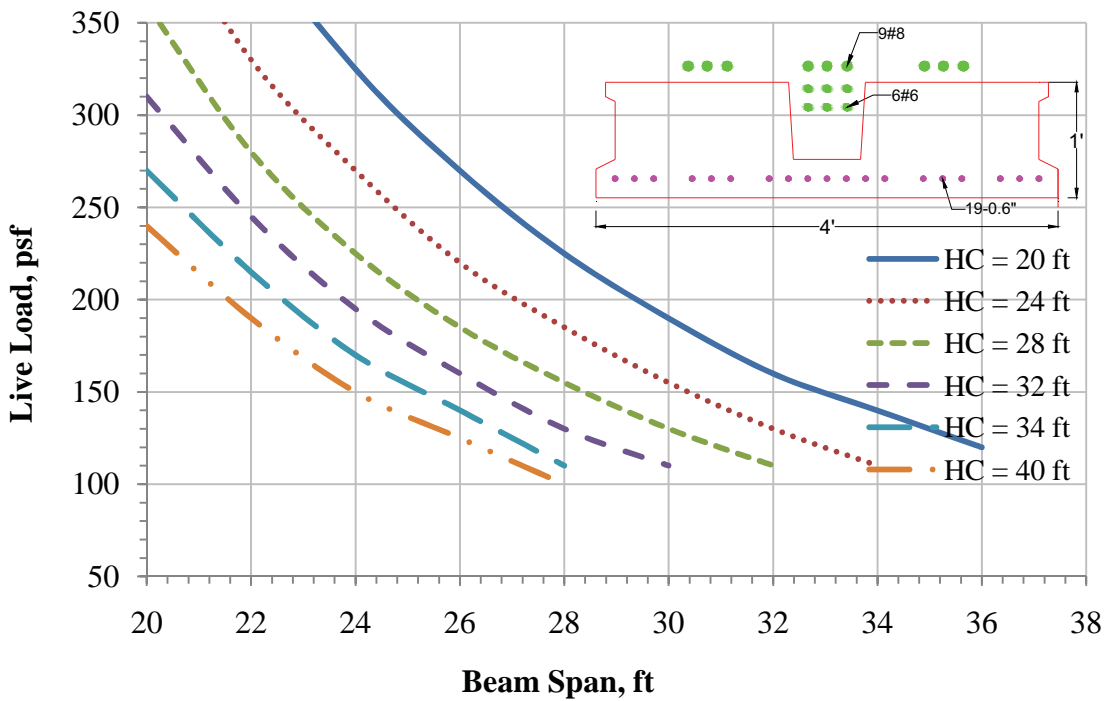


Figure 4.29: Design chart for FS 12 (9#8 and 6#6 negative reinforcement)

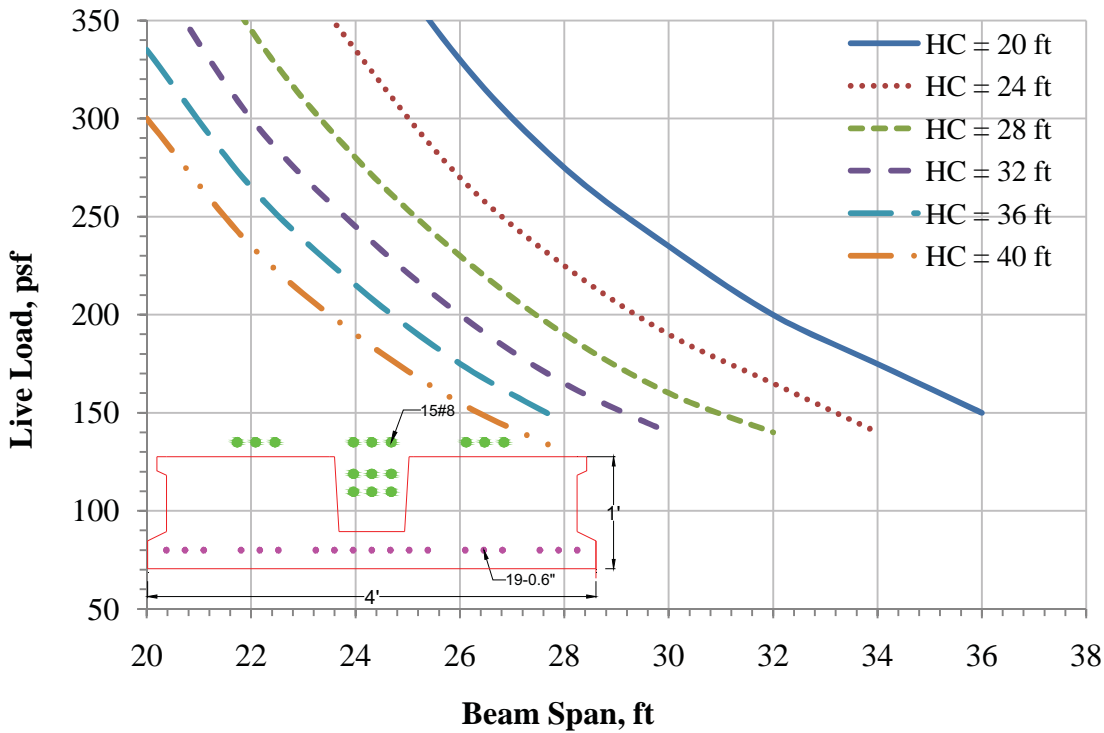


Figure 4.30: Design chart for FS 12 (15#8 negative reinforcement)

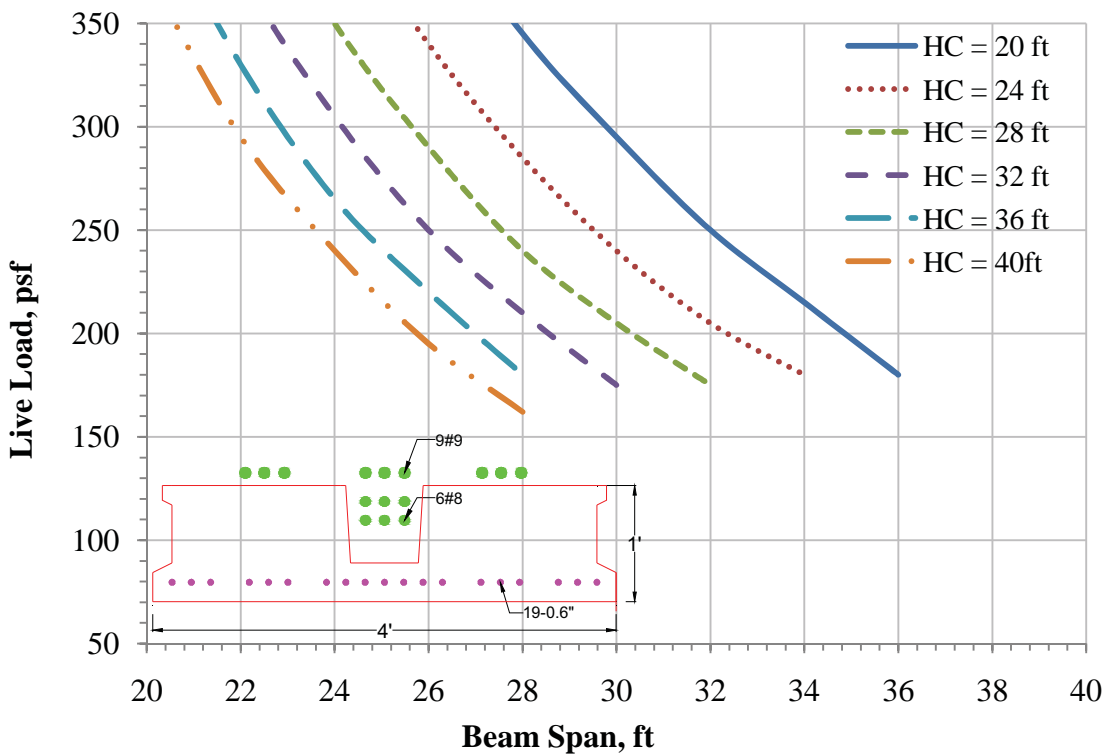


Figure 4.31: Design chart for FS 12 (9#9 and 6#8 negative reinforcement)

4.4 Constructability, Cost, and Schedule Analysis

This section compares the constructability, cost and schedule of the proposed system with a typical precast floor system. The cost and schedule analysis refers to a single 120 ft x 120 ft elevated floor slab (16 bays each bay 30 ft x 30 ft).

A. Constructability Analysis

The flat soffit precast floor system appears to have no major constructability issues. The temporary corbels are easy to install, as are the temporary beam ledges, rolling scaffold provides easy access to both. Welding the two angles to the beam end plates and column side plates take slightly longer than welding a typical inverted T beam to the column but requires no exceptional skill or equipment. Placing the beams and the HC planks are no more and no less complex than standard precast floor systems. Placing continuity reinforcement while not complex, are additional steps required for the shallow flat soffit precast floor system that requires more steel reinforcement. The grouting operation is comparable to other precast floor systems with the exception of the need for slightly more grout for the beam pocket and column opening. Placing the welded wire fabric and the concrete topping are identical operations for both the shallow flat soffit precast floor system and the typical precast floor system. Removing the temporary supports at the column and the hollow core planks is a simple, albeit additional operation.

Cost Analysis

Table 4.7 shows a cost analysis comparing the flat soffit precast floor system to a typical precast floor system. All cost data was developed using RSMeans Building Construction Cost Data 2011 unless specified otherwise. For clarity, the estimate line items in this

section coincide with the construction steps described in the proposed system section of this dissertation.

There are 25 precast concrete columns on each floor. Since the depth of the inverted-tee beams in the typical precast system are 28 in. compared to 10 in. in the flat soffit precast floor system, the typical precast columns are 12.5 ft per floor compared to 11 ft per floor for the shallow flat soffit precast floor system to provide 10 ft equivalent clearance. Columns are assumed approximately equivalent except for length since the shallow flat soffit precast floor column includes a recessed area, steel tube and bolt sleeves as compared to two heavily reinforced corbels.

Temporary corbels are attached to each shallow flat soffit precast floor system column. Installation productivity is listed at five per hour with two structural steel workers and two rolling scaffold while removal rates are estimated at 10 per hour. This is based on actual field measurements from two full-scale installations. The angles are 6 in. x 4 in. x 0.5 in. and are 2 ft long with a weight of 16 pounds per lineal foot). There are 40 reusable angles per floor at a cost of \$32 each, which results in material cost of \$1,280. Two, 1 in. diameter and 2 ft long all thread rods fasten the angles to the columns through 1-1/16 in. diameter holes precast into the 25 column. The cost for 50 rods is \$650 for a total material cost including angles of \$1,930. Assuming a reuse rate of six give a total material cost of \$322 per floor.

Twenty beams are installed in either system and installation costs are similar because of the similar weights between the two systems (RSMeans Building Construction Cost Data 2011, section (03 41 05.10 1400) There are eight spandrel beams that are the same for either system since they are concealed within the exterior wall. The cost of the eight-

spandrel beams is \$3,425 each. The beam material costs for the flat soffit beam system and the inverted-tee were priced from the manufacturer at \$150 and \$120 per lineal foot, respectively. Inserts are cast into the beam for field installation of the temporary plank supports.

Installation of the temporary plank supports is estimated at 20 supports per hour with two structural steel workers and two rolling scaffold while removal rates are estimated also at 20 per hour. This is based on measurements from full-scale field installation. The 5 ft long temporary supports are 4 in. x 4 in. x 0.125 in. tubes that weigh 12 pounds per lineal foot. There are 4 supports per plank and 120 planks. Each support is estimated to cost \$50 plus \$5 for bolt and washer resulting in total material cost of \$18,000. With six reuses, material cost per use is \$3,000 per floor.

Continuity reinforcement is only required with the flat soffit precast floor system. There are two layers as indicated in the construction sequence. There is 3.1 tons of reinforcement required in the first layer and 8.2 tons in the second.

There are 16 bays, 30 ft x 30 ft that require approximately 4 yd³ of grout for each bay regardless of operation. The flat soffit floor system requires an additional 0.5 yd³ per column to fill the beam and column pocket.

Welded wire fabric is identical for both operations as is the concrete topping. There was 15,840 ft² of welded wire fabric and 14,400 ft² of 2.5 in. concrete topping.

Schedule Analysis

The schedule results are shown in the Table 4.8. Durations were determined from the

Table 4.7: A Cost (\$US) Comparison between shallow flat soffit and typical precast floor systems per floor

Item	Shallow Flat Soffit Floor System				Typical Precast Floor System			
	Materials	Labour	Equipment	Total	Materials	Labour	Equipment	Total
Column	29,150	7,838	4,373	41,361	33,125	8,906	4,969	47,000
Temporary Corbel	322	777	160	1,259				
Beam placement	111,901	4004	2226	118,131	95,360	4,004	2,226	101,590
-angles vs. corbels ^a	750	305	122	1177		777	312	1089
HC Supports	3000	1457	300	4,757				
HC Plank Install	93,600	11,856	6,614	112,070	103,500	13,110	7,314	123,924
Continuity Reinf.	2,961	1,659	0	4,620				
Grout	7,725	1,260	420	9,405	5,974	974	325	7,273
2 nd Continuity Reinf.	6,642	3,526	0	10,168				
WWF Installation	2,995	3,960	0	6,955	2,995	4,514	0	6,954
Concrete Topping	12,240	11,376	4,032	27,648	12,240	11,376	4,032	27,648
Remove Supports		1846	380	2,226				
Total cost				339,777				315,478
Cost per square foot				\$23.6				\$21.9

^aThere are two corbel welds per column approximately 6 in. (15.24 cm) long in the overhead position from a scaffold vs. the two 36 in. (0.91 m) long angle welds in the horizontal position from the deck. It was determined that it would take approximately 15 minutes per column for the former and twice as long per column for the later at \$58.05/hour for welder and equipment.

daily output from RSMMeans. One crew was assumed for each activity in order to develop a consistent comparison. Other durations were taken from the estimated productivity

described in the previous section. Since the focus of this analysis is on the difference between shallow flat soffit precast floor system and a typical precast operation, it was determined unnecessary to incorporate factors like learning curve, mobilization, equipment delays, weather, etc. since these would have a similar effect on either floor system.

Table 4.8: A schedule comparison between shallow flat soffit and a typical precast flooring system

Item	Proposed System Days	Typical Precast Floor System Days
Step 1-Column	2.3	2.6
-Temporary Corbel	1.0	N/A
Step 2-Beam placement	1.4	1.6
-Weld angles	1.6	1
Step 3-Temporary HC Supports	1.9	N/A
Step 4-HC Plank Installation	3.5	3.8
Step 5-Continuity Reinf.	1.1	N/A
Step 6-Grout	0.5	0.4
Step 7-2 nd Continuity Reinf.	2.3	N/A
Step 8-WWF Installation	5.1	5.1
Step 9-Concrete Topping	5.4	5.4
Step 10-Remove Supports	2.4	N/A
Total durations in days	28.5	20

Chapter 5

DESIGN OF FLAT SOFFIT FLOOR SYSTEM UNDER LATERAL LOAD

5.1 Introduction

Lateral loads considered in the analysis of the proposed flat shallow floor system include the wind and seismic loads calculated according to ASCE 7-05. These loads were applied to the 75 ft high (six-story) marked frames in Figure 5.1 for both beam and hollow core directions. Two Dimensional frame analysis was performed using Structural Analysis Program (Computers and Structures, Inc. (2000)) to determine the maximum moments due to wind and seismic loading in each direction.

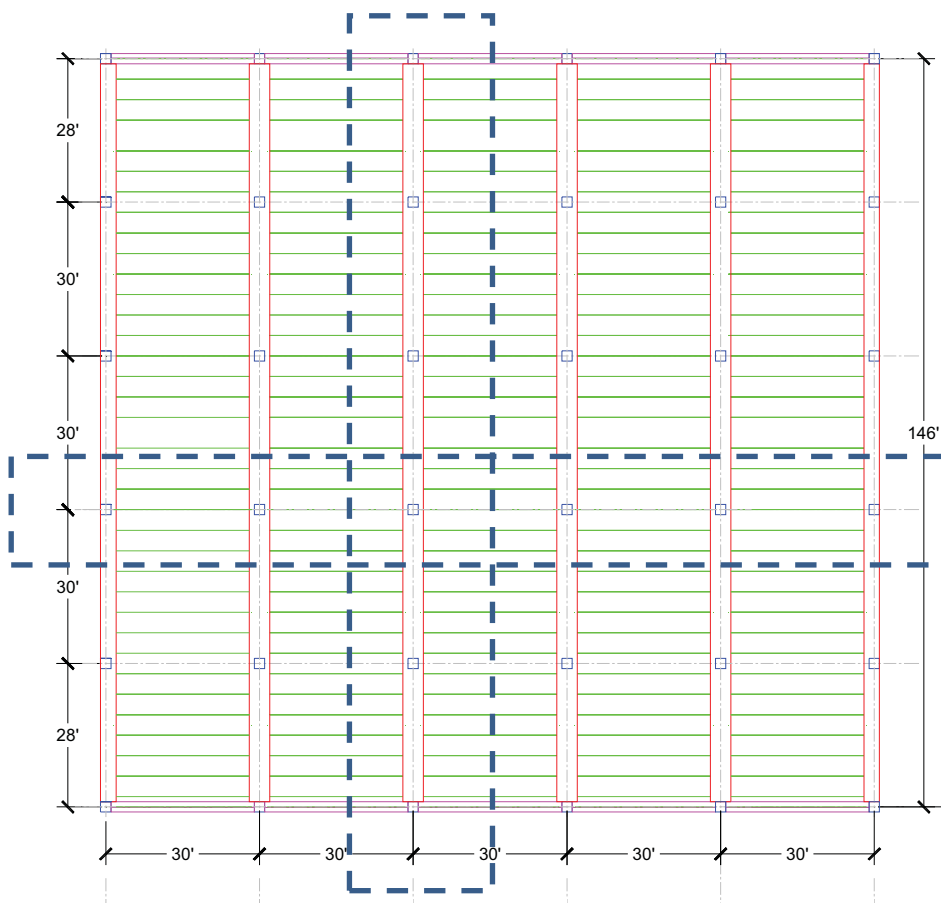


Figure 5.1: Two-dimensional frames adopted for lateral load analysis

5.2 Wind Loads

In this section, the wind loads will be calculated according to the wind speeds. Two-wind zone will be discussed in this section. The first zone is low- moderate wind zone, which located in the mid-west region. State of Nebraska was chosen as example for low-moderate windy zone. The second zone is high wind zone, which located in the south east coast. State of Florida was chosen as example for high wind zone.

5.2.1 Low-moderate Wind Zone

Wind loads were calculated according to Chapter 6 of the ASCE 7-05. The wind speed used in the analysis was 90 mph, which is the design wind speed for Nebraska State. Figure 5.2, Figure 5.3, and Figure 5.4 show, respectively, the loaded frame, bending moment diagram, and deformed shape due to wind load applied to the beam direction. Maximum unfactored bending moment was found to be 41.11 kip.ft, while maximum deflection was 0.654 in.

Table 5.1 shows wind pressure calculations with references to the ASCE 7-05 sections, tables and figures. These calculations indicate that the design wind pressure is approximately 15 psf, which results in a lateral force per floor of 5.38 kip in beam and HC directions.

Figure 5.2, Figure 5.3, and Figure 5.4 show, respectively, the loaded frame, bending moment diagram, and deformed shape due to wind load applied to the beam direction. Maximum unfactored bending moment was found to be 41.11 kip.ft, while maximum deflection was 0.654 in.

Table 5.1: Wind pressure calculations

The Basic Wind Speed (V)	90	mph	Figure 6.1
Wind Directionality Factor (K_d)	0.85		Table 6-4
Importance Factor Depends On Building Category (I&II)	1.0		Table 6-1
Velocity Pressure Exposure Coefficient Evaluated at height z (K_z)	1.23		Section 6.5.6
Topographic Factor (K_{zt})	1		Section 6.5.7
Equivalent Height Of The Structure (Z')	52.8	ft	Table 6-2
Turbulence intensity factor (C)	0.2		Table 6-2
Intensity Of Turbulence (I_z)	0.18		
Integral length Scale L	500	ft	Table 6-2
Integral length Scale Power law Exponent (ϵ)	0.2		Table 6-2
Integral Length Scale of Turbulence (L_z')	549.3		Section 6.5.8.1
Mean Roof Height (h)	72	ft	Section 6.5.8.1
Horizontal Dimension of Building Measured Normal to Wind Direction (B)	146	ft	Section 6.5.8.1
Background response factor (Q)	0.86		Section 6.5.8.1
Peak Factor for Background Response (g_Q)	3.4		Section 6.5.8.1
Peak Factor for Wind Response (g_v)	3.4		Section 6.5.8.1
Gust Effect Factor (G)	0.86		Section 6.5.8.1
External Pressure Coefficient (C_p)	0.8		Section 6.5.11
Velocity Pressure Evaluated at Height z above ground (q_z)	21.68	psf	
Design Wind Pressure (P)	14.9	psf	
Force at each node in the frame	5.36	kip	

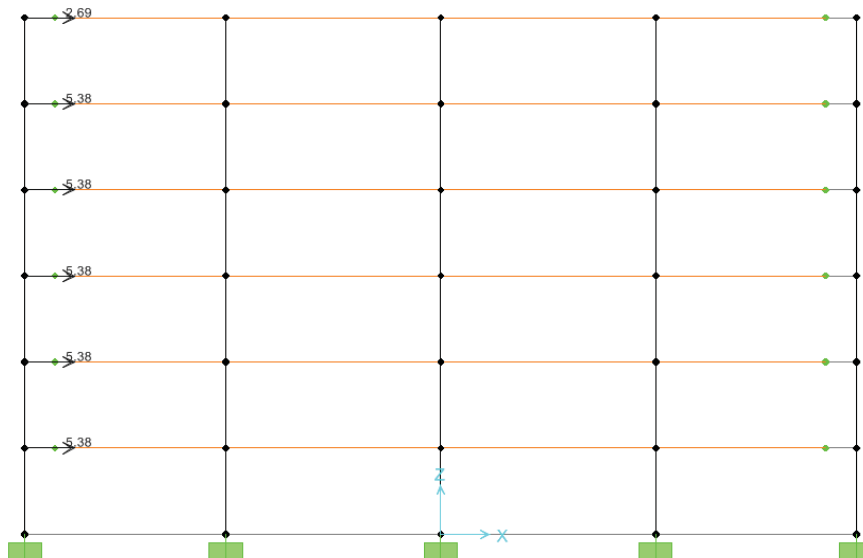


Figure 5.2: Wind load applied to the beam direction

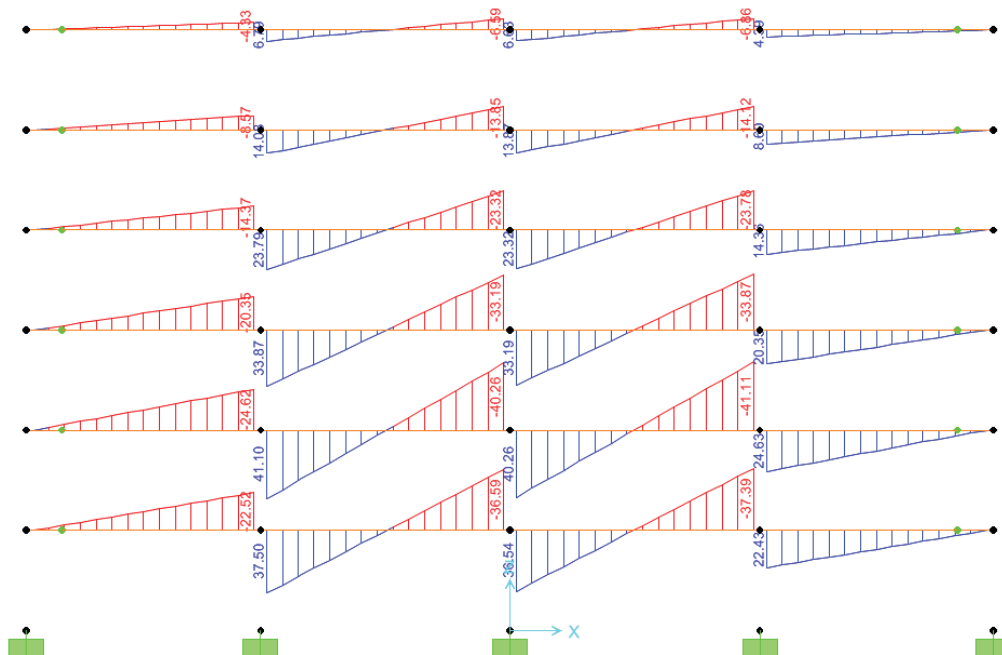


Figure 5.3: Bending moment due to wind load in the beam direction

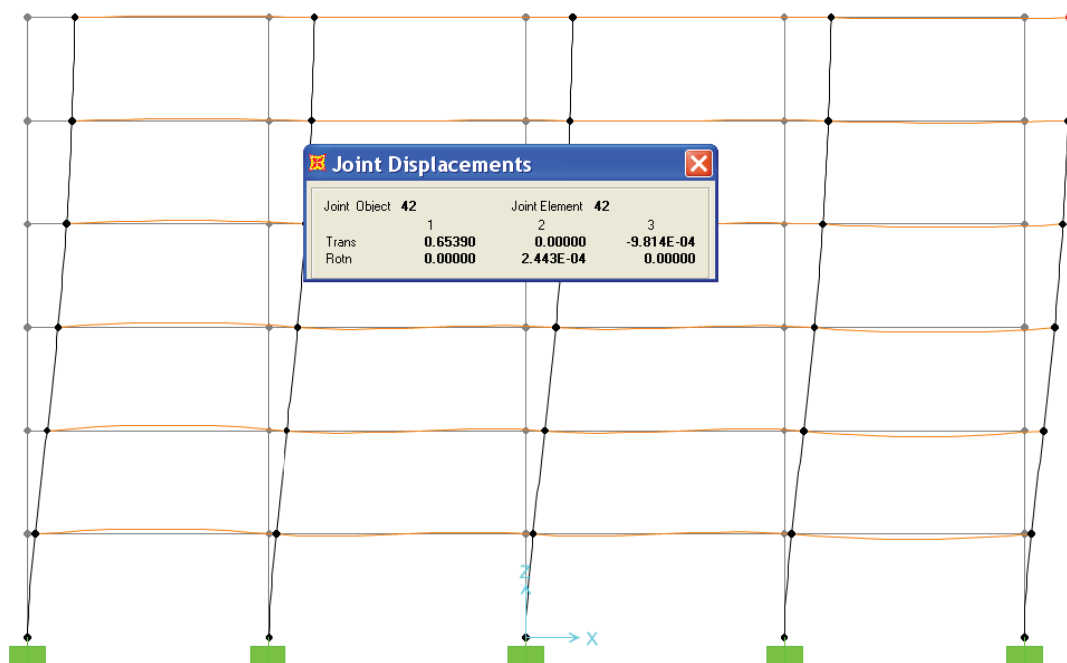


Figure 5.4: Deformed shape due to wind load in the beam direction

Figure 5.5, Figure 5.6, and Figure 5.7 show, respectively, the loaded frame, bending moment diagram, and deformed shape due to wind load applied to the HC direction. Four

hollow cores planks around the column (i.e. column strip) were modeled as a frame element that can resist negative moment only (i.e. positive moment resistance was released). Maximum unfactored bending moment was found to be 42.3 kip.ft, while maximum deflection was 0.397 in.

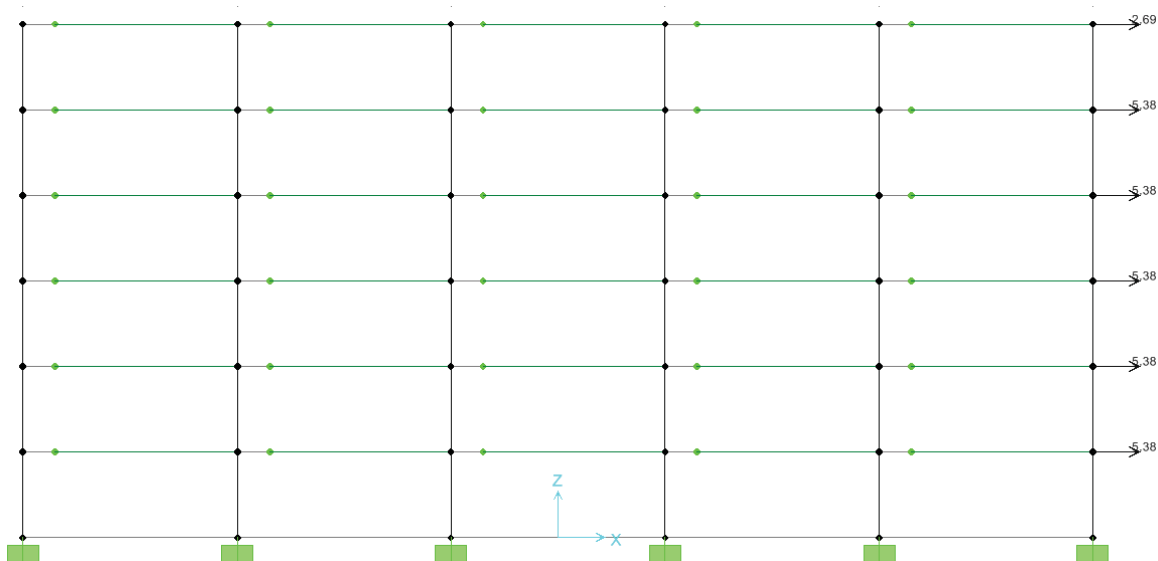


Figure 5.5: Wind load applied to the HC direction

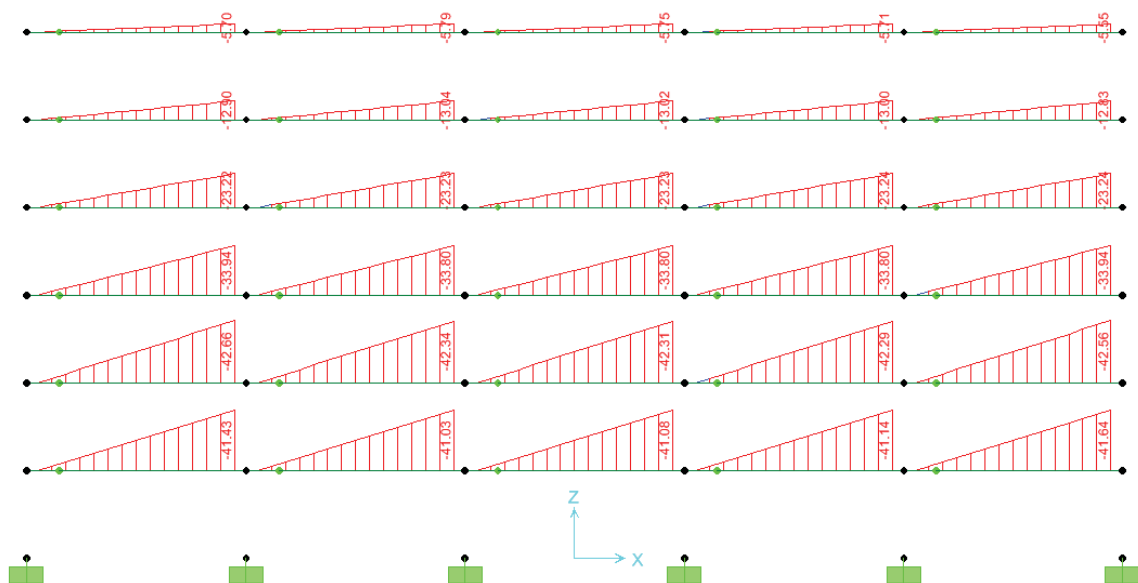


Figure 5.6: Bending moment due to wind load in the HC direction

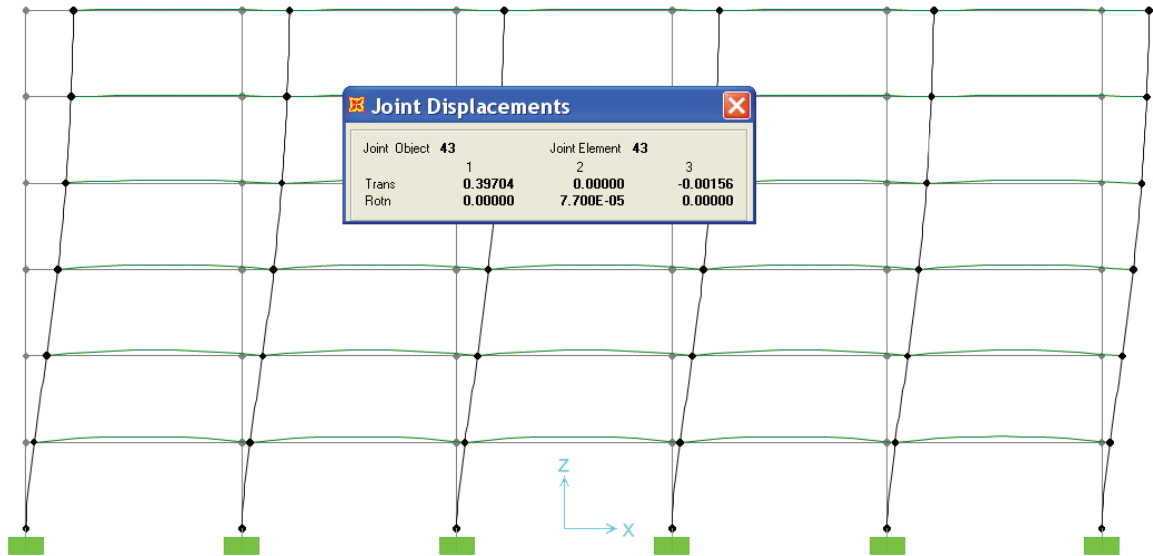


Figure 5.7: Deformed shape due to wind load in the HC direction

5.2.2 High Wind Zone

The wind speed used in the analysis was 150 mph, which is the design wind speed for Florida State. Table 5.2 shows wind pressure calculations with references to the ASCE 7-05 sections, tables and figures. These calculations indicate that the design wind pressure is approximately 41.5 psf, which results in a lateral force per floor of 14.93 kip in beam and HC directions.

The maximum unfactored bending in the beam direction moment was found to be 114.3 kip.ft, while maximum deflection was 1.8 in. In addition, the maximum unfactored bending moment in HC direction was found to be 118.1 kip.ft, while maximum deflection was 1.1 in.

Table 5.2: Wind pressure calculations

Parameter	Value	Unit	ASCE 7-05 Ref.
The Basic Wind Speed (V)	150	mph	Figure 6.1
Wind Directionality Factor (K_d)	0.85		Table 6-4
Importance Factor Depends On Building Category (I&II)	1.0		Table 6-1
Velocity Pressure Exposure Coefficient Evaluated at height z (K_z)	1.23		Section 6.5.6
Topographic Factor (K_{zt})	1		Section 6.5.7
Equivalent Height Of The Structure (Z')	43.2	ft	Table 6-2
Turbulence intensity factor (C)	0.2		Table 6-2
Intensity Of Turbulence (I_z')	0.19		
Integral length Scale L	500	ft	Table 6-2
Integral length Scale Power law Exponent (ϵ)	0.2		Table 6-2
Integral Length Scale of Turbulence (L_z')	527.7		Section 6.5.8.1
Mean Roof Height (h)	72	ft	Section 6.5.8.1
Horizontal Dimension of Building Measured Normal to Wind Direction (B)	146	ft	Section 6.5.8.1
Background response factor (Q)	0.86		Section 6.5.8.1
Peak Factor for Background Response (g_0)	3.4		Section 6.5.8.1
Peak Factor for Wind Response (g_v)	3.4		Section 6.5.8.1
Gust Effect Factor (G)	0.86		Section 6.5.8.1
External Pressure Coefficient (C_p)	0.8		Section 6.5.11
Velocity Pressure Evaluated at Height z above ground (q_z)	60.22	psf	
Design Wind Pressure (P)	41.5	psf	
Force at each node in the frame	14.93	kip	

5.3 Seismic Loads

In this section, the seismic loads will be calculated according to seismicity zones. Two zones will be discussed in this section. The first zone is the low-moderate seismicity zone (Seismic Design Categories A&B occupancy categories II and I). State of Nebraska is taken as example for that zone. The second zone is the high-moderate seismicity zone (Seismic Design Categories D and occupancy categories II and I). State of California is taken as example of that zone. The following subsections present load calculations and analysis results.

5.3.1 Low-moderate Seismicity Zone

Seismic loads were calculated according to Chapters 11 and 22 of the ASCE 7-05. The 0.2 sec. and 1.0 sec. spectral response acceleration used in the analysis were chosen for Nebraska State. Table 5.3 shows the base shear force calculations with references to the ASCE 7-05 sections, tables and figures, while Table 5.4 shows the force distribution on each floor.

Table 5.3: Base shear force calculations

Parameter	Value	ASCE 7-05 Ref.
Soil Site Class	D	Section 11.4.2
0.2 Sec. Spectral Response Acceleration S_S	0.18	Figure 22-1
1.0 Sec. Spectral Response Acceleration S_1	0.04	Figure 22-2
Site Coefficient F_a	1.6	Table 11.4-1
Site Coefficient F_v	2.4	Table 11.4-2
Modified 0.2 Sec. Spectral Response Acceleration S_{MS}	0.288	
Modified 1.0 Sec. Spectral Response Acceleration S_{M1}	0.096	
Design 0.2 Sec. Spectral Response Acceleration S_{DS}	0.192	
Design 1.0 Sec. Spectral Response Acceleration S_{D1}	0.064	
T_0 Sec.	0.067	
T_S Sec.	0.333	
T_L Sec.	4	Figure 22-15
Total Height ft	72	
C_t value for approximate period calculation	0.016	Table 12.8-2
x value for approximate period calculation	0.90	Table 12.8-2
Approximate Fundamental Period T_a Sec.	0.75	
Design Spectral Response Acceleration S_a	0.085	
Importance Category	I,II	
Importance Factor I	1.0	Table 11.5-1
Seismic Design Category	B	Table 11.6-1, 11.6-2
Seismic Force-Resisting System	Ordinary RC moment frame	
Response Modification Coefficient R	3	Table 12.2-1
Analysis Method	Equivalent Lateral Force	
Seismic Response Coefficient C_s	0.0284	
Total Weight W (kip)	12,902	
Base Shear V (kip)	366.4	

Table 5.4: Base shear force distribution on each floor

Floor No.	Weight, W (kip)	Height, h (ft)	h^k	Wh^k	C	Total Floor Force (kip)	No. of Frames in Beam Direction	Frame Force - Beam Direction (kip)	No. of Frames in HC Direction	Frame Force - HC Direction (kip)
1	2000	12	16.39	32,789	0.038	13.28	6	2.21	5	2.66
2	2000	24	35.77	71,541	0.082	28.97	6	4.83	5	5.79
3	2000	36	56.46	112,916	0.130	45.73	6	7.62	5	9.15
4	2000	48	78.05	156,093	0.179	63.21	6	10.54	5	12.64
5	2000	60	100.33	200,660	0.231	81.26	6	13.54	5	16.25
6	2,400	72	123.18	295,642	0.340	119.73	6	19.95	5	23.95
TOTAL	12,400	K	1.13	869,640	1.0	352.2		58.7		70.4

Figure 5.8, Figure 5.9, and Figure 5.10 show, respectively, the loaded frame, bending moment diagram, and deformed shape due to seismic load applied to the beam direction. Maximum unfactored bending moment was found to be 104.26 kip.ft, while maximum deflection was 1.88 in.



Figure 5.8: Seismic load applied to the beam direction

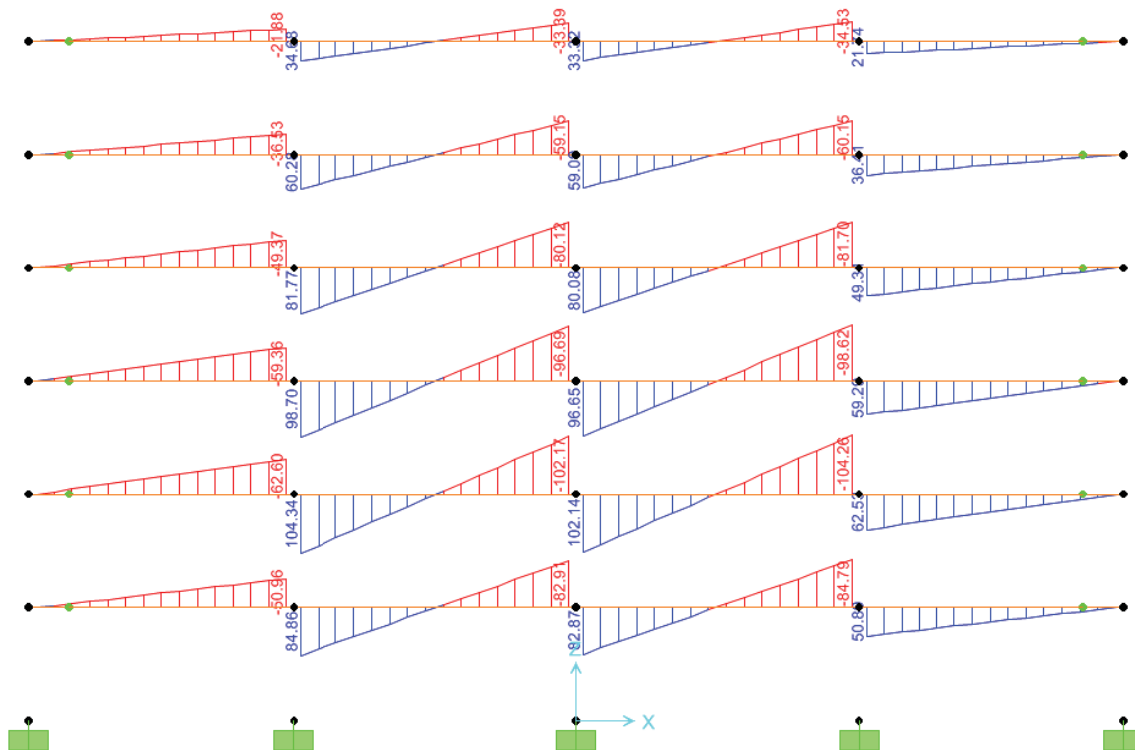


Figure 5.9: Bending moment due to seismic load in the beam direction

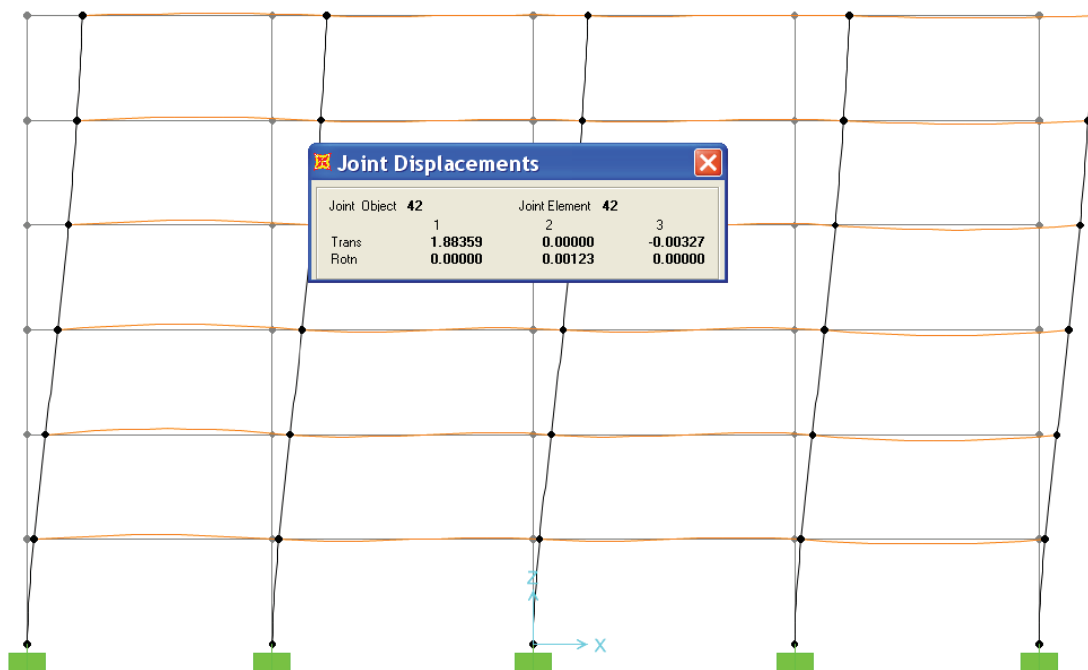


Figure 5.10: Deformed shape due to seismic load in the beam direction

Figure 5.11, Figure 5.12, and Figure 5.13 show, respectively, the loaded frame, bending moment diagram, and deformed shape due to seismic load applied to the HC direction. Four hollow cores planks around the column (i.e. column strip) modeled as a frame element that can resist negative moment only (i.e. positive moment resistance was released). Maximum unfactored bending moment was found to be 128 kip.ft, while maximum deflection was 1.36 in.

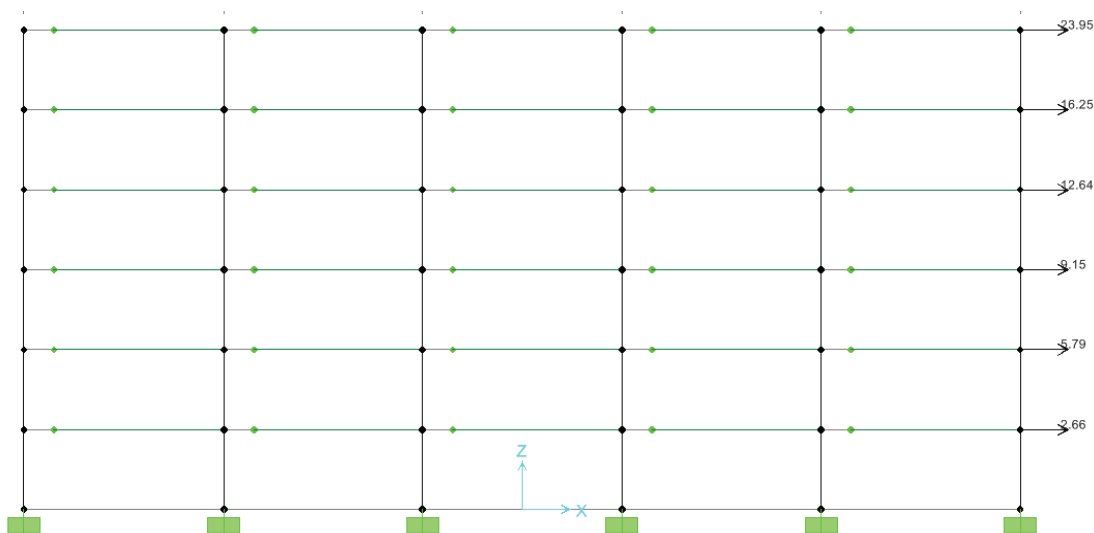


Figure 5.11: Seismic load applied to the HC direction

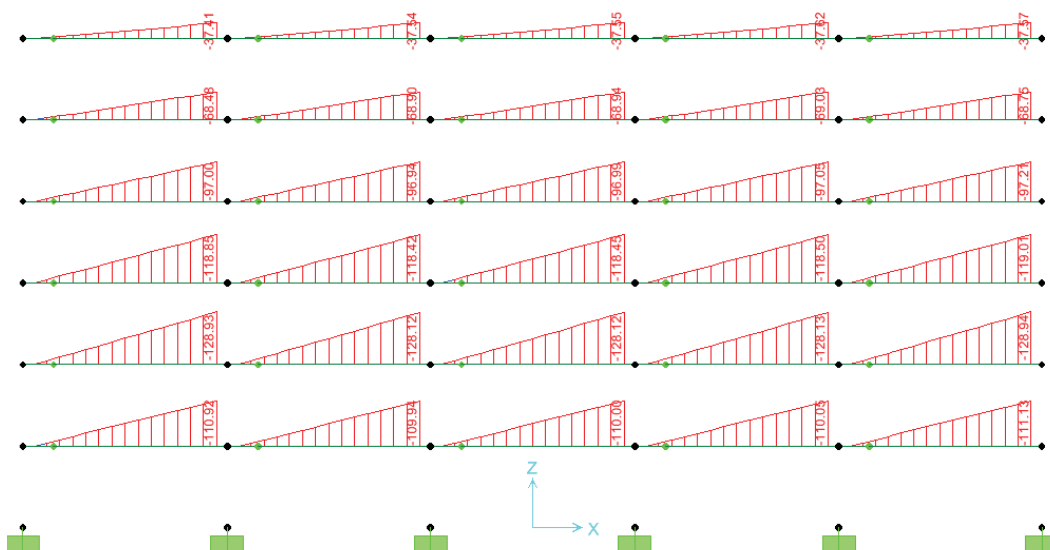


Figure 5.12: Bending moment due to seismic load in the HC direction

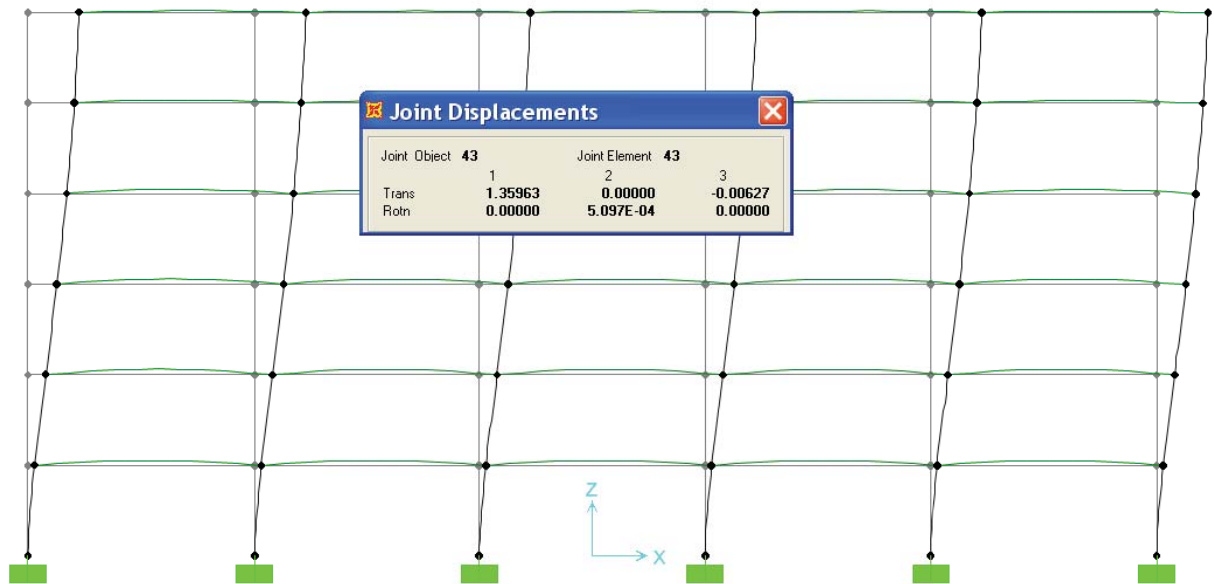


Figure 5.13: Deformed shape due to seismic load in the hc direction

5.3.1.1 Story Drift

A. Story Drift Determination

The story Drift was determined according to ASCE 7-05 section 12.8.6. Table 5.5 contains the displacements δ_{xe} obtained from the elastic analyses using the design seismic force in the beam direction and HC direction. The table also contains the design earthquake displacement δ_x computed by equation $\delta_x = C_d * \delta_{xe} / I$. The interstory drifts Δ computed from δ_x are also contained in the table. For this structures that doesn't have plan irregularity, the drift at story level (X) is determined by subtracting the design earthquake displacement at the center of mass at the bottom of the story from the design earthquake displacement at the center of mass at the top of the story.

Table 5.5: Lateral displacements and inter-story drifts due to seismic force in beam direction and HC direction

Story	δ_{xe} , (in.) Beam Direction	δ_{xe} , (in.) HC Direction	I	C_d	δ_x , (in.) Beam Direction	δ_x , (in.) HC Direction	Δ , (in.) Beam Direction	Δ , (in.) HC Direction
6	1.87	1.36	1	2.5	4.675	3.4	0.5	0.325
5	1.67	1.23			4.175	3.075	0.7	0.5
4	1.39	1.03			3.475	2.575	0.925	0.65
3	1.02	0.77			2.55	1.925	1.025	0.75
2	0.61	0.47			1.525	1.175	1	0.75
1	0.21	0.17			0.525	0.425	0.525	0.425

The design story drifts Δ must not exceed the allowable story drift Δ_a . For seismic occupancy category II, $\Delta_a = 0.020h_{sx}$. Thus for 12 ft story heights, $\Delta_a = 0.020 \times 12 \times 12 = 2.88$ in. It is evident from Table 5.5 that for all stories, the lateral drifts obtained are less than the limiting values.

5.3.2 High Seismicity Zone

The 0.2 sec. and 1.0 sec. spectral response acceleration used in the analysis were chosen for the San Francisco, CA. Table 5.6 shows the base shear force calculations for three story frame with references to the ASCE 7-05 sections, tables and figures, while Table 5.7 shows the force distribution on each floor For three-story building.

Table 5.6: Base shear force calculations

Parameter	Value	ASCE 7-05 Ref.
Soil Site Class	D	Section 11.4.2
0.2 Sec. Spectral Response Acceleration S_S	1.5	Figure 22-1
1.0 Sec. Spectral Response Acceleration S_1	0.61	Figure 22-2
Site Coefficient F_a	1	Table 11.4-1
Site Coefficient F_v	1.5	Table 11.4-2
Modified 0.2 Sec. Spectral Response Acceleration S_{MS}	1.5	
Modified 1.0 Sec. Spectral Response Acceleration S_{M1}	0.915	
Design 0.2 Sec. Spectral Response Acceleration S_{DS}	1	
Design 1.0 Sec. Spectral Response Acceleration S_{D1}	0.61	
T_0 Sec.	0.122	
T_S Sec.	0.610	
T_L Sec.	16	Figure 22-15
Total Height ft	36	
C_t value for approximate period calculation	0.016	Table 12.8-2
x value for approximate period calculation	0.90	Table 12.8-2
Approximate Fundamental Period T_a Sec.	0.40	
Design Spectral Response Acceleration S_a	1.000	
Importance Category	II	
Importance Factor I	1.0	Table 11.5-1
Seismic Design Category	D	Table 11.6-1, 11.6-2
Seismic Force-Resisting System	Ordinary RC moment frame	
Response Modification Coefficient R	8	Table 12.2-1
Analysis Method	Equivalent Lateral Force	
Seismic Response Coefficient C_s	0.1250	
Total Weight W (kip)	6,400	
Base Shear V (kip)	800.0	

Table 5.7: Base shear force distribution on each floor

Floor No.	Weight, W (kip)	Height, h (ft)	h^k	Wh^k	C	Total Floor Force (kip)	No. of Frames in Beam Direction	Frame Force - Beam Direction (kip)	No. of Frames in HC Direction	Frame Force - HC Direction (kip)
1	2000	12	12.00	24,000	0.152	121.21	6	20.20	5	24.24
2	2000	24	24.00	48,000	0.303	242.42	6	40.40	5	48.48
3	2400	36	36.00	86,400	0.545	436.36	6	72.73	5	87.27
TOTAL	6,400	K	1.00	158,400	1.0	800.0		133.3		160.0

The maximum unfactored positive and negative bending moments were found to be 196 kip. ft and 200.6 kip.ft, and maximum deflection was 1.76 in. in the beam direction, while in the HC direction the maximum negative moment was 257.82 kip.ft and maximum deflection was 1.34 in.

5.3.2.1 Story Drift

A- Story Drift Determination

Table 5.8 contains the displacements δx_e obtained from the elastic analyses using the design seismic force in the beam direction and HC direction. The table also contains the earthquake displacement δx . The inter-story drifts Δ computed from δx are also contained in the table.

Table 5.8: Lateral displacements and inter-story drifts due to seismic force

Story	δx_e , (in.) Beam Direction	δx_e , (in.) HC Direction	I	C_d	δx , (in.) Beam Direction	δx , (in.) HC Direction	Δ , (in.) Beam Direction	Δ , (in.) HC Direction
3	1.76	1.34	1	5.5	9.68	7.37	3.3	2.31
2	1.16	0.92			6.38	5.06	3.96	3.025
1	0.44	0.37			2.42	2.035	2.42	2.035

The design story drifts Δ must not exceed the allowable story drift Δ_a . For seismic occupancy category II, $\Delta_a = 0.020h_{sx}$. Thus for 12 ft story heights, $\Delta_a = 0.020 \times 12 \times 12 = 2.88$ in. It is evident from Table 5.8 that not all the cells in all stories match the limiting values. The lateral drifts in the shaded cells are higher than the allowable value. The stiffness of the building should be increase, in order to make the lateral drifts values less than the limiting value. Increasing the stiffness will be done in two ways; 1) increase the beam depth to 13 in. and 2) increase column dimension to 24 in. x 24 in. The following subsection will present the lateral displacement and drift for each way.

A-1 Increasing the Beam depth

The beam depth was increased from 10 in. to 13 in, in order to increase the building stiffness. Table 5.9 shows the lateral displacement and inter-story drifts due to the seismic force in both HC and beam direction

Table 5.9: Lateral displacements and inter-story drifts due to seismic force

Story	δx_e , (in.) Beam Direction	δx_e , (in.) HC Direction	I	C_d	δx , (in.) Beam Direction	δx , (in.) HC Direction	Δ , (in.) Beam Direction	Δ , (in.) HC Direction
3	1.46	1.04	1	5.5	8.03	5.72	2.585	1.65
2	0.99	0.74			5.445	4.07	3.3	2.42
1	0.39	0.3			2.145	1.65	2.145	1.65

It is evident from Table 5.9 that not all the cells in all stories match the limiting value.

The lateral drift in the green cell is higher than the allowable value.

A-2 Increasing the column dimension

When increasing the column dimension the maximum unfactored positive and negative bending moments were found to be 149 kip. ft and 150.53 kip.ft, and maximum deflection was 1.3 in. in the beam direction, while in the HC direction the maximum negative moment was 191.18 kip.ft and maximum deflection was 1 in.. Table 5.10 shows the lateral displacement and inter-story drifts due to the seismic force in both HC and beam direction when changing the column dimension to 24 in. x 24 in.

Table 5.10: Lateral displacements and inter-story drifts due to seismic force

Story	δx_e , (in.) Beam Direction	δx_e , (in.) HC Direction	I	C_d	δx , (in.) Beam Direction	δx , (in.) HC Direction	Δ , (in.) Beam Direction	Δ , (in.) HC Direction
3	1.3	1	1	5.5	7.15	5.5	2.695	1.87
2	0.81	0.66			4.455	3.63	2.805	2.31
1	0.3	0.24			1.65	1.32	1.65	1.32

It is evident from Table 5.10 that all the cells in all stories match the limiting value. The lateral drifts in cells are lower than the allowable value.

5.4 Load Combination for Low Seismicity Zone

Table 5.11 summarizes the 2-D analysis results of six-story building in both beam and HC directions under wind and seismic loads. To evaluate the adequacy of the proposed design to resist these loads, Table 5.12 lists the two load combinations considered in the design of the example building and compares them versus the factored resistance. The positive and negative moment capacities of the composite FS10 at the end section, and the negative moment capacity of composite HC at the end section were calculated using strain compatibility. The HC capacities were calculated for the four hollow core planks forming the column strip effective in lateral load resistance (i.e. $4 \times 56.36 = 225.44$ kip.ft). It should be noted that the positive moment capacity of the FS 10 at end section should include the permanent negative moment caused by the topping weight multiplied by 0.9 as it opposes the positive moment caused by lateral loads. Table 5.12 indicates that the proposed design of the FS 10 and HC has adequate resistance to lateral load for the example building shown in Figure 4.1. However, additional lateral load resisting system (e.g. shear wall or moment resisting frame) might be needed in the hollow core direction when different building configurations are used and/or more severe loading conditions are applied.

Table 5.11: Summary of lateral load analysis results

	Wind Load		Seismic Load	
	Moment (kip.ft)	Deflection (in)	Moment (kip.ft)	Deflection (in)
HC Direction	42.3	0.397	128	1.36
Beam Direction	41.11	0.654	104.26	1.88

Table 5.12: Comparison of factored lateral load and resistance

Load Combination	FS Beam		Four HCs
	Negative	Positive	Negative
Wind : 1.2D + 1.6W + 1.0L	-342.5	64.42	-67.58
Seismic : 1.2D + 1.0 E + 1.0 L	-381	102.26	-128
Factored Resistance	-425	155	-225.44
CHECK	OK	OK	OK

5.5 Load Combination for High Wind Zone

Table 5.13 summarizes the 2-D analysis results of three-story building in both beam and HC directions under seismic loads. To evaluate the adequacy of the proposed design to resist these loads, Table 5.14 lists the load combination considered in the design of the example building and compares them versus the factored resistance. Table 5.14 indicates that the proposed design of the FS 10 has inadequate negative moment resistance to lateral load for six-story of the example building shown in Figure 4.1. Therefore, addition negative reinforcement needs to be added to the design of the beam-column connection. Figure 5.14 shows the beam-column connection reinforcement for high-moderate windy zone. The required area of reinforcement was found to be 13.61 in² (15 # 8 + 4 #6), which was 18.2 % higher than low-moderate seismicity zone connection. The connection was designed to carry factored negative nominal moment and factored positive nominal moment equal to 461 kip.ft and 196.6 kip.ft as shown in Table 5.15

Table 5.13: Summary of lateral load analysis results

	Wind Load	
	Moment (kip.ft)	Deflection (in)
HC Direction	118.1	1.1
Beam Direction	114.3	1.8

Table 5.14: Comparison of factored lateral load and resistance

Load Combination	FS Beam		Four HCs
	Negative	Positive	Negative
Wind : 1.2D + 1.6 W + 1.0 L	-459.64	111.9	-188.96
Factored resistance	-425	155	-255.44
CHECK	NO	OK	OK

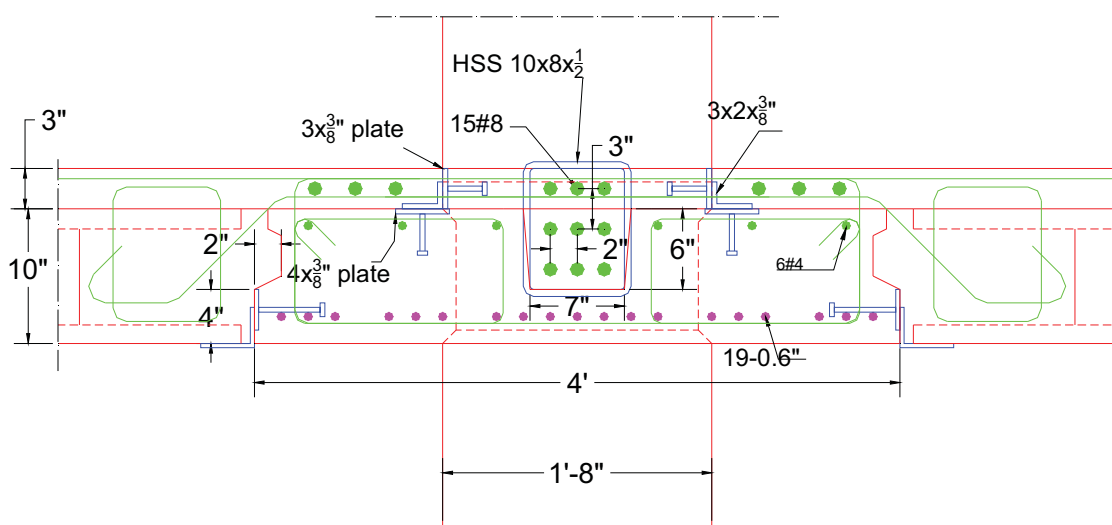


Figure 5.14: Beam-Column connection for high-moderate windy zone

Table 5.15: Comparison of factored lateral load and resistance for high-moderate windy zone.

Load Combination	FS Beam		Four HCs
	Negative	Positive	Negative
Wind : 1.2D + 1.6 W + 1.0 L	-459.64	111.9	-188.96
Factored resistance	-462	196.6	-255.44
CHECK	OK	OK	OK

5.6 Load Combination High Seismicity Zone

Table 5.16 summarizes the 2-D analysis results of three-story building in both beam and HC directions under seismic loads. To evaluate the adequacy of the proposed design to resist these loads, Table 5.17 lists the load combination considered in the design of the six-story example building and compares them versus the factored resistance. Table 5.8 and Table 5.17 indicates that the proposed design of the FS 10 and HC has 1) higher drift values than the allowable value, and 2) inadequate resistance to lateral load for three-story of the example building shown in Figure 4.1.

Table 5.16: Summary of lateral load analysis results

	Seismic Load	
	Moment (kip.ft)	Deflection (in)
HC Direction	257.8	1.34
Beam Direction	200.6	1.76

Table 5.17: Comparison of factored lateral load and resistance

Load Combination	FS Beam		Four HCs
	Negative	Positive	Negative
Seismic : 1.2D + 1.0 E + 1.0 L	-477.36	196	-257.8
Factored Resistance	-425	155	-225.44
CHECK	NO	NO	NO

A- Increasing the Column Dimension

Table 5.18 summarizes the 2-D analysis results of three-story building in both beam and HC directions under seismic loads when increasing the column dimension to 24 in. x 24 in. Table 5.19 lists the load combination considered in the design of the example building

and compares them versus the factored resistance. Table 5.10 and Table 5.19 indicates that the proposed design of the FS 10 and HC has 1) drift values lower than the allowable value, and 2) inadequate resistance to lateral load for three-story of the example building shown in Figure 4.1. Addition negative reinforcement need to be added for both beam-column connection and HC connection to be adequate for lateral load.

Table 5.18: Summary of lateral load analysis results

	Seismic Load	
	Moment (kip.ft)	Deflection (in)
HC Direction	191.18	1
Beam Direction	150.53	1.3

Table 5.19: Comparison of factored lateral load and resistance

Load Combination	FS Beam		Four HCs
	Negative	Positive	Negative
Seismic : 1.2D + 1.0 E + 1.0 L	-427.29	149.26	-257.8
Factored Resistance	-425	155	-225.44
CHECK	NO	OK	NO

In order to modify the connections to be work in high-moderate seismicity zone, Figure 5.15 shows the beam-column connection reinforcement details. All the negative reinforcement (pocket and topping bars) was changed to # 8. Also topping mesh was changed from D11@6 in. to D16@6 in. Table 5.20 shows the load combination considered in the design of the three-story and compares them versus the modified factored resistance.

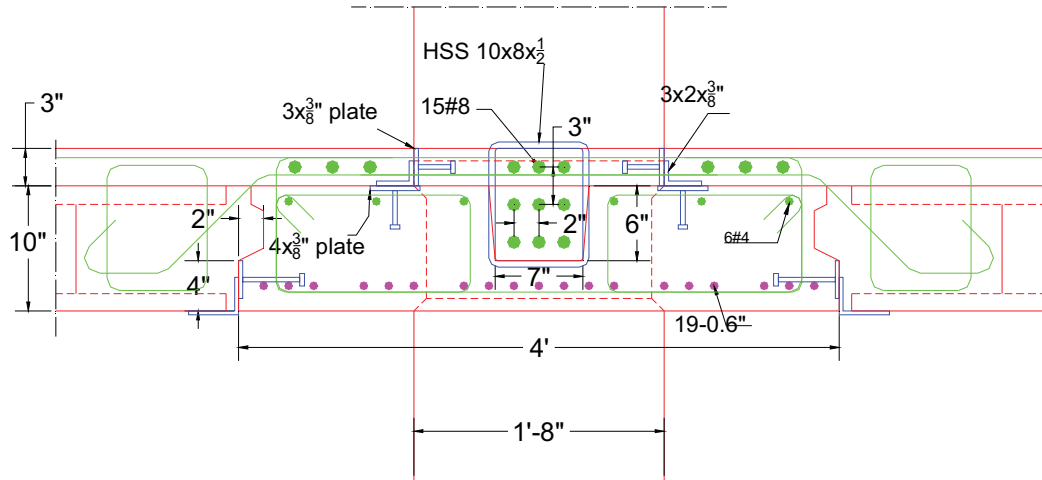


Figure 5.15: Beam-Column connection for high-moderate seismicity zone

Table 5.20: Comparison of factored lateral load and resistance

Load Combination	FS Beam		Four HCs
	Negative	Positive	Negative
Seismic : 1.2D + 1.0 E + 1.0 L	-427.29	149.26	-257.8
Factored Resistance	462	196.6	-274
CHECK	OK	OK	OK

It is clear from the analysis in this chapter that the propose system is valid to be used in low seismicity zone, high wind zone, but in high seismicity zones need to be evaluated.

Chapter 6

TESTING OF FLAT SOFFIT FLOOR SYSTEM COMPONENTS AND CONNECTIONS

6.1 Introduction

Experimental investigations were carried out to evaluate the constructability and structural performance of the developed flat soffit shallow precast floor system. beam-column connection without corbel, HC-beam connection without ledge, and flat soffit beam full-scale specimens were tested to evaluate the following:

- Flexural capacity of the beam for resisting gravity and lateral loads.
- Flexural capacity of composite hollow core planks for resisting lateral loads.
- Shear capacity of the beam-column connection without corbel
- Shear capacity of the beam-HC connection without ledge

6.2 Beam-column Connection without Corbel

This section presents the experimental investigation carried out to evaluate the performance and capacity of the beam-column connection without corbel. The dimension of the beam-column connection without corbel presented in this test is different from the dimension used in the flat soffit-building example. Despite of that difference, the design and the test prove the concepts. A full-scale specimen present approximately 20 ft x 20 ft segment of the floor around an interior column as shown in Figure 6.1. Specimen components, which include two precast beam segments, one column, and eight HC planks, were fabricated by Concrete Industries (CI) Inc., Lincoln, NE and erected and tested at the Structural Laboratory of Peter Kiewit Institute (PKI) Omaha, NE.

Figure 6.2 shows the plan view of the beam end, while Figure 6.3 illustrious the detailing of the precast column. Figure 6.4 shows the Composite beam and its connection with the column

Table 6.1: Reinforcement used in beam-column connection without corbel

Negative Moment Section Reinforcement	Number	Area (in ²)	Size
Pocket Reinforcement	6	0.44	#6
Topping Reingforcement	9	0.79	#8

Table 6.2: Comparison of Demand and Capacity at Critical Sections.

Section	Capacity ϕM_n (kip.ft)	Demand ϕM_n (kip.ft)	Check
Beam Negative Non-composite Section	-201.9	-117.8	Ok
Beam Negative Composite Section	-600.7	-600.4	Ok
Beam Positive Composite section	138	115	OK
HC Negative Composite section	162.9	126	OK

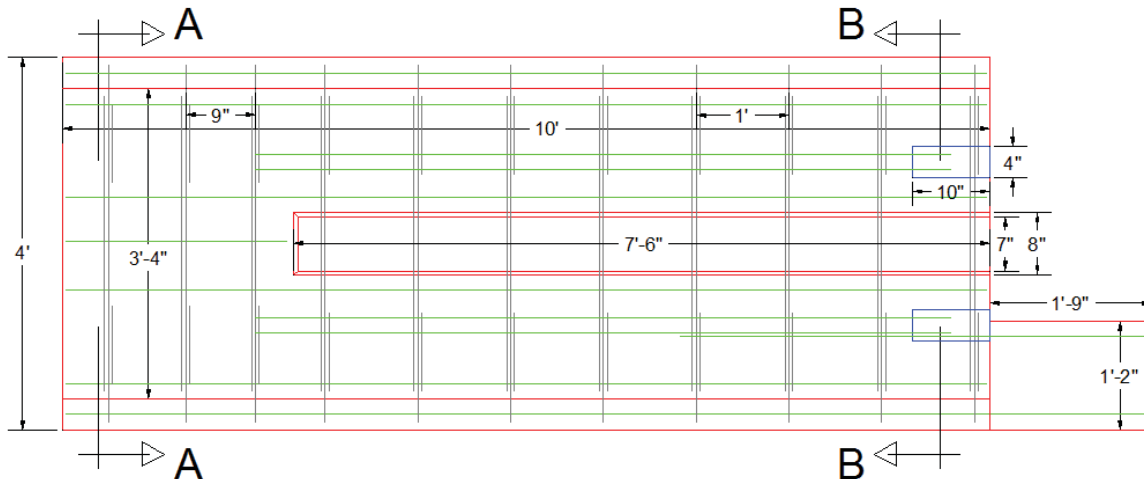


Figure 6.2: Plan View of the Beam End

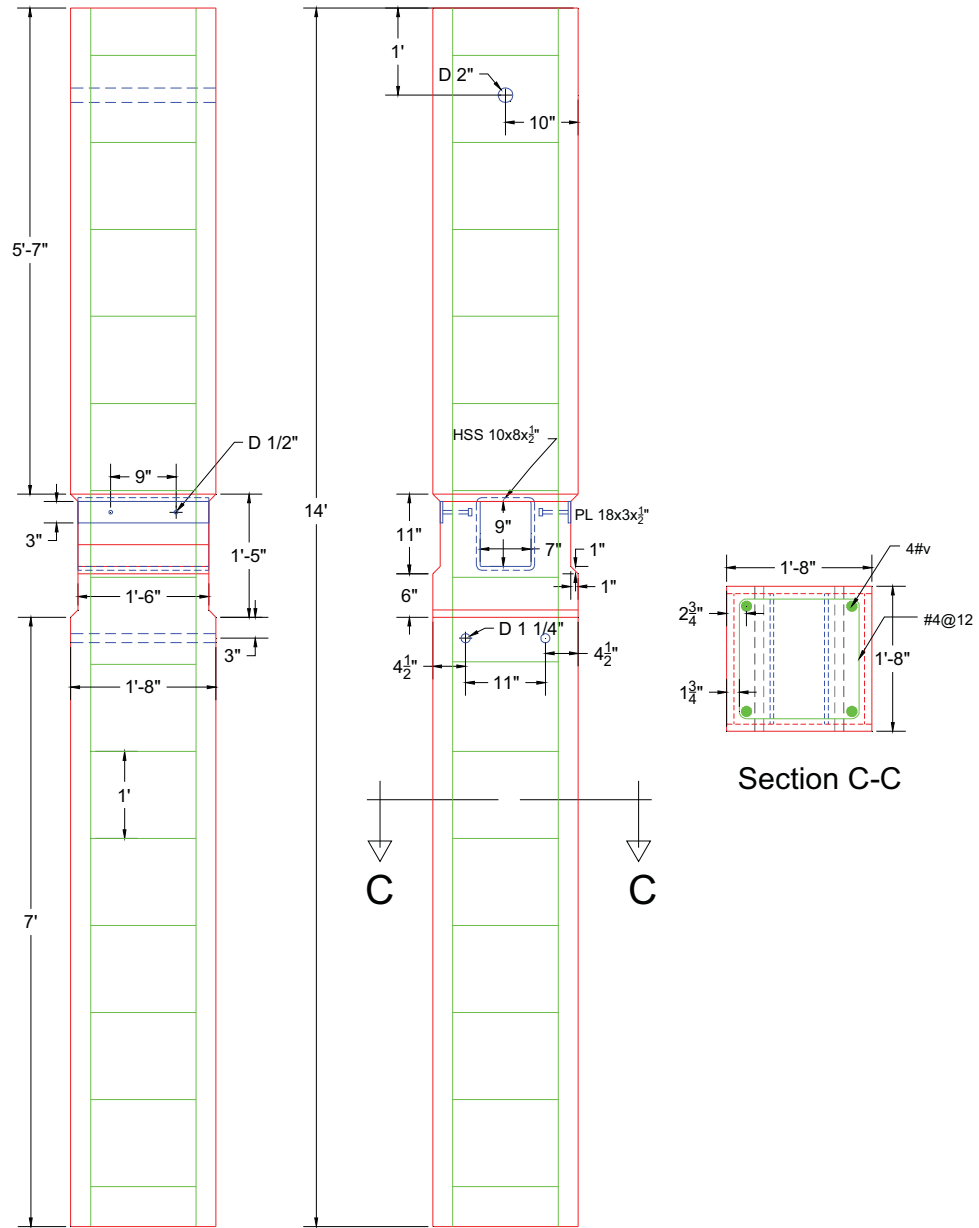


Figure 6.3: Detailing of the precast column

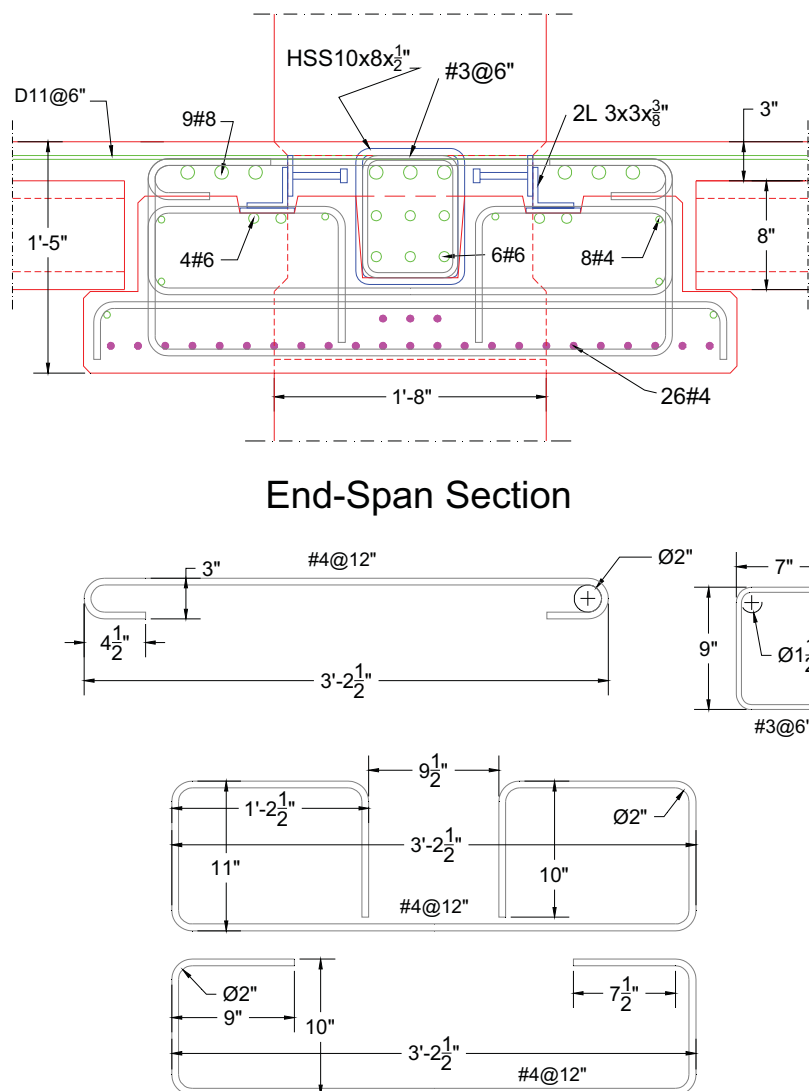


Figure 6.4: Composite beam and its connection with the column

Lateral loads considered in the analysis include the wind and seismic loads calculated as shown above in chapter 5. Table 6.3 summarizes the 2-D analysis results of the building in both beam and HC directions under wind and seismic loads. To evaluate the adequacy of the proposed design to resist these loads, Table 6.4 lists the two load combinations considered in the design and compares them versus the factored resistance. Table 6.4 indicates that the proposed design of the beam and HC has adequate resistance to lateral load.

Table 6.3: Summary of Lateral Load Analysis Results

	Wind Load	Seismic Load
	Moment (kip.ft)	Moment (kip.ft)
HC Direction	45	126
Beam Direction	47	115

Table 6.4: Comparison of Factored Lateral Load and Resistance

Load Combination	Beam	Four HCs
	Negative	Negative
Wind: 1.2 D + 1.6 W + 1.0 L	-494.6	-72
Seismic: 1.2 D + 1.0 E + 1.0 L	-534.4	-126
Factored Resistance	-601	-162.9
CHECK	OK	OK

6.2.2 Specimen Fabrication and Erection

Specimen components (two beams, one column, and eight HC planks) were fabricated at Concrete Industries Inc as shown in Appendix B. Below are the steps followed in the erection of the specimen. Appendix C shows the erection process pictures

Step 2) To achieve the stability of the column under the loads, column was erected inside a reinforced concrete base that is 4 ft x 4 ft x 3.5 ft.

Step 3) Installed the temporary corbels.

Step 4) The beams were placed on each side of the column so that the beams align to each other and the beam pockets align to the column opening

Step 5) Two 38 in. long angles (3 in. x 2.5 in. x ½ in.) were welded to the beam end plates and column side plates.

Step 6) Four HC planks were erected on each side of the beam.

Step 7) First layer of reinforcement 6#6 bars inside closed stirrups of #3@6 in. was placed in the beam pocket through the column opening.

Step 8) The HC keyways, beam pockets, and column opening were grouted using SCC Grout.

Step 9) The 9#8 bars required to provide the beam continuity for live load and the D6 @6 in. WWR required to provide HC continuity for lateral load were placed

Step 10) The topping concrete was poured using a ready mix concrete with 8 in. slump

Step 11) After the topping concrete was cured and hardened, the temporary corbel angles were removed and the specimen was ready for testing.

6.2.3 Material Properties

Table 6.5 shows the mix design for the precast, grout and topping concrete used in the production of the second specimen. Figure 6.5 shows the gain of compressive strength with time for the precast, grout, and topping concrete up to the time of testing.

Table 6.5: Concrete mixes design

Materials	Precast Components Mix	Grout Mix	Topping Mix
	Weight (lb) per cubic Yards		
Portland Cement Type I/II	632*	650	611
Fly Ash, Class C	100	100	-
Limestone 1/2"	1311	1265	950
47B Sand and Gravel	1449	1875	2190
Total Water	292	225	275
High Range Water Reducer, HRWR, Glenium 3400, Master Builders	10 oz/cwt	-	-
* Type III cement			

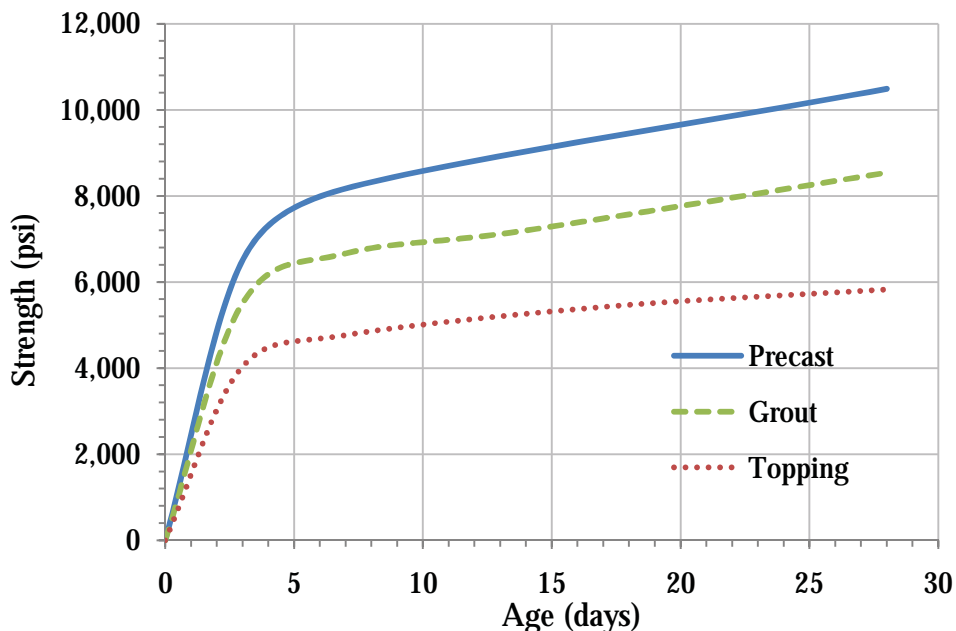


Figure 6.5: Concrete strength gain with time

Table 6.6 lists the actual and specified compressive strength of the concrete used in the production of the specimen components at the time of testing. This table indicates that the actual compressive strength of all components at the time of testing was satisfactory as it exceeded the specified strength.

Table 6.6: Specified and actual concrete compressive strength at testing

Components	Actual strength (psi)	Specified strength (psi)
Column	10,500	8,000
Grout	6,500	4,000
Topping	5,200	3,500

6.2.4 Test Setup and Procedures

Testing the beam-column connection without corbel specimen was performed on June 7, and 8, 2010. The test program includes the following four tests:

- 1- HC Negative Moment Capacity

- 2- Beam Negative Moment Capacity
- 3- Beam Positive Moment Capacity
- 4- Beam-Column Connection Shear Capacity

6.2.4.1 HC Negative Moment Capacity

The purpose of this test is to evaluate the negative moment capacity of the composite HC section for resisting lateral loads. Figure 6.6 shows the test setup, where HC planks were loaded at the unsupported end while clamping the other end to maintain specimen stability. Testing was performed by applying a uniform load on the cantilevered HC at 5 ft from the center of the column up to the capacity, while measuring the deflection at the cantilevered end.

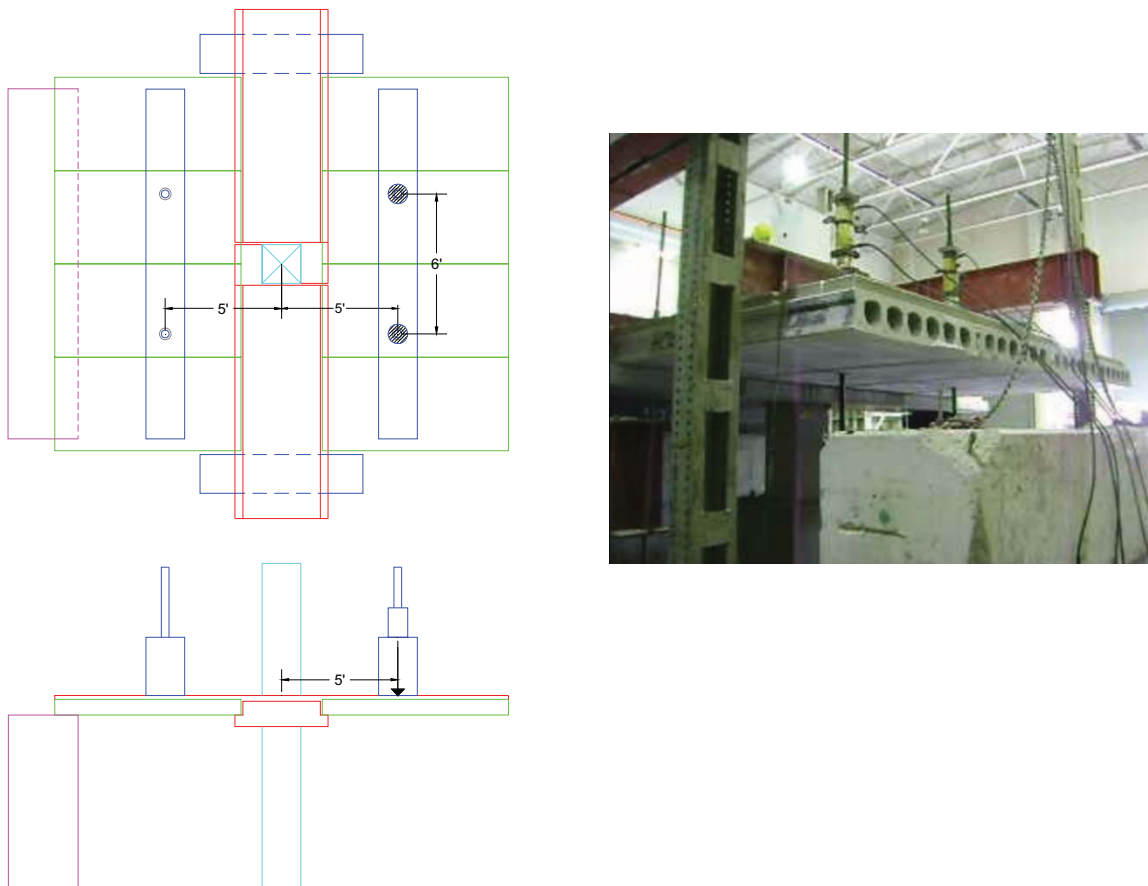


Figure 6.6: Test setup for evaluating HC negative moment capacity

Figure 6.7 plots the load-deflection relationship of this test. This plot indicates that the four composite HC planks were able to carry 61 kip, which corresponds to a total negative moment capacity of 250 kip.ft (including the moment due to the weight of the cantilevered HC). The demand for resisting lateral loads in the example building is 126 kip.ft, which is 50% less than the actual capacity. Also, the nominal capacity of the composite HC planks predicted using strain compatibility approach was found to be 181 kip.ft, which is significantly below the actual capacity. Figure 6.8 shows the cracking of the topping concrete under ultimate loads. The specimen was not loaded to failure to maintain its integrity for further testing.

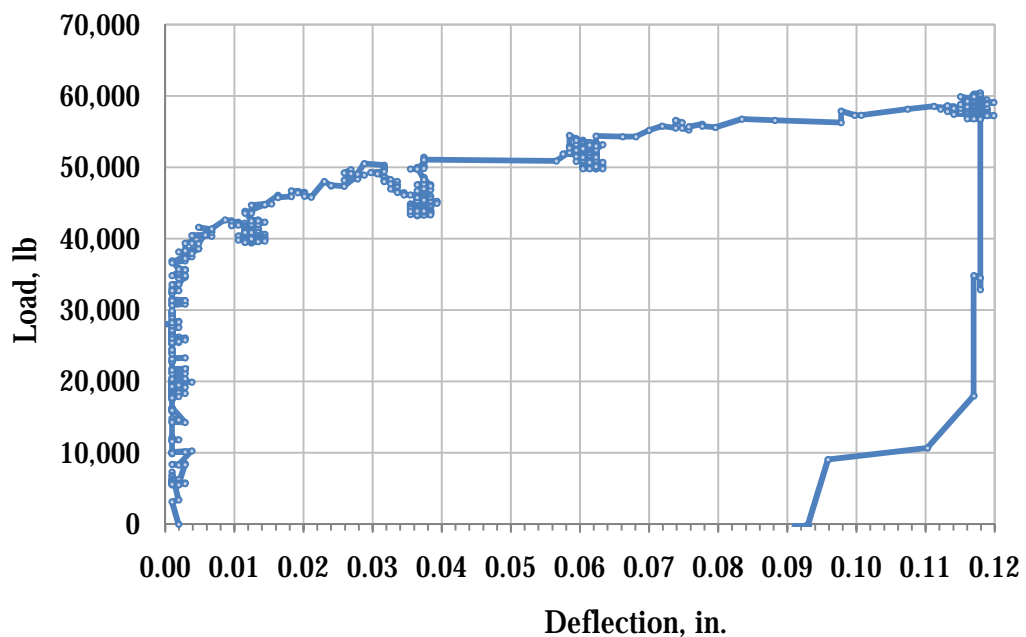


Figure 6.7: Load-deflection curve for the HC negative moment capacity test

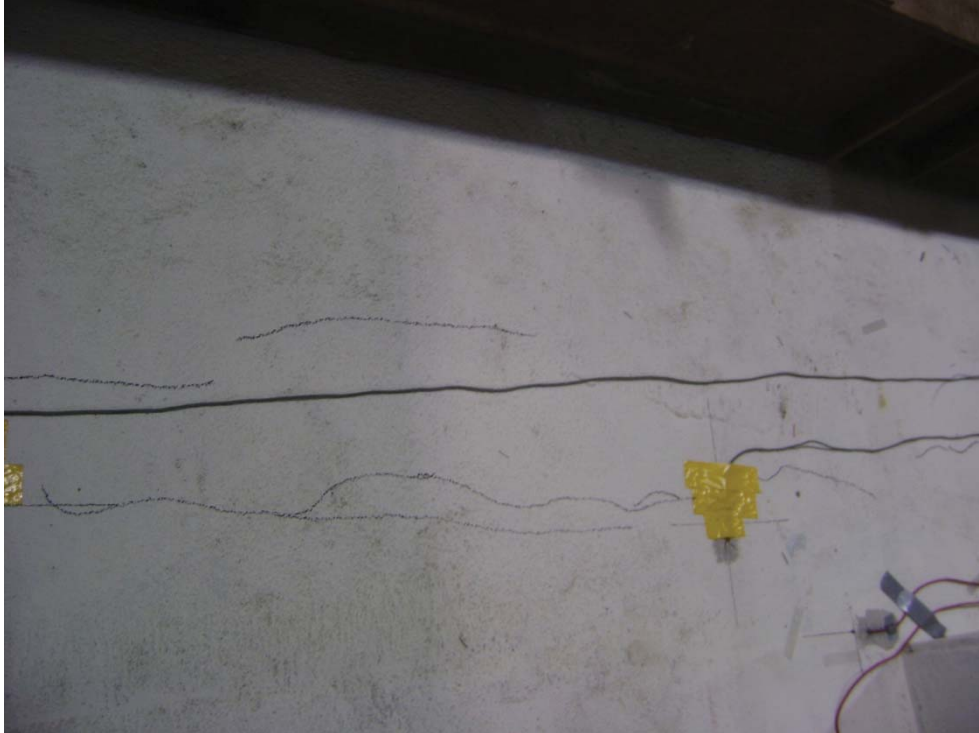


Figure 6.8: Cracking of the topping concrete at HC ultimate load

6.2.4.2 Beam Negative Moment Capacity

The purpose of this test is to evaluate the negative moment capacity at the end section of the composite beam. Figure 6.9 shows the test setup, where the load was applied at the unsupported end of the beam while clamping the other end to prevent tipping over. One 400 kip jack was used to apply a concentrated load on the beam at 9 ft from the centerline of the column, up to the nominal capacity, while measuring the deflection of the cantilevered end.

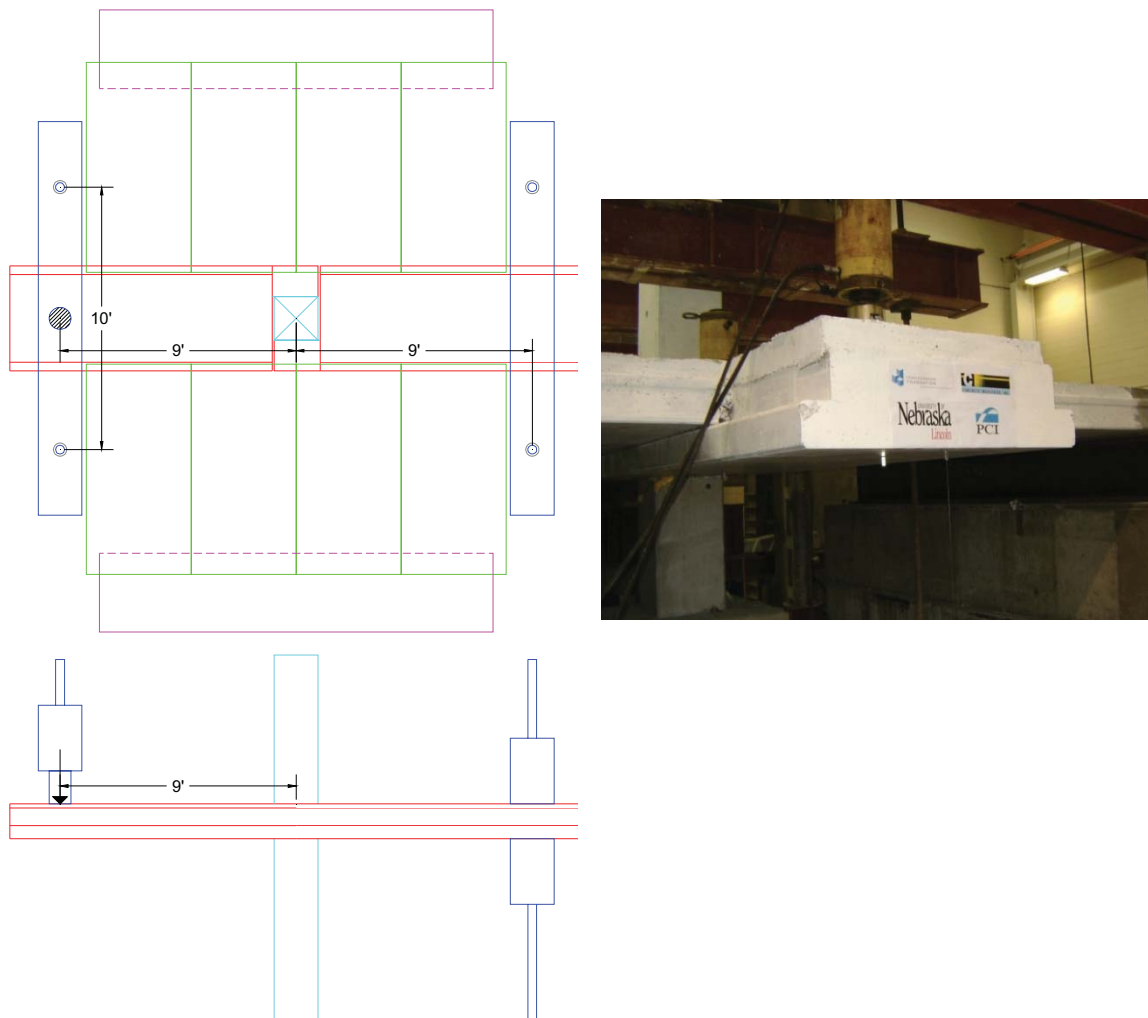
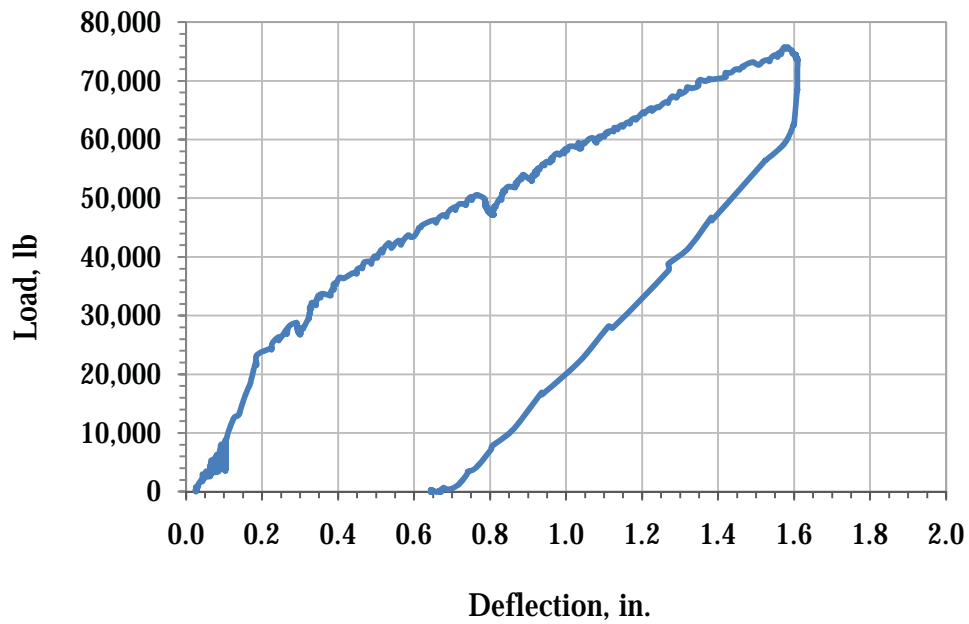


Figure 6.9: Test setup for evaluating beam negative moment capacity

Figure 6.10 shows the load-deflection relationship for this test. This plot indicates that the beam was able to carry a load up to 76 kip, which corresponds to a negative moment capacity at the critical section of 672 kip.ft (including the moment due to the weight of the cantilevered beam). The ultimate factored negative moment due to topping weight and live load was found to be 600 kip.ft, which is 11% below the actual section capacity. Also, the nominal capacity of the composite beam predicted using strain compatibility approach was found to be 667 kip.ft, which is very close to the actual capacity. Figure 6.11 shows the cracking of the top flange at the critical section under ultimate loading.



Figure

6.10: Load-deflection curve of beam negative moment capacity test

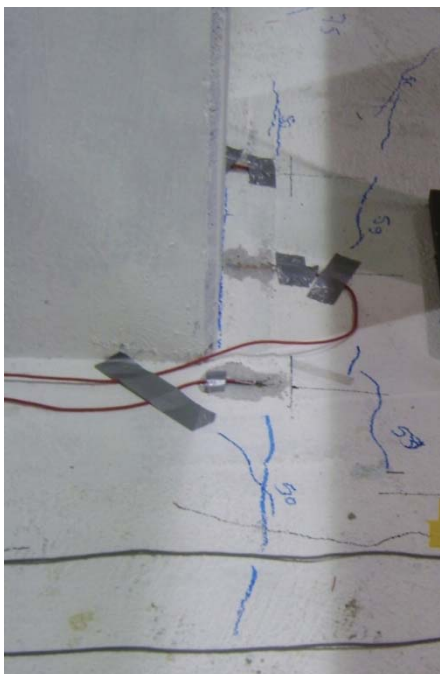


Figure 6.11: Cracking of the topping concrete at beam ultimate load

6.2.4.3 Beam Positive Moment Capacity

The purpose of this test is to evaluate the positive moment capacity of the beam end section for lateral load resistance. Figure 6.12 shows the test setup, where the load was applied upwards at the cantilevered end of the SIT beam. One 400 kip jack was used to apply a concentrated load at 9 ft from the centerline of the column up to the nominal positive moment capacity of the end section. Upward movements of the cantilevered end were recorded while loading.

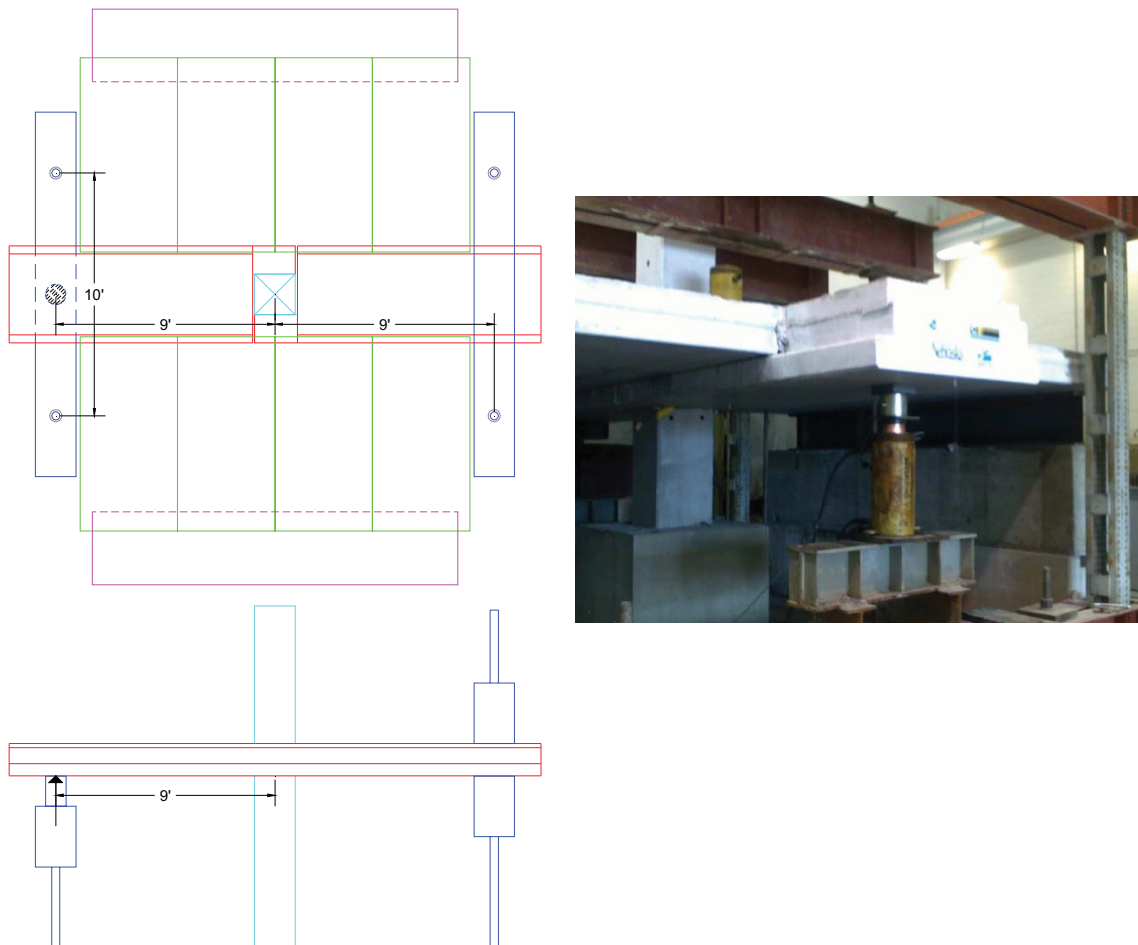


Figure 6.12: Test setup for evaluating the SIT beam positive moment capacity

Figure 6.13 shows the load-deflection curve for the beam positive moment capacity test. Cracking load was found to be 17 kip, while the maximum load was 26 kip, which corresponds to a positive moment capacity of 162 kip.ft at the critical section. This load was stopped at this value because the column base started to rise up as it was not fully anchored to the floor. This value is 40% higher than the demand (115 kip.ft) and 6% higher than the nominal capacity calculated using strain compatibility approach. Figure 6.14 shows the cracked HC soffit at the ultimate load.

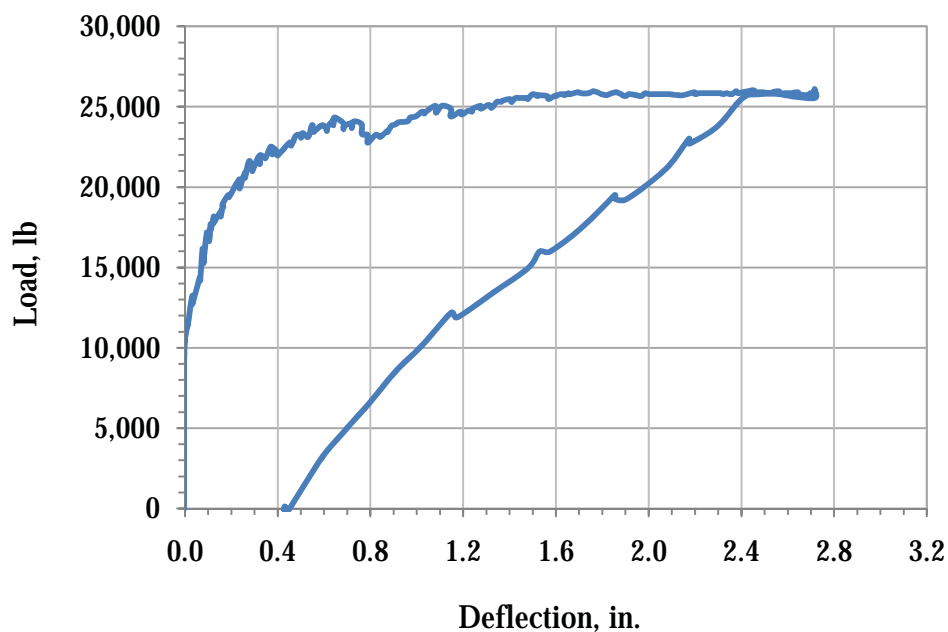


Figure 6.13: Load-deflection curve for SIT beam positive moment capacity test



Figure 6.14: Cracking of the HC soffit at ultimate load

6.2.4.4 Beam-Column Connection Shear Capacity

The purpose of this test is to evaluate the shear capacity of the modified Beam-column connection without corbel. Figure 6.15 shows the test setup, where the beams are loaded symmetrically at 3 ft from the centerline of the column on each side similar to corresponding test of the first specimen. The other end of the beams and HC planks were simply supported to stabilize the specimen. Two 400-kip loading jacks and two 12 in. square loading plates were used to apply the load on the top surface of the concrete topping up to failure.

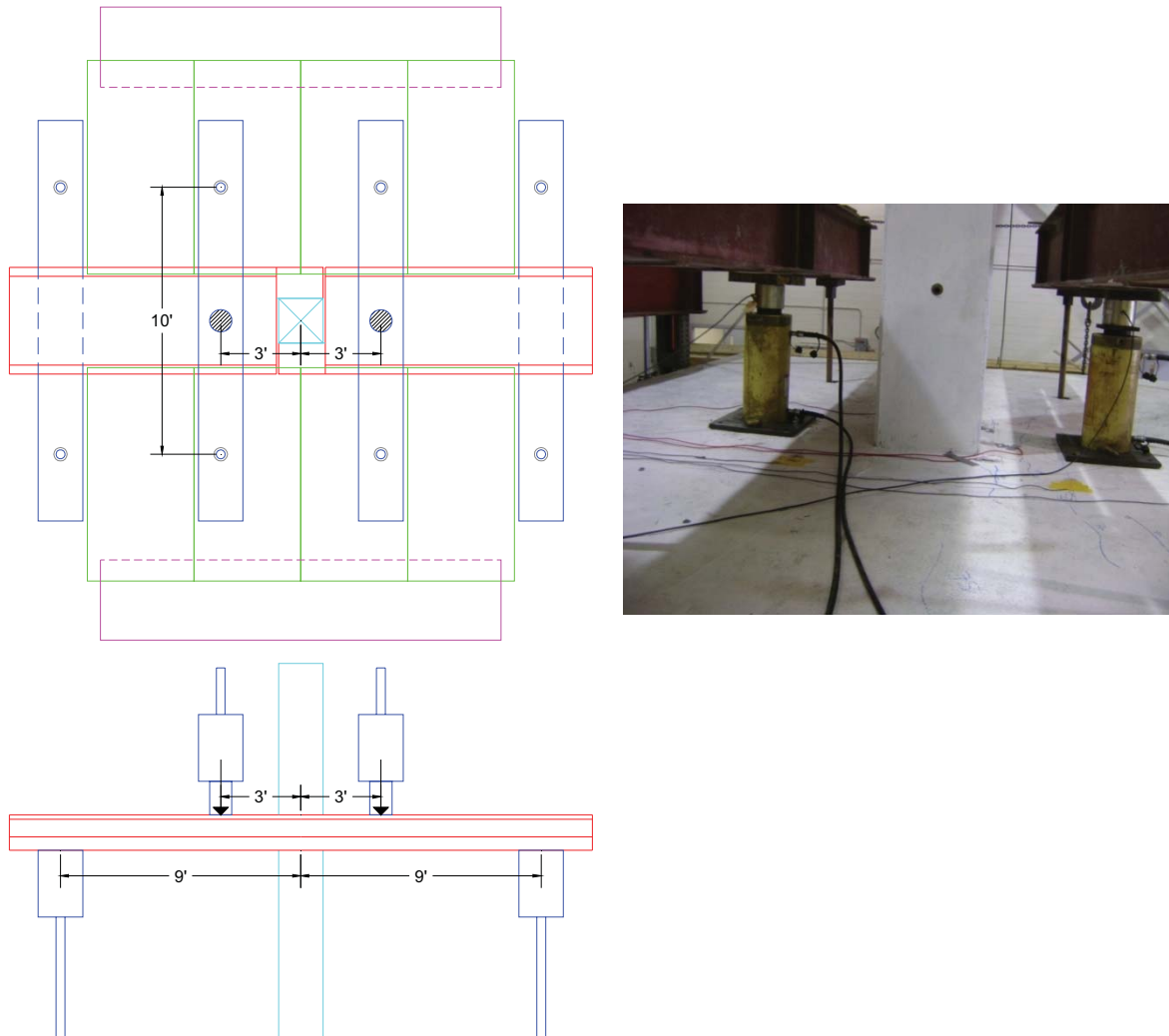


Figure 6.15: Test setup for beam-column connection shear capacity

Figure 6.16 shows load-deflection curve of that test. This curve indicates that the maximum load was 704 kip, which results in a shear force (627 kip) that is significantly higher than demand of 32 ft x 32 ft bay size loaded with 100 psf live load (308 kip) and the capacity calculated based on shear friction theory (460 kip). It should be noted that this test was performed on a cracked specimen as the beam was already tested for both positive and negative moment continuity. Figure 6.17 shows the failure mode of the specimen

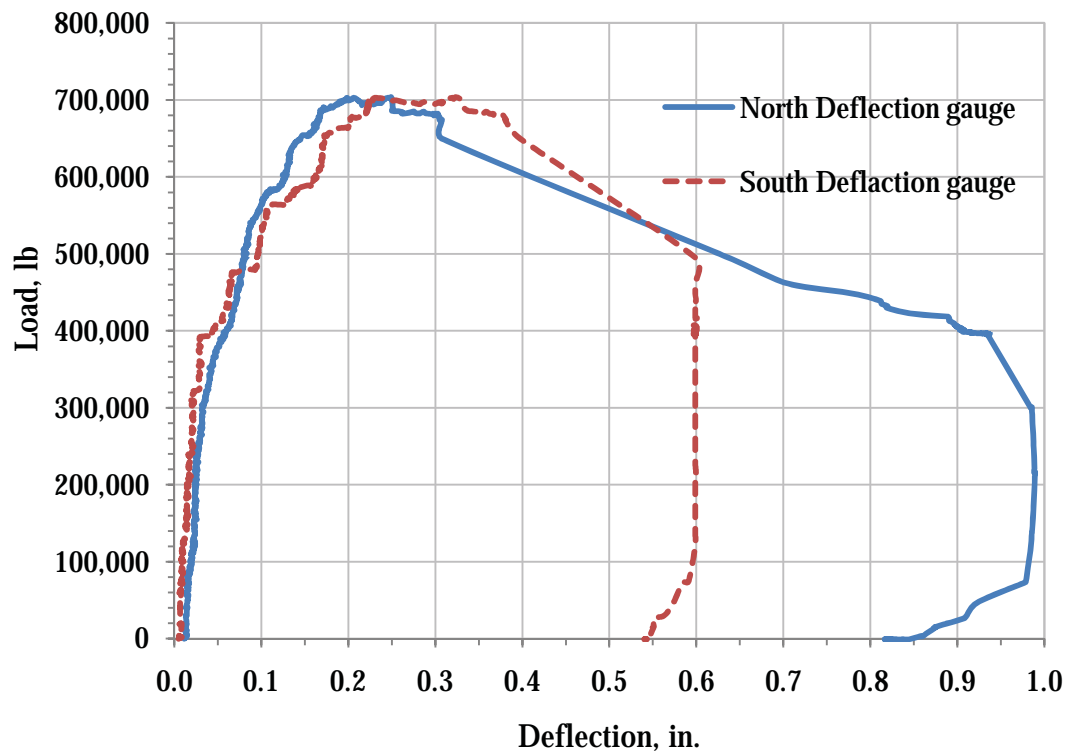


Figure 6.16: Load-deflection curve for testing beam-column connection



Figure 6.17: Failure of beam-column connection

Table 6.7 summarizes the demand, theoretical capacity, and measured capacity of the beam-column connection without corbel test. It also presents the ratios of experimental-to-theoretical capacity for each test. Based on the test results summarized in Table 6.7, the following conclusions can be made:

1. The proposed beam continuity system has adequate flexural capacity at the positive and negative moment sections to resist both gravity and lateral loads. This capacity can be accurately predicted using strain compatibility approach.
2. The proposed beam-column connection without corbel has adequate capacity to carry gravity loads even after cracking. This capacity can be accurately predicted using shear friction theory.
3. The proposed composite HC continuity system has adequate negative moment capacity to resist lateral loads. This capacity can be accurately predicted using strain compatibility approach.

6.2.5 Beam-Column Connection without Corbel Application

After the beam-column connection test was done and all the test results have been pass the design values, the concept was used in real building. Farmer's mutual building is a building under construction, which used the same technics and design. The building locates at 1220 Lincoln Mall, Lincoln, NE 68508 (the southwest corner of 13th St. and K St). The design of the building was prepared by Concrete Industries, Inc. Nebraska and e. Construct USA, LLC, Nebraska. Figure 6.18 and Figure 6.19 shows elevation view for that building and one connection details used in that building. Also Figure 6.20 shows some pictures for the building under construction.

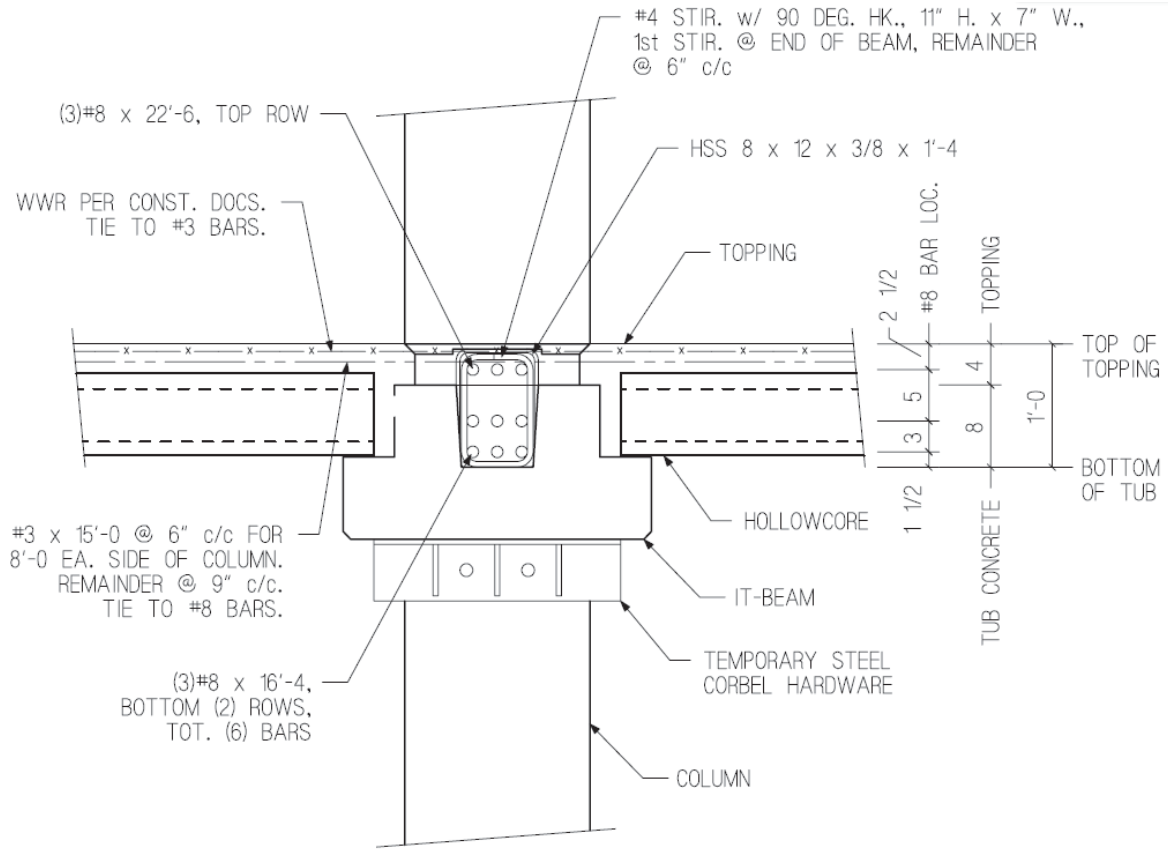


Figure 6.19: connection details





Figure 6.20: Under construction pictures for Farmer's mutual building

6.3 HC-beam Connection without Ledge

This section presents the experimental investigation carried out to evaluate the shear capacity of the HC-beam connection without ledge constructability and its performance.

In this test, the full-scale specimen consisted of 28 ft long beam that is 10 in. thick and 48 in. wide and twelve 6 ft long HC planks that are 10 in. thick and 48 in. wide each. The beam was supported by three roller supports that are 13.75 ft center to center. That test represent approximately 16 ft x 28 ft segment of the floor around an interior beam as shown in Figure 6.21. Specimen components, which include precast beam segment, and

12 HC planks, were fabricated by EnCon, Denver, Colorado and Concrete Industries (CI) Inc., Lincoln, NE respectively and erected and tested at the Structural Laboratory of Peter Kiewit Institute (PKI) Omaha, NE.

6.3.1 Specimen Design

The experimental test is focus in four different beam-HC connections. In order to investigate all these connection in the same test, the flat soffit beam was fabricated with two different sides; 1) side with shear key, and 2) side with hidden corbel. The temporary supports for HC planks were erected using two alternatives: 1) $\frac{3}{4}$ in. coil inserts embedded in the beam during the fabrication process to connect the threaded rods holding 5 ft long 4 in. x 4 in. x $\frac{1}{8}$ in. HSS and; 2). Two steel angles 4 in x 3 in. x $\frac{3}{8}$ in. were welded to side beam plates which installed during the fabrication process to acts as temporary supports and theses angles will not be moves at final stages. Each one from the two alternatives temporary HC support was used in half of flat soffit beam span. The HC have 1 ft slots in the top surface of two holes as shown in Figure 6.22. The HC key way and the two slots allowed placing the connection reinforcements.

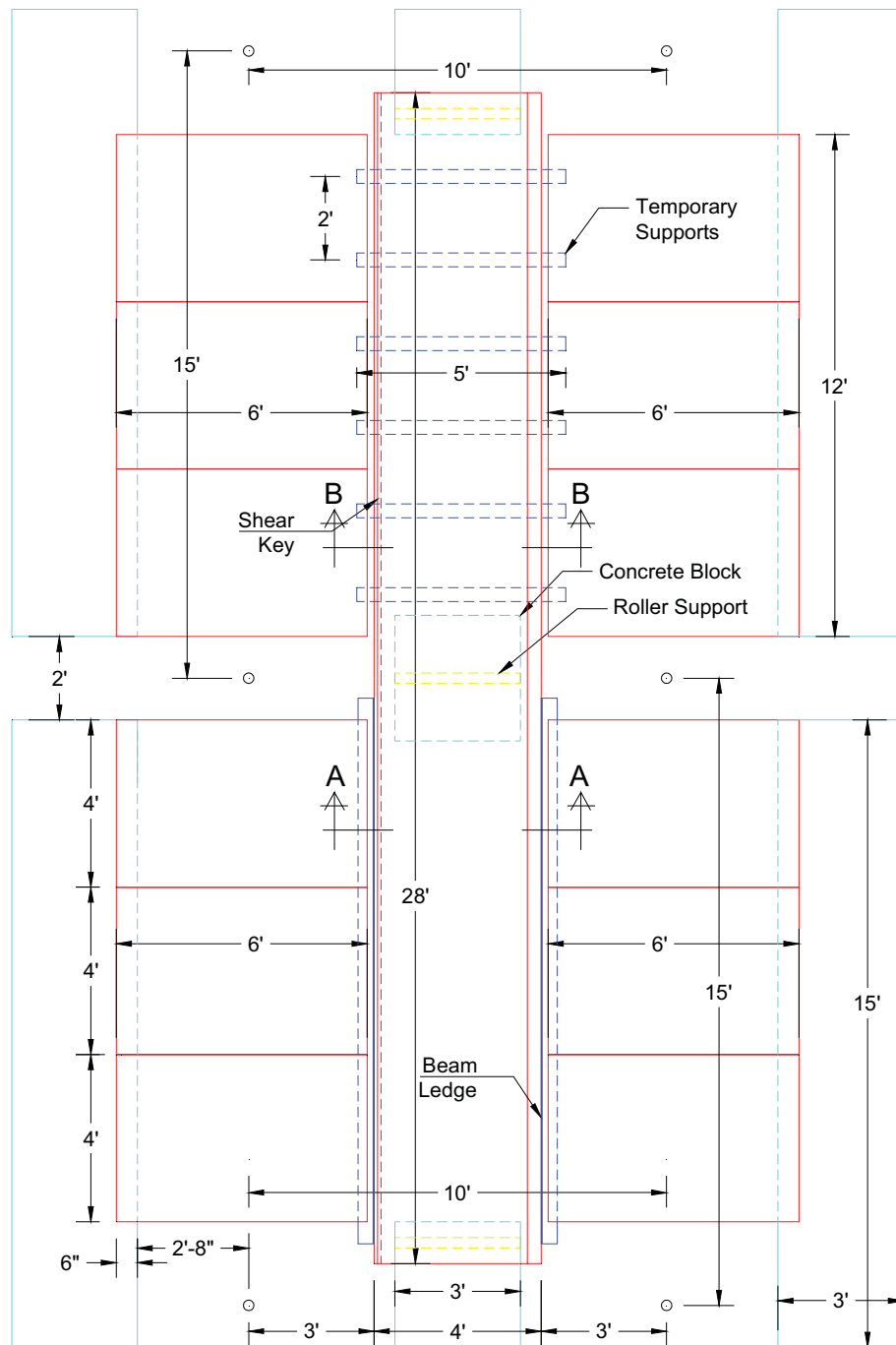


Figure 6.21: Plan view of the precast components of test specimen

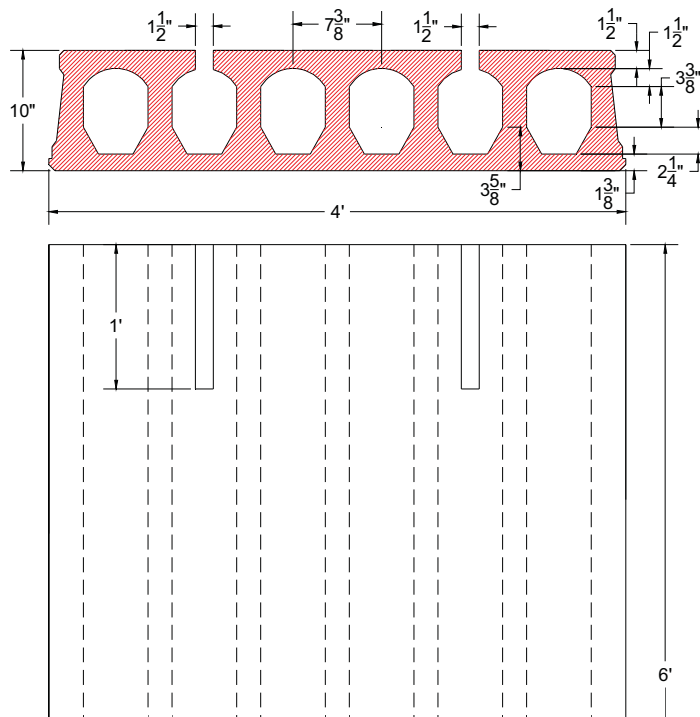
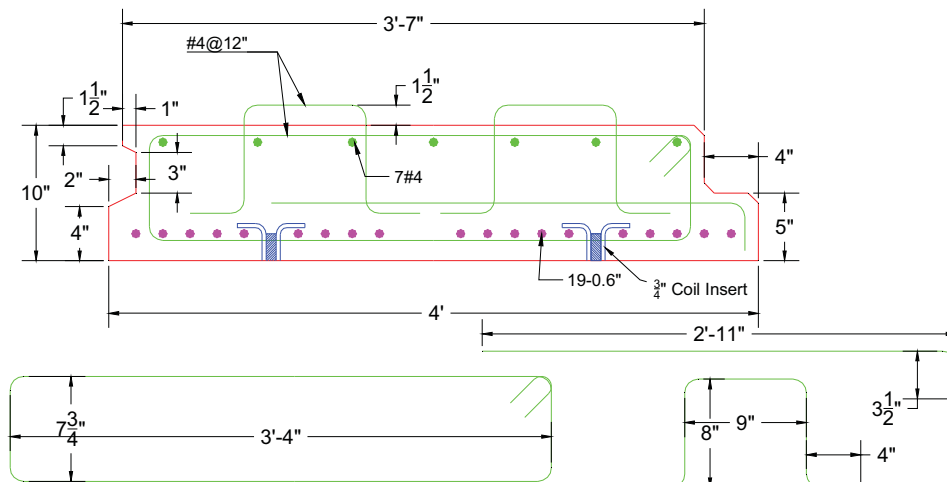


Figure 6.22: Dimensions and details of the HC specimen

Based on the design procedure shown in chapter 5 and appendix A, the HC- beam connection reinforcement were found to be #5 hat bars and #3 loop bars as shown in Figure 6.23 , which installed in each HC key way and HC slots. The factored nominal shear capacity of the HC- beam connection using shear friction theory was found 34.875 kip per each hollow core-to-beam connection, while the ultimate shearing force value due to dead and live loads was 16.5 kip.

Figure 6.24 shows the beam Dimensions and reinforcement details Figure 6.25 shows the connection details used in that test.



Section B-B

Figure 6.24: Dimensions and reinforcement details of the beam of the first specimen

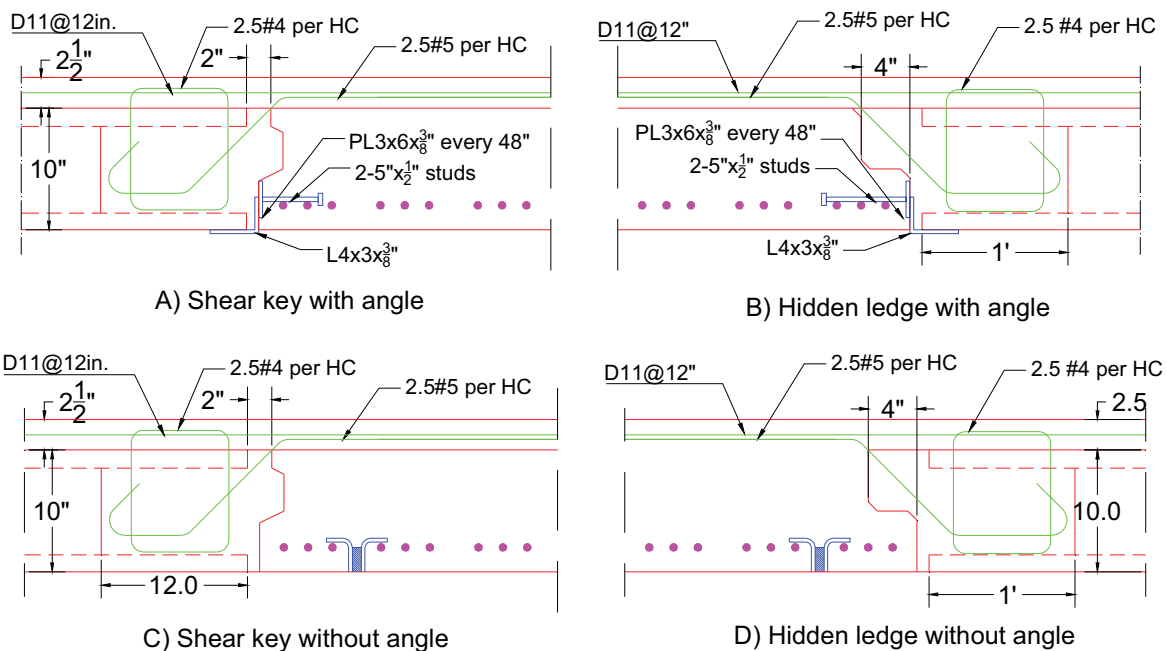


Figure 6.25: Details of the tested four HC-beam connections

The following subsection describes in details the specimen design and fabrication and tests

6.3.2 Specimen Fabrication and Erection

The beam was fabricated at EnCon, Denver, Colorado and 12 HC planks were fabricated at Concrete Industries Inc, Lincoln, Nebraska. The beam was reinforced using 19-0.6 in. diameter strands to investigate the positive moment capacity of the beam. HC planks were poured during the regular HC production. The beam fabrication pictures will be presented in appendix D. Below are the steps followed in the specimen erection, while the pictures of the erection process shown in appendix E.

Step 1) After the beam delivered to the structural lab, the beam was placed on the three roller supports.

Step 2) The beam was divided into two parts each part 14 ft. In the first half, two steel angles 3 in. x 4 in. x 3/8 in. are used as beam ledges for supporting HC planks in construction stage. The two angles are welded to beam side plates, which attached to the precast beam in the fabrication process. In the second half, HSS tubes 4 in. x 4in. x 0.1/8 in. are used to work as temporary ledges for supporting HC planks. These sections are connected to the bottom of the precast beam using 3/4 in. coil inserts and threaded rods.

Step 3) HC openings were plugged to prevent the flow of concrete inside the HC as shown in Figure 6.26 especially when a flowable concrete is used



Figure 6.26: Blocking the HC openings before erection

Step 4) Six HC planks were erected on each side of the beam as shown. The erection sequence was set to test the torsional capacity of the beam when loaded from only one side.

Step 5) Installed beam-HC connection reinforcing such as hat and loop bars reinforcement. The hat bars connecting the HC planks to the beam are placed over the beam at the HC keyways and slots. The loops placed in the HC hole opening to connecting the HC planks to the topping. Thirty-two strain gauges were placed in that test. Eight strain gauges in each corner, which are classified three in the hat bars (H), three in the loop bars (L), and two the topping reinforcement (T) as shown in Figure 6.27

Step 6) The HC keyways, HC opening, shear key between the HC and the beam were grouted. Grout (6 ksi) was delivered from Ready Mix.

Step 7) Welded wire reinforcement mesh was placed over the HC planks to reinforce the composite topping. D11 @6 in. WWR required to provide HC continuity for lateral load were placed at the top of the HC.

Step 8) The topping concrete was poured using a ready mix concrete with 8 in. slump.

Step 9) After the topping concrete was cured and hardened, the temporary ledges angles were removed and the specimen was ready for testing.

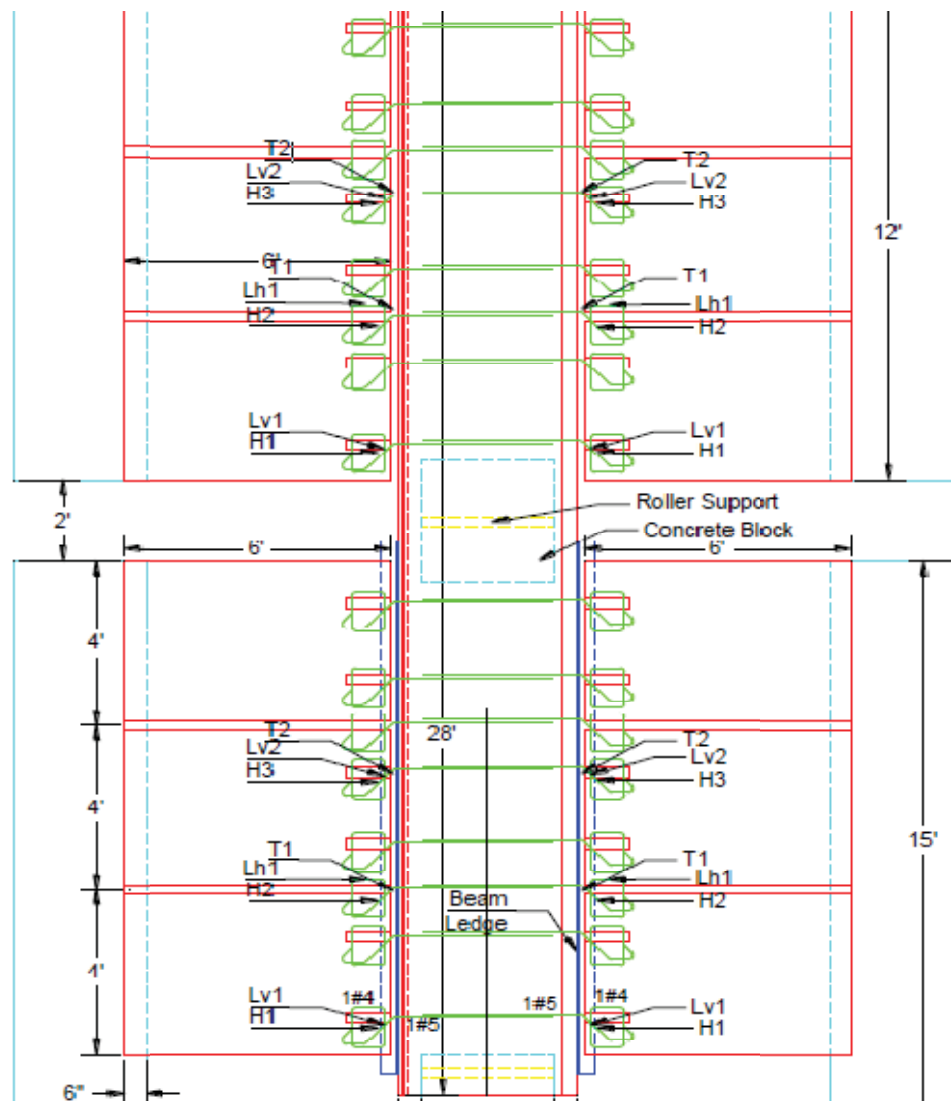


Figure 6.27: Strain gauges locations

6.3.3 Material Properties

Table 6.8 shows the mix design for the precast, grout and topping concrete used in that specimen. Figure 6.28 shows the gain of compressive strength with time for the precast, grout, and topping concrete up to the time of testing. Table 6.9 lists the actual and specified compressive strength of the concrete used in the production of the specimen components at the time of testing. This table indicates that the actual compressive strength of all components at the time of testing was satisfactory as it exceeded the specified strength.

Table 6.8: Concrete mixes design

Materials	Precast Components Mix	Grout Mix	Topping Mix
	Weight (lb) per cubic Yards		
Portland Cement Type I/II	755*	650	611
Fly Ash, Class C	0	100	-
Limestone 1/2"	1620	1265	950
47B Sand and Gravel	1405	1875	2190
Total Water	292	225	275
Water Reducer PS 1446	88 oz/cwt	-	-

* Type III cement

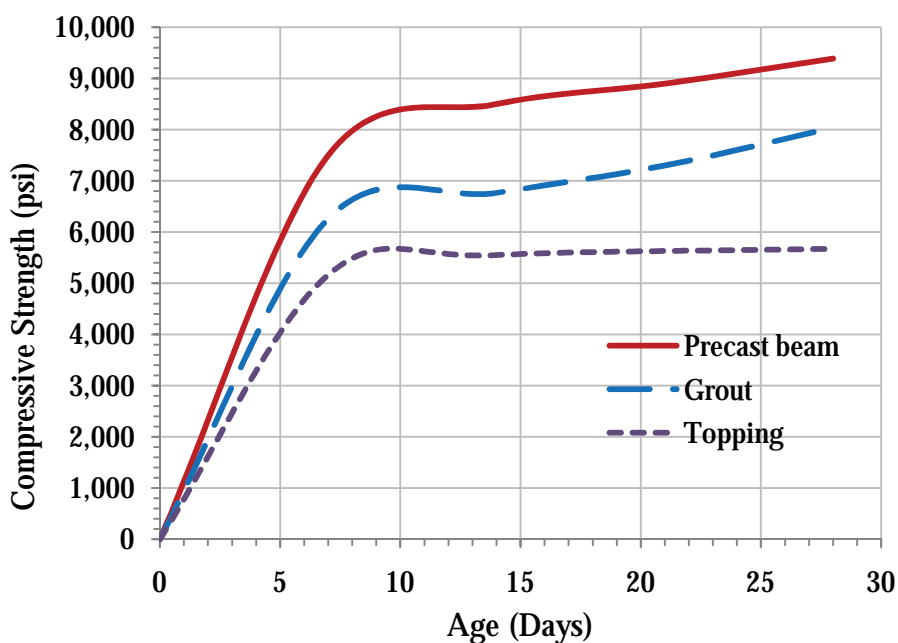


Figure 6.28: Concrete strength gain with time

Table 6.9: Specified and actual concrete compressive strength at testing

Components	Actual strength (psi)	Specified strength (psi)
Precast	9,390	8,000
Grout	8,037	4,000
Topping	5,678	3,500

6.3.4 Test Setup and Procedures

Testing the full-scale specimen was performed on January 25, to 31, 2011. The test program includes the following three tests:

- 1) Testing HC-beam connection
 - A. Hidden corbel with angle (North-West Side)
 - B. Shear key with angle (North-East side)
 - C. Hidden corbel without angle (South-West Side)
 - D. Shear key without angle (South-East Side)
 - E. Testing HC-beam connection by loading HC as cantilever
- 2) Testing the beam flexural capacity by loading at mid-span

6.3.4.1 Testing HC-beam Connection

The purpose of this test is to evaluate the shear capacity of the HC-beam connections under gravity loads. The HC planks were loaded at their mid-span in one side while clamping the other side of the beam to maintain specimen stability. Testing was performed using two jacks applying two concentrated loads to a spread steel beam to create uniform load on the HC planks at 3 ft away from the HC-beam connection as shown in Figure 6.29 . Loading continued to failure while measuring the deflection under the load using potentiometer attached to the soffit of the middle HC plank. The HC-beam connection was tested in two stages. In the first stage, HC planks were loaded up to 100 kip (50 kip each side), which creates a shearing force at the connection of 16.5 kip. This value is the ultimate shearing force due to factored dead and live loads.

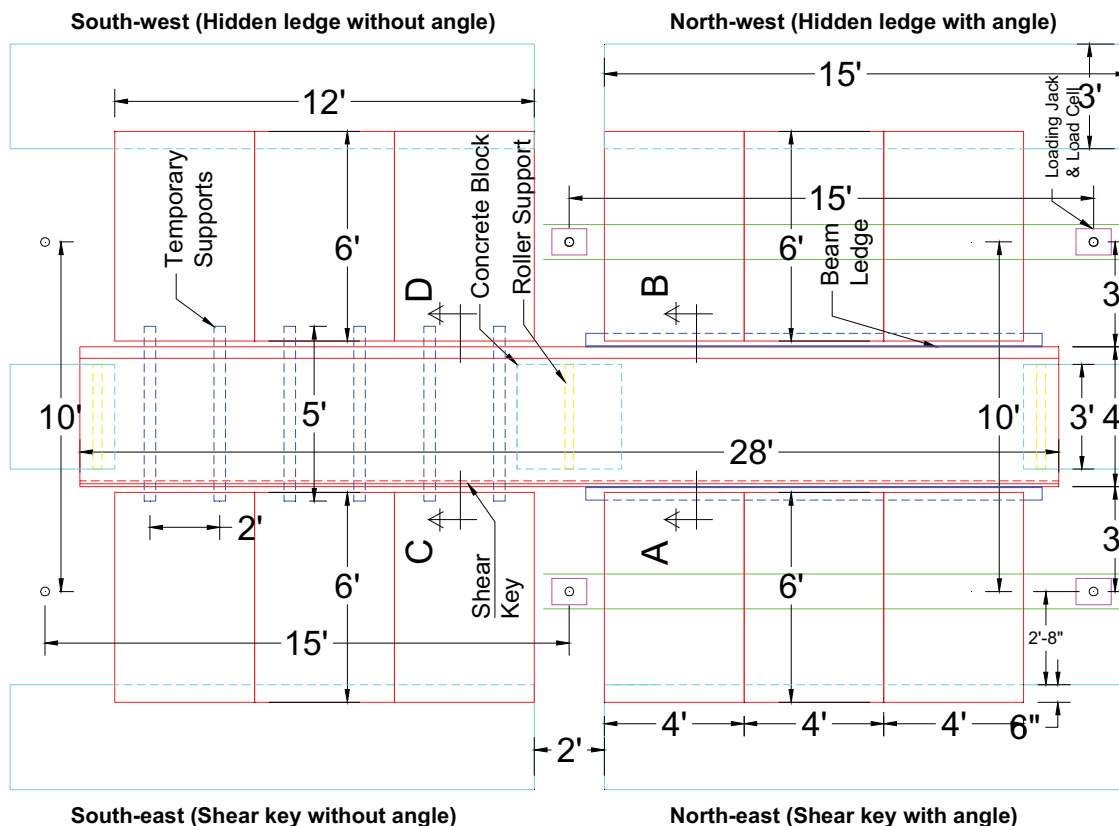


Figure 6.29: Plan view for the test specimens shows the four connections

In the second stage, HC planks were loaded up to the failure. The factored load applied to shear the HC-beam connection using shear friction theory was predicted to be 209 kip (104.5 kip each side, which is 34.9 kip per HC). Also, the factored loads applied to fail the composite HC planks in flexure and shear were predicted to be 315 kip (157.5 kip each side, which is 52.5 kip per HC) and 240 kip (120 kip each side, which is 40 kip per HC) respectively. Figure 6.30 shows the test setup as simple support.

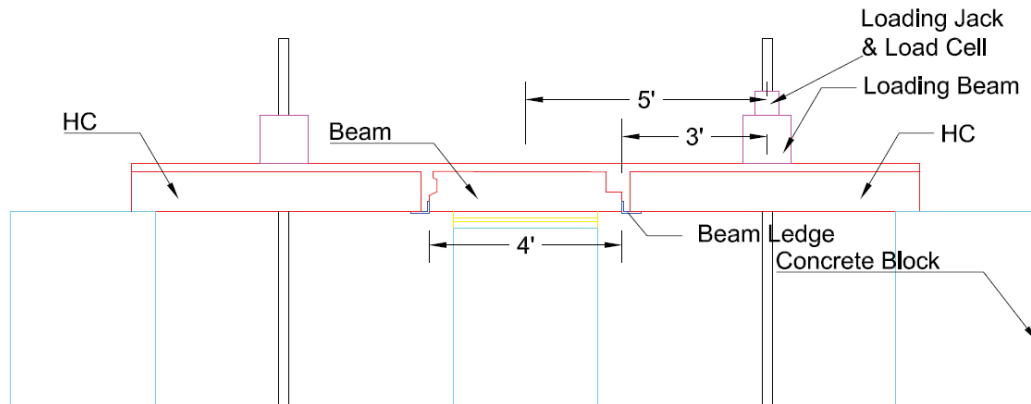


Figure 6.30: HC-beam connection setup

A. Hidden Corbel with Angle (North-West)

Two 130 kip jacks were used to test the connection. In the first stage of loading, the specimen performed well under ultimate design load with no signs of failure or cracking. In the second stage, HC planks were loaded up to 258 kip (129 kip each side). The test was stopped after reaching the ultimate load capacity of the used jacks. The applied load creates a shearing force at the hollow core-to-beam connection of 43 kip. This value is almost 2.6 times the demand and 12 % more than the design capacity of the connection. At that load, the connection did not crack, while small shear cracks were observed in the other end of HC.

B. Shear Key with Angle (North-East)

Two 400 kip jacks were used in this test. The specimen performed well under ultimate design load with no signs of failure or cracking. In the second stage, HC planks were loaded up to 240 kip (120 kip each side) without even cracking the connection. The test was stopped due to the shear failure of HC planks as shown in Figure 6.31 . The applied load created 40 kip shearing force on each HC. This value is almost 2.4 times the demand and 15 % more than the design capacity of the connection.



Figure 6.31: Failure of the HC at the critical section under ultimate loading

C. Hidden Corbel without Angle (South-West)

Two 400 kip jacks were used in this test. The specimen performed well under ultimate design load with no signs of failure or cracking. In the second stage, HC planks were loaded up to 204 kip (102 kip in each side) without even cracking the connection. The test was stopped because of the shear failure of HC planks as shown in Figure 6.32. The applied load created 34 kip shearing force on each HC. This value is almost 2.1 times the demand and equal to the design capacity of the connection.



Figure 6.32: Failure of the HC at the critical section under ultimate loading

D. Shear Key without Angle (South-East)

Two 130 kip jacks were used in this test. The specimen performed well under ultimate design load with no signs of failure or cracking. In the second stage, HC planks were loaded up to 227 kip (113.5 kip each side) without even cracking the connection. The test was stopped due to the shear failure HC planks as shown in Figure 6.33. The applied load created 37.8 kip shearing force on each HC. This value is almost 2.3 times the demand and 8 % more than the design capacity of the connection.



Figure 6.33: Failure of the HC at the critical section under ultimate loading

Figure 10 presents the load deflection relationships of the four tested connections. Also the strains in the connection reinforcement, which recorded by the strain gauges during the test were found very small.

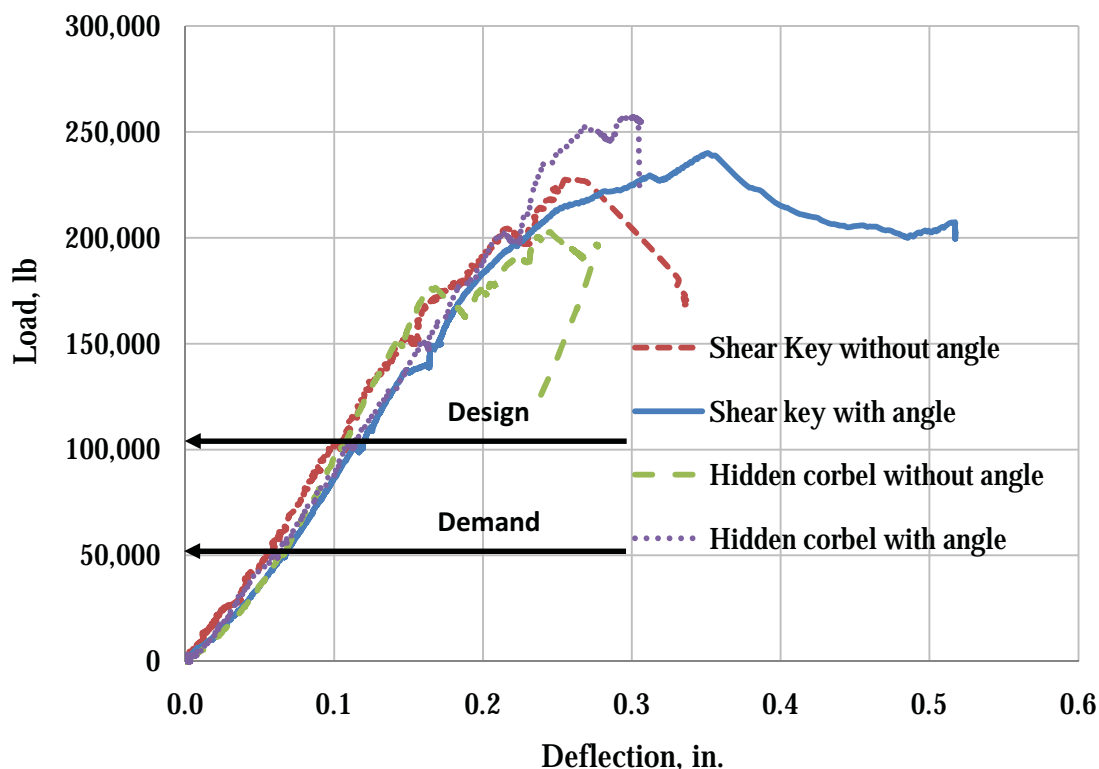


Figure 6.34: Load-deflection relationships of the four tested connections

E. Testing HC-Beam Connection by Loading HC as Cantilever

In the entire previous, the tests were done by applied the load at the mid span of the HC, and the failure occurred in the HC without even cracking the connections. Therefore, in order to investigate the full shear capacity of the connection, the HC was loaded as a cantilever. Figure 6.35 shows the test setup, where HC planks were loaded on the free end (south-west side) while clamping the other end (south-east side) to maintain specimen stability. Testing was performed to the hidden ledge connection without angle by applying a uniform load on the cantilevered HC at 4 ft from the centre of the beam,

while measuring the deflection at mid-span of the HC. The clamped side was clamped at 5 ft from the centre of the beam.

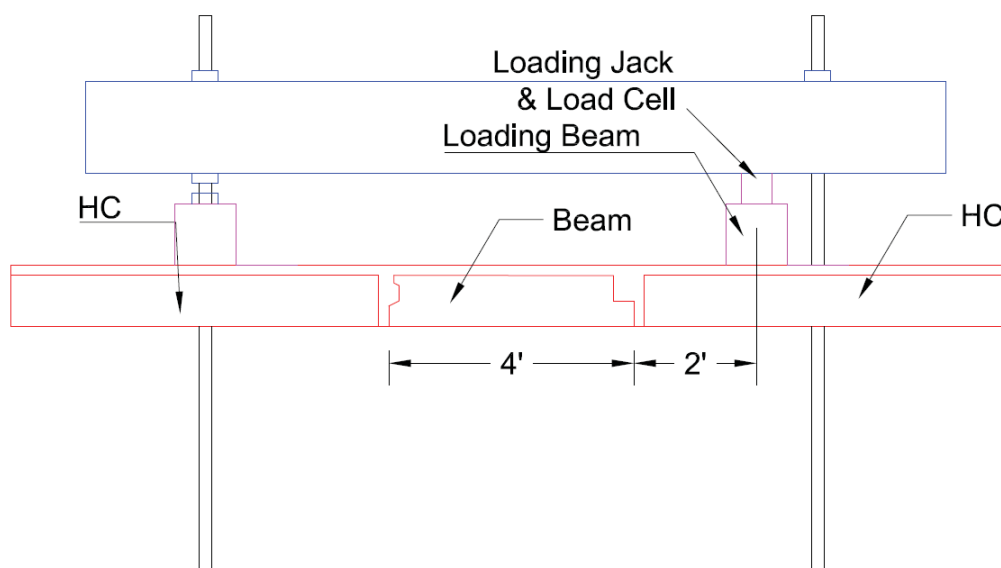


Figure 6.35: HC-beam connection setup by loading HC as cantilever

Figure 6.36 plots the load-deflection relationship. This plot indicates that the three composite HC planks in the south-west side were able to carry 140 kip, which corresponds to a total shear force 147.7 kip includes the self-weight of the HC and topping (49.2 kip per HC). This is almost 3 times the demand and 40% more than the design capacity of the HC-beam connection.

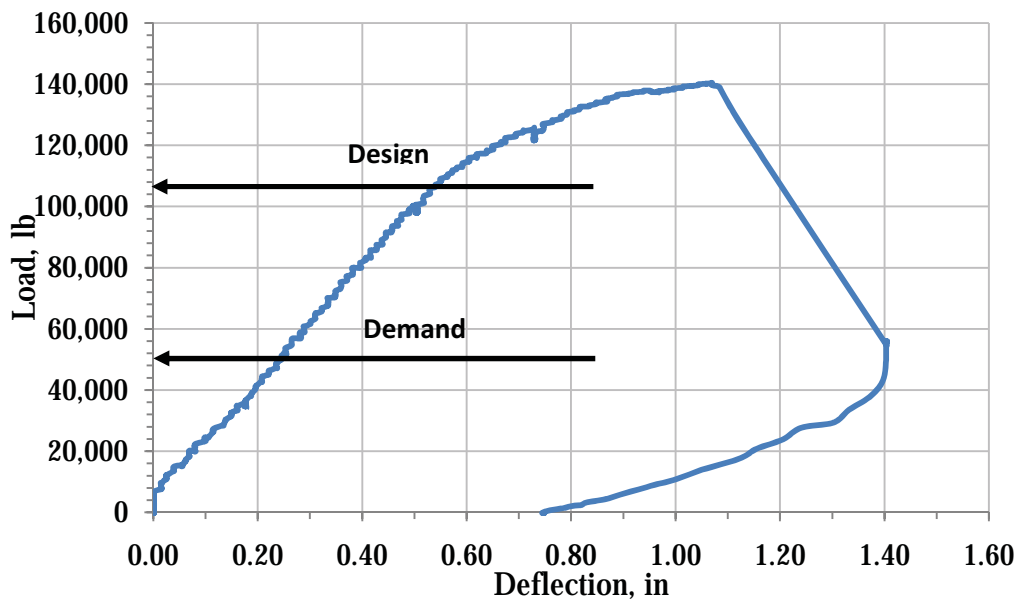


Figure 6.36: Load-deflection curve of HC-beam connection when tested as cantilever

Figure 6.37 plots the load-strain relationships for connection reinforcement, which indicate that the topping reinforcement and hat bars reached the yield stress. The test was stopped due to the shear failure of the HC at the clamped side and severe cracking of the connection. Table 6.10 summarize the previous HC-beam connections test results

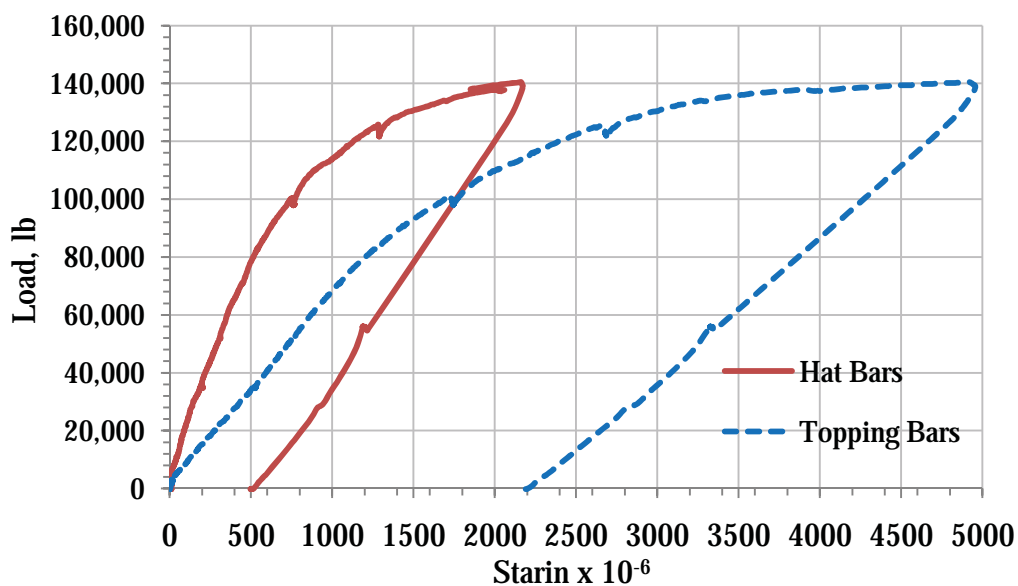


Figure 6.37: Load-strain relationships of HC-beam connection when tested as cantilever

Table 6.10 summarizes the demand, normal capacity, and measured capacity of the previous HC-beam connections test results the following summary can be made

Table 6.10: Summary results for HC-beam connections tests

Test ID	Test Title	Max. applied load (kip)/HC	Theoretical Capacity (kip)/HC	Demand (kip)/HC	HC Shear Capacity (kip)	Observation
A	Hidden ledge with angle (Three point loading)	43.0	34.9	16.5	40.0	Test stopped because of reaching the capacity of the loading jacks
B	Shear key with angle(Three point loading)	40.0				HC shear failure
C	Hidden ledge without angle (Three point loading)	34.0				HC shear failure
D	Shear key without angle(Three point loading)	37.8				HC shear failure
E	Hidden ledge without angle (HC loaded as cantilever)	49.2				HC shear failure and several cracks in the connection

1. All proposed HC-beam connections without ledge (shear key and hidden ledge with and without angles) performed very well as their shear capacity exceeded the predicted values and significantly exceeded the demand. None of these connections has failed as the tested HC planks failed in shear prior to the failure of the connections
2. The capacity of the proposed HC-beam connections without ledge can be accurately predicted using shear friction theory.
3. Since the shear capacity of the HC-beam connections without steel angle was adequate, steel angles are considered as temporary ledges that do not affect the fire rating of the building
4. The results of testing full-scale specimen do not only indicate the efficiency of the proposed system but also the consistency of its performance.

6.4 Testing the Flat Soffit Beam Flexural Capacity

The purpose of this test is to evaluate the positive moment capacity at the mid-section of the composite beam. One 400-kip jack was used to apply a concentrated load on the beam at 13.75 ft from the center line of roller supports as shown in Figure 6.38 , up to failure, while measuring the deflection under the load.



Figure 6.38: Flat soffit beam flexural test setup

Figure 6.39 shows the load-deflection relationship. The load-deflection relationships show a linear behavior up to the cracking load, which was approximately 50 kip. This plot indicates that the beam was able to carry a load up to 91 kips, which corresponds to a positive moment capacity at the critical section of 733 kip.ft (including the moment due to the self-weight of beam, HC, and topping). The ultimate positive moment due to factored dead and live loads was calculated to be 565 kip.ft (demand), which is 30% below the measured capacity. The nominal capacity of the composite beam predicted using strain compatibility approach was found to be 678 kip.ft, which is very close to the actual capacity. It should be noted that the point load equivalent to service load is approximately 49 kip and the corresponding final deflection is approximately 0.74 in.,

while the allowable deflection equal to 0.93 in. Figure 6.40 shows the flat soffit beam failure under flexural.

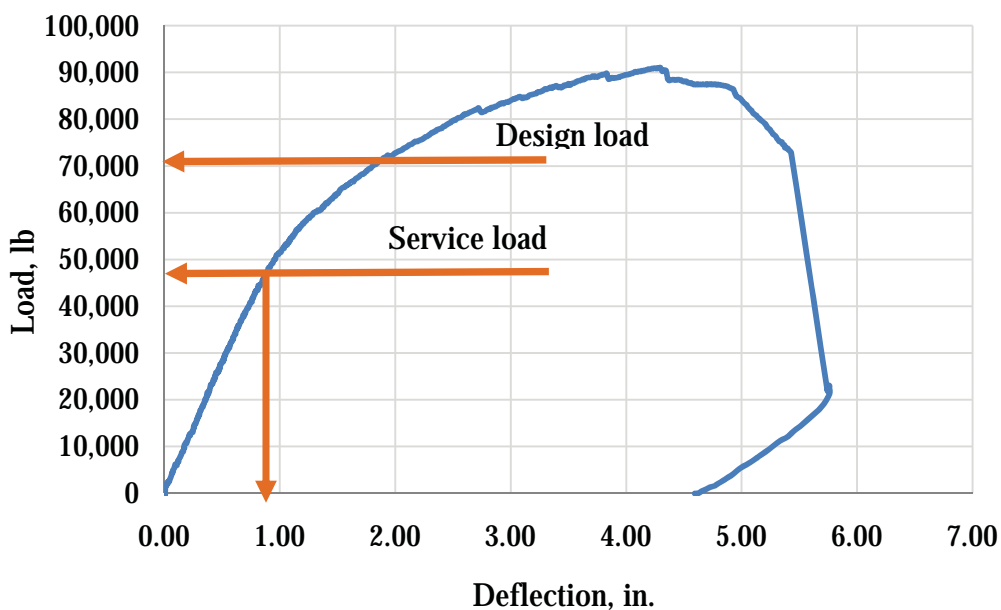


Figure 6.39: Load-deflection relationship of flat soffit beam flexural test



Figure 6.40: Failure mode of the flat soffit beam

From the test results, the flexural capacity of the flat soffit prestressed beam exceeded the demand and was accurately predicted using strain compatibility.

Chapter 7

PRECAST/PRESTRESSED SANDWICH FLOOR PANELS

7.1 Introduction

Structural floor systems represent a major portion of both the cost and weight of precast concrete building frames. Also, structural floor systems in multi-story buildings have an impact on the overall building height and design of other building systems. Many approaches have been used to improve the structural and construction efficiency of floor systems, some of these were sought to minimize the weight, depth, and cost of structural floor systems through the use of higher strength materials and improved construction techniques.

Hollow core (HC) precast prestressed concrete floor panels (Board of FIB steering committee, 1999) are the common solution for several floor applications, especially where flat soffit, long span, and lightweight floors are required. The number and size of strands in the bottom flange determine the ultimate load/span capacity of the planks. HC planks are produced using specialized equipment to ensure consistently, high quality, and efficiency of production. HC planks are grouted together to produce a diaphragm action and flat soffit. Enhanced structural performance can be achieved by using a composite topping, which can result in a span-to-depth ratio of up to 40. Despite these advantages, HC planks have poor thermal insulation, and require high initial investment for production equipment.

Rip-slab floor panels (Hanlon, et al. 2009) is a modified precast prestressed concrete double-tee with a 2 in. thick concrete slab and 8 in. deep ribs, for a total depth of 10 in. Testing the ultimate load capacity of the rib-slab with a dapped end connection has

confirmed the feasibility of this floor system. The Rip-slab floor elements are economical, structurally efficient, and can be easily produced. However, they do not provide either flat soffit or thermal insulation.

Filigree wide slab system (Mid-State filigree Systems, Inc. 1992) was originally developed in Great Britain and is presently used under the name of OMNIDEC. Filigree precast panels are thin reinforced concrete slabs with steel lattice truss that are used as formwork for the composite cast-in-place concrete topping. The steel truss ensures composite behavior between precast and cast-in-place concrete and provides the panel with the required stiffness during erection. The typical thickness of the prefabricated slab is 2.25 in., but the total thickness of the panel varies due to the spans. The panels are structurally efficient and easy to produce. They have a typical width of 8 ft and flat soffit that eliminates the need for false ceiling. The main disadvantage of this system is the low thermal insulation.

This chapter presents the development of a new precast/prestressed floor panel that is alternative to HC planks. Table 7.1 compares the proposed floor panel with the existing floor panels in terms of the criteria listed before. The proposed system consists of an internal wythe of insulation and two external wythes of concrete similar to precast concrete sandwich wall panels. The two concrete wythes are designed to be fully composite through the use of shear connectors.

Table 7.1: Comparing the proposed against existing floor systems

Criteria	Hollow core	Rip-slab	Filigree wide slab	Sandwich Floor Panel
Does not Need Special Equipment to Produce	✗	✓	✓	✓
Does not Need Cast-in-place Topping	✓	✓	✗	✓
Thermal Insulation	✗	✗	✗	✓
Flat Soffit	✓	✗	✓	✓

The proposed floor panel is expected to have flat soffit, lightweight and adequate structural capacity while being efficient in thermal insulation and does not require specialized equipment for fabrication. Sandwich panels can be used for many applications to save the energy such as roof application due to the difference in temperature between the inside and the outside. Also it can be in radial building as floor application where there is different in temperature for each story.

7.2 Panel Description and Design

Sandwich panels are used since many years in wall application. Sandwich panel does not used in floor application because of the Glass Fiber-Reinforced Polymer (GFRP) ties under sustain loads. Many works was done in Canada to determinate GFRP bars creep. When the stress in the GFRP bars should not be more than $0.2 F_u$ there is no creep problems, where F_u is the ultimate tensile strength. A typical Precast/Prestressed Concrete Sandwich Floor Panel (PCSFP) consists of two precast concrete wythes. The bottom wythe may has steel reinforcing or steel strands as main reinforcement. The two concrete wythes separated by a layer of insulation (e.g. Extruded Polystyrene (XPS)) and joined together with connectors to achieve the composite action required for flexural resistance and stiffness. These connectors can be concrete, steel, plastic ties, or any combination of these components. However, the low thermal resistance of steel and concrete connectors makes these products unattractive as they significantly reduce the thermal efficiency of the PCSFP through thermal bridging. NU-Tie (GFRP) ties is a product developed by researchers at the University of Nebraska-Lincoln (UNL) as shown in Figure 7.1 and patented in 1995 (Tadros et al. 1995).



Figure 7.1: NU Tie

The proposed panel is designed to be fully composite. The flexural capacity of the composite panel is that of a solid panel that has the same cross section as the two concrete wythes.

Shear connectors are used to transfer horizontal shear forces between the concrete wythes as shown in Figure 7.2.

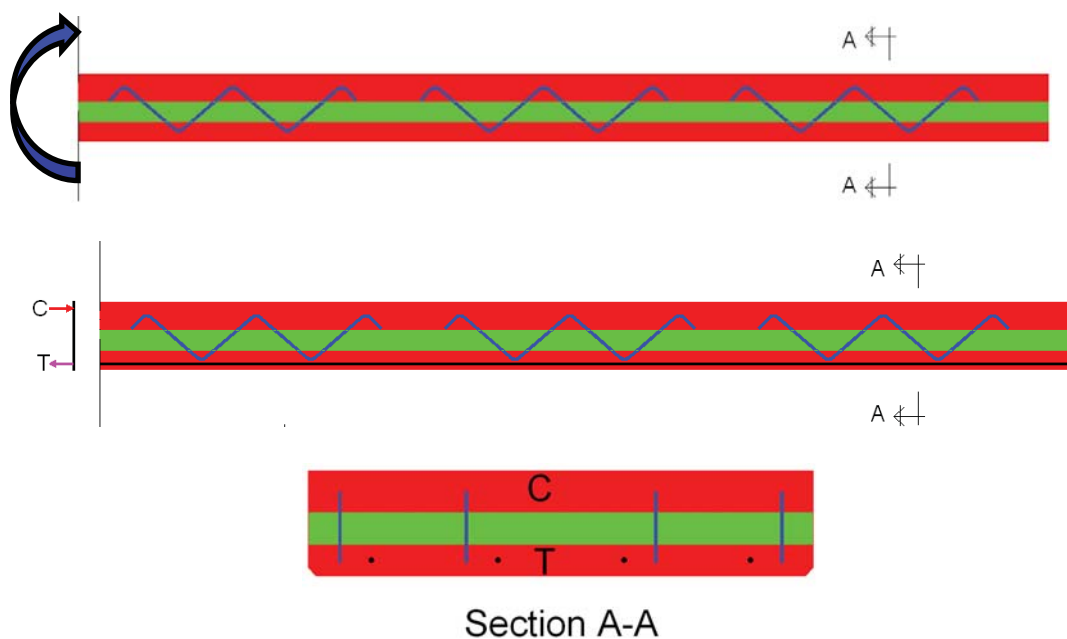


Figure 7.2: Shear connectors and horizontal shear force

This force can be calculated using the strength method given in the PCI Design Handbook, 6th Edition 2005 Section 5.3.5 “Horizontal Shear Transfer in Composite Components”. In this method, the horizontal shear force is taken as the lesser of the maximum compressive force in concrete and maximum tensile force in the

reinforcement/prestressing. This force is then used to determine the required number of shear connectors over the horizontal shear span, which is one-half the clear span for simply supported panels. Most manufacturers of shear connectors use the same method to determine the amount of shear connectors for composite panels and distribute these connectors uniformly along the horizontal shear span. In this study, another procedure was used, in addition to the PCI Design Handbook 6th Edition procedure. A triangular distribution of the horizontal shear force along the shear span is used to determine the most efficient distribution of shear connector. Also the flexural capacity was determined using the strain-compatibility for two loading stages: 1) panel without topping was designed to carry 25 psf topping weight plus 25 psf construction loads; and 2) panel with topping was designed to carry the live load (100 psf) plus any superimposed dead loads (weight of flooring or ceiling).

7.3 Thermal Performance

Glass Fiber-Reinforced Polymer (GFRP) ties connectors was introduced for its superior thermal resistance and structural strength. GFRP tie typically has a conductivity of $k = 0.5 \text{ Btu}\cdot\text{in.}/(\text{hr}\cdot\text{ft}^2\cdot^\circ\text{F})$. Compare to concrete connector ($k = 13.3 \text{ Btu}\cdot\text{in.} / (\text{hr}\cdot\text{ft}^2\cdot^\circ\text{F})$) and metal connector ($k = 314 \text{ Btu}\cdot\text{in.} / (\text{hr}\cdot\text{ft}^2\cdot^\circ\text{F})$). In order to study the thermal performances of these panels, R-Value are calculated using the “Zone Method” proposed by PCI Design Handbook 6th Edition, Section 11.1.6. Two sandwich panels will be used to calculate R-Value, 1) sandwich panel with concrete solid ends as shown Figure 7.3. the panel was 26 ft long, 4 ft wide and 8 in. thick (3-4-1), plus 2 in. concrete topping and 2) fully insulated sandwich panel as shown in Figure 7.28. The panel was 26 ft long ,4 ft wide and 8 in. thick (3-3-2), plus 2 in. concrete topping. Table 7.2 Table 7.3 show R-

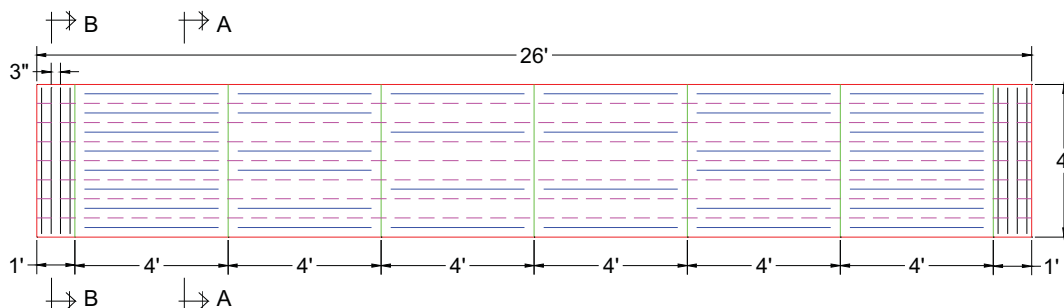
Value calculations for sandwich panel with concrete solid blocks at the ends and fully insulated sandwich panel respectively.

Table 7.2: R-Values calculations for sandwich panel with concrete solid ends

Parameter	Value	Unit	
Panel Span	26	ft	
Panel width	4	ft	$\alpha = 1 + 2.25 \left(\frac{k_{in} - 0.26}{0.26} \right)$
Thickness of the topping (t_{cf1})	2	in.	
Thickness of top wythe (t_{cf2})	2	in.	$\beta = 1 + 1.458 \left(\frac{k_{con} - 12.05}{12.05} \right)$
Thickness of insulation (t_{in})	3	in.	$E_z = 1.4 - 0.4t_{in}\alpha + (0.4t_{cf} + 0.1(t_{cb} - t_{cf}))\beta$
Thickness of bottom wythe (t_{cb})	3	in.	
Solid Concrete Block Length	1	ft	$\frac{1}{R} = \frac{A'_s}{R_s} + \frac{A'_p}{R_p}$
Insulation Conductivity Values (K_{in})	0.2	(Btu-in.)/(hr. ft ² . F)	
Concrete Conductivity Values (K_{con})	13.3	(Btu-in.)/(hr. ft ² . F)	
Alpha Coefficient (α)	0.48		
Beta Coefficient (β)	1.15		
Size of The Effective Zone (E_z)	2.98	in.	
Effective Zone Around the Solid Block	143.17	in ²	
Panel Area (A_t)	14976	in ²	
Concrete Area (A_s)	1438.33	in ²	
Insulated Area (A_p)	13537.67	in ²	
R-Value for Insulated Path in Winter	16.38	hr.ft ² .F/Btu	
R-Value for Insulated Path in summer	16.46	hr.ft ² .F/Btu	
R-Value for Concrete Path in Winter	1.60		
R-Value for Concrete Path in Summer	1.68		
Ratio of solid concrete ($A'_s = A_s/A_t$)	0.096		
Ratio of insulated concrete ($A'_p = A_p/A_t$)	0.90		
Final R-Value in Winter	8.68	hr.ft ² .F/Btu	
Final R-Value in Summer	8.93	hr.ft ² .F/Btu	

Table 7.3: R-Value calculation for fully insulated sandwich panel

Parameter	Value	Unit							
Panel Span	26	ft							
Panel width	4	ft							
Thickness of the topping (t_{cf1})	2	in.							
Thickness of top wythe (t_{cf2})	2	in.							
Thickness of insulation (t_{in})	3	in.							
Thickness of bottom wythe (t_{cb})	3	in.							
Solid Concrete Block Length	0	ft							
Insulation Conductivity Values (K_{in})	0.2	(Btu-in.)/(hr. ft ² . F)							
Concrete Conductivity Values (K_{con})	13.3	(Btu-in.)/(hr. ft ² . F)							
Alpha Coefficient (α)	0.48								
Beta Coefficient (β)	1.15								
Size of The Effective Zone (E_z)	2.98	in.							
Effective Zone Around the Solid Block	143.17	in ²							
Panel Area (A_t)	14976	in ²							
Concrete Area (A_s)	0.00	in ²							
Insulated Area (A_p)	14976	in ²							
R-Value for Insulated Path in Winter	16.38	hr.ft ² .F/Btu							
R-Value for Insulated Path in summer	16.46	hr.ft ² .F/Btu							
R-Value for Concrete Path in Winter	1.60								
R-Value for Concrete Path in Summer	1.68								
Ratio of solid concrete ($A'_s = A_s/A_t$)	0.000								
Ratio of insulated concrete ($A'_p = A_p/A_t$)	1.00								
Final R-Value in Winter	16.38	hr.ft ² .F/Btu							
Final R-Value in Summer	16.46	hr.ft ² .F/Btu							



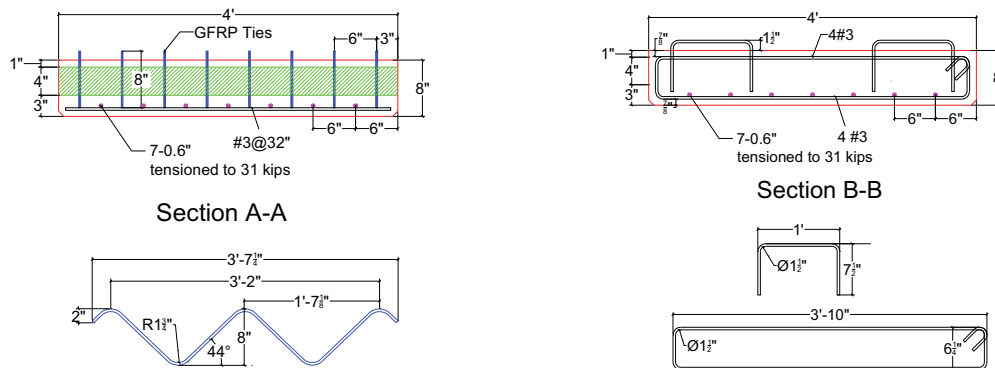


Figure 7.3: Floor panel A with GFRP ties

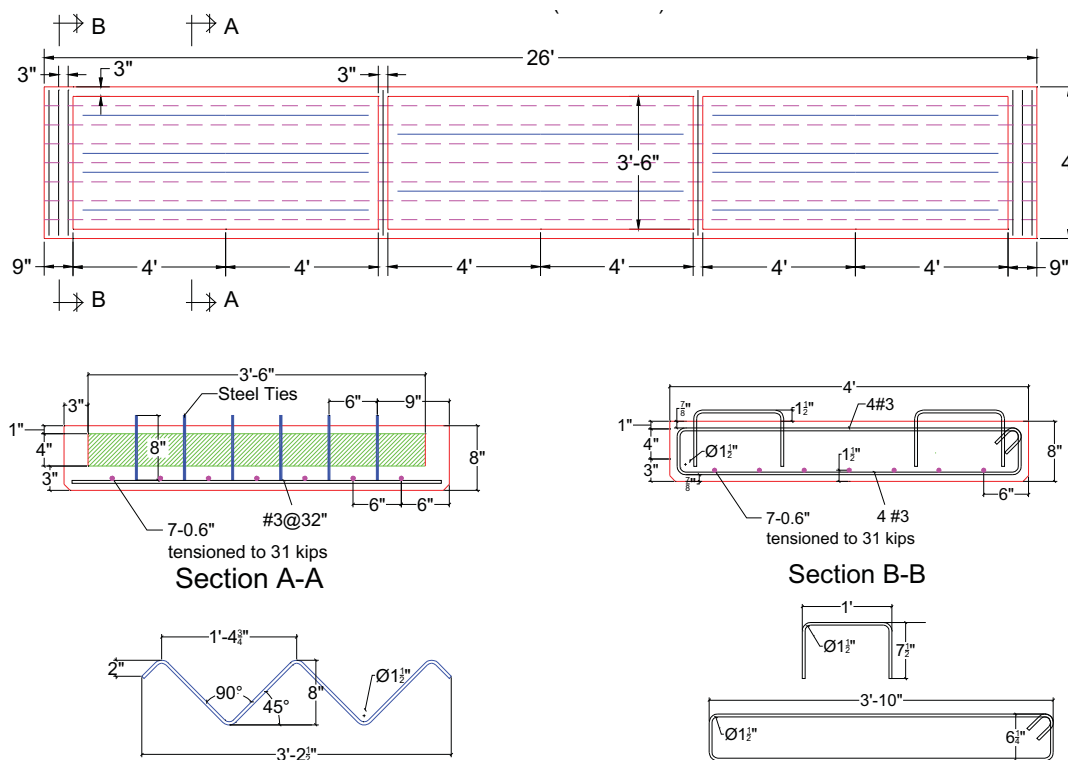


Figure 7.4: Floor panel B with steel ties

7.4 Phase I Experimental Investigation

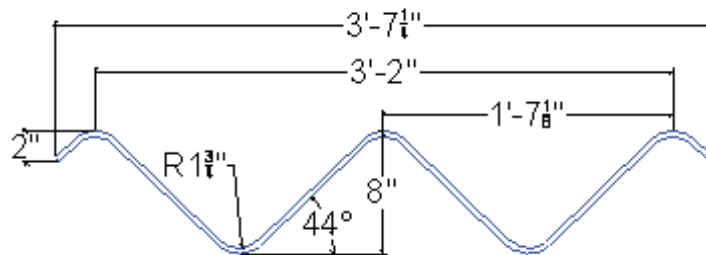
Phase I of the experimental program focused on investigating the flexural behavior of PCSFP under construction stage and final stage and the impact of such parameters as the connectors distribution, using different types of shear connectors, effects of connectors extension above the top wythe in the fabrication process, and using solid concrete blocks

at the ends. This phase allowed determination of the best and efficient design in terms of strength and cost. Based on the phase I results and the learned lessons phase II specimens were tested to develop design recommendations.

7.4.1 Specimens Design

Two panels were fabricated and tested at the Structural Laboratory of the University of Nebraska-Lincoln. Each panel was 26 ft long, 4 ft wide, and 8 in. thick. Both Panels were longitudinally reinforced with seven 0.6 in. diameter grade 270 low-relaxation prestressing strands tensioned to 31 kip, which is the maximum jacking force for 0.5 in. diameter strands. The researchers used 0.6 in. diameter due to the unavailability of 0.5 in. diameter strands at the time of panel fabrication. The 8 in. thick sandwich panels consisted of two concrete wythes. The top concrete wythe is 1 in. thick and the bottom concrete wythe is 3 in. thick and they are separated by a 4 in. thick layer of extruded polystyrene (XPS) as shown in Figure 7.3 and Figure 7.4. Glass Fiber-Reinforced Polymer (GFRP) ties were used in panel A as shear connectors in addition to 12 in. wide solid concrete block at each end as shown in Figure 7.3. Steel ties and concrete connectors were used in panel B as shear connectors plus concrete connectors. The concrete connectors were 9 in. wide solid block at each end, 3 in. wide rip in each side, and two 3 in. wide rips 8.75 ft apart from each end as shown in Figure 7.4 in addition to the gap between the steel ties and the insulation. Both the GFRP ties and the steel ties are 8 in. high, which make the ties extended above the top wyth of the panel. The following shows the calculation GFRP ties

Design of GFRB Ties



NU-Ties Properties

$$A_{\text{tie}} := 0.1 \text{ in}^2$$

$$C_e := 0.7$$

$$\alpha_{\text{tie}} := 44$$

$$C_r := 0.65$$

$$\text{Tie}_{\text{depth}} := 8 \text{ in}$$

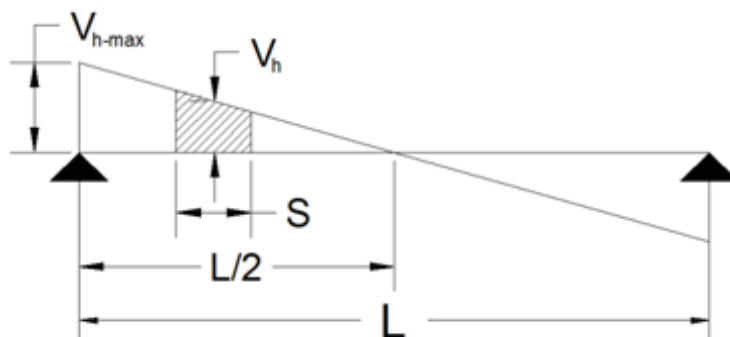
$$\phi_{\text{shear}} := 0.75$$

$$\text{Tie}_{\text{Tensile.Strength}} := 110 \text{ ksi}$$

$$F_u := \text{Tie}_{\text{Tensile.Strength}} = 1.1 \times 10^5 \text{ psi}$$

$$M_u = 98 \text{ kip}\cdot\text{ft}$$

$$\text{Span} = 28 \text{ ft}$$



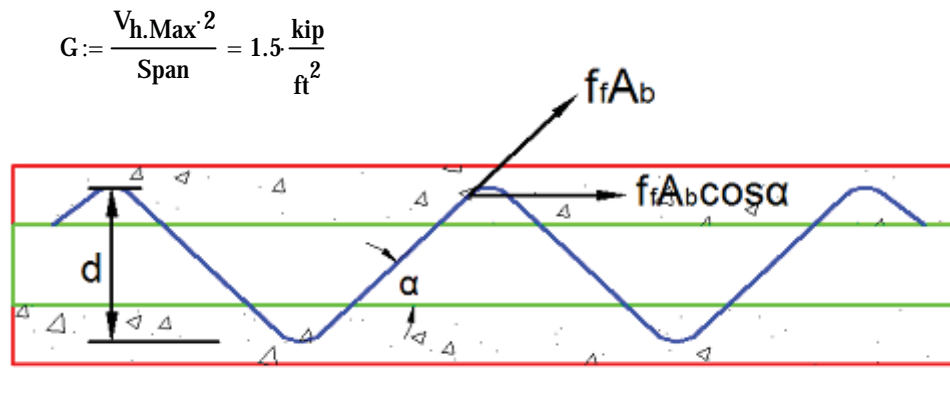
Total Horizontal Shear

$$V_{\text{h.total}} := \frac{M_u}{\text{Tie}_{\text{depth}}} = 147 \text{ kip}$$

Maximum Horizontal Shear

$$V_{\text{h.Max}} := \frac{V_{\text{h.total}} \cdot 4}{\text{Span}} = 21 \frac{\text{kip}}{\text{ft}}$$

Horizontal Shear Gradient



Factored Strength

$$F_f := \phi_{shear} \cdot F_u \cdot C_e \cdot C_r = 37.538 \text{ ksi}$$

Leg Capacity

$$F := A_{tie} \cdot F_f \cos\left(\alpha_{tie} \cdot \frac{\pi}{180}\right) = 2.97 \text{ kip}$$

The panel can be divided into segments that are multiples of 4 ft in length. Assuming 1 ft solid at each end

First segments

$$\text{First}_{segments} := 5 \text{ ft}$$

$$\text{Area}_{segment.one} := \frac{[V_{h,Max} + (V_{h,Max} - G \cdot \text{First}_{segments})]}{2} \cdot \text{First}_{segments} = 86.25 \text{ kip}$$

Number of Legs

$$\text{Number}_{Legs} := \frac{\text{Area}_{segment.one}}{F} = 29.038$$

Since one NU-Tie contains 4 legs,

$$\text{Number}_{Ties} := \frac{\text{Number}_{Legs}}{4} = 7.26$$

Take it 8 ties

Second segments

$$\text{Second}_{segments} := 4 \text{ ft}$$

$$V_{1second} := V_{h,Max} - G \cdot \text{First}_{segments} = 13.5 \frac{kip}{ft}$$

$$V_{2.\text{second}} := V_{1.\text{second}} - G \cdot \text{Second}_{\text{segments}} = 7.5 \frac{\text{kip}}{\text{ft}}$$

$$\text{Area}_{\text{segment.second}} := \frac{(V_{1.\text{second}} + V_{2.\text{second}})}{2} \cdot \text{Second}_{\text{segments}} = 42 \cdot \text{kip}$$

Number of Legs

$$\text{Number}_{\text{Legs.}} := \frac{\text{Area}_{\text{segment.second}}}{F} = 14.14$$

Since one NU-Tie contains 4 legs,

$$\text{Number}_{\text{Ties.}} := \frac{\text{Number}_{\text{Legs.}}}{4} = 3.535 \quad \text{Take it 6 ties}$$

Third segments

Take number of the tie = 4 ties

7.4.2 Specimens Erection

The panels were fabricated and cast in the prestressing bed at the PKI structural Laboratory. Figure 7.5 shows the casting orientation and the nomenclature of the panel.

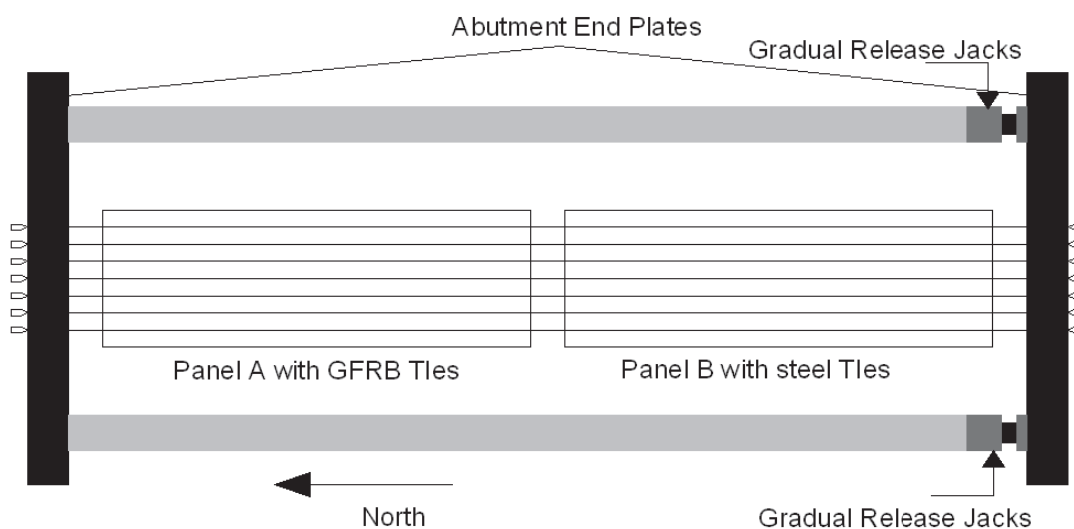


Figure 7.5: floor panels casting position and nomenclature for the panels

Below are the steps followed in the erection of phase I specimens.

Step 1) Production of GFRP and steel ties as shown in Figure 7.6

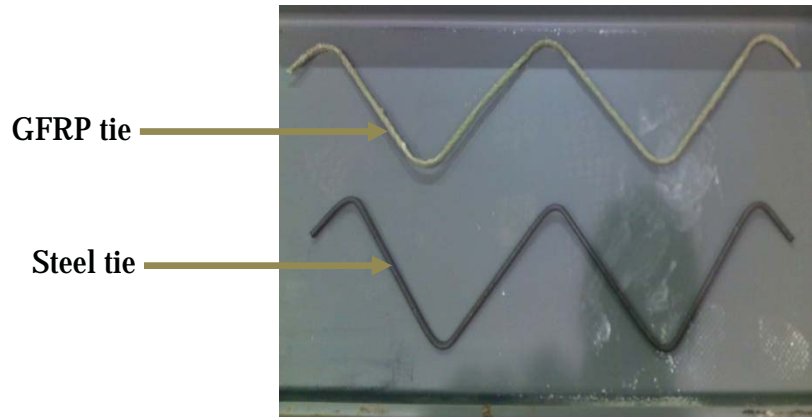


Figure 7.6: GFRP and steel ties profile.

Step 2) Preparation of XPS Foam Panels. The preparation of the XPS foam panels starts from hot melting slots for inserting the ties connectors. This is done by a prefabricated machine and should be accompanied by using exhaust containment hoods and adequate ventilation to deal with smoke and fumes associated with the melting of slots. A picture of this machine can be seen in Figure 7.7. After the blanks are ready, GFRP tie is inserted into the foam and the remaining gaps are filled with canned expanding foam insulation as shown in Figure 7.8. Excess foam is removed with a long, flat fine tooth blade.



Figure 7.7: Hot melt slots into the foam blanks

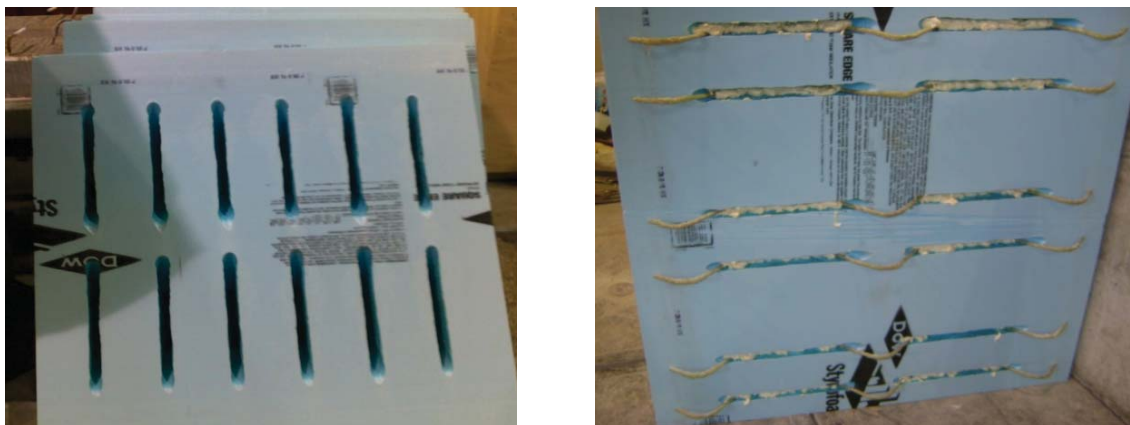
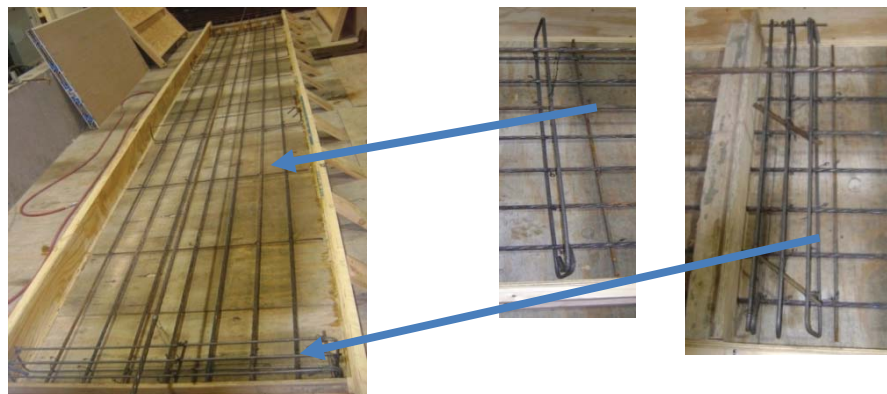


Figure 7.8: Insert GFRP tie into the XPS slot and filling the gap with expanding foam insulation

Step 3) Setup the forms and lubricate the bed for concrete placement and tension the strands and place the reinforcement. First, chamfer was stapled to the bed at the appropriate spacing; then, the seven 0.6 in. diameter strands were threaded through the south abutment plates, through the appropriate plywood end plates and confinement reinforcement, then finally through the north abutment plates as shown in Figure 7.9. Each strand was chucked at both ends and tensioned to 31 kip. The formwork for the floor panel was prepared using plywood 0.75 in thickness and 8 in. height. These plywood pieces were fixed to the floor, preventing horizontal movement due to the force of the fresh concrete.



Panel A (4 steel stirrups at each end)



Panel B (3 steel stirrups at each end and one stirrup at one-third of the span)

Figure 7.9: Setup the forms and tension the strands

Step 4) Pouring the concrete, SCC concrete was delivered by Ready Mix truck to the PKI structural laboratory. Spread diameter was taken upon arrival and was found to be 25 in. Cylinder samples were taken following the adequate spread diameter and pouring of the panels commenced. First placed the bottom wythe, then place XPS panels with GFRP ties on the fresh concrete of the bottom wythe and place the concrete of the top wythe as shown in Figure 7.10.



Figure 7.10: Casting the bottom wythe, installing foam panels, and casting the top wythe
In case of panel B the XPS panels was placed without the ties, then placed the top concrete wythe, finally install the steel ties. Casting of the panel required no vibration and

little labor due to the concrete's flowing ability. The two panels were completed, as shown in Figure 7.11, in approximately 60 minutes using a crane bucket. Wet burlap curing commenced after the specimens had setup such that the burlap would not damage the surface or lifting points, as shown in Figure 7.12.



Figure 7.11: Completing casting the panels



Figure 7.12: Wet Burlap Curing

Step 5) Release and cut the strands. After three days, the forms were stripped and strands were released gradually. At that time the concrete strength reached 8400 psi

7.4.3 Material Properties

Table 7.4 shows the mix designs used for precast panels and for the coming topping, while Figure 7.13 shows compressive strength versus age relationships for precast concrete panels and the used topping

Table 7.4: Concrete design mix for precast panel

Materials	Weight (lb) per cubic Yards	
	Precast	Topping
Portland Cement Type I	705	611
Fly Ash, Class C	378	-
Limestone (LBRS)	1340	950
Sand (S47B)	980	2190
Sand (S4110)	420	-
Total Water	260	275
Water Reducer (AGLEN)	13 oz/cwt	-

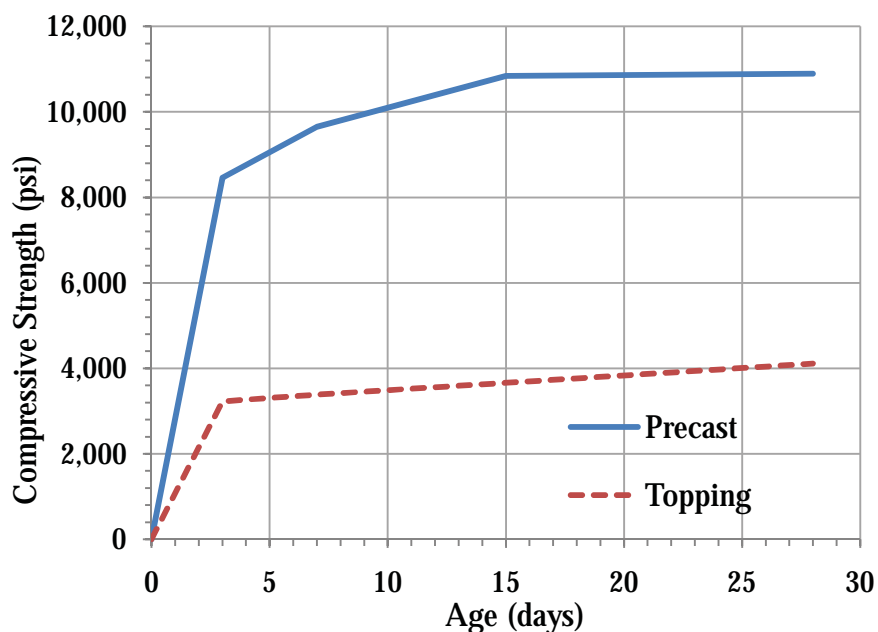


Figure 7.13: Concrete strength gain with time

7.4.4 Test Setup and Procedures

Testing of the first phase specimens was performed on March 24, and April 1 and 2 2010.

This includes the following three tests:

- 1- First test (without topping)
- 2- Second test (with topping)

7.4.4.1 First Test (Without Topping)

The proposed panels will be used as floor panels instead of the hollow core planks. At the stage of construction the panels should carry its own weight, plus the weight of the topping and the construction loads. The construction loads assumed 25 psf plus 25 psf topping weight. The first test was conducted to determine the behavior of the panels without topping. At the time of the first test, the concrete strength was 9.6 ksi. One point load was applied at mid-span of the panel using hydraulic jack and load cell. Roller supports were placed 25.67 ft center to center. Specimen deflection was recorded using one potentiometer located at mid-span under the point load as shown in Figure 7.14. The net camber (after subtracting the self-weight deflection) of the two panels was approximately 0.25 in.

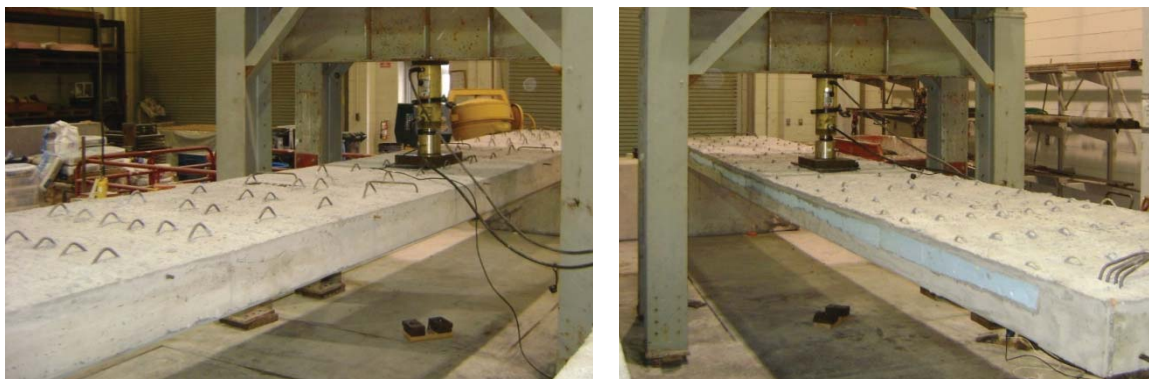
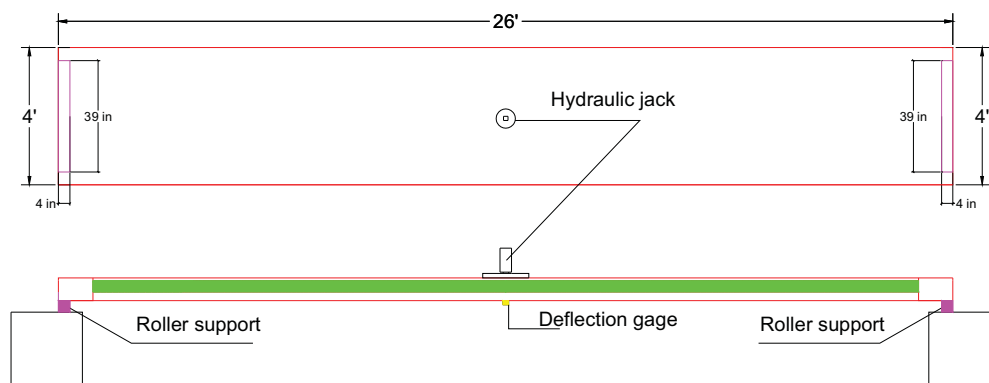


Figure 7.14: Test Setup

After setting up the panel, Panels were slowly loaded using the hydraulic jack. Deflection was recorded during loading. The test was stopped when the load reaches the cracking load. Figure 7.15 plots the load-deflection relationships of the two panels when loaded up to the cracking load. The left vertical axis shows the applied load in pounds, while the right axis shows the corresponding uniform load (i.e that results in similar deflection) in pound per square foot. The plot indicates that the relationship of panel A is non-linear, and the relationship of panel B is linear. Panel A showed a higher level of ductility than panel B, which can be explained by the fact that GFRP ties have significantly lower modulus of elasticity than steel ties, which allows higher relative movements between the top and bottom concrete wythes. In addition, panel B has more concrete connectors that restrain this relative movement. The figure illustrated that the construction loads plus the weight of the topping are equal to 3100 lb approximately. Also the deflection caused by that load is 0.25 in. approximately which makes the panels has zero deflection finally.

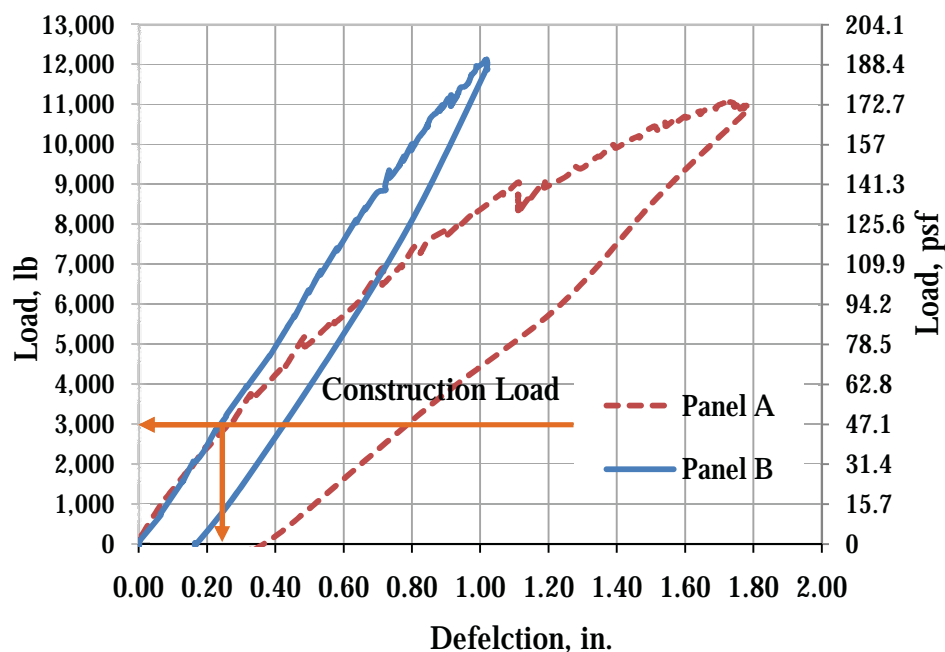


Figure 7.15: Load-deflection relationships for panel A, and B without topping

7.4.4.2 Second Test (With Topping)

After the first test was done, the panels moved to the bed, then 2 in. concrete topping was casting over the top of the two panels, after placing #4@32 in. as transverse reinforcement as shown in Figure 7.16. The concrete was delivered by Ready Mix truck to the PKI structural laboratory. Table 7.4 shows the topping mix design. After the topping concrete strength reached 3.4 ksi, the two panels were moved again to testing. The second test setup is similar to the first one as shown in Figure 7.17. Concrete strain gauges were attached to the top surface to measure the strain in extreme compression fibers as shown in Figure 7.18. At the time of the second test, the compressive strength for the panels and the topping was 10.8 ksi and 3.4 ksi respectively. These values represent the average compressive strength of the tested cylinders.



Figure 7.16: Built the form for the topping and cast the concrete topping



Figure 7.17: Second test setup

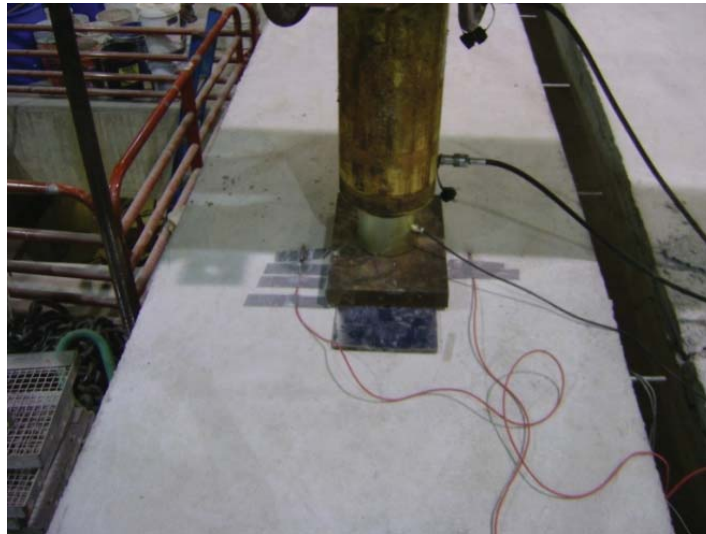


Figure 7.18: Strain Gauges at the top surface

Figure 7.19 shows the load deflection relationships of the two panels. In this figure, the left vertical axis shows the applied load in pounds, while the right axis shows the corresponding uniform load (i.e that results in similar deflection) in pound per square foot. The load-deflection relationships show a linear behavior up to the cracking load, which was approximately 15 kip for the two panels. A non-linear relationship continued until the ultimate load was reached, which was approximately 33, kip for panel A and 34

kip for panel B. It should be noted that the point load equivalent to a live load of 100 psf is 6.5 kip and the corresponding deflection is 0.4 in and 0.2 in. for panel A and B respectively. This values of deflection are less than 0.85 in. which corresponding to the limits of $L/360$

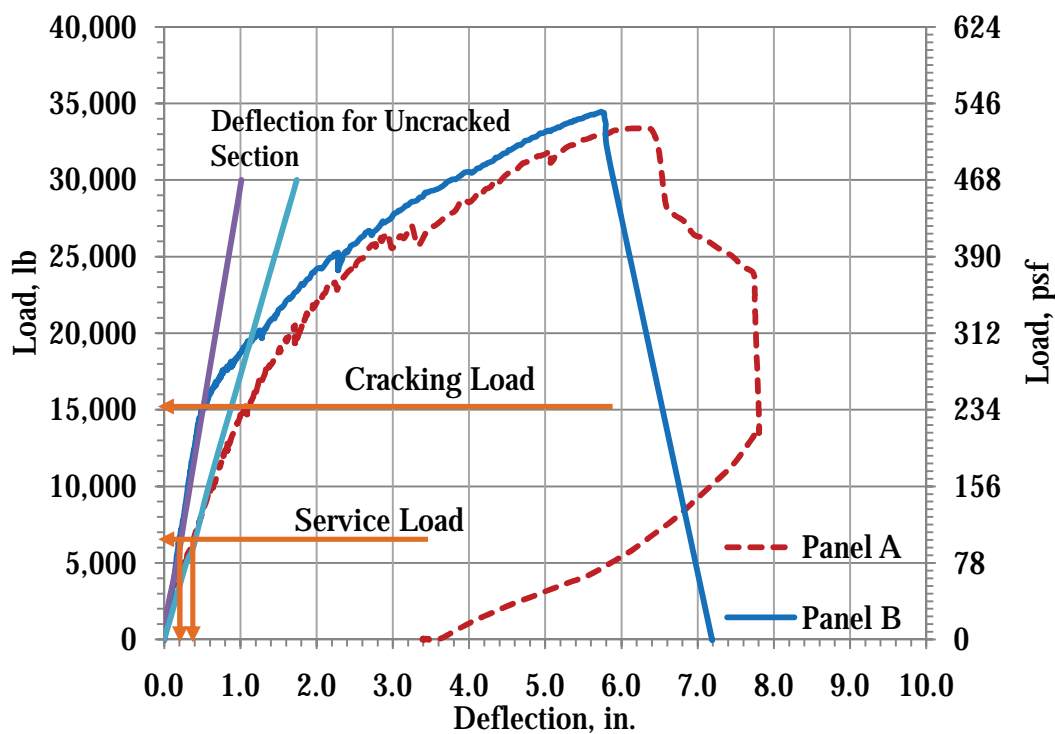


Figure 7.19: Load-deflection relationship for the two panels with topping

Prestress loss calculations were performed according to the 7th Edition of the PCI Design Handbook (2010), which resulted in a total prestress loss of approximately 18%. The nominal flexural capacity of the panel section (ϕM_n) was calculated using strain compatibility and assuming a fully composite section and a resistance factor (ϕ) of 1.0. This resulted in a theoretical capacity of 226 kip.ft, depth of compression block of 2.224 in, and ultimate stress in prestressing strands of 270 ksi. It should be noted that the two panels were made of the same concrete and had the same prestressing force.

Figure 7.20 shows load strain relationships of the two panels at top fiber. The strain at mid-span top fibers in panel A indicates that the concrete strain did not reach 0.003, while it reached 0.003 in panel B. This behavior explains the failure mode of each panel, which is shown in Figure 7.21 and Figure 7.22. Figure 7.21 shows that Panel A had tension-controlled flexural failure. Also several cracks appeared in the top surface at each ends, where the concrete end blocks restrained the panel rotation (i.e. partial fixity). Figure 7.22 shows that panel B has compression-controlled flexural failure as the topping concrete reached its ultimate strain.

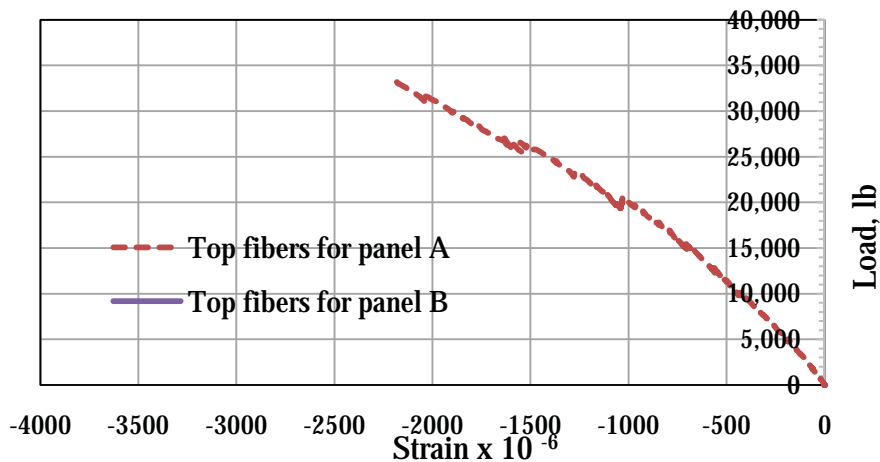


Figure 7.20: Load-strain relationships of top fibers at mid-span

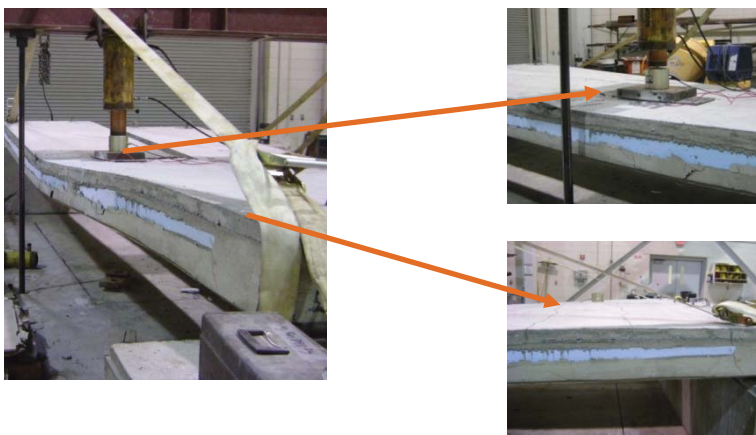


Figure 7.21: Failure mode of panel A

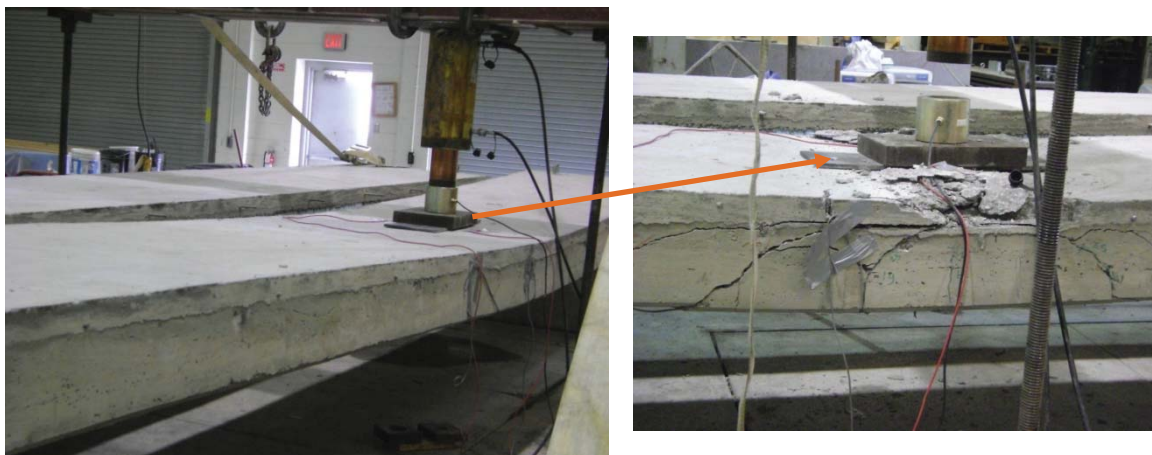


Figure 7.22: Failure mode of panel B

Table 7.5 compares the theoretical flexural capacity of each specimen with its measured flexural capacity obtained from testing. The ratios of measured-to-theoretical capacity indicate that panels A and B have flexural capacity higher than the theoretical capacity of a fully composite section. This means that the section is fully composite. The ratios of measured -to-theoretical capacity in Table 7.5 also indicate that GFRP ties in panel A and steel ties in panel B have achieved the full composite action.

Table 7.5: Comparing the theoretical against measured flexural capacity of phase I test specimens

Panel	L_e (in.)	$M_{\text{theoretical}}$ (kip. In.)	$W_{O.W}$ (kip/in.)	$M_{O.W}$ (Kip.in.)	P_{measured} (kip)	M_{measured} (kip. in.)	$M_{\text{total-measured}}$ (kip. in.)	$M_{\text{total.measured}} / M_{\text{theoretical}}$
Panel A	308	2712	0.026	308.3	33.4	2571.8	2880.1	1.06
Panel B	308	2712	0.028	332.0	34.5	2656.5	2988.5	1.10

7.5 Design Optimization and Erection Simplification

Based on fabrication and erection experience of phase I specimens, the following changes were recommended and made to the design and detailing of phase II specimens:

- 1- The height of ties was changed from 8 in. to 7 in., which eliminate the extension of the ties above the top wyth of the panel that is making the finishing of the top wyth much easier and faster. See Figure 7.23



Figure 7.23: Changing the ties height in phase I (top) and phase II (bottom).

- 2- Eliminating any thermal bridges such as the solid concrete parts at the ends, which increase the panel thermal efficient. For bearing at the ends, thermal plastic lamber 6 in. x 3 in. x 48 in. were places. See Figure 7.24

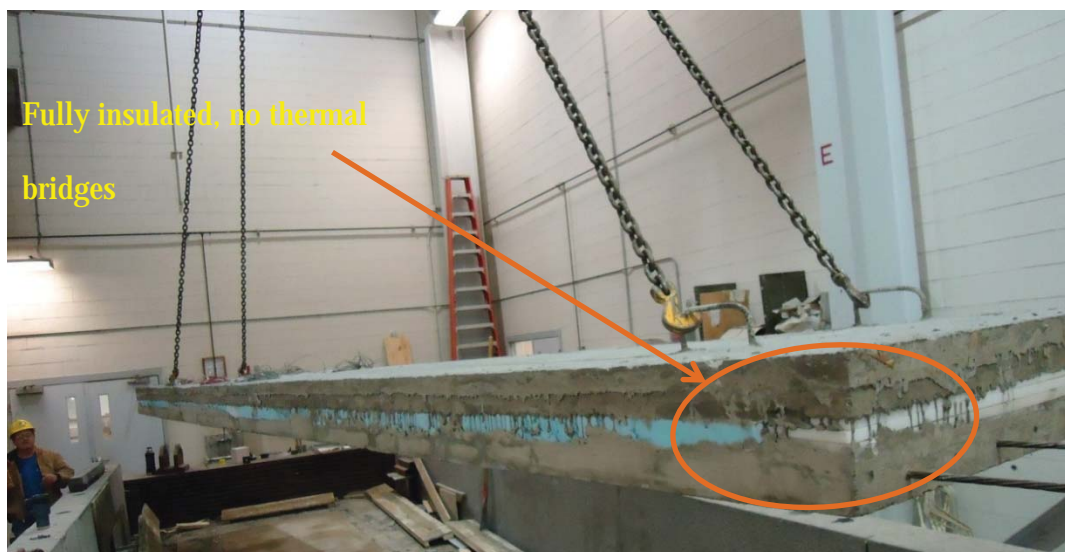
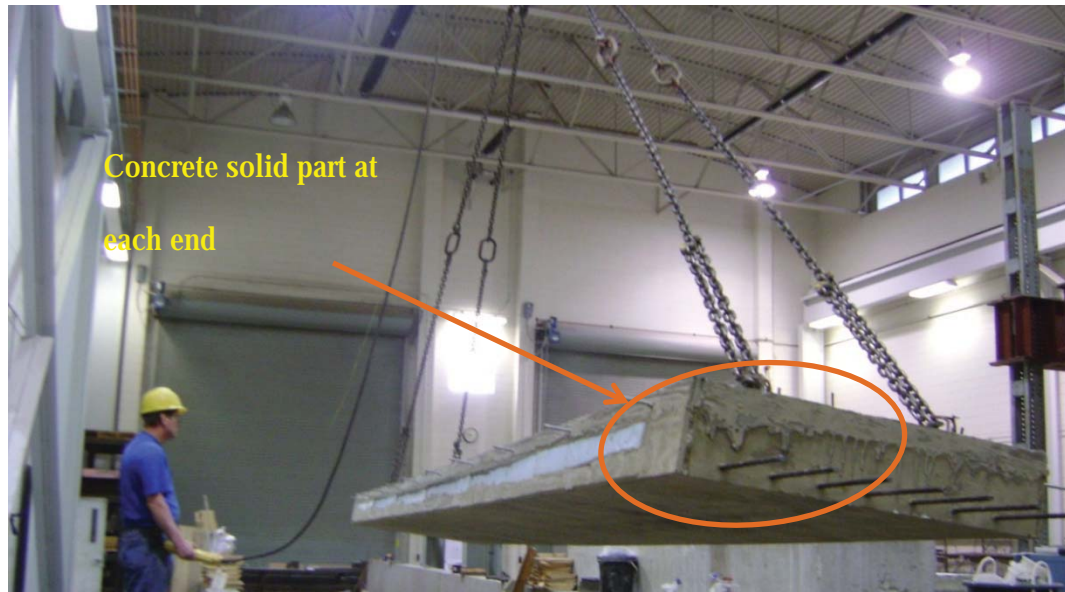


Figure 7.24: The end of the panels in phase I (top) and phase II (bottom).

- 3- Topping reinforcement in the longitudinal direction was changed to be D5xD5 (6 in. X 18 in.) instead of using #4@32 in the transvers direction. See Figure 7.25

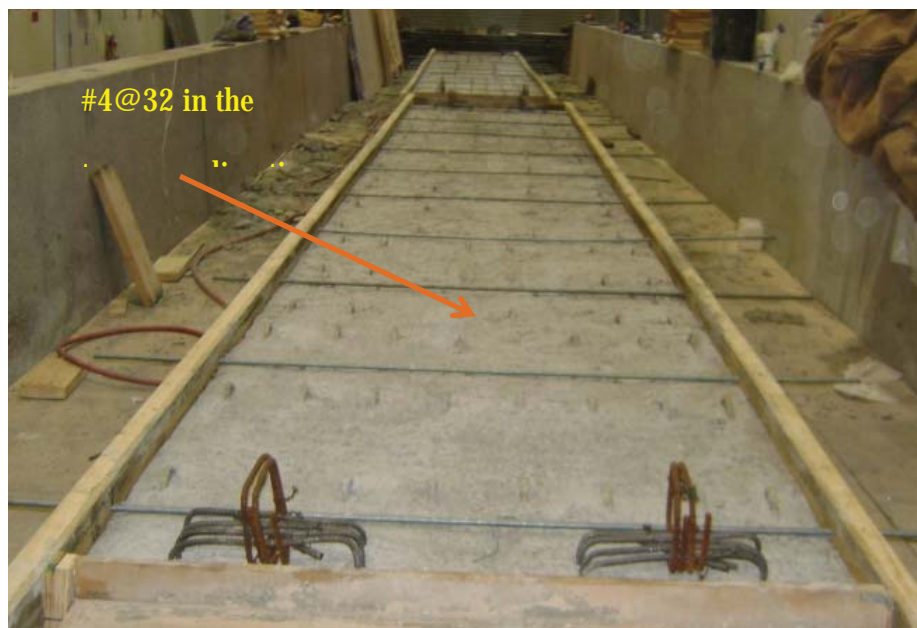


Figure 7.25: Topping reinforcement phase I (top) and phase II (bottom).

- 4- Optimize the design by using 24 ties and 4-0.5 strand instead of using 36 ties and 7-0.5 strand in the panel. See Figure 7.26



Figure 7.26: Optimize number of strands and number of ties for phase I (top) and phase II (bottom).

5- Re-distribute the 8 in. height from 3-4-1 to 3-2-2. See Figure 7.27

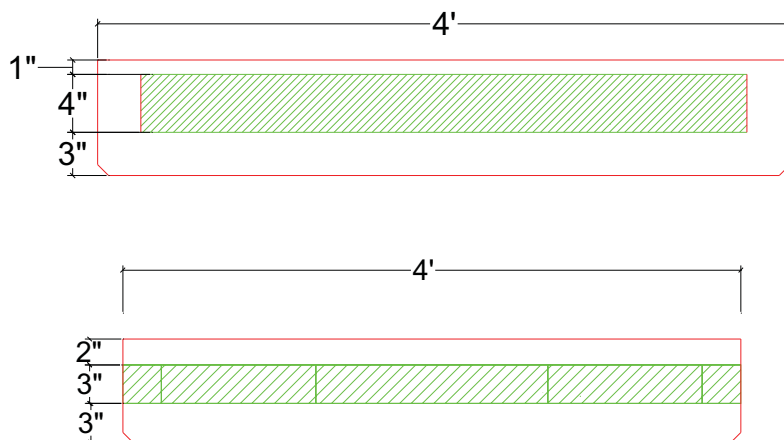


Figure 7.27: changes in the cross section for phase I (top) and phase II (bottom).

7.6 Phase II Experimental Investigation

Based on the results of Phase I and the learning lessons, fully thermal insulated panels will be investigated in Phase II, using GFRP ties as shear connectors.

7.6.1 Specimens Design

Two panels C and D were fabricated and tested at the Structural Laboratory of the University of Nebraska-Lincoln. Each panel was 26 ft long, 4 ft wide, and 8 in. thick. Both Panels were longitudinally reinforced with four 0.5 in. diameter grade 270 low-relaxation prestressing strands tensioned to 31 kip, which is the maximum jacking force for 0.5 in. diameter strands. The 8 in. thick, sandwich panels consisted of two concrete wythes. The top concrete wythe is 2 in. thick and the bottom concrete wythe is 3 in. thick and they are separated by a 3 in. thick layer of extruded polystyrene (XPS) as shown in Figure 7.28. Glass Fiber-Reinforced Polymer (GFRP) ties were used in the two panels as shear connectors. The design of the GFRP ties and the distribution will be presented in the next subsection

Design of GFRB Ties

NU-Ties Properties

$$A_{\text{tie.no3}} := 0.11 \text{ in}^2$$

$$C_e := 0.7$$

$$\alpha_{\text{tie.no3}} := 40$$

$$C_r := 0.65$$

$$\text{Tie}_{\text{Tensile.Strength}} := 110 \text{ ksi}$$

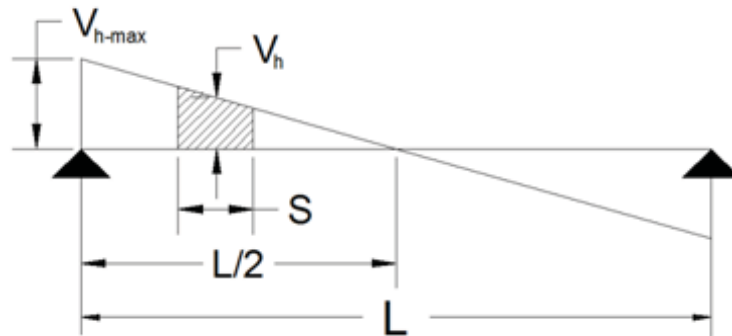
$$\text{Tie}_{\text{depth.no3}} := 7 \text{ in}$$

$$\phi_{\text{shear}} := 0.75$$

$$M_u := \text{Factor}_{\text{Load.Final}} = 1.06 \frac{\text{kip}}{\text{ft}}$$

$$\text{Span} = 26 \text{ ft}$$

$$M_u = 89.57 \text{ kip}\cdot\text{ft}$$



Total Horizontal Shear

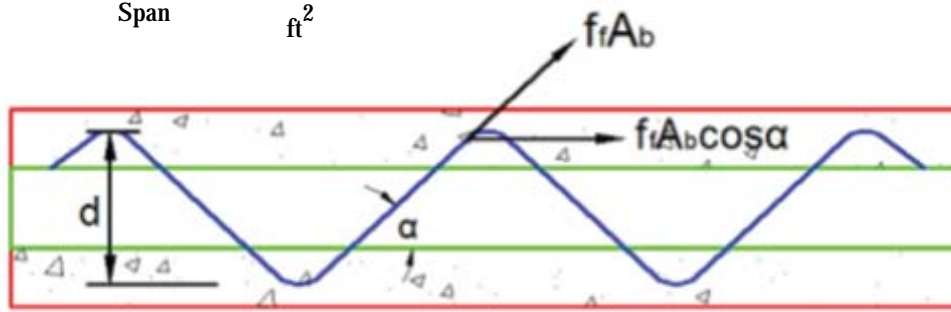
$$V_{h,\text{total}} := \frac{M_u}{\text{Tie}_{\text{depth.no3}}} = 153.55 \text{ kip}$$

Maximum Horizontal Shear

$$V_{h,\text{Max}} := \frac{V_{h,\text{total}} \cdot 4}{\text{Span}} = 23.62 \frac{\text{kip}}{\text{ft}}$$

Horizontal Shear Gradient

$$G := \frac{V_{h,\text{Max}} \cdot 2}{\text{Span}} = 1.82 \frac{\text{kip}}{\text{ft}^2}$$



$$F_{f.no3} := \phi_{\text{shear}} \cdot T_{ie} \cdot T_{ensile} \cdot Strength \cdot C_e \cdot C_r = 37.54 \text{ ksi} \quad \# 3$$

$$F_{no3} := A_{tie.no3} \cdot F_{f.no3} \cdot \cos\left(\alpha_{tie.no3} \cdot \frac{\pi}{180}\right) = 3.16 \text{ kip} \quad \# 3 \text{ Leg}$$

Since the length of NU-Tie is approximately 4 ft, the panel can be divided into segments that are 4 ft in length.

First segments

$$\text{First}_{\text{segments}} := 4 \text{ ft}$$

$$\text{Area}_{\text{segment.one}} := \frac{[V_{h.\text{Max}} + (V_{h.\text{Max}} - G \cdot \text{First}_{\text{segments}})]}{2} \cdot \text{First}_{\text{segments}} = 79.95 \text{ kip}$$

$$\text{Number}_{\text{Legs.segment1}} := \frac{\text{Area}_{\text{segment.one}}}{F_{no3}} = 25.28$$

Second segments

$$\text{Second}_{\text{segments}} := 4 \text{ ft}$$

$$V_{1\text{second}} := V_{h.\text{Max}} - G \cdot \text{First}_{\text{segments}} = 16.35 \frac{\text{kip}}{\text{ft}}$$

$$V_{2.\text{second}} := V_{1\text{second}} - G \cdot \text{Second}_{\text{segments}} = 9.09 \frac{\text{kip}}{\text{ft}}$$

$$\text{Area}_{\text{segment.second}} := \frac{(V_{1\text{second}} + V_{2.\text{second}})}{2} \cdot \text{Second}_{\text{segments}} = 50.88 \text{ kip}$$

$$\text{Number}_{\text{Legs.segment2}} := \frac{\text{Area}_{\text{segment.second}}}{F_{no3}} = 16.09$$

Third segments

$$V_{1\text{third}} := V_{2.\text{second}} = 2.92 \times 10^5 \frac{\text{lb}}{\text{s}^2}$$

$$\text{Third}_{\text{segments}} := 4 \text{ ft}$$

$$V_{2.\text{third}} := V_{1\text{third}} - G \cdot \text{Third}_{\text{segments}} = 1.82 \frac{\text{kip}}{\text{ft}}$$

$$\text{Area}_{\text{segment.third}} := \frac{(V_{1\text{third}} + V_{2.\text{third}})}{2} \cdot \text{Third}_{\text{segments}} = 21.81 \text{ kip}$$

$$\text{Number}_{\text{Legs.segment3}} := \frac{\text{Area}_{\text{segment.third}}}{F_{no3}} = 6.89$$

$$\text{Total}_{\text{legs}} := \text{Number}_{\text{Legs.segment3.}} + \text{Number}_{\text{Legs.segment2.}} + \text{Number}_{\text{Legs.segment1}} = 48.26$$

$$\text{Number}_{\text{ties}} := \frac{\text{Total}_{\text{legs}}}{4} = 12.06$$

Check the stresses in the ties under sustain Load

$$M_{\text{Sustain}} := \frac{(W_{\text{topping}} + W_{\text{panel}}) \cdot \text{Span}^2 \cdot 1.2}{8} = 35.49 \text{ kip} \cdot \text{ft}$$

$$V_{\text{h.total.sustain.loads}} := \frac{M_{\text{Sustain}}}{\text{Tie}_{\text{depth.no3}}} = 60.84 \text{ kip}$$

$$\text{Actual Stress in the ties due to Sustain Load} \quad \text{Actual}_{\text{no3.legs}} := 48$$

$$\text{Actual}_{\text{leg.force}} := \frac{V_{\text{h.total.sustain.loads}}}{\text{Actual}_{\text{no3.legs}}} = 1.27 \text{ kip}$$

$$\text{Actual}_{\text{leg.Stress}} := \frac{\text{Actual}_{\text{leg.force}}}{A_{\text{tie.no3}} \cdot \cos\left(\alpha_{\text{tie.no3}} \cdot \frac{\pi}{180}\right)} = 15.04 \text{ ksi} \quad \text{Less than 18 ksi}$$

$$V_{\text{h.total.Live.load}} := \frac{M_{\text{L.L.factor}}}{\text{Tie}_{\text{depth.no3}}} = 92.71 \text{ kip}$$

Actual Stress in the ties due to Live Load

$$\text{Actual}_{\text{leg.force.}} := \frac{V_{\text{h.total.Live.load}}}{\text{Actual}_{\text{no3.legs}}} = 1.93 \text{ kip}$$

$$\text{Actual}_{\text{leg.Stress.}} := \frac{\text{Actual}_{\text{leg.force.}}}{A_{\text{tie.no3}} \cdot \cos\left(\alpha_{\text{tie.no3}} \cdot \frac{\pi}{180}\right)} = 22.92 \text{ ksi} \quad \text{Less than 30 ksi}$$

The ties were distributed to be uniform as shown in Figure 7.28

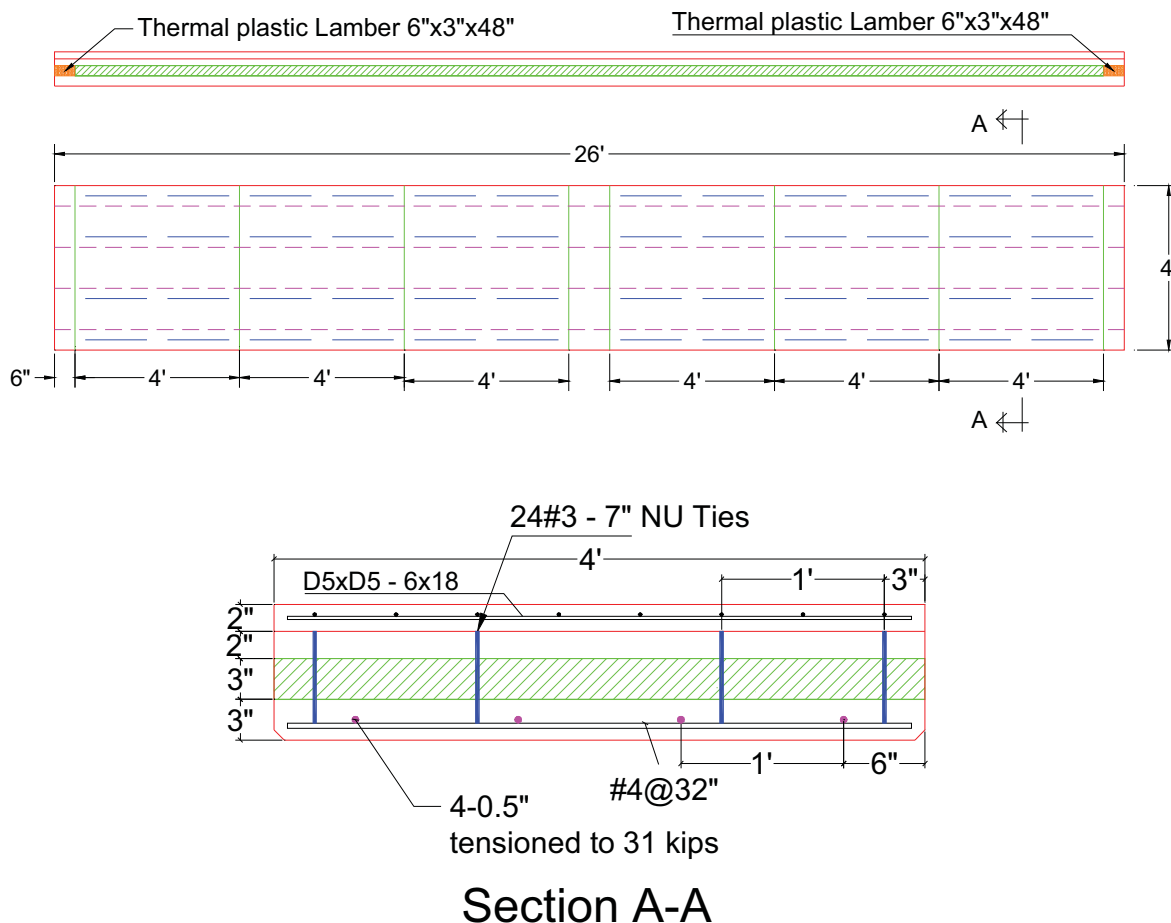


Figure 7.28: Fully insulated floor panels C and D

7.6.2 Specimens Erection

The panels C and D were fabricated and cast in the same bed as panels A and B. Below are the steps followed in the erection of phase II specimens. Fabrication process pictures were shown in Appendix F

Step 1) Preparation of XPS foam panels

Step 2) Production of GFRP, then linear strain gauges were connected to the tension legs of the GFRP ties before concrete pouring. After the insulation blanks are ready, GFRP-tie is inserted into the foam and the remaining gaps are filled with canned expanding foam insulation as shown in Figure 7.29.

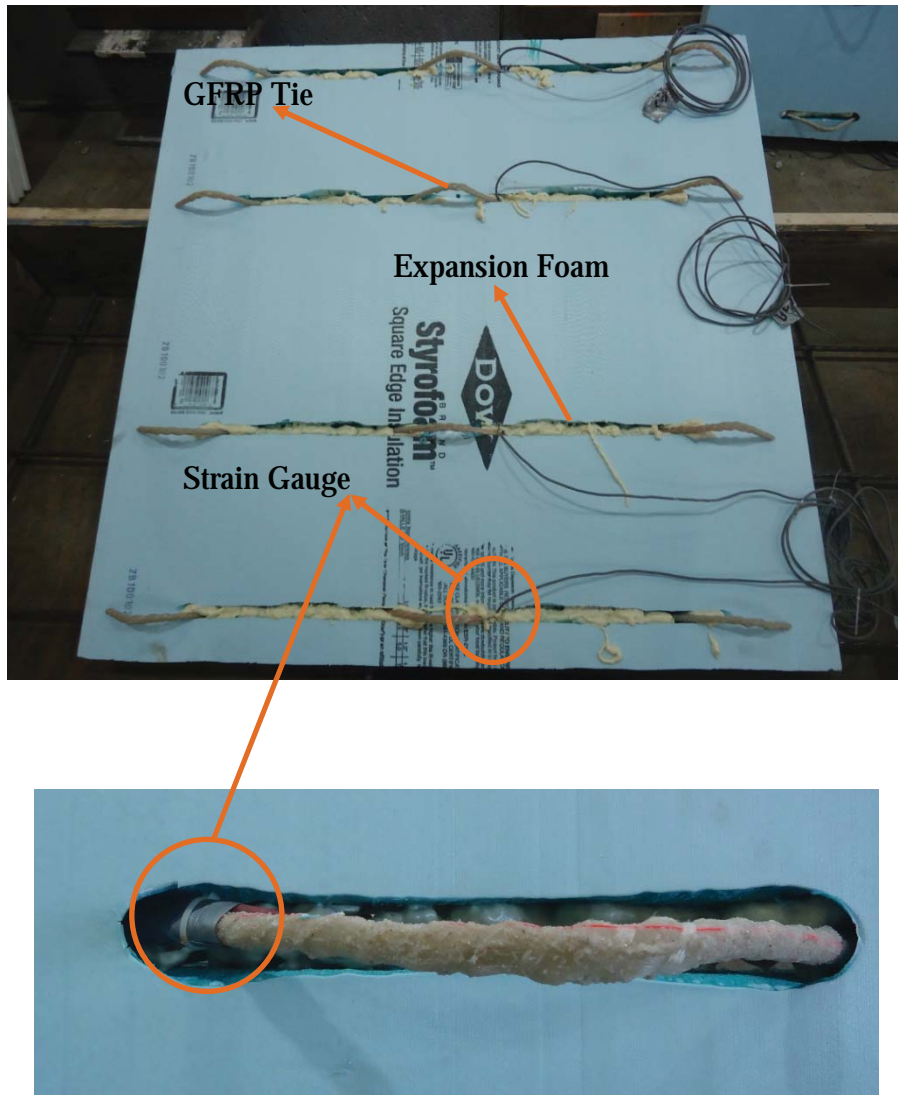


Figure 7.29: Insert GFRP tie into the XPS slot and filling the gap with expanding foam insulation

Step 3) Setup the forms and lubricate the bed for concrete placement and tension the strands and place the reinforcement.

Step 4) Pour the concrete. SCC concrete was delivered by Ready Mix truck to the PKI structural laboratory. Spread diameter was taken upon arrival and was found to be 22 in. First placed the bottom wythe, then Place XPS panels with GFRP ties on the fresh concrete of the bottom wythe and Place the concrete of the top wythe. Lifting points were then inserted into the still fresh concrete at each end. Wet burlap curing commenced after the specimens had setup such that the burlap would not damage the surface or lifting points.

Step 5) Release and cut the strands, after three days, the concrete strength reached 8034psi, then the strands were released gradually.

Step 6) place topping reinforcement D5 x D5 @ 6 in. x 18 in. and casting 2 in. the concrete topping

7.6.3 Material Properties

The same mixes, which used in panel A and B was used in panel C and D as shown in Table 7.4. Figure 7.30 shows compressive strength versus age relationships for precast concrete and the topping.

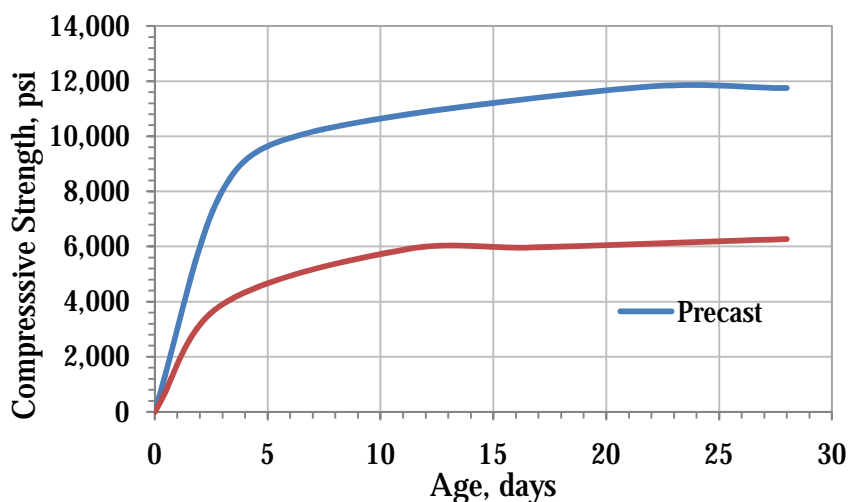


Figure 7.30: Concrete strength gain with time

7.6.4 Test Setup and Procedures

Testing of the phase II specimens was performed on December 1, 2, and 3, 2011 to investigate the flexural and shear behavior of panel C and D under different type of loading. The test program includes the following tests:

- 1- Flexural test
 - A. Using two point loads
 - B. Using one point loads
- 2- Shear test
 - A. Test 1
 - B. Test 2
 - C. Test 3

7.6.4.1 Flexural Test

A. Using Two Point Loads

The purpose of this test is to investigate the flexural behavior of panel C under two point loads, also to evaluate the positive moment capacity of the composite panel for resisting gravity loads. Figure 7.31 shows the test setup, where the panel was loaded as simply supported. At the time of the test, the concrete strength was reached 11.5 ksi. Testing was performed by applying two point loads at 9 ft from the center of the roller. Concrete strain gauges were attached to the top surface to measure the strain in extreme compression fibers. Specimen deflection was recorded using one potentiometer located at mid-span, in addition to measure the strains in the GFRP ties. Figure 7.32 shows the GFRP ties strain gauges locations. The relative movement between the top wythe and the bottom wythe was recorded as shown in Figure 7.33. The deflection of panels C and D

due to self-weight plus topping weight was measured after setup the panels using laser device as shown in Figure 7.31 and was found 0.385 in. Also the deflection was checked using the analytical models (truss and FE model), and was found 0.35 in. after subtracted the camber from the self-weight. See Figure 7.62

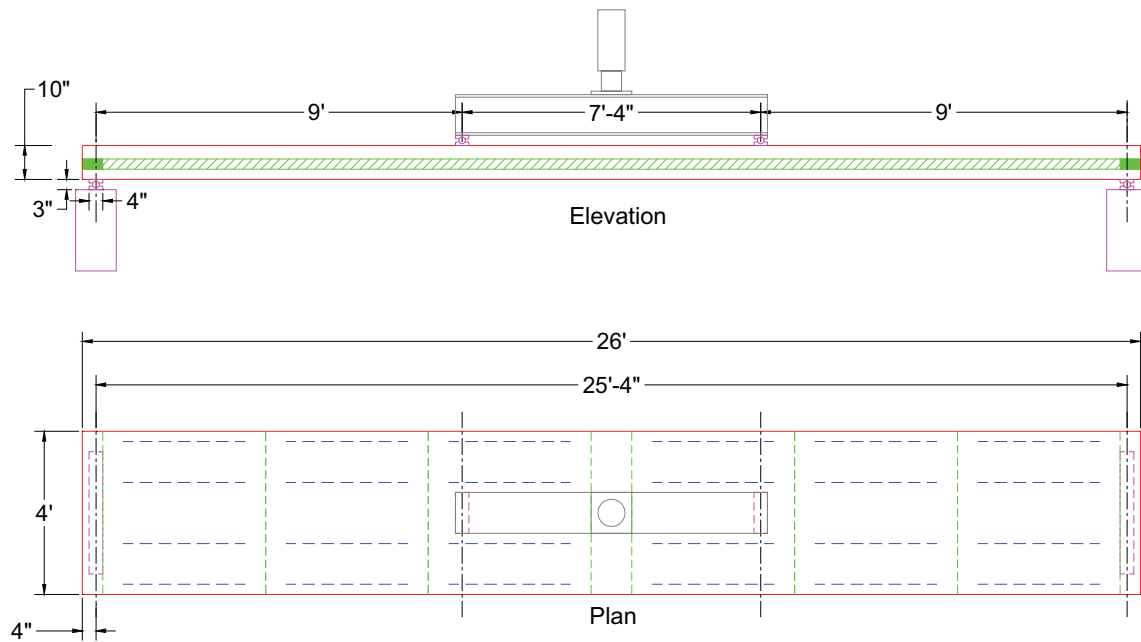


Figure 7.31: Test setup for panel C

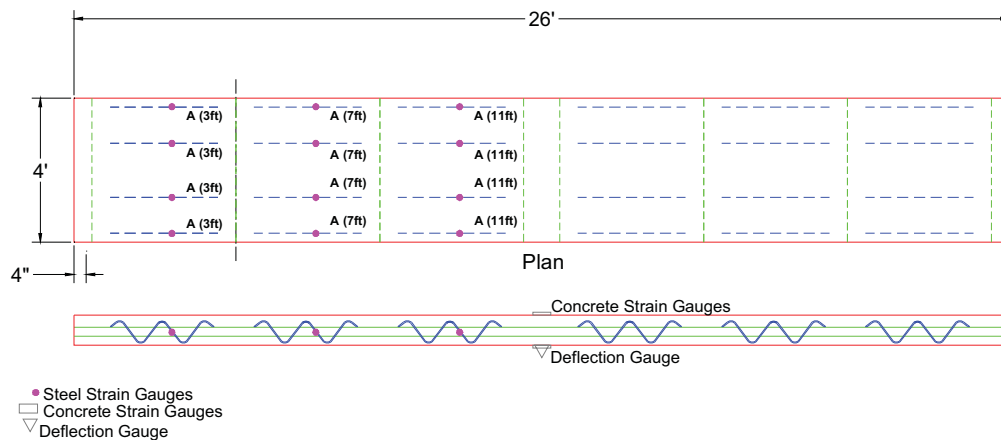


Figure 7.32: Specimen instrumentation



Figure 7.33: Measuring the relative movement between the bottom and top wythes

Figure 7.34 plots the load deflection relationships of panel C. In this plot, the left vertical axis shows the applied load in pounds, while the right axis shows the corresponding uniform load (i.e that results in similar deflection) in pound per square foot. This plot indicates that the composite panel was able to carry 13.3 kip, which corresponds to a total positive moment capacity (Measured capacity) equal to 87.9 kip.ft (including the moment due to the self-weight of the panel and the topping weight). The demand for resisting the

loads is 89.57 kip.ft, which is 1.9% large than the actual capacity. Also, the nominal capacity (theoretical capacity) of the composite panel predicted using strain compatibility approach was found to be 112 kip.ft, which is significantly higher than the actual capacity. The load-deflection relationships show a linear behavior up to 7 kip. It should be noted that the point load equivalent to a live load of 100 psf is 8 kip and the corresponding deflection is 0.85 in. approximately.

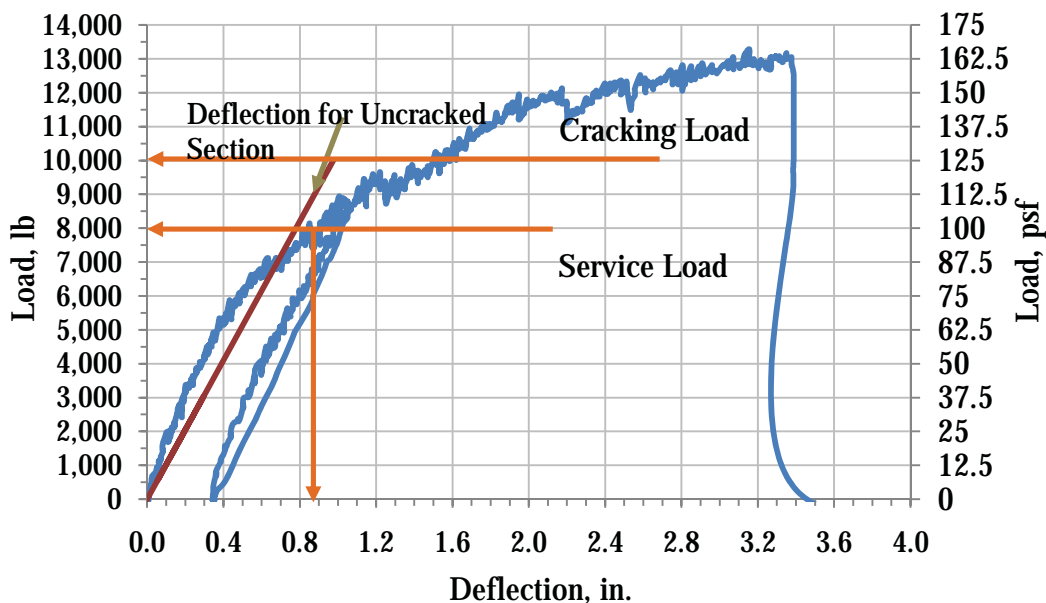


Figure 7.34: Load-deflection relationship for the panel C

Figure 7.35 and Figure 7.36 plot the load-strain relationships at the top concrete surface and in the tension legs of several GFRP ties respectively. Figure 7.35 indicates that the maximum compressive strain in the concrete at mid-span was 0.00046, which is below 0.003 (ultimate compressive strain). Figure 7.36 indicates that the maximum strain in the GFRP ties is approximately 0.0067, which occurred at the ties located 3 ft and 7 ft from the panel end. This strain corresponds to a stress of approximately 40.2 ksi using modulus of elasticity of 6000 ksi. This stress level is below the design stress of the ties after

considering the exposure and interaction coefficients ($110 \times 0.7 \times 0.65 = 50$ ksi). Figure 7.36 also indicates that the ties located 3 ft and 7 ft from the panel end have small differences in the strains values. Ties located 11 ft from panel have strains less than 0.0008 in. That strain corresponds to a stress of approximately 4.8 ksi (i.e. very little loads was carried by these ties). It also should be noted that the horizontal shear distribution in the tested panel is the combination of the triangular distribution due to self-weight and the rectangular distribution due to applied load, which explains why the strain values are not linearly proportioned to the tie location and why the ties located 11 ft from the panel end have less strains because there is no shear force due to the applied load at that location. The measured mid-span deflections under the self-weight and service load were found to be 0.385 in. and 0.85 in. respectively. Figure 7.37 illustrates the relative movement between the two connected wythes (bottom wyth and the top wyth). The figure shows that 0.1 in. is the maximum movement can be occurs between the two connected wythes. It also should be noted that this movement was recorded for the end which has no failure.

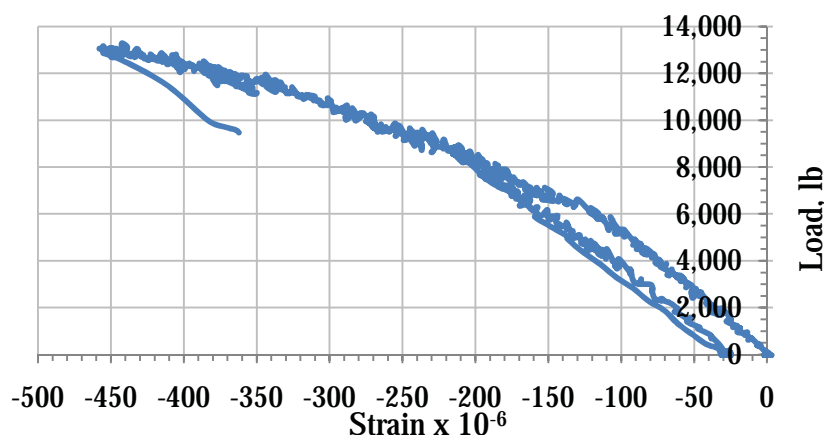


Figure 7.35: Load-strain relationship at the top concrete surface

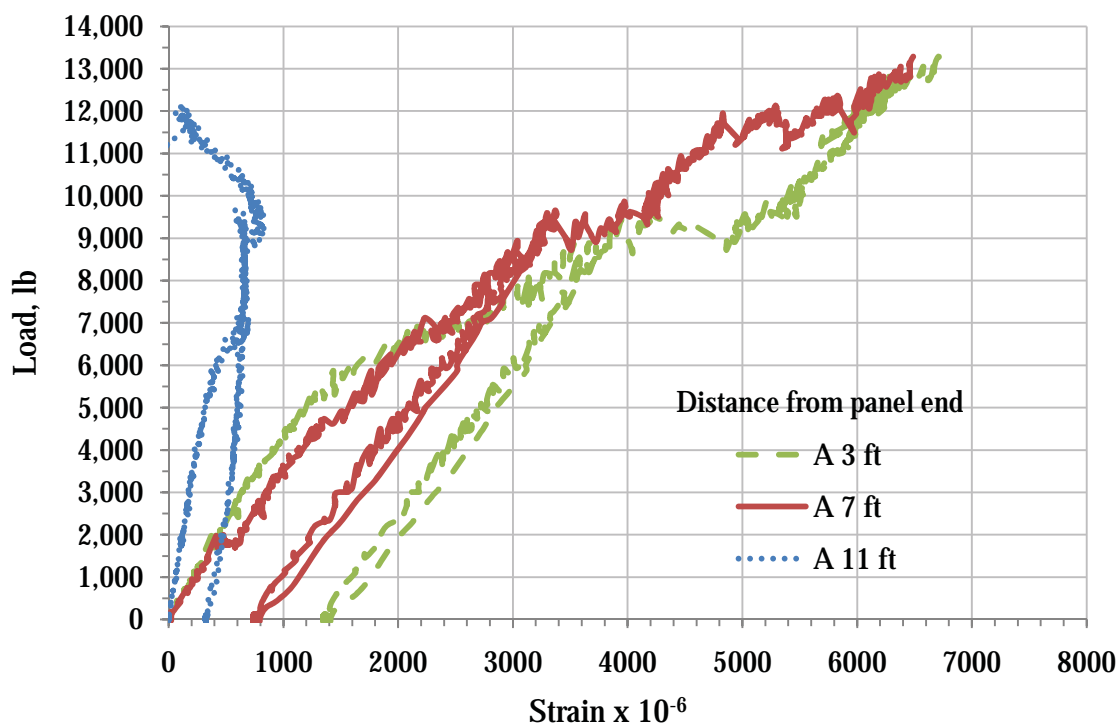


Figure 7.36: Load-strain relationship for GFRP ties at different locations

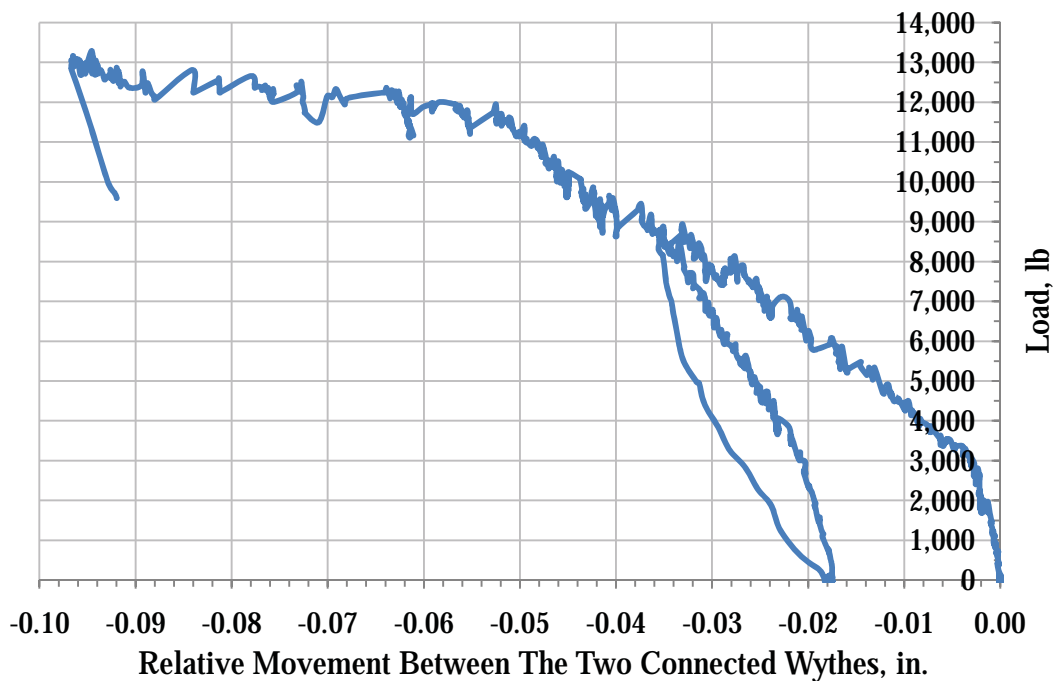


Figure 7.37: Load-relative movement relationship for connected wythes

Figure 7.38 shows the mode failure of panel C. Because of the rectangular distribution of shear diagram between the load and the support, the failure occurred due to the horizontal shear. The horizontal shear caused the pullout of some ties from the bottom concrete wythe. No cracks or deformation have been seen or recorded in middle part (between the two loads) due to the zero shear diagrams in that area.

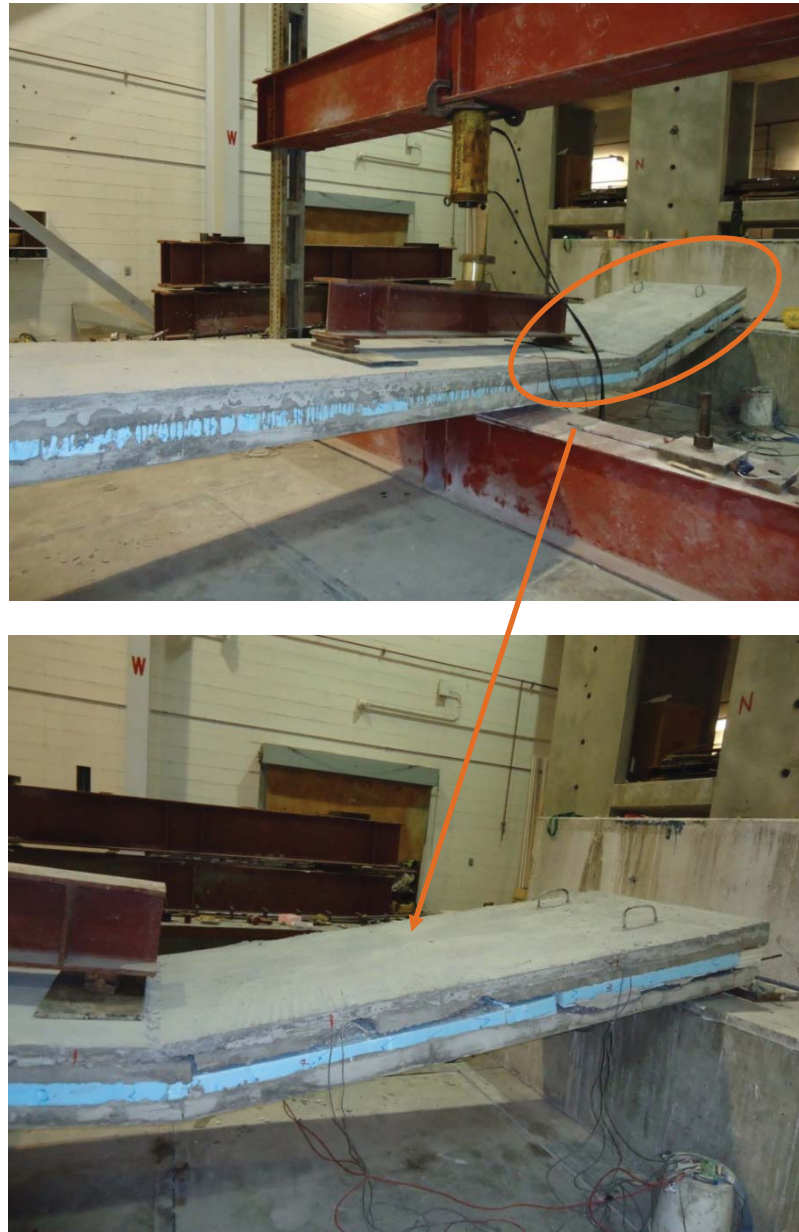


Figure 7.38: Pull out of GFRP tie at failure

B. Using One Point Load

Figure 7.39 shows panel D test setup, where the panel was loaded as simply supported. Testing was performed by applying one point load at mid-span at 12.67 ft from the center of the roller. Concrete strain gauges were attached to the top surface to measure the strain in extreme compression fibers. Specimen deflection was recorded using one potentiometer located at mid-span; also, the relative movement between the top wythe and the bottom wythe was recorded. The strains in the GFRP ties were measured. Figure 7.40 shows the GFRP ties strain gauges locations.

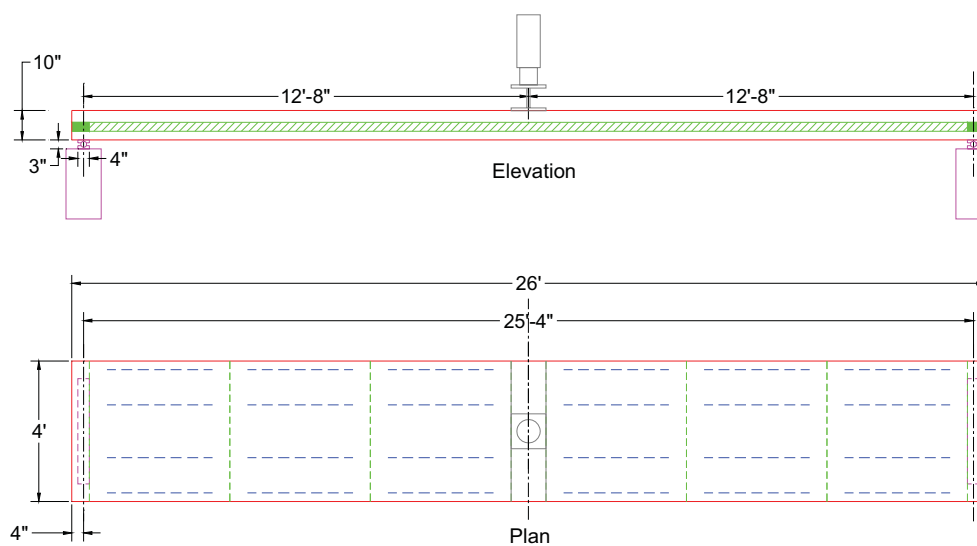


Figure 7.39: Test setup for panel D

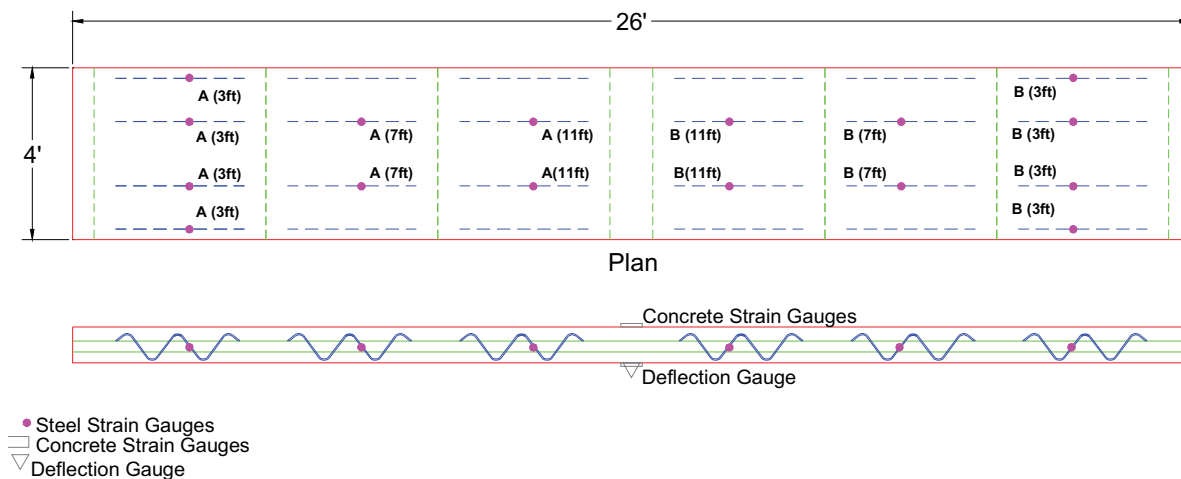


Figure 7.40: Specimen instrumentation

Figure 7.41 plots the load deflection relationships of panel D. In this plot, the left vertical axis shows the applied load in pounds, while the right axis shows the corresponding uniform load (i.e that results in similar deflection) in pound per square foot. This plot indicates that the composite panel was able to carry 15.012 kip, which corresponds to a total positive moment capacity (Measured capacity) of 123.2 kip.ft (including the moment due to the self-weight of the panel and the topping weight). The demand for resisting the loads is 89.57 kip.ft, which is 37.5% less than the actual capacity. Also, the nominal capacity (theoretical capacity) of the composite panel predicted using strain compatibility approach was found to be 112 kip.ft, which is significantly less than the actual capacity. The load-deflection relationships show a linear behavior up to 8 kip approximately. The measured mid-span deflections under the self-weight and cracking load were found to be 0.385 in. and 0.4 in. respectively. It should be noted that the point load equivalent to a live load of 100 psf is 6.3 kip and the corresponding deflection is 0.36 in. approximately.

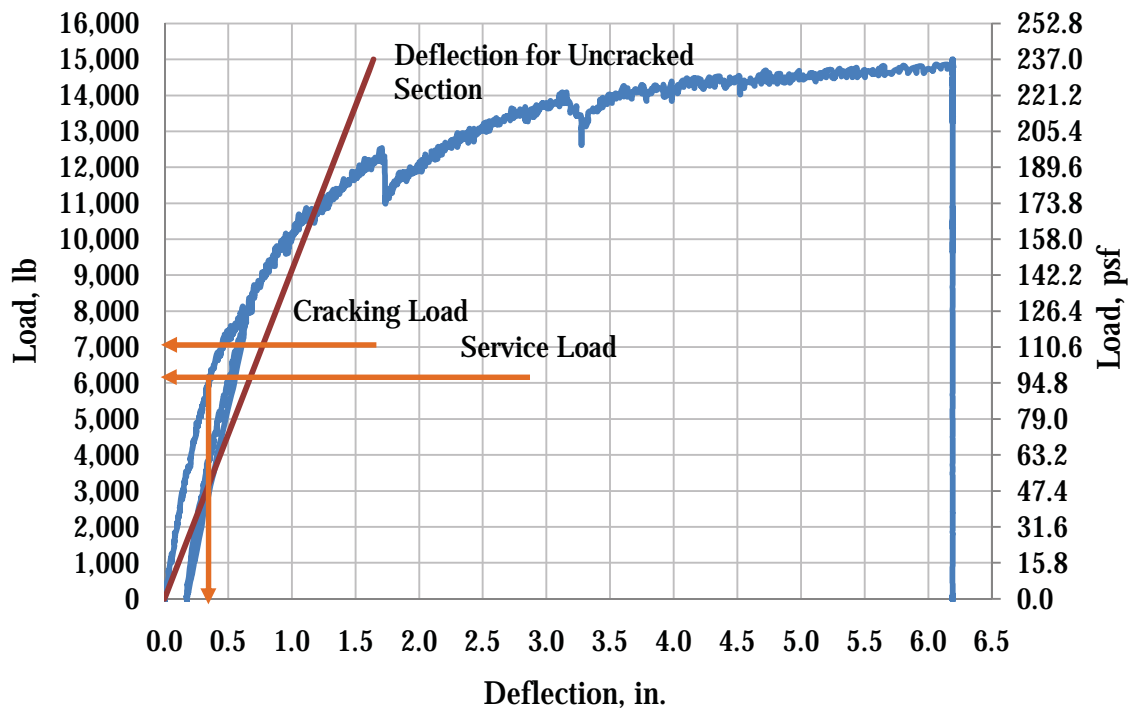


Figure 7.41: Load-deflection relationships for the panel D

Figure 7.42 and Figure 7.43 plot the load-strain relationships at the top concrete surface and in the tension legs of several GFRP ties respectively. Figure 7.42 indicates that the maximum compressive strain in the concrete at mid-span was 0.00161, which is well below 0.003 (ultimate compressive strain). Figure 7.43 indicates that the maximum strain in the GFRP ties is approximately 0.0074, which occurred at the ties located 7 ft from the panel end. This strain corresponds to a stress of approximately 44.4 ksi using modulus of elasticity of 6000 ksi. This stress level is below the design stress of the ties after considering the exposure and interaction coefficients ($110 \times 0.7 \times 0.65 = 50$ ksi). Figure 7.43 also indicates that the ties located 3 ft, 7 ft, and 11 ft from the panel end have the same strain behavior, but with small differences in the strains values. It also should be noted that the horizontal shear distribution in the tested panel is the combination of the triangular distribution due to self-weight and the rectangular distribution due to applied

load, which explains why the strain values are not linearly proportioned to the tie location. Figure 7.44 shows the mode failure of panel D. The figure illustrates that no horizontal shear failure. The failure occurs due to the yielding of the strands.

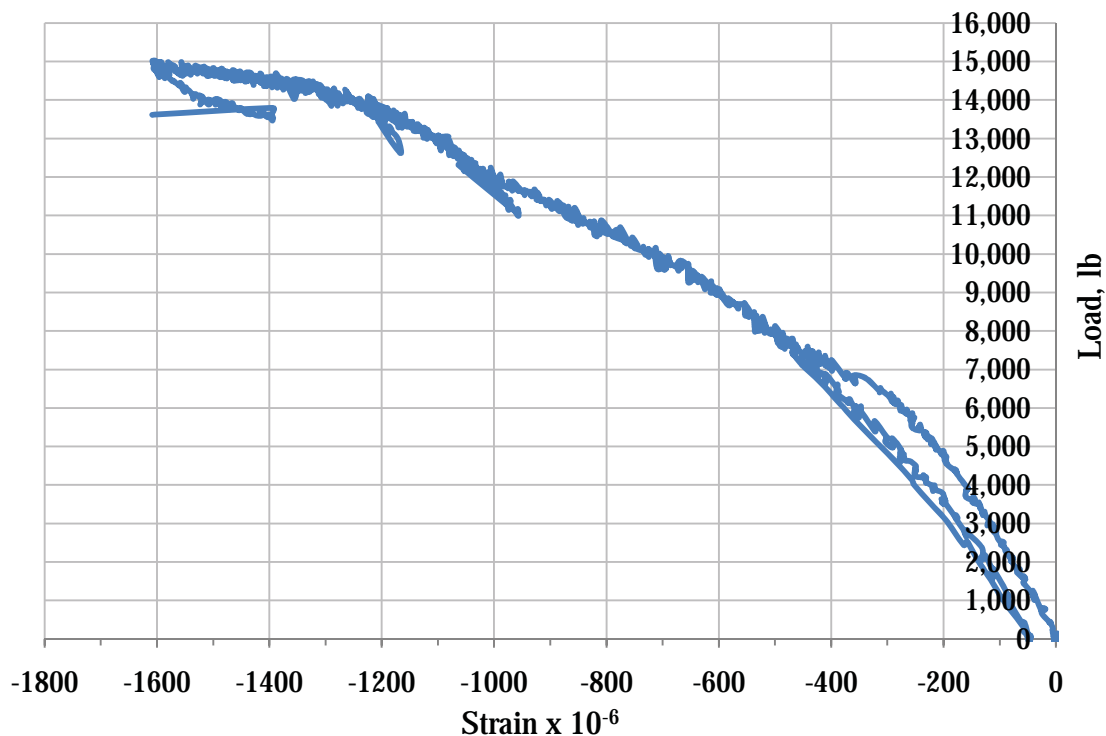


Figure 7.42: Load-strain relationship at the top concrete surface

Table 7.6 compares the theoretical flexural capacity of each specimen with its measured flexural capacity obtained from testing. The ratios of measured-to-theoretical capacity indicate that panel C has flexural capacity less than the theoretical capacity due to the horizontal shear failure; in the contrary panel D has flexural capacity higher than the theoretical capacity of a fully composite section. This means that the section is fully composite. The ratios of measured -to-theoretical capacity in Table 7.6 also indicate that GFRP ties in panel D have achieved the full composite action.

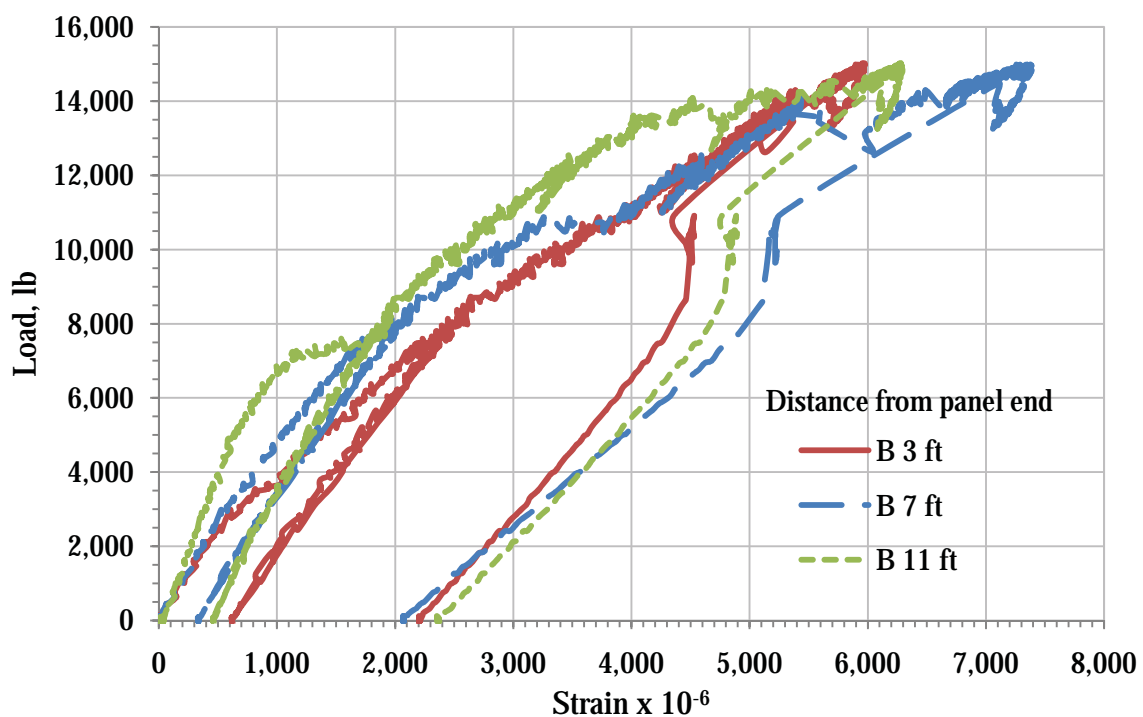
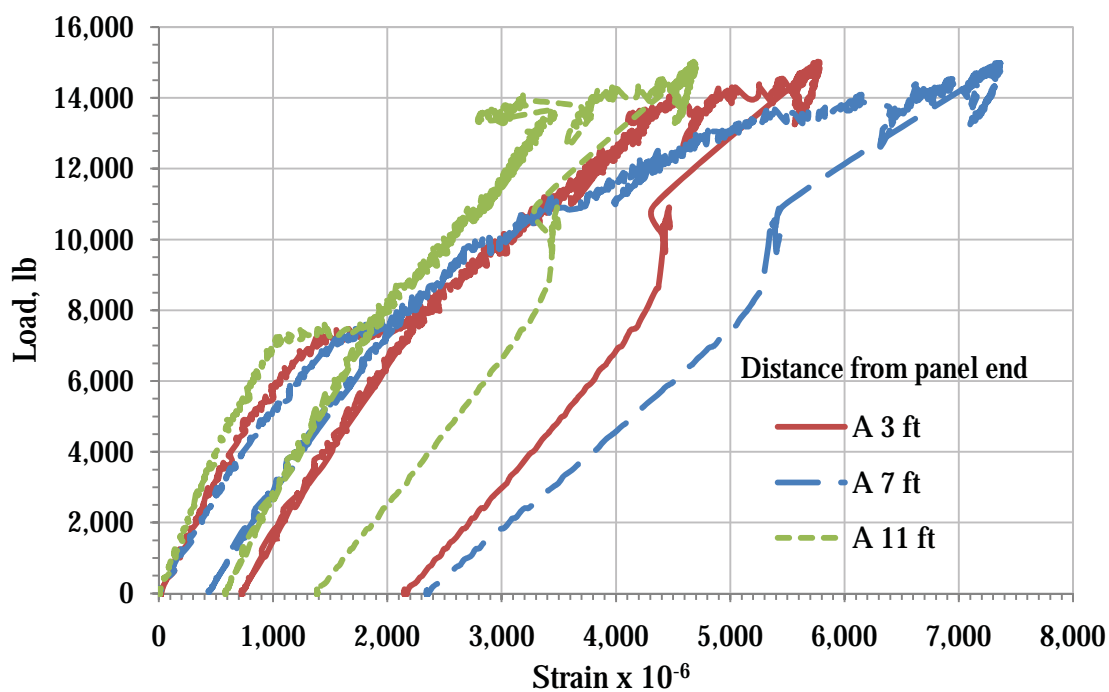


Figure 7.43: Load-strain relationship for GFRP ties at different locations left side (Top) and right side (bottom)



Figure 7.44: Failure mode of panel D

Table 7.6: Comparing the theoretical against measured flexural capacity of phase II test specimens

Panel	L_e (in.)	$M_{\text{theoretical}}$ (kip. In.)	$W_{O.W}$ (kip/in.)	$M_{O.W}$ (Kip.in.)	P_{measured} (kip)	M_{measured} (kip. in.)	$M_{\text{total-measured}}$ (kip. in.)	$M_{\text{total.measured}} / M_{\text{theoretical}}$
Panel C	304	1344	0.0292	336.9	13.3	718.2	1055.1	0.79
Panel D	304	1344	0.0292	336.9	15	1140	1476.9	1.10

7.6.4.2 Shear Test

The shear test was done on some parts of panels C and D to investigate the shear behavior of the precast sandwich panel. The following section will discuss the shear behavior in details.

A. Test 1

Test 1 was done on the middle part of panel C. Figure 7.45 shows the test setup, where the load was applied at the mid-span at 3.5 ft from the center of the roller. Specimen deflection was recorded using one potentiometer located at mid-span; also the strains in the GFRP ties were measured. Figure 7.46 shows the GFRP ties strain gauges locations.

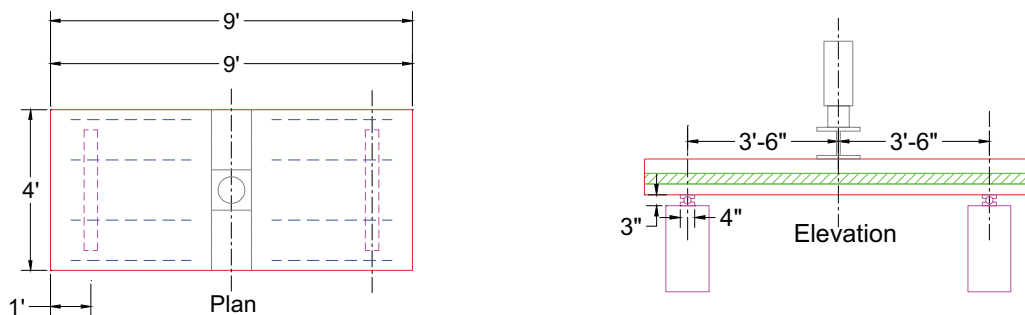


Figure 7.45: Test 1 setup

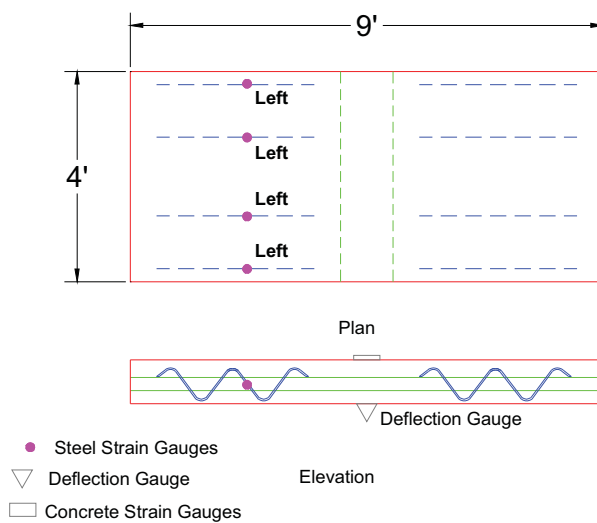


Figure 7.46: Test 1 specimen instrumentation

Figure 7.47 plots the load deflection relationships of test 1. This plot indicates that the composite panel was able to carry 30.7 kip, which corresponds to shear capacity

(measured capacity) of 16.6 kip (including the load due to the self-weight of the panel and the topping weight). The demand is 13 kip.ft, which is 27.7% less than the actual capacity.

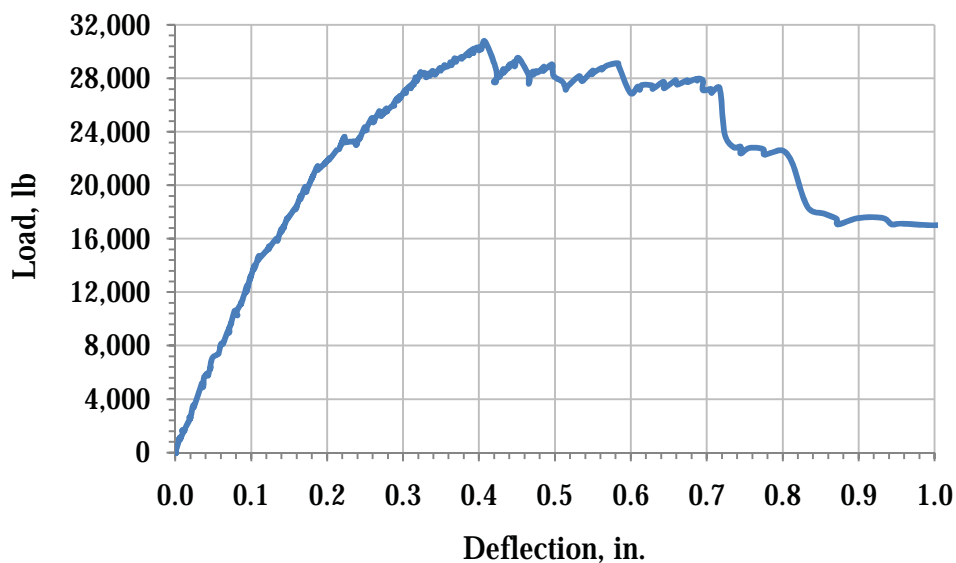


Figure 7.47: Load-deflection relationship for test 1

Figure 7.48 plot the load-strain relationships in the tension legs of several GFRP ties respectively. Figure 7.48 indicates that the maximum strain in the GFRP ties is approximately 0.0108, which occurred at the ties located at the left side of the panel end. This strain corresponds to a stress of approximately 64.8 ksi using modulus of elasticity of 6000 ksi. This stress level is above the design stress of the ties after considering the exposure and interaction coefficients ($110 \times 0.7 \times 0.65 = 50$ ksi).

Figure 7.49 shows the failure of test 1. The failure occurred due to the horizontal shear. The horizontal shear caused the pullout of some ties from the bottom concrete wythe

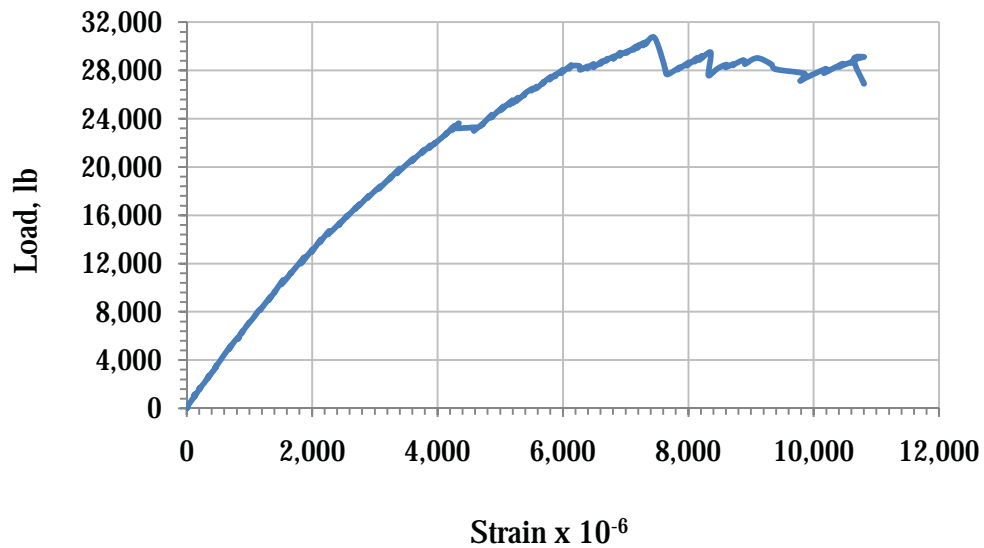


Figure 7.48: Load-strain relationship for GFRP ties at left



Figure 7.49: Shear failure of test 1

B. Test 2 & 3

Test 2 and test 3 were done in two parts of panel D. Figure 7.50 shows the test setup, where the load was applied at the mid-span at 4 ft from the center of the roller support. Specimen deflection was recorded using one potentiometer located at mid-span; also the strains in the GFRP ties were measured. Figure 7.51 shows the GFRP ties strain gauges locations.

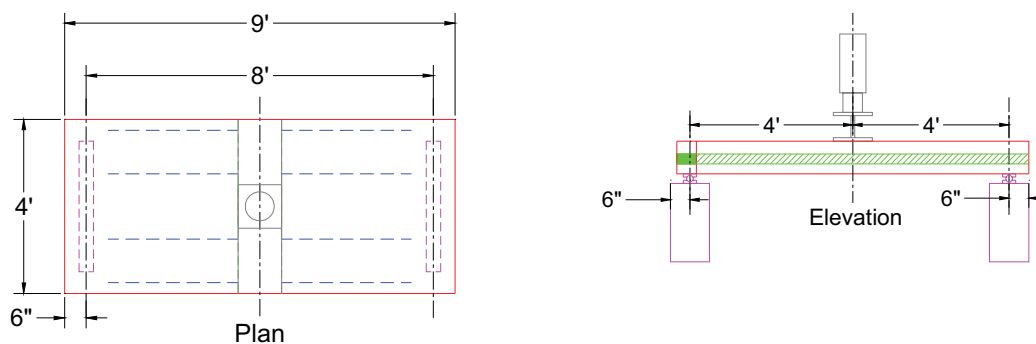


Figure 7.50: Test 2 setup

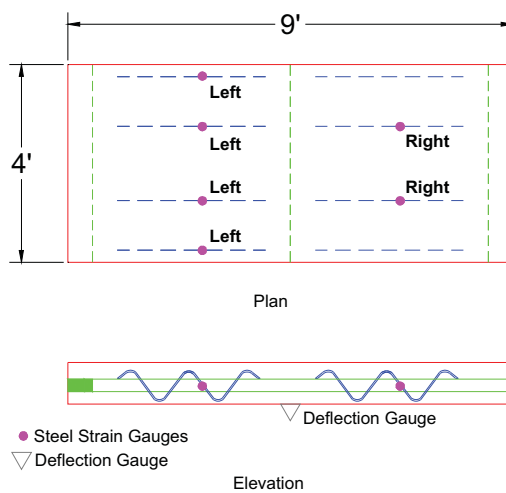


Figure 7.51: Test 2 specimen instrumentation

Figure 7.52 plots the load deflection relationships of test 2 and 3. In this plot, the left vertical axis shows the applied load in pounds. This plot indicates that the composite panel was able to carry 21.535 kip and 20.85 kip, which corresponds to shear capacity

(measured capacity) of 12.2 kip and 11.8 (including the load due to the self-weight of the panel and the topping weight). While the demand was 13 kip.ft, which is 6.5% and 10% higher than the actual capacity for test 2 and 3 respectively. The measured shear capacity is less than the demand due to the flexural test effects, which decrease the composite action due to loss in bond between the GFRP ties and the concrete.

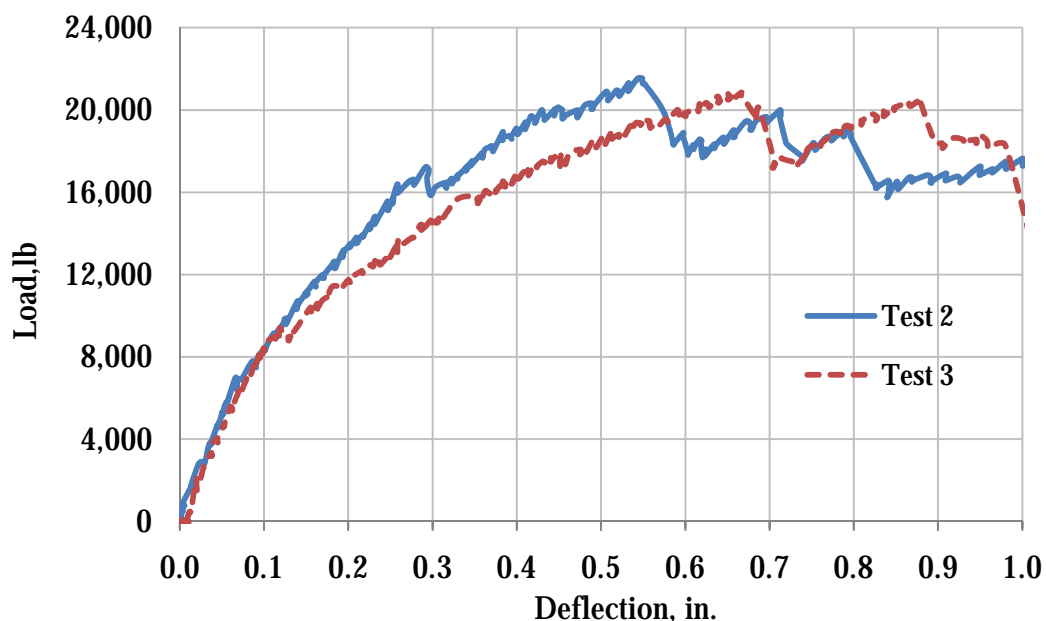


Figure 7.52: Load-deflection relationship for test 2&3

Figure 7.53 and Figure 7.54 plots the load-strain relationships in the tension legs of several GFRP ties. The plot indicates that the maximum strain in the GFRP ties is approximately 0.00686 and 0.0073 in test 2 and 3 respectively. This strain corresponds to a stress of approximately 41.16 ksi and 43.7 ksi using modulus of elasticity of 6000 ksi. This stress level is below the design stress of the ties after considering the exposure and interaction coefficients ($110 \times 0.7 \times 0.65 = 50$ ksi).

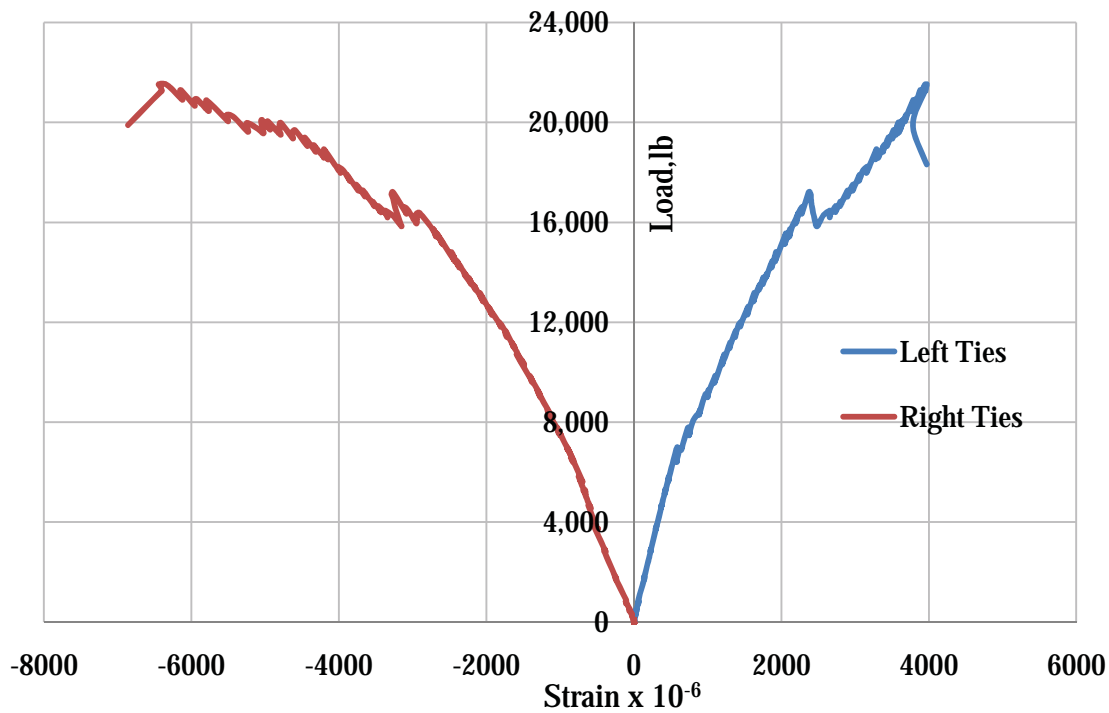


Figure 7.53: Load-strain relationship of GFRP ties for test 2

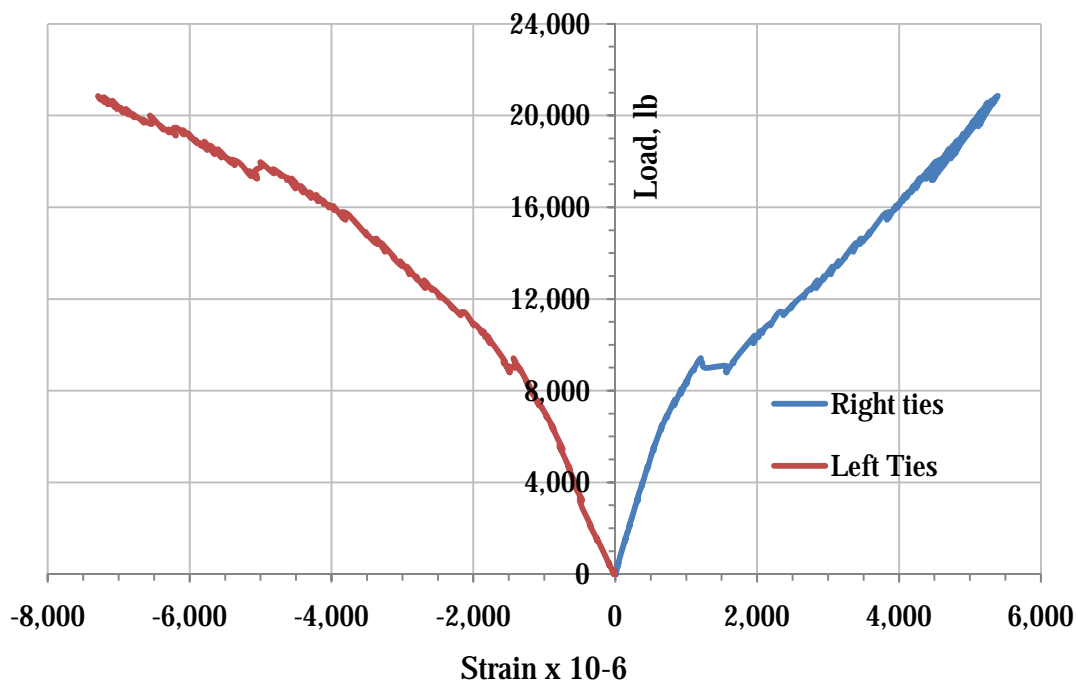


Figure 7.54: Load-strain relationship of GFRP ties for test 3

Figure 7.55 show the mode failure of test 2 and 3. The failure occurred due to the horizontal shear. The horizontal shear caused the pullout of ties from the top concrete wythe.



Figure 7.55: Shear failure of test 2 &3

7.7 Analytical Models

In order to predict the behavior of precast concrete sandwich floor panels with different number and distribution of ties, two modeling methods were investigated. The first method is the planar truss method in which the top-chord members represent the top wythe, bottom-chord members represent the bottom wythe, and diagonal members represent tie legs. Figure 7.56 shows the two planar truss models developed for panel A, B, C, and D. In each model, truss elements are assumed to be located at the centerlines of actual elements and have the equivalent section properties. For example, the geometric properties of a diagonal member in the end of the panel A are equal to eight times the geometric properties of one tie leg. Connections between the diagonal members and top and bottom chord members are assumed to be pinned with rigid end zone equal to the portion of tie leg embedded in concrete. The truss models of panel A, B, and D are assumed to be simply supported and subjected to 6.5 kip, 6.5 kip, and 6.3 kip one point loads respectively, while panel C model subjected to 4 kip two point load which represents the equivalent service live load 100 psf in terms of deflection.

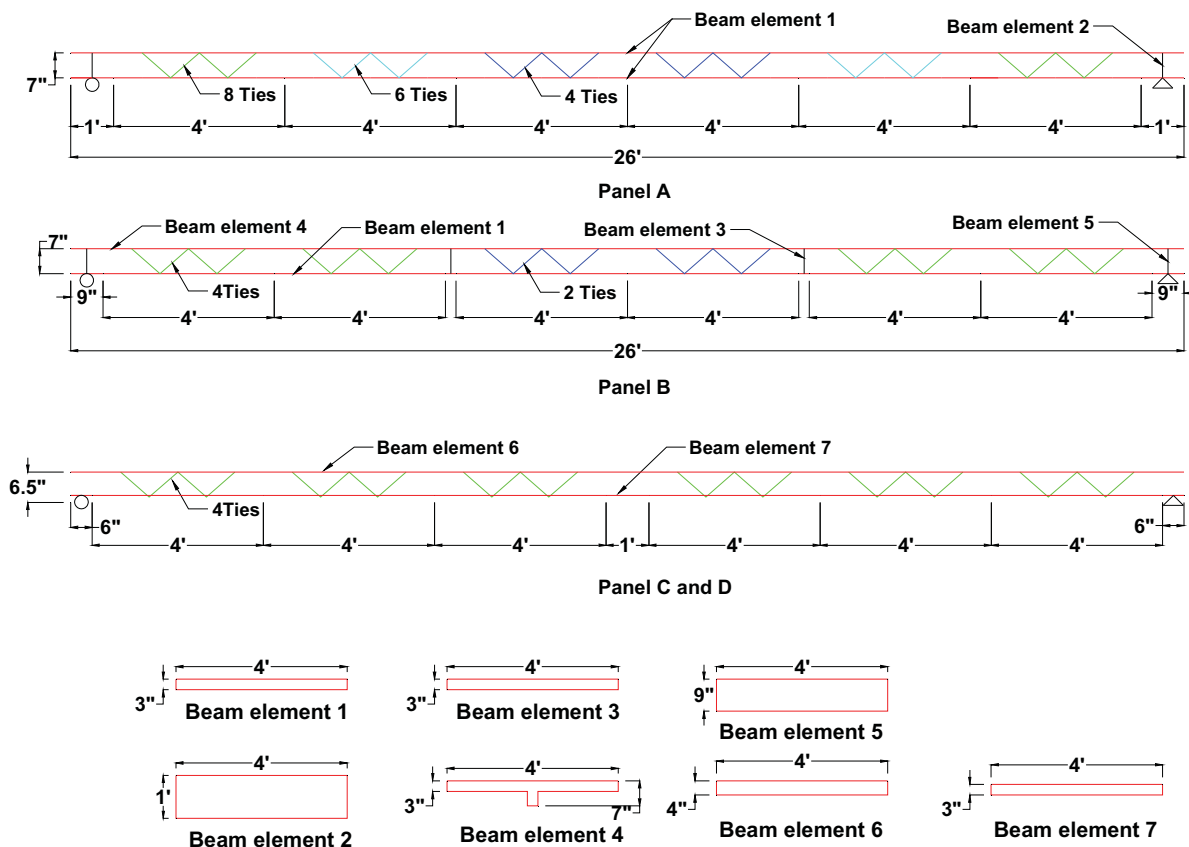


Figure 7.56: Truss models of panel A, B, C, and D

The second modeling method is developing three-dimensional FE models in which the top and bottom wythes are modeled as shell elements, and tie legs are modeled as frame elements. Figure 7.57 shows the model developed for the panel A, B, C, and D. In each model, shell and frame elements are assumed to be located at the centerlines of actual elements and have their exact section properties. Connections between the frame and shell elements are assumed to be pinned with rigid end zone equal to the portion of tie leg embedded in concrete. Also the FE models of panel A, B, and D are assumed to be simply supported and subjected to 6.5 kip, 6.5 kip, and 6.3 kip point loads respectively, while panel C subjected to 4 kip two point load which represents the equivalent service live load 100 psf in terms of deflection. Figure 7.58, Figure 7.59, Figure 7.60, and Figure

7.61 illustrate the deflection values for the truss model and the deflection contour lines for FE model of panel A, B, C, and D respectively under service load. Also the analysis results of the truss and FE models are listed in Table 6.4.

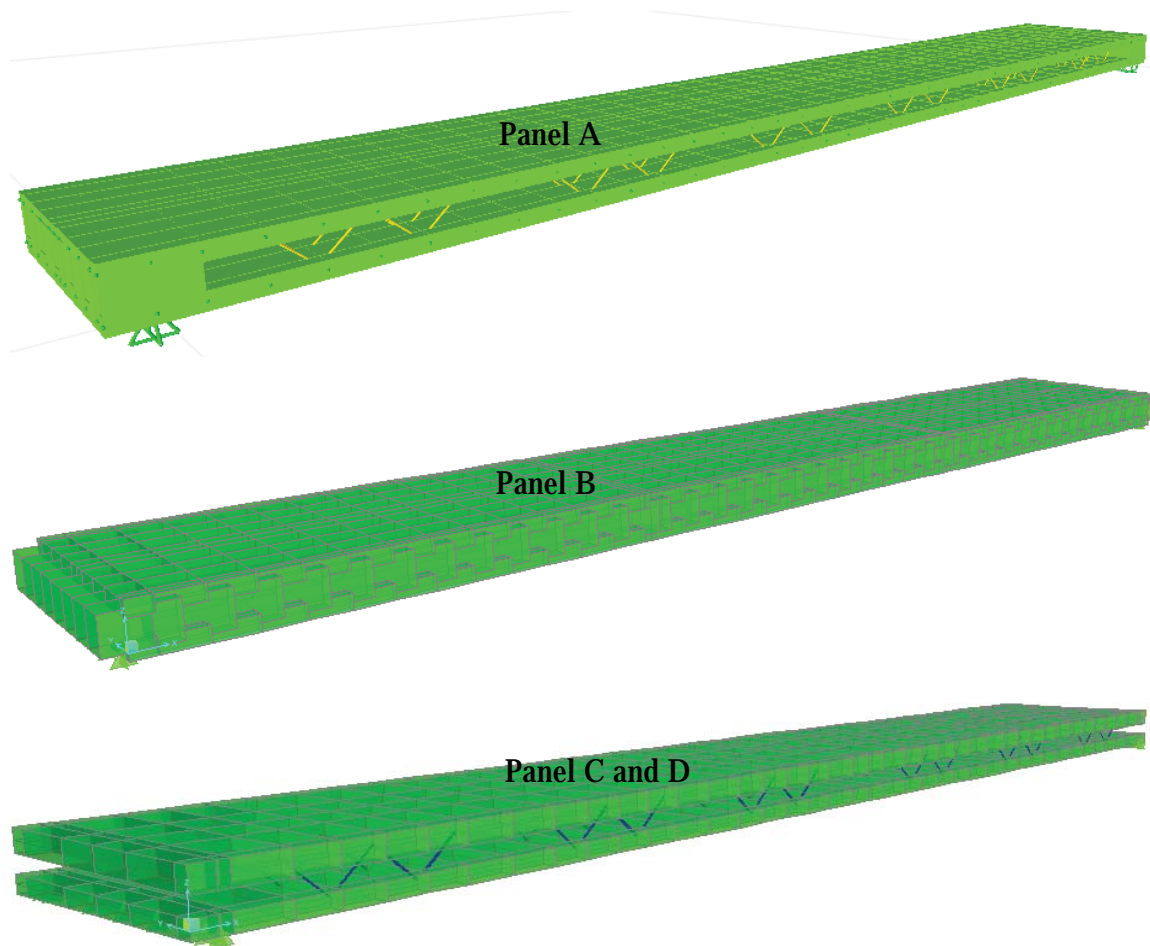
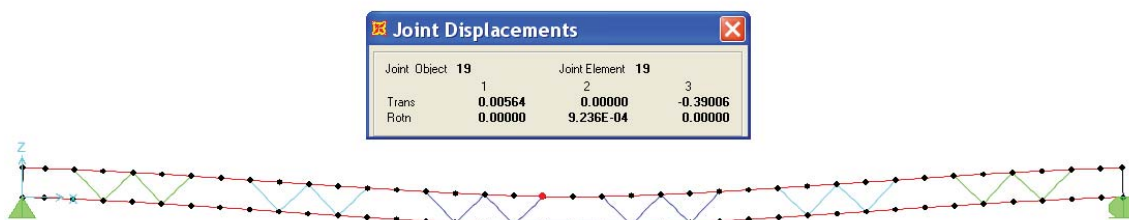


Figure 7.57: 3D FE model of panel A, B, C, and D



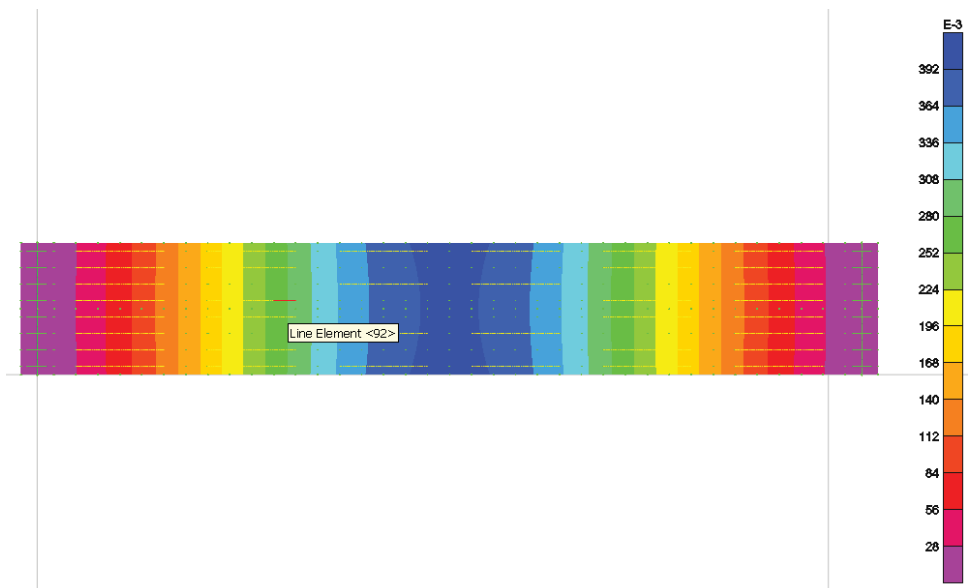


Figure 7.58: Service load deflection of panel A using the truss model and FE model

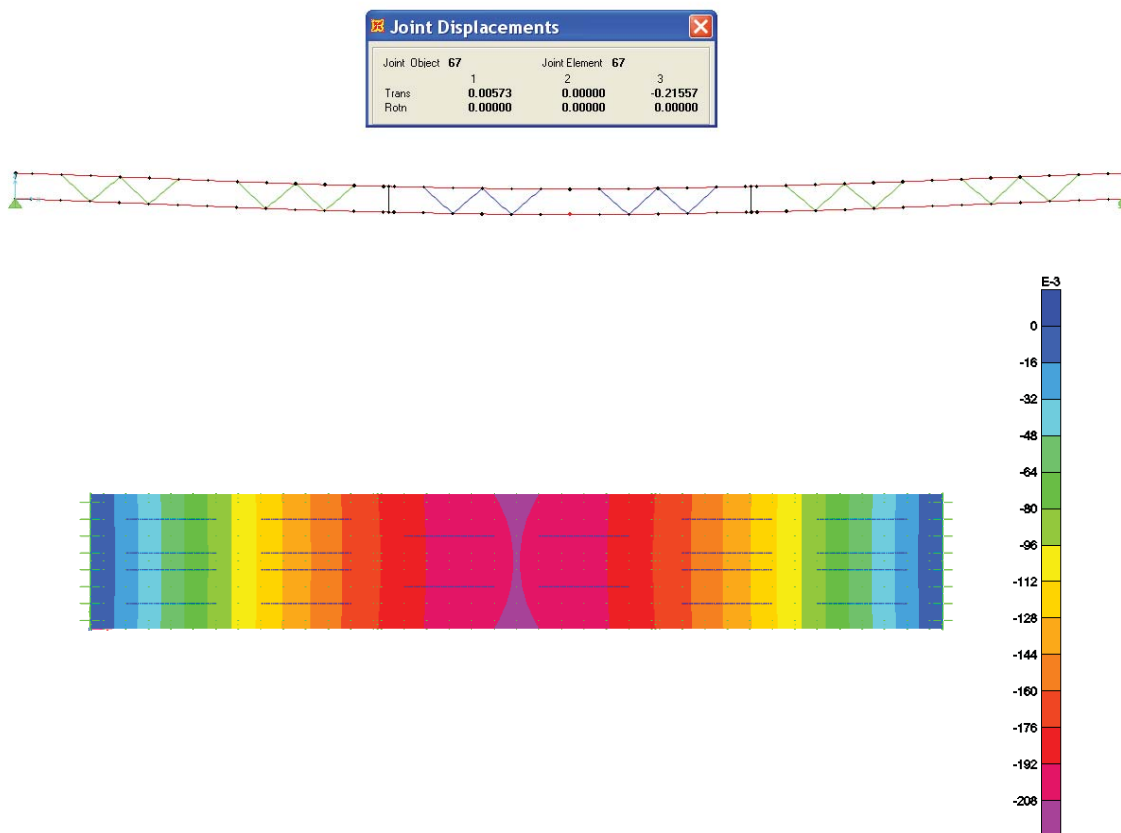


Figure 7.59: Service load deflection of panel B using the truss model and FE model

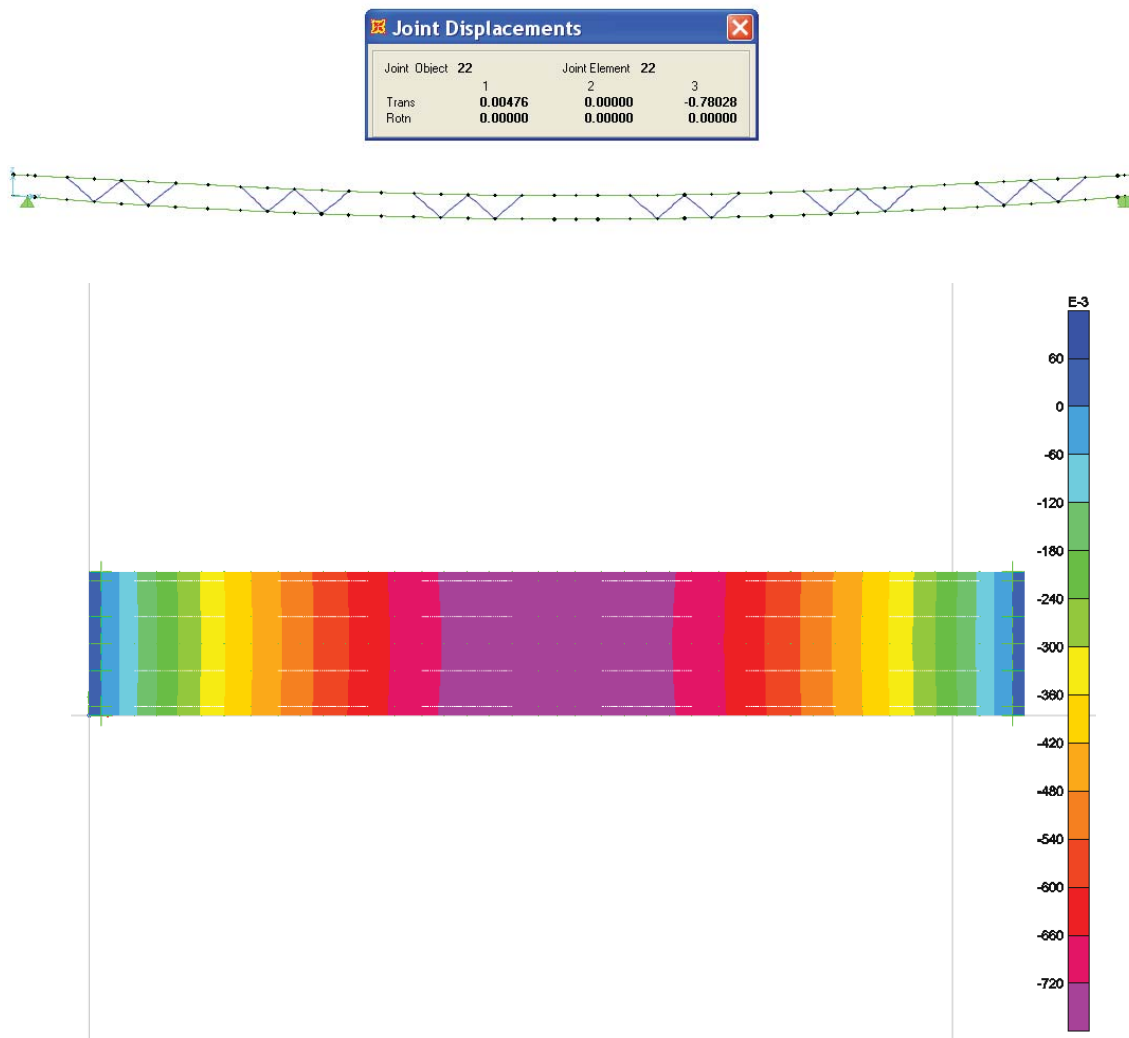
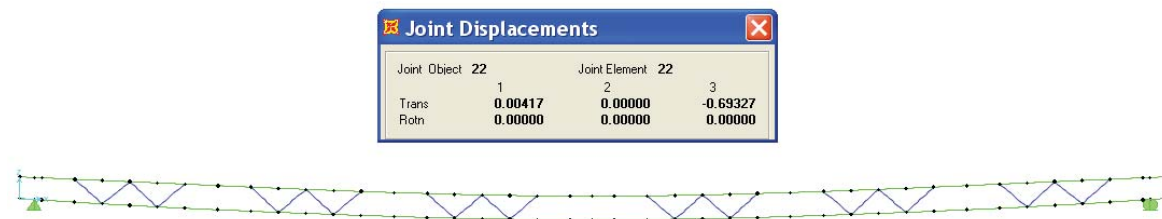


Figure 7.60: Service load deflection of panel C using the truss model and FE model



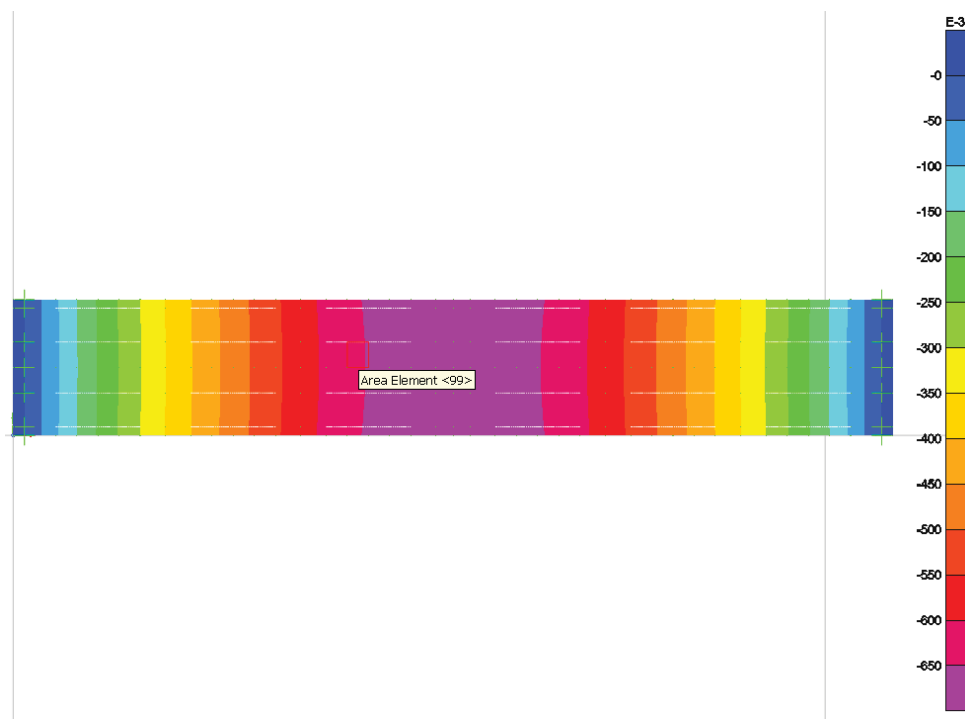


Figure 7.61: Service load deflection of panel D using the truss model and FE model

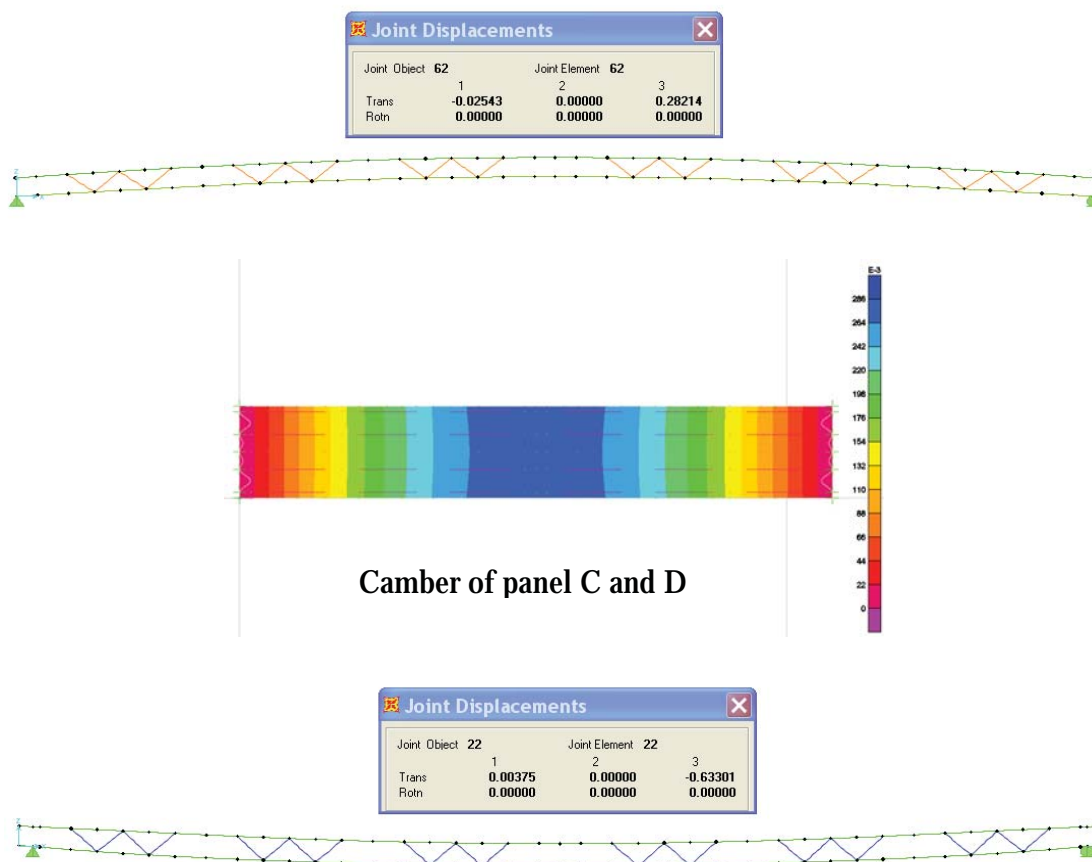
Table 7.7 presents the theoretical deflections of the four specimens calculated using truss and FE models under 6.5 kip point load applied at mid-span. Comparing these values against the actual deflections measured during testing indicates that both planar truss models and 3D FE models provide very reasonable estimates of panel deflections under service load. Also it is shown that there is a high difference between the analytical deflection model and the actual deflection for panel D. This difference was due to problems in measuring the actual deflection, which lead to inaccurate values.

Table 7.7: Comparing the theoretical against measured flexural capacity of phase II test specimens

Panel	L_e (in.)	E(ksi)	I_g (in. ⁴)	P (Kip)	D_{truss} (in.)	D_{FE} (in.)	D_{actual} (in.)	D_{actual} / D_{truss}	D_{actual} / D_{FE}
Panel A	308	5813	2975	6.5	0.38	0.39	0.40	1.05	1.03
Panel B	308	5813	3016	6.5	0.22	0.21	0.20	0.91	0.95
Panel C	304	6112	3370	8*	0.78	0.72	0.85	1.09	1.18
Panel D	304	6112	3370	6.3	0.693	0.65	0.36	0.52	0.55

* Two point load each one equal 4 kip

Figure 7.62 shows the values of the camber and self-weight deflection obtained from the analytical models of panel C and D. the final deflection after subtract the camber is 0.35 in. which is very close to the obtain values using the leaser



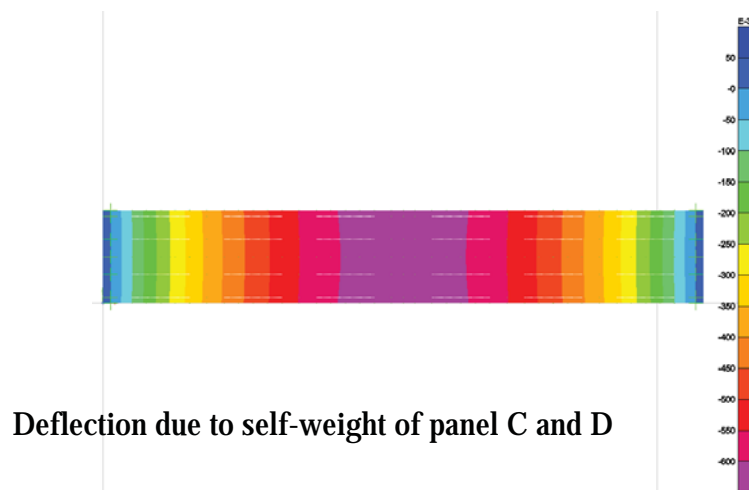
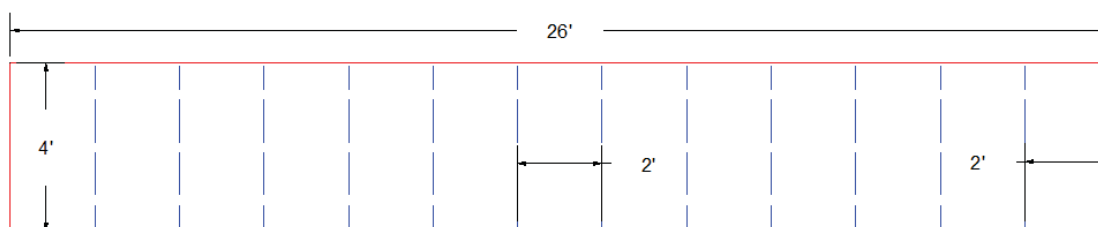


Figure 7.62: Camber and self-weight deflection of panel C and D

7.8 Embedment Depth of GFRP Ties

The common failure in sandwich panel is the horizontal shear failures due to the pull out of the GFRP ties from the concrete wythes. In this section, experimental work performed to investigate the capacity of three specimens made of 1/4, 3/8, and 1/2 in. diameter GFRP ties with embedment depths ranging from 0.5 in. to 2.5 in. Each specimen was a 26 ft long, 4 ft wide and 4 in. thick slab with 12 GFRP-ties embedded at 2 ft spacing as shown in Figure 7.63. The slabs were reinforced with 3#3 bars in the longitudinal direction and made of 8 ksi self-consolidating concrete. Three ties were embedded at each of the four-embedment depths shown in Table 7.8 (total of 12 ties per size).



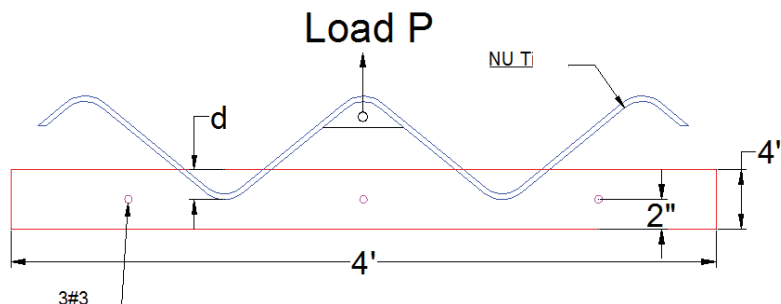


Figure 7.63: Plan and Section view of the test specimen

Specimens were tested by pulling out each tie from its mid-point using a specially manufactured handle, a 1/8 in. thick rubber pad, and a hydraulic jack as shown in Figure 7.64. This handle was specifically made to distribute the tensile forces on the tie legs with minimal bending effects. Table 7.8 lists the ultimate pull out force in pounds for the three tests performed on each tie-embedment combination (36 tests). The table also indicates whether the failure occurred by the pull out of the tie from the concrete, as shown in Figure 7.65, or the rupture of the tie, as shown in Figure 7.66. Testing results presented in Table 7.8 indicate that there is a significant variation in the pull out capacity of the three tests performed on each case (coefficient of variation greater than 40% in some cases). These high values for the coefficient of variation are due to the small number of tests conducted on each case (i.e. three tests), and can be reduced if more tests are conducted. Also, the use of a steel handle with rubber pad to grip the tie for pull out testing does not perfectly simulate the embedment of the tie in concrete, and in some cases results in higher stress concentrations and rupture of ties.

Table 7.8: GFRP-tie size-embedment combinations and test results

NU-Tie Diameter (in.)	Embedment Depth (in.)	Ultimate Load (lb)					
		Test #1	Test #2	Test #3	Failure Mode	Average	Coefficient of Variation
1/4	0.5	251	496	319	Pull-out	355	0.36
	1	1,196	2,012	2,807	Tie rupture	2,005	0.40
	1.5	3,391	2,406	1,363	Tie rupture	2,387	0.42
	2	3,244	3,136	2,289	Tie rupture	2,890	0.18
3/8	0.75	525	623	479	Pull-out	542	0.14
	1	1,594	906	1,431	Pull-out	1,310	0.27
	1.5	3,091	3,534	1,686	Pull-out	2,770	0.35
	2	6,145	6,387	5,565	Tie rupture	6,032	0.07
1/2	1	1,396	2,445	2,093	Pull-out	1,978	0.27
	1.5	3,556	5,539	5,565	Pull-out	4,887	0.24
	2	7,453	4,199	7,606	Pull-out	6,419	0.30
	2.5	10,237	6,804	8,005	Tie rupture	8,349	0.21



Figure 7.64: Test specimen and setup

Figure 7.67 plots the average of three tests for each tie-embedment combination. This histogram clearly indicates that the deeper the GFRP-tie embedment, the higher the pull out force. It also shows that the smaller the bar size, the higher the probability of the bar

rupture before pulling out from the concrete. The use of large bar sizes with small embedment depths does not improve the tie capacity, as it reduces the amount of concrete around the bar and increases the probability of the tie to pull out from concrete.



Figure 7.65: Pull-out of the tie from the concrete



Figure 7.66: Rupture of the tie

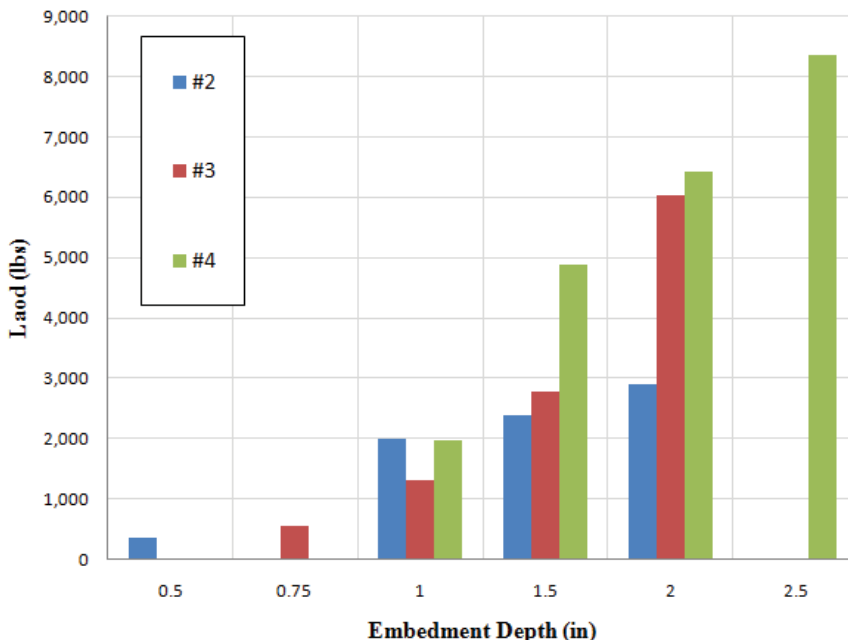


Figure 7.67: Average ultimate load for different tie size and embedment combination

From the previous results, the following conclusion can be mad

- The deeper the GFRP-tie embedment, the higher the pull-out force. Also the smaller the bar size, the higher the probability that the bar will rupture before pulling out from the concrete.
- Using large bar sizes with small embedment depths does not improve the tie capacity, as it reduces the amount of concrete around the bar and increases the probability of the tie to pull out from concrete.
- The minimum embedment depth recommended for GFRP ties is as follows:
 - 1.5 in. for 1/4 in. diameter ties
 - 2.0 in. for 3/8 in. diameter ties
 - 2.5 in. for 1/2 in. diameter ties

7.9 Summary

Based on the results of the experimental and analytical investigations, the following summaries are made:

1. The fabrication of proposed panels using the procedure presented in the paper is simple, efficient, economical, and does not required specialized equipment
2. The number and distribution of ties required to achieve full composite action should be calculated using the PCI Design Handbook method for horizontal shear in composite members. This distribution should be follow the shear diagram , for example using triangular distribution of the horizontal shear along the shear span in case of uniform loads.
3. The proposed panels A, B, D have full composite action under ultimate load. Their ultimate flexural capacity exceeded the theoretical capacity calculated using strain compatibility, on the contrary panel C doesn't reached the capacity which prove the last the shear connector distribution concept.
4. Calculating deflections of the proposed floor panels using the truss models and FE models results in consistent and realistic deflection predictions. Truss models are recommended due to their simplicity and computational efficiency.

Chapter 8

SUMMARY, CONCLUSIONS AND RECOMMENDATIONS FOR Future WORK

8.1 Summary

The only option for constructing flat soffit shallow floors in multi-story buildings is using post-tensioned cast-in-place concrete flat slab, which is complicated, costly, and time-consuming. Current precast concrete floor systems require the use of beam ledges to support hollow core planks and column corbels to support beams, which result in projections that further reduce the clear floor height in addition to the already low span-to-depth ratio. Moreover, conventional precast floor systems do not have adequate resistance to lateral loads without shear walls. The proposed floor system solves this problem by developing a flat soffit shallow precast concrete floor system that is eliminates the need for beam ledges and column corbels, and provides a flat soffit. This system has adequate resistance to lateral loads, which minimizes need for shear walls, and makes it a total precast floor that can be rapidly erected without false or formwork operations that are time-consuming and labor intensive. Economy, structural efficiency, ease and speed of construction, and aesthetics are the main advantages of the proposed system. The dissertation presented the construction sequence and summarized the design of the proposed system for six-story building with 30 ft x 30 ft bay size under 100 psf live load and lateral loads such as wind loads and seismic loads. Full-scale testing of beam-column connection without corbel, the HC-beam connection without ledge and flat soffit beam indicated that the proposed system components and connections are practical, economical, and have adequate structural capacity for the design loads.

Also the dissertation discussed the development of new precast/prestressed panels for floor systems that is alternative to HC planks. The proposed panels are sandwich panels that have comparative weight and structural capacity to HC planks while being efficient in thermal and sound insulation. These panels can be easily produced, as they do not require specialized equipment for fabrication, which eliminates the need for high initial investment. The proposed floor panels consist of an internal wythe of insulation and two external wythes of concrete similar to precast concrete sandwich wall panels. The two concrete wythes are designed to be fully composite using shear connectors. To minimize the reduction of thermal performance of the shear connectors, GFRP-tie was introduced for its superior thermal resistance and structural strength. Four full-scale testing of sandwich panel with different tie distribution was tested. The test result indicated that the proposed panels practical, easy to produce, and have adequate structural capacity for the design loads.

8.2 Conclusions

Below are the main conclusions of this research:

1. The proposed flat soffit beam continuity system has adequate flexural capacity at the positive and negative moment sections to resist both gravity and lateral loads. This capacity can be accurately predicted using strain compatibility approach.
2. The proposed beam-column connection has adequate capacity to carry gravity loads. This capacity can be accurately predicted using shear friction theory.
3. The proposed composite HC continuity system has adequate negative moment capacity to resist lateral loads. This capacity can be accurately predicted using strain compatibility approach.

4. All beam-HC connections performed very well in all tests as their capacities exceeded the predicted capacities and significantly exceeded the demand. None of these connections has failed as the tested HC planks failed in shear prior to the failure of the connections.
5. The ratios of experimental-to-theoretical capacity of the full-scale specimens do not only indicate the efficiency of the proposed system but also the consistency of its performance.
6. The capacity of the proposed HC-beam connection can be accurately predicted using shear friction theory.
7. Since the shear capacity of the HC-beam connections without steel angle was adequate, steel angles are considered as temporary ledges that do not affect the fire rating of the building.
8. The fabrication of proposed sandwich panels using the procedure presented in chapter 7 is simple, efficient, economical, and does not required specialized equipment
9. The number and distribution of ties required to achieve full composite action should be calculated using the PCI Design Handbook method for horizontal shear in composite members. This distribution should be following the shear diagram, for example using triangular distribution of the horizontal shear along the shear span in case of uniform loads.
10. The proposed panels A, B, D have full composite action under ultimate load. Their ultimate flexural capacity exceeded the theoretical capacity calculated using

strain compatibility. On the contrary, panel C does not reached the capacity, which proves the shear distribution concept.

11. Calculating deflections of the proposed floor panels using the truss models and FE models results in consistent and realistic deflection predictions. Truss models are recommended due to their simplicity and computational efficiency.

8.3 Recommendations for Future Works

Several experimental investigations were conducted to examine the seismic behavior of precast concrete moment-resisting frames and connections, none of these investigations have dealt with flat soffit shallow precast beams with no corbels and continuity connections similar to those of the proposed system. Therefore, the proposed system and its connection should be redesign and test for high seismicity zones (Seismic Design Categories E, and F). There is a need for experimentally investigate the proposed interior and exterior beam-column connections for their strength, failure mode, stiffness degradation, ductility, and energy dissipation under cyclic loads. These connections may include a non-post-tensioned connection and a post-tensioned hybrid connection with mild steel reinforcement for both interior and exterior columns. Figure 8.1 shows the proposed test setup as well as an example beam-column connection. Test procedures will comply with the scheme specified in the ACI document “Acceptance Criteria for Moment Frames Based on Structural Testing”. The output of these tests will include the lateral load versus story drift response, cracking pattern, failure mode for forward and backward loading cycles, and bond degradation among precast concrete, grout, and reinforcement. Also a refined structural analysis of six-story building will be conducted using finite

element to account for mass distribution and determine the dynamic response of the structure.

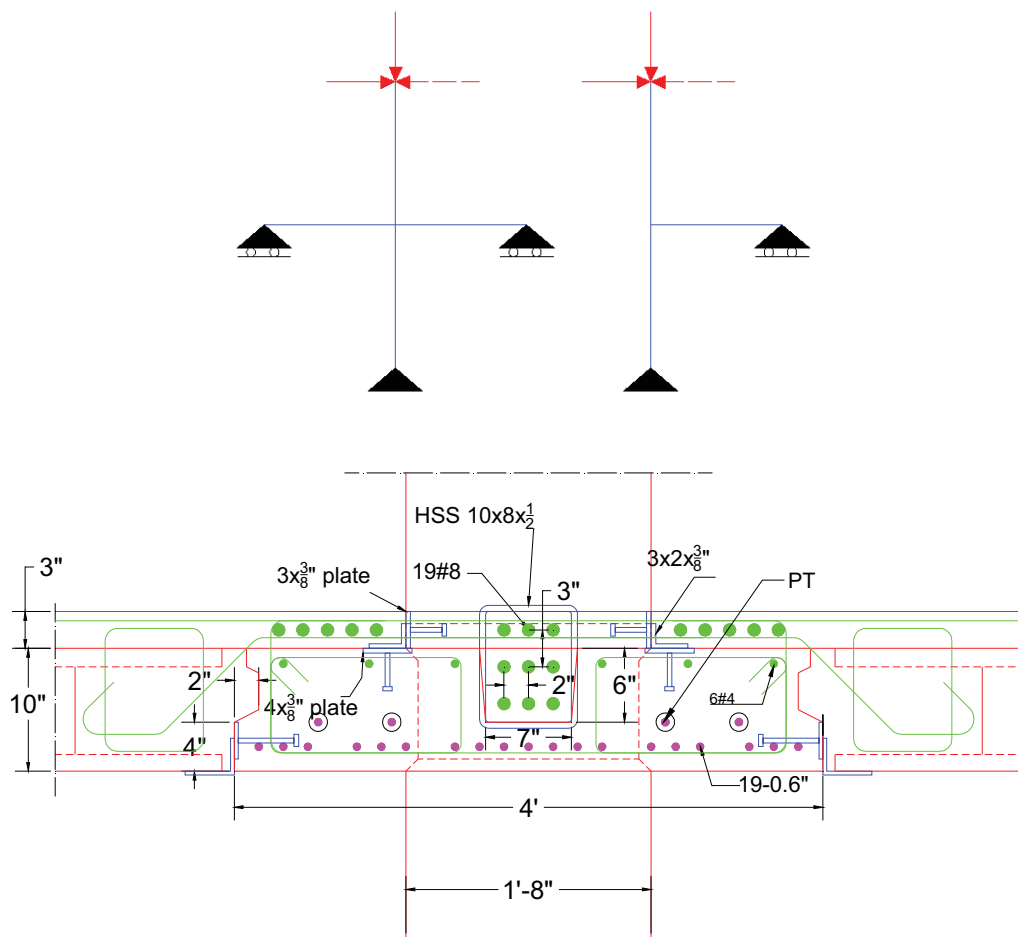


Figure 8.1: Proposed Testing Setup and a Preliminary Design of Post-tensioned Hybrid Connection

REFERENCES

- American Concrete Institute, (ACI), (2008). **Building Code Requirements for Structural Concrete and Commentary**, June. Farmington Hills, Michigan.
- American Institute of Steel Construction, (AISC), (2008). **Steel Construction Manual**, Thirteenth Edition.
- American Society of Civil Engineers (ASCE 7-05), (2005). **Minimum Design Loads for Buildings and Other Structures**. Reston, Virginia.
- Board of Federation International Du Beton (FIB) Steering Committee, (1999) "Special Design consideration for Precast Prestressed Hollow Core floors," No. 6, October 1999.
- Compton, L. A. (2002) "Retractable Hangers for Mounting Precast Concrete Beams and the Like in Buildings" US Patent number 2002/0062616 A1.
- Composite Dycore Office Structures (1992), Company literature - Finforck Industries, Inc., Orlando, Florida.
- Computers and Structures, Inc. (2000). "Structural Analysis Program Advanced 14.1.0", Berkeley, CA.
- Fawzy F. (2009) "Shallow Precast Concrete Hollow-core Floor System" Master Thesis, University of Nebraska-Lincoln.
- Girder-Slab Technologies LLC of Cherry Hill, NJ. (2002). **Composite steel and precast system, Design Guide V.1.4**. <http://www.girder-slab.com/designguide.asp>.
- Hanlon J., Dolan C. W., Figurdki D., Deng J., and Dolan J. G., (2009) "Precast concrete building system components for the Westin Resort Hotel" part 1, *PCI Journal*, Vol. 54, No. 2 Spring, pp.88-96.
- John C., (2003) "Coordinated Construction," *Modern Steel Construction*, July.

Hanlon, J.W. (1990) "Building System Using Modular precast Concrete Components" United States Patent, Patent number: United States Patent, Patent number 4,903,448.

Low S., Tadros M. K., and Nijhawan J. C., (1991) "A New Framing System for Multistory Buildings," Concrete International, Vol. 13, No. 9, September, pp. 54-57.

Low S., Tadros, M., Einea A., and Magana, R., (1996) "Seismic Behavior of a Six Story Precast Concrete Office Building," PCI Journal, Vol. 41, No. 6, November/December, pp.56-75.

Mid-State filigree Systems, Inc. 1992 "The Filigree Widesslab Method of concrete Deck Construction" Company Literature -, Cranbury, NJ

Morcous. G. and Tadros K. M., (2010) "Shallow Flat Soffit Precast Concrete Floor System" 3rd fib International Congress, Washington, D.C.

Pessiki S., Prior R., Sause R., and Slaughter S., (1995) "Review of Existing precast concrete gravity load floor framing systems". PCI Journal, Vol. 40, No. March-April, pp.70-83

Precast/Prestressed Concrete Institute. (1998). Design of Hollow Core Slabs Manual 2nd Edition, Chicago, Illinois

Peter A. N., (2001) "Steel and Precast Slab Construction System for Mid and High Rise Residential Buildings," Modern Steel Construction, May.

Prestressed Concrete Institute (PCI), (2005). PCI Design Handbook, 6th Edition, Chicago, IL.

Post Tensioning Institute (PTI). (2006). Post-tensioning Manual 6th Edition, Phoenix, Arizona.

Peikko Group, Peikko News, (2010) "Delta Beam Composite Beams" <http://www.peikko.com>, june 12

Quincy Joist Company, (2012), "Standard Specifications for Joist Girders"].
<http://www.quincyjoist.com/resources/downloads/default.asp>, February 6

Reay, A. M. (1997) "Method of Construction Using Precast Floor Units" US, Patent number 5,660,020.

Rahimzadeh, H. (2003) "Composite Structural Framing System" US Patent number 6,543,195 B2.

Rafael B., and Orid P., (2010) "NEW Precast Light Flooring System" 3rd fib International Congress .

RSMMeans Construction publishers & Consultants, 2011. "RSMMeans Building Construction Cost Data" Kingston, MA

Simanjuntak, J. H. (1998) "System for Joining Precast Concrete Columns and Slabs" US, Patent number 5,809,712.

Steel Joist Institute (SJI). (2007). First Edition Composite Steel Joist Catalog.

Tadros M. K., Salmon D. C., Einea A., and Culp T. D. "Precast Concrete Sandwich Panels," US Patent number 5,440,845, 1995.

Tadros, k. M., and Low, S. (1996) "Concrete Framing System" US Patent number 5,507,124.

Thompson and Pessiki, (2004) "Behavior and Design of Precast/Prestressed Inverted Tee Girders with Multiple Web Openings for Service Systems," ATLSS Report 04-07, Lehigh University, pp. 156.

Veitas R., (2002) "Slab Solution," Modern Steel Construction, May.

Wise, H. H. (1973) "Composite Concrete Construction of Two-Way Slabs and Flat Slabs" US Patent number 3,763,613.

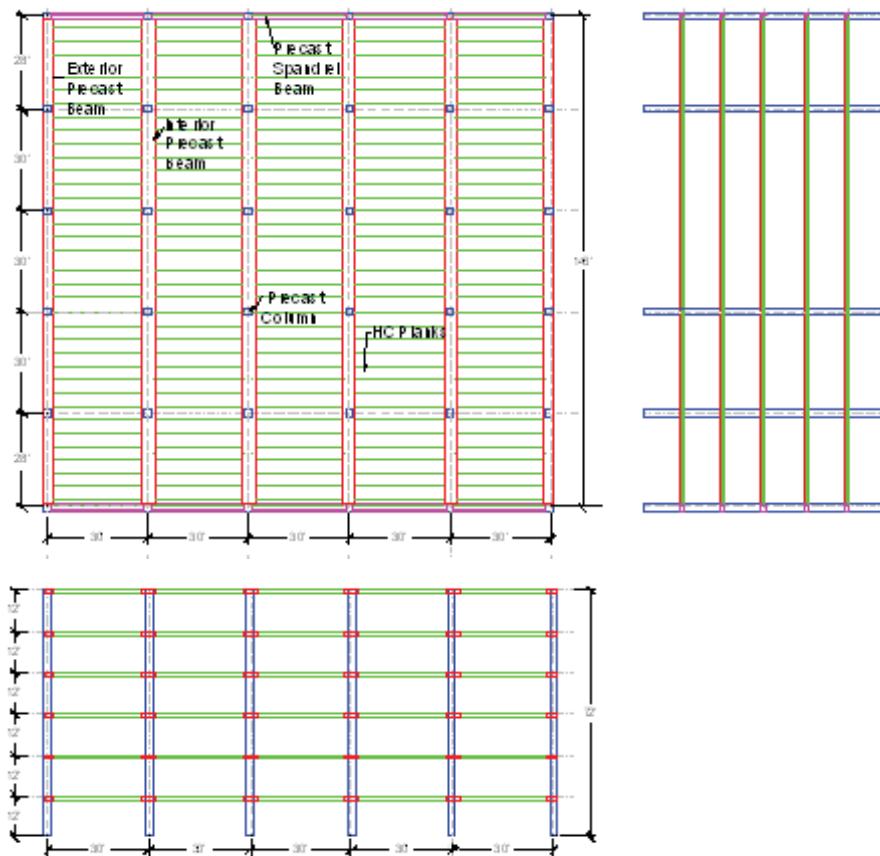
Wise, H. H., and Meade, B. (1978) "Building Structure Utilizing Precast Concrete Elements" US Patent number 4,081,935, Apr. 4, 1978.

Appendix A

DETAILED DESIGN EXAMPLE FOR SHALLOW FLAT SOFFIT PRECAST

CONCRETE FLOOR SYSTEM (BEAM WITH SHEAR KEY)

The design was done on a 6-story building for estimating design loads. The following Figure shows plane, elevation, and side views of the example building



Plane, elevation, and side views for the example building

1. Design of Hollow Core (HC)

Hollow core planks are designed as simply supported composite beam with loads including self-weight, topping weight, and live load.

$$\text{Beam}_{\text{width}} := 4\text{ft}$$

$$\text{HC}_{\text{width}} := 4\text{ft}$$

$$\text{HC}_{\text{span}} := 30\text{ft}$$

$$\text{Clear}_{\text{span.HC.direction}} := \text{HC}_{\text{span}} - \text{Beam}_{\text{width}} = 26\text{ft}$$

$$L_{\text{HC}} := \text{Clear}_{\text{span.HC.direction}} = 26\text{ft}$$

$$HC_{sw} := HC_{weight.sq.ft} \cdot HC_{width} = 0.3 \cdot \frac{\text{kip}}{\text{ft}}$$

$$A_{avg.thickness.top} := 2.5 \text{ in} \quad \gamma_c := 0.15 \frac{\text{kip}}{\text{ft}^3}$$

$$Top_{sw.sq.ft} := A_{avg.thickness.top} \cdot \gamma_c = 0.03 \cdot \frac{\text{kip}}{\text{ft}^2}$$

$$L_L := 0.1 \frac{\text{kip}}{\text{ft}^2}$$

Positive Moment

$$W_{HC.DL} := (HC_{sw} + Top_{sw.sq.ft} \cdot HC_{width}) = 0.43 \cdot \frac{\text{kip}}{\text{ft}}$$

$$W_{LL} := (L_L \cdot HC_{width}) = 0.4 \cdot \frac{\text{kip}}{\text{ft}}$$

$$M_{HC} := W_{HC.DL} \cdot 1.2 \cdot \frac{L_{HC}^2}{8} + \frac{W_{LL} \cdot 1.6 \cdot L_{HC}^2}{8} = 97.17 \cdot \text{kip} \cdot \text{ft}$$

Design

The HC will be designed according to the design chart of the 10" thick HC with 2" composite topping used in the example building. This chart obtained from the HC Load Tables produced by Concrete Industries, Inc. The chart is very simple to use for a typical building floor. Given the Load in psf (live load and superimposed dead load), as shown in the vertical axis, the maximum span of a specific HC size is obtained in feet, as shown in the horizontal axis. For other types of HC produced by other manufacturer, the manufacturer tables should be used on the generic spreadsheet.

Hollow -Core Continuity will be design according to the lateral loads (Wind and Seismic loads)

Precast section properties

$$I_{HC} := 3214 \text{ in}^4$$

$$A_{HC} := 267 \text{ in}^2$$

$$h_{HC} := 10 \text{ in}$$

$$Y_{b.HC} := 5.04 \text{ in}$$

$$Y_{t.HC} := h_{HC} - Y_{b.HC} = 4.96 \cdot \text{in}$$

$$f_{\text{ctop}} := 4000 \text{ psi} \qquad f_{\text{cHC}} := 6000 \text{ psi}$$

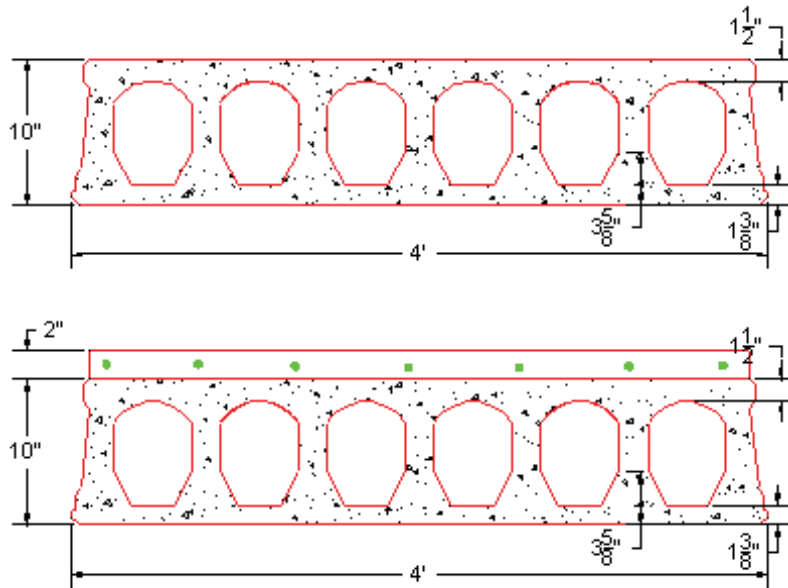
$$n_{\text{HC}} := \left(\frac{f_{\text{ctop}}}{f_{\text{cHC}}} \right)^{0.5} = 0.82$$

Composite section

$$h_{\text{cHC}} := 12 \text{ in} \qquad t_{\text{top}} := 2.5 \text{ in}$$

$$d_{\text{top}} := h_{\text{HC}} + \frac{t_{\text{top}}}{2} = 11.25 \cdot \text{in}$$

$$Y_{\text{bc.HC}} := \left[\frac{[(A_{\text{HC}} \cdot Y_{\text{b.HC}}) + (t_{\text{top}} \cdot \text{HC}_{\text{width}} \cdot n_{\text{HC}} \cdot d_{\text{top}})]}{A_{\text{HC}} + t_{\text{top}} \cdot \text{HC}_{\text{width}} \cdot n_{\text{HC}}} \right] = 6.71 \cdot \text{in}$$



$$Y_{\text{tc.HC}} := h_{\text{cHC}} - Y_{\text{bc.HC}} = 5.29 \cdot \text{in}$$

$$I_{\text{c.top}} := \frac{n_{\text{HC}} \cdot \text{HC}_{\text{width}} \cdot t_{\text{top}}^3}{12} + n_{\text{HC}} \cdot \text{HC}_{\text{width}} \cdot t_{\text{top}} \cdot \left(Y_{\text{tc.HC}} - \frac{t_{\text{top}}}{2} \right)^2$$

$$I_{\text{c.top}} = 1.65 \times 10^3 \cdot \text{in}^4$$

$$I_{\text{c.HC}} := \left[I_{\text{HC}} + A_{\text{HC}} \cdot (Y_{\text{bc.HC}} - Y_{\text{b.HC}})^2 \right] + I_{\text{c.top}} = 5.61 \times 10^3 \cdot \text{in}^4$$

Design

$$f_{yb.welded.wire} := 75 \text{ ksi} \qquad \beta_{1HC} := 0.75$$

$$\varepsilon_c := 0.003$$

Try

$$C_{comp.block} := 0.36 \text{ in}$$

$$a_{comp.block} := C_{comp.block} \cdot \beta_{1HC} = 0.27 \cdot \text{in}$$

$$\varepsilon_{steel.1} := \varepsilon_c \cdot \frac{(d_{top} - C_{comp.block})}{C_{comp.block}} = 0.09$$

$$Force_{comp} := 0.85 \cdot f_{cHC} \cdot HC_{width} \cdot a_{comp.block} = 66.1 \cdot \text{kip}$$

$$\text{Use D.11 @ 6 in} \qquad A_{b3} := 0.11 \text{ in}^2$$

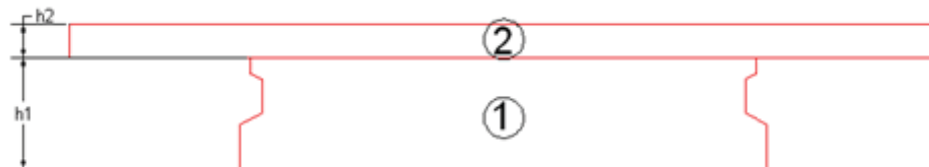
$$A_{steel} := \frac{A_{b3} \cdot HC_{width}}{6 \text{ in}} = 0.88 \text{ in}^2$$

$$Force_{ten} := A_{steel} \cdot f_{yb.welded.wire} = 66 \cdot \text{kip}$$

Moment at the bottom fibers

$$Mn_{HC.comp.} := Force_{comp} \cdot \frac{a_{comp.block}}{2} + Force_{ten} \cdot d_{top} = 62.62 \text{ ft} \cdot \text{kip}$$

$$\phi := 0.9 \qquad \phi \cdot Mn_{HC.comp.} = 56.36 \cdot \text{kip} \cdot \text{ft}$$

2. Shallow Inverted Tee (SIT) Beam Design2.1 Section Properties

$$W_1 := 48 \text{ in}$$

$$h_1 := 10 \text{ in}$$

$$A_1 := W_1 \cdot h_1 = 480 \cdot \text{in}^2$$

$$t := 2 \cdot \text{in}$$

$$h_2 := t = 2 \cdot \text{in}$$

$$W_1 + 16 \cdot h_2 = 80 \cdot \text{in}$$

$$b_{\text{eff}} := W_1 + 16 \cdot h_2 = 80 \cdot \text{in}$$

From ACI 318-08 section 8.12

$$W_2 := b_{\text{eff}} = 80 \cdot \text{in}$$

$$A_2 := W_2 \cdot h_2 = 160 \cdot \text{in}^2$$

$$h_{\text{nc}} := h_1 = 10 \cdot \text{in}$$

$$h_c := h_{\text{nc}} + h_2 = 12 \cdot \text{in}$$

2.1.1 Non-Composite Section

$$A_{\text{nc}} := A_1 = 480 \cdot \text{in}^2$$

$$Y_{\text{nc}} := \frac{h_1}{2} = 5 \cdot \text{in}$$

$$Y_{\text{bnc}} := Y_{\text{nc}} = 5 \cdot \text{in}$$

$$Y_{\text{tnc}} := h_{\text{nc}} - Y_{\text{nc}} = 5 \cdot \text{in}$$

$$I_{\text{nc}} := \left[\frac{W_1}{12} \cdot (h_1)^3 + A_1 \cdot \left(Y_{\text{bnc}} - \frac{h_1}{2} \right)^2 \right] = 4 \times 10^3 \cdot \text{in}^4$$

$$S_{\text{bnc}} := \frac{I_{\text{nc}}}{Y_{\text{bnc}}} = 800 \cdot \text{in}^3$$

$$S_{\text{tnc}} := \frac{I_{\text{nc}}}{Y_{\text{tnc}}} = 800 \cdot \text{in}^3$$

2.1.2 Composite Section

$$F_{\text{cbeam}} := 8000 \text{psi}$$

$$F_{\text{ctop}} := 4000 \text{psi}$$

$$n := \sqrt{\left(\frac{F_{\text{ctop}}}{F_{\text{cbeam}}} \right)} = 0.71$$

$$A_c := A_{\text{nc}} + A_2 \cdot n = 593.14 \cdot \text{in}^2$$

$$Y_c := \frac{\left[A_{\text{nc}} \cdot Y_{\text{nc}} + A_2 \cdot n \cdot \left(h_{\text{nc}} + \frac{h_2}{2} \right) \right]}{A_c} = 6.14 \cdot \text{in}$$

$$Y_{\text{bc}} := Y_c = 6.14 \cdot \text{in}$$

$$Y_{\text{tc}} := (h_{\text{nc}} + h_2) - Y_{\text{bc}} = 5.86 \cdot \text{in}$$

$$I_{\text{cA1}} := W_1 \cdot \frac{h_1^3}{12} + A_1 \cdot \left(Y_{\text{bc}} - \frac{h_1}{2} \right)^2 = 4.63 \times 10^3 \cdot \text{in}^4$$

$$I_{cA2} := W_2 \cdot \frac{h_2^3}{12} + A_2 \cdot \left(h_1 + \frac{h_2}{2} - Y_{bc} \right)^2 = 3.83 \times 10^3 \cdot \text{in}^4$$

$$I_c := I_{cA1} + I_{cA2} = 8.45 \times 10^3 \cdot \text{in}^4$$

2.2 Loads

$$\text{Inter}_{\text{beam.span}} := 30 \text{ft}$$

$$\text{Exter}_{\text{beam.span}} := 28 \text{ft}$$

$$\text{Span}_{\text{HC.direction}} := 30 \text{ft}$$

$$\text{Column}_{\text{width}} := 20 \text{in}$$

$$\text{Span}_{\text{external.beam}} := \text{Exter}_{\text{beam.span}} - \text{Column}_{\text{width}} - 0.167 \text{ft} = 26.17 \cdot \text{ft}$$

$$\text{Span}_{\text{internal.beam}} := \text{Inter}_{\text{beam.span}} - \text{Column}_{\text{width}} - 0.167 \text{ft} = 28.17 \cdot \text{ft}$$

$$\text{Span}_{\text{beam.Avg.}} := \frac{(\text{Span}_{\text{external.beam}} + \text{Span}_{\text{internal.beam}})}{2} = 27.17 \cdot \text{ft}$$

$$W_{\text{beam}} := A_{nc} \cdot \gamma_c = 0.5 \cdot \frac{\text{kip}}{\text{ft}} \quad \text{HC}_{\text{sw}} = 0.3 \cdot \frac{\text{kip}}{\text{ft}}$$

$$W_{\text{H.C}} := \text{HC}_{\text{sw}} \cdot \frac{L_{\text{HC}}}{4 \text{ft}} = 1.95 \cdot \frac{\text{kip}}{\text{ft}}$$

$$W_{\text{D.L}} := W_{\text{beam}} + W_{\text{H.C}} = 2.45 \cdot \frac{\text{kip}}{\text{ft}}$$

$$W_{\text{top}} := A_{\text{avg}} \cdot \text{thickness}_{\text{top}} \cdot \gamma_c \cdot \text{Span}_{\text{HC.direction}} = 0.94 \cdot \frac{\text{kip}}{\text{ft}}$$

$$W_{\text{Hc.and.top}} := W_{\text{top}} + W_{\text{H.C}} = 2.89 \cdot \frac{\text{kip}}{\text{ft}}$$

$$W_{\text{L.L}} := L_L \cdot \text{Span}_{\text{HC.direction}} = 3 \cdot \frac{\text{kip}}{\text{ft}}$$

Bending moments Calculations

Stage one:

Simple supported non-composite section under beam self-weight, and HC self-weight

$$M_{\text{non.comp.simple.external.beam}} := \frac{W_{\text{D.L}} \text{Span}_{\text{external.beam}}^2}{8} = 209.68 \cdot \text{kip} \cdot \text{ft}$$

$$M_{\text{non.comp.simple.internal.beam}} := W_{\text{D.L}} \cdot \frac{\text{Span}_{\text{internal.beam}}^2}{8} = 242.96 \cdot \text{kip} \cdot \text{ft}$$

$$V_{\text{non.comp.external.beam}} := W_{\text{D.L}} \cdot \frac{\text{Span}_{\text{external.beam}}}{2} = 32.05 \cdot \text{kip}$$

Stage Two:

Continuous non-composite section under topping weight

$$M_{\text{non.comp.con.external.beam}} := W_{\text{top}} \cdot \frac{\text{Span}_{\text{beam.Avg.}}^2}{14} = 49.42 \cdot \text{kip} \cdot \text{ft}$$

$$M_{\text{non.comp.con.internal.beam}} := W_{\text{top}} \cdot \frac{\text{Span}_{\text{beam.Avg.}}^2}{16} = 43.24 \cdot \text{kip} \cdot \text{ft}$$

$$M_{\text{negative.non.simple.comp.}} := -W_{\text{top}} \cdot \frac{\text{Span}_{\text{beam.Avg.}}^2}{11} = -62.9 \cdot \text{kip} \cdot \text{ft}$$

$$V_{\text{non.comp.con.external.beam}} := 1.15 W_{\text{top}} \cdot \frac{\text{Span}_{\text{beam.Avg.}}}{2} = 14.64 \cdot \text{kip}$$

Stage Three:

Continuous composite section under live loads

$$M_{\text{comp.con.external.beam}} := W_{\text{L.L}} \cdot \frac{\text{Span}_{\text{beam.Avg.}}^2}{14} = 158.14 \cdot \text{kip} \cdot \text{ft}$$

$$M_{\text{comp.con.internal.beam}} := W_{\text{L.L}} \cdot \frac{\text{Span}_{\text{beam.Avg.}}^2}{16} = 138.38 \cdot \text{kip} \cdot \text{ft}$$

$$M_{\text{negative.comp.}} := -W_{\text{L.L}} \cdot \frac{\text{Span}_{\text{beam.Avg.}}^2}{11} = -201.28 \cdot \text{kip} \cdot \text{ft}$$

$$V_{\text{comp.con.external.beam}} := 1.15 \cdot W_{\text{L.L}} \cdot \frac{\text{Span}_{\text{beam.Avg.}}}{2} = 46.86 \cdot \text{kip}$$

Factor moments in non-composite section

$$M_{n.c.s.ex} := M_{non.comp.simple.external.beam} = 209.68 \cdot \text{kip} \cdot \text{ft}$$

$$M_{n.c.c.ex} := M_{non.comp.con.external.beam} = 49.42 \cdot \text{kip} \cdot \text{ft}$$

$$M_{non.comp.external.beam} := 1.2 \cdot M_{n.c.s.ex} + 1.2 \cdot M_{n.c.c.ex} = 310.92 \cdot \text{kip} \cdot \text{ft}$$

$$M_{n.c.s.in} := M_{non.comp.simple.internal.beam} = 242.96 \cdot \text{kip} \cdot \text{ft}$$

$$M_{n.c.c.in} := M_{non.comp.con.internal.beam} = 43.24 \cdot \text{kip} \cdot \text{ft}$$

$$M_{non.comp.internal.beam} := 1.2 \cdot M_{n.c.s.in} + 1.2 \cdot M_{n.c.c.in} = 343.44 \cdot \text{kip} \cdot \text{ft}$$

$$M_{negative.non.comp.f} := 1.2 \cdot M_{negative.non.simple.comp.} = -75.48 \cdot \text{kip} \cdot \text{ft}$$

Factor moments in composite section

$$M_{c.c.ex} := 1.6 M_{comp.con.external.beam} = 253.03 \cdot \text{kip} \cdot \text{ft}$$

$$M_{c.c.in} := 1.6 \cdot M_{comp.con.internal.beam} = 221.4 \cdot \text{kip} \cdot \text{ft}$$

$$M_{comp.external.beam} := M_{non.comp.external.beam} + M_{c.c.ex} = 563.96 \cdot \text{kip} \cdot \text{ft}$$

$$M_{comp.internal.beam} := M_{non.comp.internal.beam} + M_{c.c.in} = 564.85 \cdot \text{kip} \cdot \text{ft}$$

$$M_{n.c} := 1.6 \cdot M_{negative.comp.} = -322.04 \cdot \text{kip} \cdot \text{ft}$$

$$M_{negative.comp} := M_{negative.non.comp.f} + M_{n.c} = -397.52 \cdot \text{kip} \cdot \text{ft}$$

Factor Shear in non-composite section

$$V_{n.c.s.ex} := 1.2 \cdot V_{non.comp.external.beam} = 38.46 \cdot \text{kip}$$

$$V_{c.c.ex} := 1.2 \cdot V_{non.comp.con.external.beam} = 17.57 \cdot \text{kip}$$

$$V_{noncomposite} := V_{n.c.s.ex} + V_{c.c.ex} = 56.04 \cdot \text{kip}$$

Factor shear in composite section

$$V_{\text{composite}} := V_{\text{noncomposite}} + 1.6 \cdot V_{\text{comp.con.external.beam}} = 131.02 \cdot \text{kip}$$

2.3 Determination of Approximate Number of Strand Based on Flexural Strength.

Based on the analysis results shown above, the exterior span of the SIT beam was found to be the most critical at both positive and negative moment sections.

$$M_{U,\text{positive}} := M_{\text{comp.external.beam}} = 563.96 \cdot \text{kip} \cdot \text{ft}$$

$$\text{Tension}_{\text{force}} := \frac{(M_{U,\text{positive}})}{[0.9(h_c - 3\text{in})]} = 835.49 \cdot \text{kip}$$

$$f_{pu} := 270 \text{ksi}$$

$$F_{sp} := 0.9 \cdot f_{pu} = 243 \cdot \text{ksi}$$

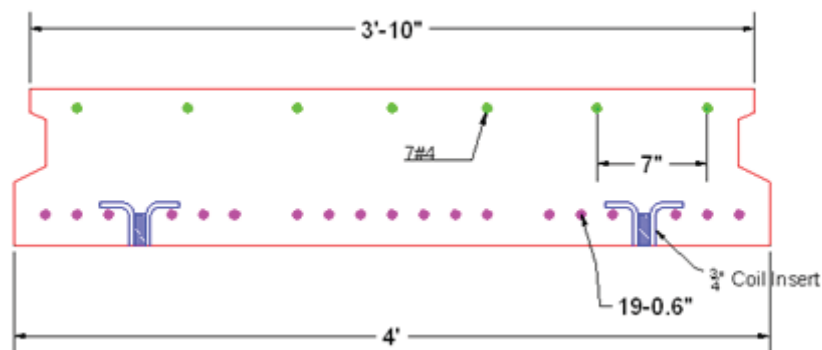
$$A_{\text{sp.apx}} := \frac{\text{Tension}_{\text{force}}}{F_{sp}} = 3.44 \cdot \text{in}^2$$

$$N_{\text{strand.apx}} := \frac{A_{\text{sp.apx}}}{0.217 \text{in}^2} = 15.84$$

Take the number of strand equal to 19 - 0.6in

Prestressing steel

(19)-0.6in. diameter 270k low-relaxation strand



$$N_{\text{strands}} := 19$$

$$A_{\text{strand}} := 0.217 \text{in}^2$$

$$A_{ps} := N_{strands} \cdot A_{strand} = 4.12 \cdot \text{in}^2 \quad Y_{ps} := 2 \text{in}$$

$$e := Y_{nc} - Y_{ps} = 3 \cdot \text{in}$$

2.4 Prestress losses

Prestress loss calculations performed according to the PCI Design Handbook 6th Edition method outlined in section 4.7.

$$f_{ci.beam} := 6500 \text{psi}$$

$$f_{c.beam} := 8000 \text{psi}$$

$$A_g := A_{nc} = 480 \cdot \text{in}^2$$

$$I_g := I_{nc} = 4 \times 10^3 \cdot \text{in}^4$$

$$V := 1 \text{in} \cdot (A_{nc}) = 480 \cdot \text{in}^3$$

$$S := 2 \cdot (W_1 + h_{nc}) = 116 \cdot \text{in}$$

$$RH := 70$$

$$\frac{V}{S} = 4.14 \cdot \text{in}^2$$

$$A_{ps} = 4.12 \cdot \text{in}^2$$

$$e = 3 \cdot \text{in}$$

$$f_{pu} = 270 \cdot \text{ksi}$$

$$f_{pj} := 0.75 \cdot f_{pu} = 202.5 \cdot \text{ksi}$$

$$P_i := f_{pj} \cdot A_{ps} = 834.91 \cdot \text{kip}$$

$$E_{ps} := 28500 \text{ksi}$$

$$E_{ci} := 57000 \text{psi}^{0.5} \cdot \sqrt{f_{ci.beam}} = 4.6 \times 10^3 \cdot \text{ksi}$$

$$E_c := 57000 \cdot \text{psi}^{0.5} \cdot \sqrt{f_{c.beam}} = 5.1 \times 10^3 \cdot \text{ksi}$$

$$M_g := \frac{W_{beam} \text{Span}_{external.beam}^2}{8} = 42.79 \cdot \text{kip} \cdot \text{ft}$$

$$M_{dl} := \left(\frac{HC_{sw}}{1 \text{ft}} \cdot \frac{L_{HC}}{4} \cdot \frac{\text{Span}_{external.beam}^2}{8} \right) + W_{top} \cdot \frac{(\text{Span}_{external.beam})^2}{8}$$

$$M_{dl} = 247.13 \cdot \text{kip} \cdot \text{ft}$$

2.4.1 Elastic Shortening Losses

$$K_{es} := 1 \quad \text{For pretension members}$$

$$K_{cir} := 0.9 \quad \text{For pretension members}$$

$$f_{cir} := K_{cir} \cdot \left(\frac{P_i}{A_g} + P_i \cdot \frac{e^2}{I_g} \right) - M_g \cdot \frac{e}{I_g} = 2.87 \cdot \text{ksi}$$

$$ES := K_{es} \cdot \frac{E_{ps}}{E_{ci}} \cdot f_{cir} = 17.81 \cdot \text{ksi}$$

2.4.2 Creep Losses

$$K_{cr} := 2 \quad \text{For normal weight concrete}$$

$$f_{c ds} := M_{dl} \cdot \frac{e}{I_g} = 2.22 \cdot \text{ksi}$$

$$CR := K_{cr} \cdot \frac{E_{ps}}{E_c} \cdot (f_{cir} - f_{c ds}) = 7.23 \cdot \text{ksi}$$

2.4.3 Shrinkage Losses

$$K_{sh} := 1 \quad \text{For pretension members}$$

$$SH := 8.2 \cdot 10^{-6} \cdot K_{sh} \cdot E_{ps} \cdot \left[1 - 0.06 \left(\frac{1}{\text{in}^2} \cdot \frac{V}{S} \right) \right] \cdot (100 - RH) = 5.27 \cdot \text{ksi}$$

2.4.4 Relaxation Losses

$$K_{re} := 5000 \text{ psi}$$

$$J := .037$$

$$C := 1$$

$$RE := \left[K_{re} - J \cdot (SH + CR + ES) \right] \cdot C = 3.88 \cdot \text{ksi}$$

2.4.5 Total Losses

$$TL := ES + CR + SH + RE = 34.19 \text{ ksi}$$

$$\text{Losses\%} := \frac{TL \cdot 100}{f_{pj}} = 16.88$$

$$f_p := f_{pj} - TL = 168.31 \text{ ksi}$$

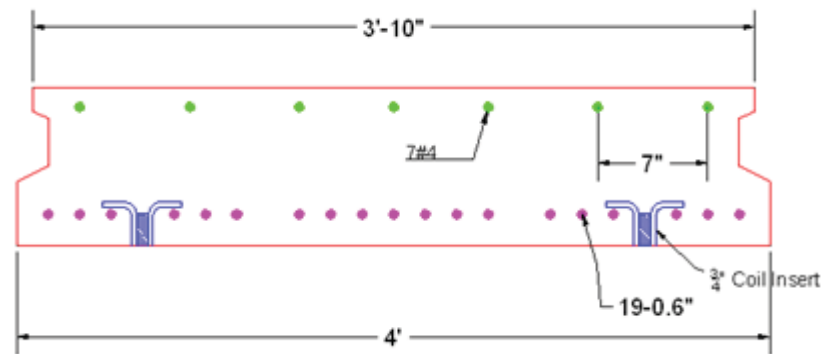
$$P_o := (f_{pj} - ES) \cdot A_{ps} = 761.5 \text{ kip}$$

$$P := A_{ps} \cdot (f_p) = 693.96 \text{ kip}$$

2.5 Flexural Strength

2.5.1 Flexural Strength for Positive Mid-Span Section

2.5.1.1 Non-Composite Section



Strain compatibility approach was used to calculate the section strength

$$A_{ps} = 4.12 \cdot \text{in}^2$$

$$b_{\text{eff}} = 80 \cdot \text{in}$$

$$Y_{ps} = 2 \cdot \text{in}$$

From the bottom of the beam

From ACI 318-08 section 8.12 (T-beam Construction)

$$f_{c\text{beam}} := 8 \text{ ksi}$$

$$\epsilon_c = 3 \times 10^{-3}$$

$$\beta_{1\text{beam}} := 0.65$$

Try

$$C_{\text{non.comp.positive}} := 4.05 \text{ in}$$

$$a_{\text{non.comp.positive}} := \beta_{1\text{beam}} \cdot C_{\text{non.comp.positive}} = 2.63 \cdot \text{in}$$

$$C_{1\text{non.comp.positive}} := 0.85 \cdot a_{\text{non.comp.positive}} \cdot W_1 \cdot f_{\text{cbeam}} = 859.25 \cdot \text{kip}$$

$$d_{1\text{non.comp.positive}} := h_{\text{nc}} - Y_{\text{ps}} = 8 \cdot \text{in}$$

$$d_{\text{upperbars}} := 1 \text{in}$$

$$\varepsilon_{s1\text{non.comp.positive}} := \varepsilon_c \cdot \frac{(d_{1\text{non.comp.positive}} - C_{\text{non.comp.positive}})}{C_{\text{non.comp.positive}}}$$

$$\varepsilon_{s1\text{non.comp.positive}} = 2.93 \times 10^{-3}$$

$$\varepsilon_{\text{upperbars}} := \varepsilon_c \cdot \frac{(C_{\text{non.comp.positive}} - d_{\text{upperbars}})}{C_{\text{non.comp.positive}}} = 2.26 \times 10^{-3}$$

$$F_{\text{sbars}} := 60 \text{ksi}$$

$$\varepsilon_{\text{ps1non.comp.positive}} := \varepsilon_{s1\text{non.comp.positive}} + \left(\frac{f_p}{E_{\text{ps}}} \right) = 8.83 \times 10^{-3}$$

$$f_p = 1.68 \times 10^5 \text{psi}$$

$$Q_{\text{ps1}} := 887 + \frac{27613}{\left[1 + (112.4 \cdot \varepsilon_{\text{ps1non.comp.positive}})^{7.36} \right] \left(\frac{1}{7.36} \right)} = 2.61 \times 10^4$$

$$f_{\text{ps1non.comp.positive}} := \varepsilon_{\text{ps1non.comp.positive}} \cdot (Q_{\text{ps1}}) \cdot 1000 \text{psi} = 230.59 \cdot \text{ksi}$$

$$T_{1\text{non.comp.positive}} := f_{\text{ps1non.comp.positive}} \cdot N_{\text{strands}} \cdot A_{\text{strand}} = 950.72 \cdot \text{kip}$$

$$\text{Tension}_{\text{total.non.comp.positive}} := T_{1\text{non.comp.positive}} = 950.72 \cdot \text{kip}$$

$$C_{2.\text{upperbars}} := F_{\text{sbars}} \cdot 0.2 \text{in}^2 \cdot 7 = 84 \cdot \text{kip}$$

$$\text{Compression}_{\text{total.non.comp.positive}} := C_{1\text{non.comp.positive}} + C_{2.\text{upperbars}}$$

$$\text{Compression}_{\text{total.non.comp.positive}} = 943.25 \cdot \text{kip}$$

Σ Moment at the top fibers

$$M_{19.Strand} := T_{1non.comp.positive} \cdot d_{1non.comp.positive} = 633.81 \cdot \text{kip} \cdot \text{ft}$$

$$M_{comp.1} := C_{1non.comp.positive} \cdot \frac{a_{non.comp.positive}}{2} = 94.25 \cdot \text{kip} \cdot \text{ft}$$

$$M_{comp.2} := C_{2.upper.bars} \cdot d_{upperbars} = 7 \cdot \text{kip} \cdot \text{ft}$$

$$M_{comp.block} := M_{comp.1} + M_{comp.2} = 101.25 \cdot \text{kip} \cdot \text{ft}$$

$$\Sigma M_{Ten..non.comp.positive} := M_{19.Strand} = 633.81 \cdot \text{kip} \cdot \text{ft}$$

$$\Sigma M_{Comp.non.comp.positive} := M_{comp.block} = 101.25 \cdot \text{kip} \cdot \text{ft}$$

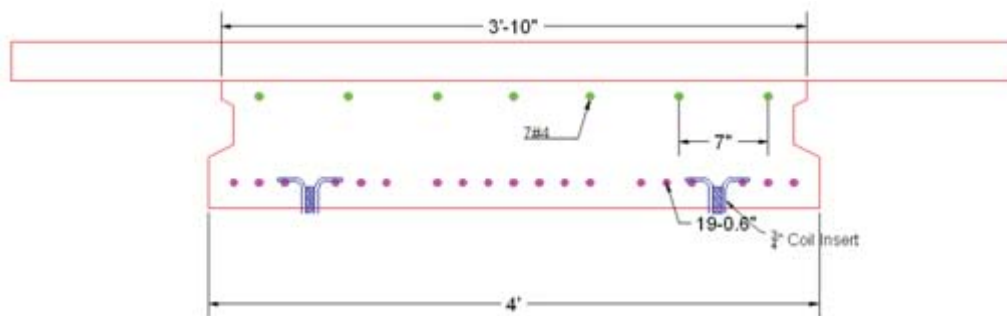
$$M_{n.c.positive} := \Sigma M_{Ten..non.comp.positive} - \Sigma M_{Comp.non.comp.positive}$$

$$M_{n.c.positive} = 532.57 \cdot \text{kip} \cdot \text{ft}$$

$$\phi := 0.48 + 83 \cdot \varepsilon_{s1non.comp.positive} = 0.72$$

$$\phi M_{n.c.positive} := \phi \cdot M_{n.c.positive} = 384.97 \cdot \text{kip} \cdot \text{ft}$$

2.5.1.2 Composite Section



$$f_{ctop} = 4 \times 10^3 \text{ psi}$$

$$f_{cbeam} = 8 \times 10^3 \text{ psi}$$

$$\beta_{1top} := 0.85 - \frac{(f_{ctop} - 4000\text{psi})}{1000\text{psi}} \cdot 0.05 = 0.85$$

$$\beta_{1\text{beam}} = 0.65$$

Try

$$c_{\text{comp.positive}} := 4.15\text{in}$$

$$h_{\text{top}} := h_2 + 0.5\text{in} = 2.5 \cdot \text{in}$$

$$b_{\text{eff2}} := 16 \cdot h_{\text{top}} + W_1 = 88 \cdot \text{in}$$

$$\beta_{1\text{average}} := \frac{\beta_{1\text{top}} \cdot f_{\text{ctop}} \cdot (h_{\text{top}} \cdot b_{\text{eff2}}) + \beta_{1\text{beam}} \cdot f_{\text{cbeam}} \cdot W_1 \cdot (c_{\text{comp.positive}} - h_{\text{top}})}{[W_1 \cdot (c_{\text{comp.positive}} - h_{\text{top}}) \cdot f_{\text{cbeam}} + (h_{\text{top}} \cdot b_{\text{eff2}}) \cdot f_{\text{ctop}}]}$$

$$\beta_{1\text{average}} = 0.77$$

$$a_{\text{comp.positive}} := c_{\text{comp.positive}} \cdot \beta_{1\text{average}} = 3.18 \cdot \text{in}$$

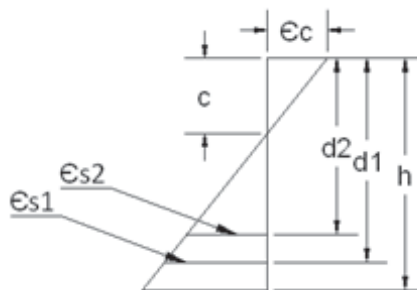
$$C_{1\text{comp.positive}} := 0.85 \cdot f_{\text{ctop}} \cdot (h_{\text{top}} \cdot b_{\text{eff2}}) = 748 \cdot \text{kip}$$

$$C_{2\text{comp.positive}} := 0.85 \cdot f_{\text{cbeam}} \cdot W_1 \cdot (a_{\text{comp.positive}} - h_{\text{top}}) = 221.97 \cdot \text{kip}$$

$$h := h_c = 12 \cdot \text{in}$$

$$d_{\text{Strand.}} := h_c + 0.5\text{in} - 2\text{in} = 10.5 \cdot \text{in}$$

$$d_{1\text{Comp}} := 1.25 \text{in}$$



$$d_{2.\text{Comp}} := h_{\text{top}} + \frac{(a_{\text{comp.positive}} - h_{\text{top}})}{2} = 2.84 \cdot \text{in}$$

$$d_{3.\text{bars}} := 3.5 \text{in}$$

$$\varepsilon_{s1\text{comp. positive}} := \varepsilon_c \cdot \frac{(d_{\text{Strand.}} - c_{\text{comp. positive}})}{c_{\text{comp. positive}}} = 4.59 \times 10^{-3}$$

$$\varepsilon_{\text{comp. bars}} := \varepsilon_c \cdot \frac{(c_{\text{comp. positive}} - d_{3.\text{bars}})}{c_{\text{comp. positive}}} = 4.7 \times 10^{-4}$$

$$F_{s.\text{bars}} := \varepsilon_{\text{comp. bars}} \cdot 29000\text{ksi} = 13.63 \cdot \text{ksi}$$

$$C_{3.\text{bars}} := F_{s.\text{bars}} \cdot 0.2\text{in}^2 \cdot 7 = 19.08 \cdot \text{kip}$$

$$\varepsilon_{ps1\text{comp. positive}} := \varepsilon_{s1\text{comp. positive}} + \frac{f_p}{E_{ps}} = 0.01$$

Using the Power formula

$$Q_{ps1\text{comp. positive}} := 887 + \frac{27613}{\left[1 + \left(112.4 \cdot \varepsilon_{ps1\text{comp. positive}} \right)^{7.36} \right]^{\left(\frac{1}{7.36} \right)}}$$

$$f_{ps1\text{comp. positive}} := \varepsilon_{ps1\text{comp. positive}} \cdot (Q_{ps1\text{comp. positive}}) \cdot 1000\text{psi} = 246.47 \cdot \text{ksi}$$

$$T_{1\text{comp. positive}} := 19 \cdot A_{\text{strand}} \cdot f_{ps1\text{comp. positive}} = 1.02 \times 10^3 \cdot \text{kip}$$

$$C_{\text{total}} := C_{1\text{comp. positive}} + C_{2\text{comp. positive}} + C_{3.\text{bars}} = 989.05 \cdot \text{kip}$$

$$T_{\text{total}} := T_{1\text{comp. positive}} = 1.02 \times 10^3 \cdot \text{kip}$$

Σ Moment at the top fiber

$$\Sigma M_{\text{comp. strand}} := T_{1\text{comp. positive}} \cdot d_{\text{Strand.}} = 889.17 \cdot \text{kip} \cdot \text{ft}$$

$$M_{C.1\text{comp}} := C_{1\text{comp. positive}} \cdot d_{1\text{Comp}} = 77.92 \cdot \text{kip} \cdot \text{ft}$$

$$M_{C.2\text{comp}} := C_{2\text{comp. positive}} \cdot (d_{2.\text{Comp}}) = 52.53 \cdot \text{kip} \cdot \text{ft}$$

$$M_{C.3\text{comp}} := C_{3.\text{bars}} \cdot d_{3.\text{bars}} = 5.56 \cdot \text{kip} \cdot \text{ft}$$

$$\Sigma M_{\text{comp.concrete}} := M_{\text{C.1comp}} + M_{\text{C.2comp}} + M_{\text{C.3comp}} = 136.01 \cdot \text{kip} \cdot \text{ft}$$

$$M_{\text{nc.comp.positive}} := \Sigma M_{\text{comp.strand}} - \Sigma M_{\text{comp.concrete}} = 753.15 \cdot \text{kip} \cdot \text{ft}$$

$$\phi_{\text{com.pv}} := 0.9$$

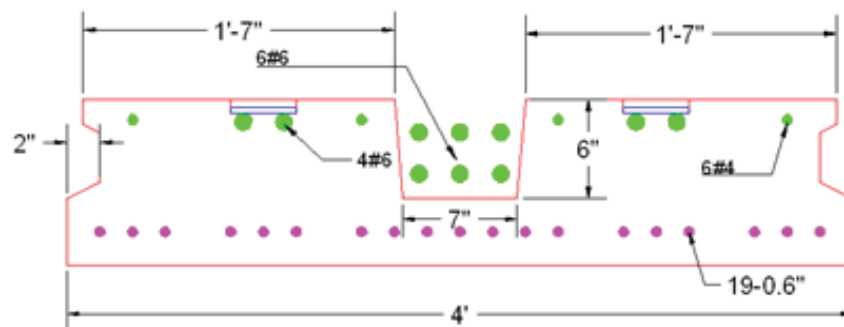
$$\phi_{\text{com.pv}} \cdot M_{\text{nc.comp.positive}} = 677.84 \cdot \text{kip} \cdot \text{ft}$$

This provided strength much higher than the required strength.

OK

2.5.2 Flexural Strength for Negative End-Section

2.5.2.1 Non-Composite Section



Strain Compatibility approach was used to calculate the section strength.

Use the top reinforcement as the following

First row = 3 # 6

$$N1_{\text{first.row.non.comp.}} := 3 \quad A_{\text{No.6}} := 0.44 \text{in}^2$$

$$A1_{\text{steel.first.row.non.comp}} := N1_{\text{first.row.non.comp.}} \cdot A_{\text{No.6}} = 1.32 \cdot \text{in}^2$$

$$d1_{\text{first.row.non.comp.}} := h_{\text{nc}} - 1.5 \text{in} = 8.5 \cdot \text{in}$$

First row = 4 # 6

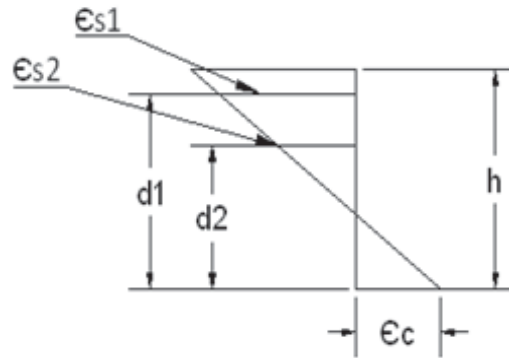
$$N2_{\text{first.row.non.comp.}} := 4 \quad A_{\text{No.6}} = 0.44 \cdot \text{in}^2$$

$$A2_{\text{steel.first.row.non.comp}} := N2_{\text{first.row.non.comp.}} \cdot A_{\text{No.6}} = 1.76 \cdot \text{in}^2$$

$$d_{\text{second.row.non.comp.}} := h_{\text{nc}} - 4.5\text{in} = 5.5\text{in}$$

$$d_1 := d_{\text{first.row.non.comp.}} = 8.5\text{in}$$

$$d_2 := d_{\text{second.row.non.comp.}} = 5.5\text{in}$$



$$h_{\text{nc}} = 10\text{in}$$

Try

$$C_{\text{non.comp.negative}} := 1.44\text{in} \quad \text{use strength for the grout}$$

$$f_{\text{cgrout}} := 6000\text{psi} \quad \beta_{1\text{grout}} := 0.75$$

$$a_{\text{non.comp.negative}} := \beta_{1\text{grout}} \cdot C_{\text{non.comp.negative}} = 1.08\text{in}$$

$$C_{1\text{non.comp.negative}} := 0.85 \cdot W_1 \cdot a_{\text{non.comp.negative}} \cdot f_{\text{cgrout}} = 264.38\text{kip}$$

$$\varepsilon_{s1\text{non.comp.negative}} := \varepsilon_c \cdot \frac{(d_1 - C_{\text{non.comp.negative}})}{C_{\text{non.comp.negative}}} = 0.01$$

$$\varepsilon_{s2\text{non.comp.negative}} := \varepsilon_c \cdot \frac{(d_2 - C_{\text{non.comp.negative}})}{C_{\text{non.comp.negative}}} = 8.46 \times 10^{-3}$$

$$\phi = 0.9 \quad f_{yb} := 60000\text{psi}$$

$$T1_{\text{first.row.non.comp}} := A1_{\text{steel.first.row.non.comp}} \cdot f_{yb} = 79.2\text{kip}$$

$$T2_{\text{first.row.non.comp}} := A2_{\text{steel.first.row.non.comp}} \cdot f_{yb} = 1.06 \times 10^5\text{lbf}$$

$$T_{\text{second.row.non.comp}} := A_{\text{steel.second.row.non.comp}} \cdot f_{yb} = 79.2 \cdot \text{kip}$$

$$T_{\text{first.row.non.comp}} := T1_{\text{first.row.non.comp}} + T2_{\text{first.row.non.comp}} = 184.8 \cdot \text{kip}$$

$$\Sigma T_{\text{non.comp.negative}} := T_{\text{first.row.non.comp}} + T_{\text{second.row.non.comp}} = 264 \cdot \text{kip}$$

$$\Sigma C_{\text{non.comp.negative}} := C_{1\text{non.comp.negative}} = 264.38 \cdot \text{kip}$$

Σ Moment at the bottom fibers

$$\Sigma M_{\text{steel}} := T_{\text{first.row.non.comp}} \cdot d_1 + T_{\text{second.row.non.comp}} \cdot d_2 = 167.2 \cdot \text{kip} \cdot \text{ft}$$

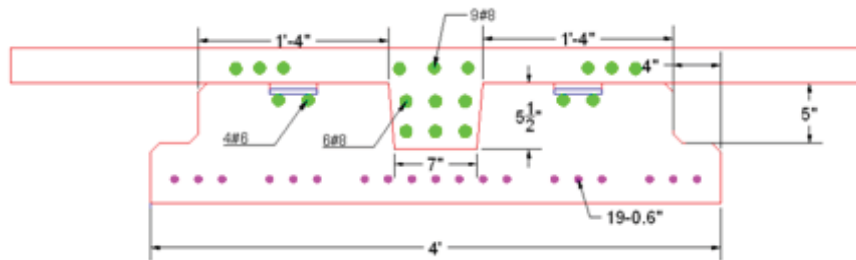
$$\Sigma M_{\text{concrete}} := C_{1\text{non.comp.negative}} \cdot \frac{a_{\text{non.comp.negative}}}{2} = 11.9 \cdot \text{kip} \cdot \text{ft}$$

$$M_{\text{non.comp.negative}} := \Sigma M_{\text{steel}} - \Sigma M_{\text{concrete}} = 155.3 \cdot \text{kip} \cdot \text{ft}$$

$$\phi \cdot M_{\text{non.comp.negative}} = 139.77 \cdot \text{kip} \cdot \text{ft} \quad \phi = 0.9$$

Thus the provided strength much higher than the required strength

2.5.2.2. Composite Section

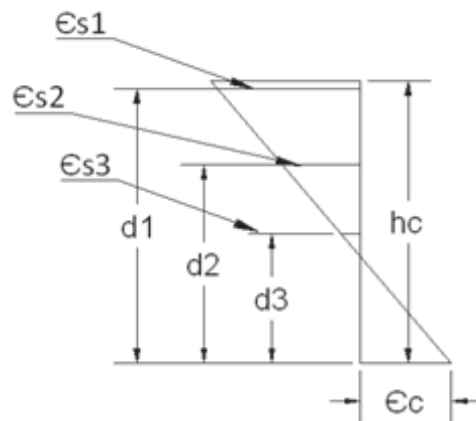


First row 9 # 8

$$N_{\text{first.row.comp.negative}} := 9 \quad A_{\text{No.8}} := 0.79 \text{in}^2$$

$$A_{\text{first.row.comp}} := N_{\text{first.row.comp.negative}} \cdot A_{\text{No.8}} = 7.11 \cdot \text{in}^2$$

$$d_{\text{first.row.comp.negative}} := h_c + 1\text{in} - 2\text{in} = 11 \cdot \text{in}$$



Second row = 3 # 6

$$N1_{\text{second.row.non.comp.}} := 3$$

$$A1_{\text{steel.second.row.non.comp.}} := N1_{\text{first.row.non.comp.}} \cdot A_{\text{No.6}} = 1.32 \cdot \text{in}^2$$

$$d1_{\text{second.row.non.comp.}} := h_{\text{nc}} - 1.5 \text{in} = 8.5 \cdot \text{in}$$

Second row = 4 # 6

$$N2_{\text{second.row.non.comp.}} := 4 \quad A_{\text{No.6}} = 0.44 \cdot \text{in}^2$$

$$A2_{\text{steel.second.row.non.comp.}} := N2_{\text{first.row.non.comp.}} \cdot A_{\text{No.6}} = 1.76 \cdot \text{in}^2$$

$$d2_{\text{second.row.non.comp.}} := h_{\text{nc}} - 1.5 \text{in} = 8.5 \cdot \text{in}$$

Third row 3 # 6

$$N_{\text{third.row.comp.negative}} := 3$$

$$A_{\text{third.row.comp.}} := N_{\text{third.row.comp.negative}} \cdot A_{\text{No.6}} = 1.32 \cdot \text{in}^2$$

$$d_{\text{third.row.comp.negative}} := h_c + 1 \text{in} - 7.5 \text{in} = 5.5 \cdot \text{in}$$

$$f_{\text{cgrout}} = 6 \times 10^3 \text{ psi}$$

$$\beta_{1\text{grout}} = 0.75$$

Try

$$C_{\text{comp.negative}} := 3.65 \text{ in} \quad E_{\text{sb}} := 29000 \text{ ksi}$$

$$a_{\text{comp.negative}} := \beta_1 \text{grout} \cdot C_{\text{comp.negative}} = 2.74 \cdot \text{in}$$

$$C_{1\text{comp.negative}} := 0.85 \cdot f_{\text{cgrout}} \cdot a_{\text{comp.negative}} \cdot W_1 = 670.14 \cdot \text{kip}$$

$$\varepsilon_{s1c} := \varepsilon_c \cdot \frac{(d_{\text{first.row.comp.negative}} - C_{\text{comp.negative}})}{C_{\text{comp.negative}}} = 6.04 \times 10^{-3}$$

$$\varepsilon_{s2c} := \varepsilon_c \cdot \frac{(d_{2\text{second.row.non.comp.}} - C_{\text{comp.negative}})}{C_{\text{comp.negative}}} = 3.99 \times 10^{-3}$$

$$\varepsilon_{s3c} := \varepsilon_c \cdot \frac{(d_{\text{third.row.comp.negative}} - C_{\text{comp.negative}})}{C_{\text{comp.negative}}} = 1.52 \times 10^{-3}$$

$$T_1 := A_{\text{first.row.comp}} \cdot f_{yb} = 426.6 \cdot \text{kip}$$

$$T_2 := (A_{1\text{steel.second.row.non.comp.}} + A_{2\text{steel.second.row.non.comp.}}) \cdot f_{yb}$$

$$T_2 = 184.8 \cdot \text{kip}$$

$$T_3 := A_{\text{third.row.comp}} \cdot (\varepsilon_{s3c} \cdot 29000 \text{ ksi}) = 58.21 \cdot \text{kip}$$

$$\Sigma T_c := T_1 + T_2 + T_3 = 669.61 \cdot \text{kip}$$

$$\Sigma C_c := C_{1\text{comp.negative}} = 670.14 \cdot \text{kip}$$

$$M_{\text{first.row}} := T_1 \cdot d_{\text{first.row.comp.negative}} = 391.05 \cdot \text{kip} \cdot \text{ft}$$

$$M_{\text{second.row}} := T_2 \cdot d_{2\text{second.row.non.comp.}} = 130.9 \cdot \text{kip} \cdot \text{ft}$$

$$M_{\text{third.row}} := T_3 \cdot d_{\text{third.row.comp.negative}} = 26.68 \cdot \text{kip} \cdot \text{ft}$$

$$\Sigma M_{\text{steel.comp}} := M_{\text{first.row}} + M_{\text{second.row}} + M_{\text{third.row}} = 548.63 \cdot \text{kip} \cdot \text{ft}$$

$$\Sigma M_{\text{concrete.comp}} := C_{1\text{comp.negative}} \cdot \frac{a_{\text{comp.negative}}}{2} = 76.44 \cdot \text{kip} \cdot \text{ft}$$

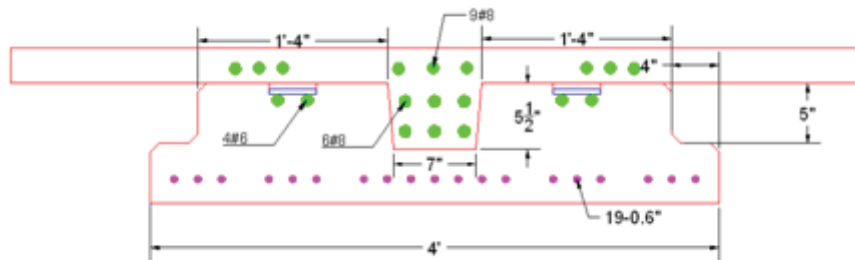
$$M_{n\text{comp.}} := \Sigma M_{\text{steel.comp}} - \Sigma M_{\text{concrete.comp}} = 472.19 \cdot \text{kip} \cdot \text{ft}$$

$$\phi \cdot M_{n\text{comp.}} = 424.97 \cdot \text{kip} \cdot \text{ft}$$

Thus the provided strength much higher than the required strength

2.5.3 Flexural Strength For End-Section (Positive Moment)

2.5.3.1 Composite Section



First row 9 # 8

$$N_{\text{first.row.comp.positive}} := 9 \quad A_{\text{No.8}} = 0.79 \cdot \text{in}^2$$

$$A_{\text{first.row.positive}} := N_{\text{first.row.comp.negative}} \cdot A_{\text{No.8}} = 7.11 \cdot \text{in}^2$$

$$d_{\text{first.row.comp.positive}} := 1.5 \text{in}$$

Second row = 3 # 6

$$N_{1\text{second.row.non.positive.}} := 3$$

$$A_{1\text{steel.second.row.non.positive}} := N_{1\text{first.row.non.comp.}} \cdot A_{\text{No.6}} = 1.32 \cdot \text{in}^2$$

$$d_{1\text{second.row.non.positive}} := 4.5 \text{in}$$

Second row = 4 # 6

$$N_{2\text{second.row.non.positive}} := 4 \quad A_{\text{No.6}} = 0.44 \cdot \text{in}^2$$

$$A2_{\text{steel.second.row.non.positive}} := N2_{\text{first.row.non.comp.}} \cdot A_{\text{No.6}} = 1.76 \cdot \text{in}^2$$

$$d2_{\text{second.row.non.positive}} := 4.5 \text{ in}$$

Third row 3 # 6

$$N_{\text{third.row.comp.positive}} := 3$$

$$A_{\text{third.row.positive}} := N_{\text{third.row.comp.negative}} \cdot A_{\text{No.6}} = 1.32 \cdot \text{in}^2$$

$$d_{\text{third.row.comp.positive}} := 7.5 \text{ in}$$

$$\beta_{\text{topping}} := 0.85$$

$$C_{\text{comp.positive.}} := 1.38 \text{ in}$$

$$a_{\text{comp.positive.}} := \beta_{\text{topping}} \cdot C_{\text{comp.positive.}} = 1.17 \cdot \text{in}$$

$$C_{1\text{comp.positive.}} := 0.85 \cdot f_{\text{ctop}} \cdot a_{\text{comp.positive.}} \cdot W_2 = 319.06 \cdot \text{kip}$$

$$\varepsilon_{s1c.} := \varepsilon_c \cdot \frac{(d_{\text{first.row.comp.positive}} - C_{\text{comp.positive.}})}{C_{\text{comp.positive.}}} = 2.61 \times 10^{-4}$$

$$\varepsilon_{s2c.} := \varepsilon_c \cdot \frac{(d2_{\text{second.row.non.positive}} - C_{\text{comp.positive.}})}{C_{\text{comp.positive.}}} = 6.78 \times 10^{-3}$$

$$\varepsilon_{s3c.} := \varepsilon_c \cdot \frac{(d_{\text{third.row.comp.positive}} - C_{\text{comp.positive.}})}{C_{\text{comp.positive.}}} = 0.01$$

$$E_s := 29000 \text{ ksi}$$

$$T_1 := A_{\text{first.row.positive}} \cdot \varepsilon_{s1c.} \cdot E_s = 53.79 \cdot \text{kip}$$

$$T_2 := (A1_{\text{steel.second.row.non.positive}} + A2_{\text{steel.second.row.non.positive}}) \cdot f_{yb}$$

$$T_2 = 184.8 \cdot \text{kip}$$

$$T_{3.} := A_{\text{third.row.positive}} \cdot f_{yb} = 79.2 \cdot \text{kip}$$

$$\Sigma T_t := T_{2.} + T_{3.} = 264 \cdot \text{kip}$$

$$\Sigma C_c := C_{1\text{comp.positive.}} - T_{1.} = 265.27 \cdot \text{kip}$$

$$M_{\text{first.row.}} := T_{1.} \cdot d_{\text{first.row.comp.positive}} = 6.72 \cdot \text{kip} \cdot \text{ft}$$

$$M_{\text{second.row.}} := T_{2.} \cdot d_{\text{second.row.non.positive}}^2 = 69.3 \cdot \text{kip} \cdot \text{ft}$$

$$M_{\text{thired.row.}} := T_{3.} \cdot d_{\text{third.row.comp.positive}} = 49.5 \cdot \text{kip} \cdot \text{ft}$$

$$\Sigma M_{\text{steel.comp.}} := M_{\text{first.row.}} + M_{\text{second.row.}} + M_{\text{thired.row.}} = 125.52 \cdot \text{kip} \cdot \text{ft}$$

$$\Sigma M_{\text{concrete.comp.}} := C_{1\text{comp.positive.}} \cdot \frac{a_{\text{comp.positive.}}}{2} = 15.59 \cdot \text{kip} \cdot \text{ft}$$

$$M_{n\text{comp.positive.}} := \Sigma M_{\text{steel.comp.}} - \Sigma M_{\text{concrete.comp.}} = 109.93 \cdot \text{kip} \cdot \text{ft}$$

$$\phi \cdot M_{n\text{comp.positive.}} = 98.94 \cdot \text{kip} \cdot \text{ft}$$

Thus the provided strength much higher than the required strength

2.6 Service Design

For serviceability design requirements

See PCI Design Handbook 6th Edition Section 4.2.2

See ACI 318-08 Section 18.4.2

Non-Composite Section

$$A_{nc} = 480 \cdot \text{in}^2$$

$$I_{nc} = 4 \times 10^3 \cdot \text{in}^4$$

$$Y_{bnc} = 5 \cdot \text{in}$$

$$Y_{tnc} = 5 \cdot \text{in}$$

Composite Section

$$A_c = 593.14 \cdot \text{in}^2$$

$$I_c = 8.45 \times 10^3 \cdot \text{in}^4$$

$$Y_{bc} = 6.14 \cdot \text{in}$$

$$Y_{tc} = 5.86 \cdot \text{in}$$

$$M_{\text{beam}} := W_{\text{beam}} \cdot \frac{\text{Span}_{\text{external.beam}}^2}{8} = 42.79 \cdot \text{kip} \cdot \text{ft}$$

$$M_{\text{H.C}} := W_{\text{H.C}} \cdot \frac{\text{Span}_{\text{external.beam}}^2}{8} = 166.89 \cdot \text{kip} \cdot \text{ft}$$

$$M_{\text{top}} := W_{\text{top}} \cdot \frac{\text{Span}_{\text{external.beam}}^2}{16} = 40.12 \cdot \text{kip} \cdot \text{ft}$$

$$M_{\text{L.L}} := W_{\text{L.L}} \cdot \frac{\text{Span}_{\text{external.beam}}^2}{16} = 128.38 \cdot \text{kip} \cdot \text{ft}$$

2.6.1 At Release (Section at Distance = 2.5 ft from the End)

$$D_{\text{ps}} := 0.6 \text{ in} \qquad L_{\text{t}} := 50 \cdot D_{\text{ps}} = 30 \cdot \text{in}$$

$$M_{\text{end}} := W_{\text{beam}} \cdot \frac{\text{Span}_{\text{external.beam}}}{2} \cdot (L_{\text{t}}) - W_{\text{beam}} \cdot L_{\text{t}} \cdot \frac{L_{\text{t}}}{2} = 14.79 \cdot \text{kip} \cdot \text{ft}$$

$$f_{\text{top.end}} := \frac{P_{\text{o}}}{A_{\text{g}}} - \left[\frac{(P_{\text{o}} \cdot e)}{I_{\text{g}}} \cdot Y_{\text{tnc}} \right] + \left(\frac{M_{\text{end}}}{I_{\text{g}}} \cdot Y_{\text{tnc}} \right) = -1.05 \cdot \text{ksi} \qquad \text{Tension}$$

It should less than $6(f_{\text{ci}})^{0.5}$

$$f_{\text{top.all.end}} := -6(\text{psi}^{0.5}) \sqrt{f_{\text{ci.beam}}} = -0.48 \cdot \text{ksi}$$

$$f_{\text{top.end}} \geq f_{\text{top.all.end}} \qquad \text{it should have top steel}$$

$$f_{\text{bot.end}} := \left[\frac{P_{\text{o}}}{A_{\text{g}}} + \frac{(P_{\text{o}} \cdot e)}{I_{\text{g}}} \cdot Y_{\text{bnc}} \right] - \frac{M_{\text{end}}}{I_{\text{g}}} \cdot Y_{\text{bnc}} = 4.22 \cdot \text{ksi} \qquad \text{Compression}$$

It should less than $0.7f_{\text{ci}}$

$$f_{\text{bot.all.end}} := 0.7 \cdot f_{\text{ci.beam}} = 4.55 \cdot \text{ksi} \qquad \text{Ok}$$

Steel Reinforcement Required at the Top

$$D_{\text{tension.depth}} := f_{\text{top.end}} \cdot \frac{h_{\text{nc}}}{(-f_{\text{top.end}} + f_{\text{bot.end}})} = -1.99 \cdot \text{in}$$

$$A_{\text{s.end}} := \frac{0.5 \cdot W_1 \cdot D_{\text{tension.depth}} \left[f_{\text{top.end}} + 6(\text{psi}^{0.5}) \sqrt{f_{\text{ci.beam}}} \right]}{30000 \text{psi}} = 0.9 \cdot \text{in}^2$$

2.6.2 At Release (Mid - Span Section)

$$f_{\text{top.mid}} := \frac{P_o}{A_g} - \left[\frac{(P_o \cdot e)}{I_g} \cdot Y_{\text{tnc}} \right] + \left(\frac{M_{\text{beam}}}{I_g} \cdot Y_{\text{tnc}} \right) = -0.63 \cdot \text{ksi} \quad \text{Tension}$$

It should less than $3(f_{\text{ci}})^{0.5}$

$$f_{\text{top.all.mid}} := -3\text{psi}^{0.5} \cdot \sqrt{f_{\text{ci.beam}}} = -0.24 \cdot \text{ksi}$$

$$f_{\text{top.mid}} \geq f_{\text{top.all.mid}} \quad \text{it should have top steel}$$

$$f_{\text{bot.mid}} := \frac{P_o}{A_g} + \frac{(P_o \cdot e)}{I_g} \cdot Y_{\text{bnc}} - \frac{M_{\text{beam}}}{I_g} \cdot Y_{\text{bnc}} = 3.8 \cdot \text{ksi} \quad \text{Compression}$$

It should less than $0.6f_{\text{ci}}$

$$f_{\text{bot.all.mid}} := 0.6 \cdot f_{\text{ci.beam}} = 3.9 \cdot \text{ksi}$$

$$f_{\text{bot.mid}} \leq f_{\text{bot.all.mid}}$$

Steel Reinforcement Required at the Top

$$D_{\text{tension.depth.mid}} := f_{\text{top.mid}} \cdot \frac{(h_{\text{nc}})}{-f_{\text{top.mid}} + f_{\text{bot.mid}}} = -1.42 \cdot \text{in}$$

$$A_{\text{s.top.mid}} := 0.5 \cdot D_{\text{tension.depth.mid}} \cdot W_2 \cdot \frac{(f_{\text{top.mid}} - f_{\text{top.all.mid}})}{30000 \text{psi}} = 0.73 \cdot \text{in}^2$$

Use 7#4

2.6.3 During Construction (Mid-Span Section)

$$P = 693.96 \cdot \text{kip}$$

$$f_{\text{top.con.}} := \frac{P}{A_g} - \left[\frac{(P \cdot e)}{I_g} \cdot Y_{\text{tnc}} \right] + \frac{(M_{\text{beam}} + M_{\text{H.C}} + M_{\text{top}})}{I_g} \cdot Y_{\text{tnc}} = 2.59 \cdot \text{ksi}$$

It should less than $0.45f_c$

$$f_{\text{top.con.all}} := 0.45 \cdot f_{c.\text{beam}} = 3.6 \cdot \text{ksi} \quad f_{\text{top.con}} \geq f_{\text{top.con.all}} \quad \text{Ok}$$

$$f_{\text{bot.con}} := \left[\frac{P}{A_g} + \frac{(P \cdot e)}{I_g} \cdot Y_{\text{tnc}} \right] - \frac{(M_{\text{beam}} + M_{\text{H.C}} + M_{\text{top}})}{I_g} \cdot Y_{\text{tnc}} = 0.3 \cdot \text{ksi}$$

No Limit

2.6.4 At Final (Mid-Span Section)

$$f_{\text{int.final}} := f_{\text{top.con.}} + \frac{M_{\text{L.L.}}}{I_c} \cdot (Y_{\text{tc}} - h_c + h_{\text{nc}}) = 3.29 \cdot \text{ksi} \quad \text{Compression}$$

It should less than $0.6f_c$ (beam)

$$f_{\text{int.all.final}} := 0.6 \cdot f_{c.\text{beam}} = 4.8 \cdot \text{ksi}$$

$$f_{\text{int.final}} \leq f_{\text{int.all.fina}}$$

$$f_{\text{bot.final}} := f_{\text{bot.con}} - \frac{M_{\text{L.L.}}}{I_c} \cdot (Y_{\text{bc}}) = -0.82 \cdot \text{ksi}$$

$$\text{Class}_U := 7.5 \text{psi}^{0.5} \cdot f_{c.\text{beam}}^{0.5} = 0.67 \cdot \text{ksi}$$

$$\text{Class}_T := 12 \text{psi}^{0.5} \cdot f_{c.\text{beam}}^{0.5} = 1.07 \cdot \text{ksi}$$

It is Ok for class T

2.7 Development Length

2.7.1 Strands

The required length to develop the strength of the strand, however is much longer, and is specified in ACI 12.9.1

$$f_{se} := f_p = 168.31 \cdot \text{ksi} \quad d_{bs} := D_{ps} = 0.6 \cdot \text{in}$$

$$f_{ps} := f_{ps1 \text{ comp. positive}} = 246.47 \cdot \text{ksi}$$

$$l_{ds} := \left(\frac{f_{se}}{3000 \text{psi}} \right) \cdot d_{bs} + \frac{(f_{ps} - f_{se})}{1000 \text{psi}} \cdot d_{bs} = 80.56 \cdot \text{in}$$

2.7.2 Welded Wire Reinforcement in Tension

yield strength of welded wire

$$f_y := 75000 \frac{\text{lb}}{\text{in}^2} \quad d_{bw} := 0.375 \text{ in}$$

Welded wire deformed reinforcement factor (1) is the greater of the following as shown in ACI 318.08 section 12.7

$$\frac{\left(f_y - 35000 \frac{\text{lb}}{\text{in}^2} \right)}{f_y} = 0.53 \quad \frac{(5 \cdot d_{bw})}{6} = 0.31 \cdot \text{in}$$

$$\psi_w := 0.533$$

$$\psi_{tw} := 1.0$$

$$\psi_{ew} := 1.2$$

$$\psi_{sw} := 0.8$$

For simplicity take $K_{tr}=0$

$$C_b := 1 \text{ in}$$

$$F_{ctop} = 27.78 \frac{\text{ft}^2}{\text{lb}} \cdot \frac{\text{lb}}{\text{in}^2} \text{psi}$$

$$K_{tr} := 0$$

$$\frac{C_b + K_{tr}}{d_{bw}} = 2.67$$

$$x = 2.5$$

$$x := \begin{cases} 2.5 & \text{if } \frac{C_b + K_{tr}}{d_{bw}} \geq 2.5 \\ \frac{C_b + K_{tr}}{d_{bw}} & \text{otherwise} \end{cases}$$

$$L_{dw} := \left[\frac{3}{40} \frac{\text{lb}}{\text{in}^2} \cdot \frac{f_y}{\sqrt{4000}} \cdot \frac{(\psi_{tw} \cdot \psi_{ew} \cdot \psi_{sw})}{x} \right] \cdot d_{bw} = 1.07 \cdot \text{ft}$$

L.dw actual after multiplying by WWR factor (0.533)

$$L_{dw\text{actual}} := \psi_w \cdot L_{dw} = 0.57 \cdot \text{ft}$$

2.7.3 Rebars

2.7.3.1 Rebars in Tension

According to ACI 318-08 section 12.2.3

For # 8 bars

$$f_{yb} = 60 \cdot \text{ksi}$$

$$f_{ctop} = 4 \times 10^3 \text{ psi}$$

$$\psi_{tb8} := 1.3$$

$$\psi_{eb8} := 1.0$$

$$\psi_{sb8} := 1.0$$

$$d_{b8} := 1 \text{ in}$$

$$A_{tr4} := 0.2 \text{ in}^2$$

$$s := 12 \text{ in}$$

$$n_{b8} := 9$$

$$C_{bb8} := 1 \text{ in}$$

$$K_{trb8} := \frac{(940 \cdot A_{tr4})}{12 \text{ in} \cdot 9} = 0.67 \cdot \text{in}$$

$$\frac{(C_{bb8} + K_{trb8})}{d_{b8}} = 1.67$$

$$Z := \begin{cases} 2.5 & \text{if } \left[\frac{(C_{bb8} + K_{trb8})}{d_{b8}} \right] \geq 2.5 \\ \left[\left[\frac{(C_{bb8} + K_{trb8})}{d_{b8}} \right] \right] & \text{otherwise} \end{cases}$$

$$Z = 1.67$$

$$L_{db8} := \left[\frac{3}{40 \text{ psi}^{0.5}} \cdot \frac{f_{yb}}{\sqrt{f_{ctop}}} \cdot \frac{(\psi_{tb8} \cdot \psi_{eb8} \cdot \psi_{sb8})}{Z} \right] \cdot d_{b8} = 55.5 \cdot \text{in}$$

For # 6 bars

$$\psi_{tb6} := 1.3$$

$$\psi_{eb6} := 1.0$$

$$\psi_{sb6} := 0.8$$

$$d_{b6} := 0.75 \cdot \text{in}$$

$$A_{tr8} := 0.2 \text{ in}^2$$

$$s := 6 \text{ in}$$

$$n_{b6} := 6$$

$$C_{bb6} := 1 \text{ in}$$

$$K_{trb6} := \frac{(640 \cdot A_{tr8})}{s \cdot n_{b6}} = 0.67 \cdot \text{in}$$

$$\frac{(C_{bb6} + K_{trb6})}{d_{b6}} = 2.22$$

$$k := \begin{cases} 2.5 & \text{if } \left[\frac{(C_{bb6} + K_{trb6})}{d_{b6}} \right] \geq 2.5 \\ \left[\left[\frac{(C_{bb6} + K_{trb6})}{d_{b6}} \right] \right] & \text{otherwise} \end{cases}$$

$$k = 2.22$$

$$L_{db6} := \left[\frac{3}{40 \text{ psi}^{0.5}} \cdot \frac{f_{yb}}{\sqrt{f_{c.beam}}} \cdot \frac{(\psi_{tb6} \cdot \psi_{eb6} \cdot \psi_{sb6})}{k} \right] \cdot d_{b6} = 1.47 \cdot \text{ft}$$

2.7.3.2 Rebars in Compression

According to ACI 318-08 section 12.3

Development length for Rebars in compression is the greater of X or Y

For # 6

$$d_{b6} = 0.75 \cdot \text{in}$$

$$X := 0.02 \cdot \frac{f_{yb}}{1 \text{ psi}^{0.5} \sqrt{f_{c.beam}}} \cdot d_{b6} = 10.06 \cdot \text{in}$$

$$Y := 0.0003 \cdot f_{yb} \cdot \frac{d_{b6}}{1 \text{ psi}} = 13.5 \cdot \text{in}$$

$$L_{dc6} := \begin{cases} X & \text{if } X \geq Y \\ Y & \text{otherwise} \end{cases}$$

$$L_{dc6} = 13.5 \cdot \text{in}$$

For # 8

$$d_{b8} = 1 \cdot \text{in}$$

$$F_{ctop} = 4 \times 10^3 \cdot \text{psi}$$

$$X := 0.02 \cdot \frac{f_{yb}}{\sqrt{f_{ctop}} \cdot 1 \text{psi}^{0.5}} \cdot d_{b6} = 14.23 \cdot \text{in}$$

$$Y := 0.0003 \cdot f_{yb} \cdot d_{b8} \cdot \frac{1}{1 \text{psi}} = 18 \cdot \text{in}$$

$$L_{dc8} := \begin{cases} X & \text{if } X \geq Y \\ Y & \text{otherwise} \end{cases}$$

$$L_{dc8} = 18 \cdot \text{in}$$

2.8. Shear Design

Using the simplified Method ACI 318-08 Section 11.3.1

The critical section located at $h/2$ from the face of the support,

$$M_u := -M_{\text{negative.comp}} - 100 \text{kip} \cdot \text{ft} = 297.52 \cdot \text{kip} \cdot \text{ft}$$

$$V_u := V_{\text{composite}} = 131.02 \cdot \text{kip}$$

$$d_p := h_c - Y_{ps} = 10 \cdot \text{in}$$

$$b_w := W_1 = 48 \cdot \text{in}$$

$$d := 10 \text{in}$$

$$G := \begin{cases} 1 & \text{if } \frac{V_u}{M_u} \cdot d_p > 1 \\ \left(\frac{V_u}{M_u} \cdot d_p \right) & \text{otherwise} \end{cases}$$

$$G = 0.37$$

$$V_c := \left[0.6 \cdot 1\text{psi}^{0.5} \cdot (f_c.\text{beam})^{0.5} + (700 \cdot G)\text{psi} \right] \cdot b_w \cdot d = 149.06 \cdot \text{kip}$$

$$V_{\text{Con.shear}} := \begin{cases} 2 \cdot 1\text{psi}^{0.5} \cdot (f_c.\text{beam})^{0.5} \cdot b_w \cdot d & \text{if } V_c < 2 \cdot 1\text{psi}^{0.5} \cdot (f_c.\text{beam})^{0.5} \cdot b_w \cdot d \\ \left[5 \cdot 1\text{psi}^{0.5} \cdot (f_c.\text{beam})^{0.5} \cdot b_w \cdot d \right] & \text{if } V_c > 5 \cdot 1\text{psi}^{0.5} \cdot (f_c.\text{beam})^{0.5} \cdot b_w \cdot d \\ V_c & \text{otherwise} \end{cases}$$

$$V_{\text{Con.shear}} = 149.06 \cdot \text{kip}$$

$$\phi_{\text{sh}} := 0.75$$

$$V_s := \frac{V_u}{0.75} - V_{\text{Con.shear}} = 25.63 \cdot \text{kip}$$

$$S_{\text{st}} := 12\text{in}$$

$$A_v := S_{\text{st}} \cdot \frac{V_s}{f_{yb} \cdot d} = 0.51 \cdot \text{in}^2 \quad f_{yb} = 6 \times 10^4 \text{psi}$$

$$A_{\text{vmin1}} := 0.75 \cdot 1\text{psi}^{0.5} \cdot (f_c.\text{beam})^{0.5} \cdot b_w \cdot \frac{S_{\text{st}}}{f_{yb}} = 0.64 \cdot \text{in}^2$$

$$A_{\text{vmin2}} := \frac{(50\text{psi} \cdot b_w \cdot S_{\text{st}})}{f_{yb}} = 0.48 \cdot \text{in}^2$$

$$A_{\text{vmin}} := \begin{cases} A_{\text{vmin1}} & \text{if } A_{\text{vmin1}} > A_{\text{vmin2}} \\ A_{\text{vmin2}} & \text{otherwise} \end{cases}$$

$$A_{\text{shear}} := \begin{cases} A_{\text{vmin}} & \text{if } A_{\text{vmin}} < \frac{(A_{\text{ps}} \cdot f_{\text{pu}} \cdot S_{\text{st}})}{80 \cdot f_{yb} \cdot d} \cdot \left(\frac{d}{b_w} \right)^{0.5} \\ \frac{(A_{\text{ps}} \cdot f_{\text{pu}} \cdot S_{\text{st}})}{80 \cdot f_{yb} \cdot d} \cdot \left(\frac{d}{b_w} \right)^{0.5} & \text{if } \left| \frac{(A_{\text{ps}} \cdot f_{\text{pu}} \cdot S_{\text{st}})}{80 \cdot f_{yb} \cdot d} \cdot \left(\frac{d}{b_w} \right)^{0.5} < A_{\text{vmin}} \right. \\ & \left. \frac{(A_{\text{ps}} \cdot f_{\text{pu}} \cdot S_{\text{st}})}{80 \cdot f_{yb} \cdot d} \cdot \left(\frac{d}{b_w} \right)^{0.5} > A_v \right. \\ A_v & \text{otherwise} \end{cases}$$

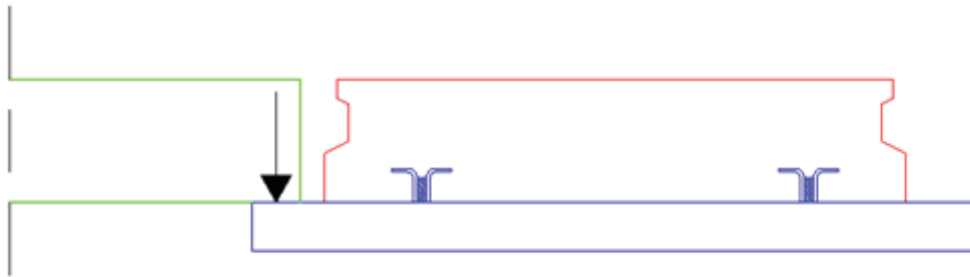
$$A_{\text{shear}} = 0.51 \cdot \text{in}^2$$

$$A_{\text{min.}} := 0.127 \text{in}^2$$

Use 2 legs # 4 stirrups @ 12 in

2.9 Torsion Design

Based to PCI Design Handbook 6th Edition section 4.4 and ACI 318-08 section 11.5, in prestressed members the critical section located at distance $h/2$ from the face of the support



At Construction Stage

Step 1: Determine the design shear (V_u) and the torsional moment (T_u) at the critical section

Assume that placed the HC on one side

$$HC_{sw} = 0.3 \cdot \frac{\text{kip}}{\text{ft}}$$

$$W_{\text{construction.load}} := 0 \frac{\text{kip}}{\text{ft}^2}$$

$$W_{\text{load.on.ledge}} := \frac{(HC_{sw} \cdot L_{HC} \cdot 0.5 + W_{\text{construction.load}} \cdot L_{HC} \cdot 0.5 \cdot 4\text{ft})}{HC_{\text{width}}} = 0.98 \cdot \frac{\text{kip}}{\text{ft}}$$

Critical section at distance 5 in from the face of the support

$$\frac{h_{nc}}{2} = 5 \cdot \text{in}$$

$$V_{Tu} := 1.4 \cdot W_{\text{load.on.ledge}} \cdot \frac{(\text{Span}_{\text{external.beam}} - h_{nc})}{2} = 17.29 \cdot \text{kip}$$

$$\text{Torsion}_{\text{arm}} := 11.5 \text{in}$$

$$T_u := V_{Tu} \cdot \text{Torsion}_{\text{arm}} = 16.57 \cdot \text{kip} \cdot \text{ft}$$

Step 2: Determine if the torsion can be neglected, i.e., is $T_u \leq T_{u(\text{min})}$

$$\phi_{\text{sh}} = 0.75$$

$$\lambda := 1$$

$$f_{\text{cbeam}} = 8 \times 10^3 \text{ psi}$$

$$P = 693.96 \cdot \text{kip}$$

$$f_{\text{pc}} := \frac{P}{A_g} = 1.45 \cdot \text{ksi}$$

$$\gamma := \left(1 + 10 \cdot \frac{f_{\text{pc}}}{f_{\text{cbeam}}} \right)^{0.5} = 1.68$$

$$X_f := h_{\text{nc}} = 10 \cdot \text{in}$$

$$Y_f := W_2 = 80 \cdot \text{in}$$

$$V_{\text{vol}} := X_f^2 \cdot Y_f = 8 \times 10^3 \cdot \text{in}^3$$

$$V_{\text{vol}} = \sum x^2 y$$

$$T_{u.\text{min}} := \phi_{\text{sh}} \cdot \left[0.5 \text{psi}^{0.5} \cdot \lambda \cdot (f_{\text{cbeam}})^{0.5} \cdot V_{\text{vol}} \right] \cdot \gamma = 37.46 \cdot \text{kip} \cdot \text{ft}$$

$$T_u < T_{u.\text{min}}$$

2.10 Design the End-Zone Reinforcement

By Using PCI Handbook Equation

$$f_s := 30 \text{ ksi}$$

$$A_s := \frac{0.021 \cdot P_o \cdot h_{\text{nc}}}{f_s \cdot L_t} = 0.18 \cdot \text{in}^2$$

Therefore, at least 0.18 in^2 of vertical reinforcement must be placed within $h/2$ from the beam end. at least $A_s/2$ should be placed at $h/8$ from the end and $A_s/2$ reinforcement at $3h/8$ from the end.

2.11.Camber and Deflection

From PCI Design Hand book 6th Edition section 4.8

For Span 30 ft

2.11.1. Stage I: At Release

$$f_{\text{c.beam}} = 8 \times 10^3 \text{ psi}$$

$$f_{\text{ci.beam}} = 6.5 \times 10^3 \text{ psi}$$

$$E_c = 5.1 \times 10^6 \text{ psi}$$

$$E_{ci} = 4.6 \times 10^6 \text{ psi}$$

$$\gamma_c = 0.15 \cdot \frac{\text{kip}}{\text{ft}^3}$$

$$I_g = 4 \times 10^3 \cdot \text{in}^4$$

$$A_g = 480 \cdot \text{in}^2$$

$$A_{ps} = 4.12 \cdot \text{in}^2$$

$$e = 3 \cdot \text{in}$$

$$L_1 := \text{Span}_{\text{external.beam}} = 26.17 \cdot \text{ft}$$

$$P_o = 761.5 \cdot \text{kip}$$

$$P = 693.96 \cdot \text{kip}$$

Initial Camber

$$\Delta_{1c} := \frac{-P_o \cdot e \cdot L_1^2}{8 \cdot E_{ci} \cdot I_g} = -1.53 \cdot \text{in}$$

Own Weight Deflection

$$W_{\text{beam}} = 0.5 \cdot \frac{\text{kip}}{\text{ft}}$$

$$\Delta_{1D} := \frac{(5 \cdot W_{\text{beam}} \cdot L_1^4)}{384 \cdot E_c \cdot I_g} = 0.26 \cdot \text{in}$$

Net Camber/Deflection

$$\Delta_{\text{net.camber.deflection.span1}} := \Delta_{1c} + \Delta_{1D} = -1.27 \cdot \text{in}$$

2.11.2. Stage II: At Erection

$$W_{H.C} = 1.95 \cdot \frac{\text{kip}}{\text{ft}}$$

$$W_{\text{top}} = 0.94 \cdot \frac{\text{kip}}{\text{ft}}$$

$$\Delta_{1D.\text{due.HC}} := \frac{(5 \cdot W_{H.C} \cdot L_1^4)}{384 \cdot E_c \cdot I_g} = 1.01 \cdot \text{in}$$

$$\Delta_{1D.\text{due.top}} := \frac{W_{\text{top}} \cdot L_1^4}{145 \cdot E_c \cdot I_g} = 0.26 \cdot \text{in}$$

$$\text{Net}_{\text{camber.deflection}} := 1.85 \cdot \Delta_{1D} + 1.8 \cdot \Delta_{1c} + \Delta_{1D.\text{due.HC}} + \Delta_{1D.\text{due.top}}$$

$$\text{Net}_{\text{camber.deflection}} = -1.01 \cdot \text{in}$$

2.11.3 Stage III: At Final

$$W_{L.L} = 3 \cdot \frac{\text{kip}}{\text{ft}}$$

$$I_C = 8.45 \times 10^3 \cdot \text{in}^4$$

$$b := W_2 = 80 \cdot \text{in}$$

$$d_p = 10 \cdot \text{in}$$

$$f_T := -7.5 \text{psi}^{0.5} \cdot (f_{c,\text{beam}})^{0.5} = -0.67 \cdot \text{ksi}$$

$$M_{L.L} = 128.38 \cdot \text{kip} \cdot \text{ft}$$

$$f_L := -M_{L.L} \cdot \frac{Y_{bc}}{I_C} = -1.12 \cdot \text{ksi}$$

$$f_{tL} := f_{\text{bot.final}} = -0.82 \cdot \text{ksi}$$

$$\rho_b := \frac{A_{ps}}{b \cdot d_p} = 5.15 \times 10^{-3}$$

$$\frac{E_{ps}}{E_c} = 5.59$$

$$I_{cr} := \frac{E_{ps}}{E_c} \cdot A_{ps} \cdot d_p^2 \cdot \left[1 - 1.6 \cdot \left(\frac{E_{ps}}{E_c} \cdot \rho_b \right)^{0.5} \right] = 1.68 \times 10^3 \cdot \text{in}^4$$

$$\left[1 - \left[\frac{(f_{tL} - f_T)}{f_L} \right] \right] = 0.87$$

$$\text{Ratio}_{\text{Mcr.Ma}} := 1 - \left[\frac{(f_{tL} - f_T)}{f_L} \right] = 0.87$$

$$I_e := \left[1 - \left[\frac{(f_{tL} - f_T)}{f_L} \right] \right]^3 \cdot I_C + \left[1 - \left[1 - \left[\frac{(f_{tL} - f_T)}{f_L} \right] \right]^3 \right] \cdot I_{cr} = 6.11 \times 10^3 \cdot \text{in}^4$$

$$\Delta_{L.L} := \frac{W_{L.L} \cdot L_1^4}{145 \cdot E_c \cdot I_e} = 0.54 \cdot \text{in}$$

$$\Delta_{\text{final}} := 2.4 \cdot \Delta_{1c} + \Delta_{1D} \cdot 2.2 + 3 \cdot \Delta_{1D.\text{due.HC}} + 2.3 \cdot \Delta_{1D.\text{due.top}} + \Delta_{L.L}$$

$$\Delta_{\text{final}} = 1.05 \cdot \text{in}$$

3. Design of Temporary and Hidden Corbels

3.1 Design of Temporary Corbels

3.1.1 Loads

The design of the temporary corbels is carried out according to the shear-friction design method ACI 318-08 section 11.6.4

$$h_c = 12 \cdot \text{in}$$

$$W_{\text{beam}} = 0.5 \cdot \frac{\text{kip}}{\text{ft}}$$

$$\text{Inter}_{\text{beam.span}} = 30 \cdot \text{ft}$$

$$\text{Exter}_{\text{beam.span}} = 28 \cdot \text{ft}$$

$$\text{HC}_{\text{weight.sq.ft}} = 0.08 \cdot \frac{\text{kip}}{\text{ft}^2}$$

$$\text{Aver}_{\text{gthickness.top}} = 2.5 \cdot \text{in}$$

$$\text{Span}_{\text{HC.direction}} = 30 \cdot \text{ft}$$

$$\text{Construction}_{\text{L.L}} := 0.015 \frac{\text{kip}}{\text{ft}^2}$$

$$V_{\text{D.from.beam}} := W_{\text{beam}} \cdot \frac{\text{Inter}_{\text{beam.span}}}{2} = 7.5 \cdot \text{kip}$$

$$V_{\text{D.from.HC}} := \text{HC}_{\text{weight.sq.ft}} \cdot \text{L}_{\text{HC}} \cdot \frac{\text{Inter}_{\text{beam.span}}}{2} = 29.25 \cdot \text{kip}$$

$$V_{\text{D.from.top}} := \text{Aver}_{\text{gthickness.top}} \cdot \gamma_c \cdot \text{HC}_{\text{span}} \cdot \frac{\text{Inter}_{\text{beam.span}}}{2} = 14.06 \cdot \text{kip}$$

$$V_{\text{Dead.per.corbel}} := V_{\text{D.from.beam}} + V_{\text{D.from.HC}} + V_{\text{D.from.top}} = 50.81 \cdot \text{kip}$$

$$V_{\text{live.per.corbel}} := \text{Construction}_{\text{L.L}} \cdot \text{HC}_{\text{span}} \cdot \frac{\text{Inter}_{\text{beam.span}}}{2} = 6.75 \cdot \text{kip}$$

$$V_{\text{U.per.corbel}} := 1.4 \cdot (V_{\text{Dead.per.corbel}} + V_{\text{live.per.corbel}}) = 80.59 \cdot \text{kip}$$

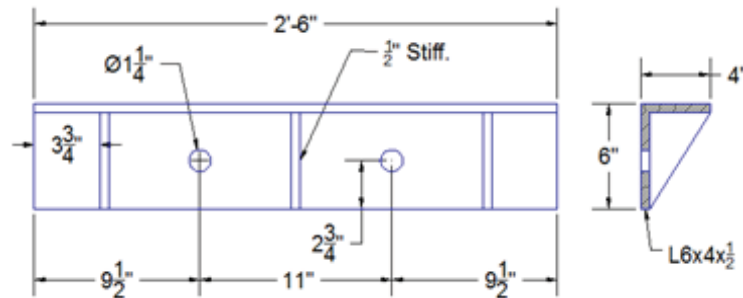
3.1.2 Resistance

$$\text{Diameter}_{\text{TR}} := 1 \cdot \text{in}$$

$$A_{\text{net.TR}} := 0.85 \text{in}^2$$

$$f_{\text{uTR}} := 150 \text{ksi}$$

$$f_{\text{yTR}} := 120 \text{ksi}$$



$$\mu := 0.7$$

$$\phi_{sh} = 0.75$$

$$\text{Number}_{TR} := 2$$

$$\text{Column}_{width} = 20 \cdot \text{in}$$

$$F_{ccolumn} := 8000 \text{ psi}$$

$$V_n := \mu \cdot \text{Number}_{TR} \cdot f_{yTR} \cdot A_{net,TR} = 142.8 \cdot \text{kip}$$

$$\phi_{sh} \cdot V_n = 107.1 \cdot \text{kip}$$

$$\text{MinAngle.depth} := \frac{V_{U,per.corbel}}{\phi_{sh} \cdot \text{Column}_{width} \cdot 0.2 \cdot F_{ccolumn}} = 3.36 \cdot \text{in}$$

3.1.3 Stiffener Design

Chosen Angle = L6*4*1/2

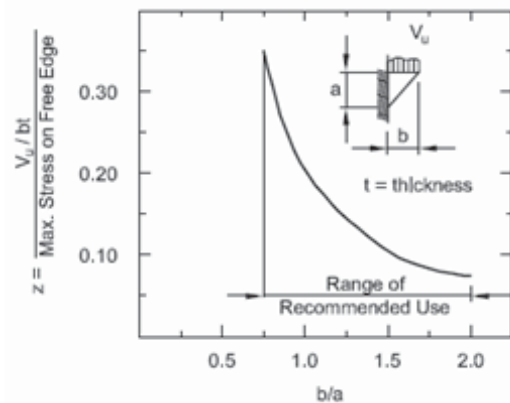
$$\text{Stiffner}_{height,a} := 5.5 \text{ in}$$

$$\text{Stiffner}_{width,b} := 3.5 \text{ in}$$

$$a := 5.5 \text{ in}$$

$$b := 3.5 \text{ in}$$

$$\frac{b}{a} = 0.64$$



$$z := 0.44$$

$$f_{y,stiff} := 50 \text{ ksi}$$

$$\phi_{SR} := 0.85$$

$$t := \frac{V_{U,\text{per.corbel}}}{\phi \cdot S_R \cdot f_{y,\text{stiff}} \cdot b \cdot z} = 1.23 \cdot \text{in}$$

3.2 Design of Hidden Corbels

The design of the hidden corbel is performed according to the shear-friction design method
Using ACI 318-08 section 11.6.4

3.2.1 Loads

$$h_c = 12 \cdot \text{in}$$

$$W_{\text{beam}} = 0.5 \cdot \frac{\text{kip}}{\text{ft}}$$

$$\text{Inter}_{\text{beam.span}} = 30 \cdot \text{ft}$$

$$\text{HC}_{\text{weight.sq.ft}} = 0.08 \cdot \frac{\text{kip}}{\text{ft}^2}$$

$$\text{HC}_{\text{span}} = 30 \cdot \text{ft}$$

$$L_L = 0.1 \cdot \frac{\text{kip}}{\text{ft}^2}$$

$$\text{Aver}_{\text{gthickness.top}} = 2.5 \cdot \text{in}$$

$$V_{\text{Dead.beam}} := W_{\text{beam}} \cdot \text{Inter}_{\text{beam.span}} = 15 \cdot \text{kip}$$

$$V_{\text{Dead.HC}} := \text{HC}_{\text{weight.sq.ft}} \cdot \text{Inter}_{\text{beam.span}} \cdot L_{\text{HC}} = 58.5 \cdot \text{kip}$$

$$V_{\text{Dead.Top}} := \text{Aver}_{\text{gthickness.top}} \cdot \gamma_c \cdot \text{HC}_{\text{span}} \cdot \text{Inter}_{\text{beam.span}} = 28.12 \cdot \text{kip}$$

$$V_{\text{Dead.Load}} := V_{\text{Dead.beam}} + V_{\text{Dead.HC}} + V_{\text{Dead.Top}} = 101.63 \cdot \text{kip}$$

$$V_{\text{Live.Load}} := L_L \cdot \text{HC}_{\text{span}} \cdot \text{Inter}_{\text{beam.span}} = 90 \cdot \text{kip}$$

$$V_U := 1.2 \cdot V_{\text{Dead.Load}} + 1.6 \cdot V_{\text{Live.Load}} = 265.95 \cdot \text{kip}$$

3.2.2 Resistance

$$\text{Area}_{\text{steel}} := 0.79 \text{in}^2 \cdot 3 + 0.44 \text{in}^2 \cdot 6 = 5.01 \cdot \text{in}^2$$

$$f_{yb} = 60 \cdot \text{ksi}$$

$$\text{Depth}_{\text{hidden.corbel}} := 9 \text{in}$$

$$\text{Width}_{\text{hidden.corbel}} := 7 \text{in}$$

$$\text{Column}_{\text{width}} = 20 \cdot \text{in} \qquad \text{Depth}_{\text{beam}} := 12 \text{in}$$

$$\mu_{\text{pocket}} := 1.4 \cdot \frac{(\text{Depth}_{\text{hidden.corbel}} \cdot \text{Width}_{\text{hidden.corbel}})}{(\text{Column}_{\text{width}} \cdot \text{Depth}_{\text{beam}})} = 0.37$$

$$\mu_{\text{precast}} := \left[0.6 \cdot \frac{(\text{Column}_{\text{width}} \cdot \text{Depth}_{\text{beam}} - \text{Depth}_{\text{hidden.corbel}} \cdot \text{Width}_{\text{hidden.corbel}})}{(\text{Column}_{\text{width}} \cdot \text{Depth}_{\text{beam}})} \right]$$

$$\mu_{\text{precast}} = 0.44$$

$$\mu_{\text{avg}} := \mu_{\text{pocket}} + \mu_{\text{precast}} = 0.81 \qquad f_{\text{ctop}} = 4 \times 10^3 \cdot \text{psi}$$

$$V_{\text{n1}} := (\text{Area}_{\text{steel}} \cdot f_{\text{yb}} \cdot \mu_{\text{avg}}) \cdot 2 = 486.97 \cdot \text{kip}$$

$$V_{\text{n2}} := (0.2 \cdot f_{\text{ctop}} \cdot \text{Column}_{\text{width}} \cdot \text{Depth}_{\text{beam}}) \cdot 2 = 384 \cdot \text{kip}$$

$$V_{\text{n3}} := (480 \text{psi} + 0.08 f_{\text{ctop}}) \cdot (\text{Column}_{\text{width}} \cdot \text{Depth}_{\text{beam}}) \cdot 2 = 384 \cdot \text{kip}$$

$$V_{\text{n.min}} := \begin{cases} V_{\text{n2}} & \text{if } V_{\text{n2}} \leq V_{\text{n3}} \\ V_{\text{n3}} & \text{otherwise} \end{cases}$$

$$V_{\text{n.min}} = 384 \cdot \text{kip}$$

$$V_{\text{n.final}} := \begin{cases} V_{\text{n1}} & \text{if } V_{\text{n1}} < V_{\text{n.min}} \\ V_{\text{n.min}} & \text{otherwise} \end{cases}$$

$$V_{\text{n.final}} = 384 \cdot \text{kip}$$

$$\phi_{\text{sh}} \cdot V_{\text{n.final}} = 288 \cdot \text{kip}$$

$$V_{\text{U}} = 265.95 \cdot \text{kip}$$

4. Design of Hidden Ledge

The design of the hidden corbel is performed according to the shear-friction design method

Using ACI 318-08 section 11.6.4

4.1 Loads

$$h_c = 12 \cdot \text{in}$$

$$W_{\text{beam}} = 0.5 \cdot \frac{\text{kip}}{\text{ft}}$$

$$\text{Inter}_{\text{beam.span}} = 30 \cdot \text{ft}$$

$$\text{HC}_{\text{weight.sq.ft}} = 0.08 \cdot \frac{\text{kip}}{\text{ft}^2}$$

$$\text{HC}_{\text{span}} = 30 \cdot \text{ft}$$

$$L_L = 0.1 \cdot \frac{\text{kip}}{\text{ft}^2}$$

$$\text{Aver}_{\text{gthickness.top}} = 2.5 \cdot \text{in}$$

$$L_{\text{HC}} = 26 \text{ ft}$$

$$V_{\text{Dead.HC.}} := \text{HC}_{\text{weight.sq.ft}} \cdot \frac{L_{\text{HC}}}{2} \cdot \text{HC}_{\text{width}} = 3.9 \cdot \text{kip} \quad \text{Per HC}$$

$$V_{\text{Dead.Top.}} := \text{Aver}_{\text{gthickness.top}} \cdot c \cdot \frac{\text{HC}_{\text{span}}}{2} \cdot \text{HC}_{\text{width}} = 1.87 \cdot \text{kip}$$

$$V_{\text{Dead.Load.}} := V_{\text{Dead.HC.}} + V_{\text{Dead.Top.}} = 5.77 \cdot \text{kip}$$

$$V_{\text{Live.Load.}} := L_L \cdot \frac{\text{HC}_{\text{span}}}{2} \cdot \text{HC}_{\text{width}} = 6 \cdot \text{kip}$$

$$V_U := 1.2 \cdot V_{\text{Dead.Load.}} + 1.6 \cdot V_{\text{Live.Load.}} = 16.53 \cdot \text{kip}$$

4.2 Resistance

$$\text{Area}_{\text{steel.}} := 2.5 \cdot .31 \text{ in}^2 = 0.78 \cdot \text{in}^2$$

$$f_{\text{yb}} = 60 \cdot \text{ksi}$$

$$\mu := 1$$

$$f_{\text{ctop}} = 4 \times 10^3 \cdot \text{psi}$$

$$V_{\text{n1.}} := (\text{Area}_{\text{steel.}} \cdot f_{\text{yb}} \cdot \mu) = 46.5 \cdot \text{kip}$$

$$\text{HC}_{\text{width}} = 4 \text{ ft}$$

$$\text{Depth}_{\text{beam}} = 1 \text{ ft}$$

$$V_{\text{n2.}} := (0.2 \cdot f_{\text{ctop}} \cdot \text{HC}_{\text{width}} \cdot \text{Depth}_{\text{beam}}) \cdot 2 = 921.6 \cdot \text{kip}$$

$$V_{n3} := (480\text{psi} + 0.08f_{ctop}) \cdot (HC_{width} \cdot Depth_{beam}) \cdot 2 = 921.6 \cdot \text{kip}$$

$$V_{n.min.} := \begin{cases} V_{n2} & \text{if } V_{n2} \leq V_{n3} \\ V_{n3} & \text{otherwise} \end{cases}$$

$$V_{n.min.} = 921.6 \cdot \text{kip}$$

$$V_{n.final.} := \begin{cases} V_{n1} & \text{if } V_{n1} < V_{n.min.} \\ V_{n.min.} & \text{otherwise} \end{cases}$$

$$V_{n.final.} = 46.5 \cdot \text{kip}$$

$$\phi_{sh} \cdot V_{n.final.} = 34.88 \cdot \text{kip}$$

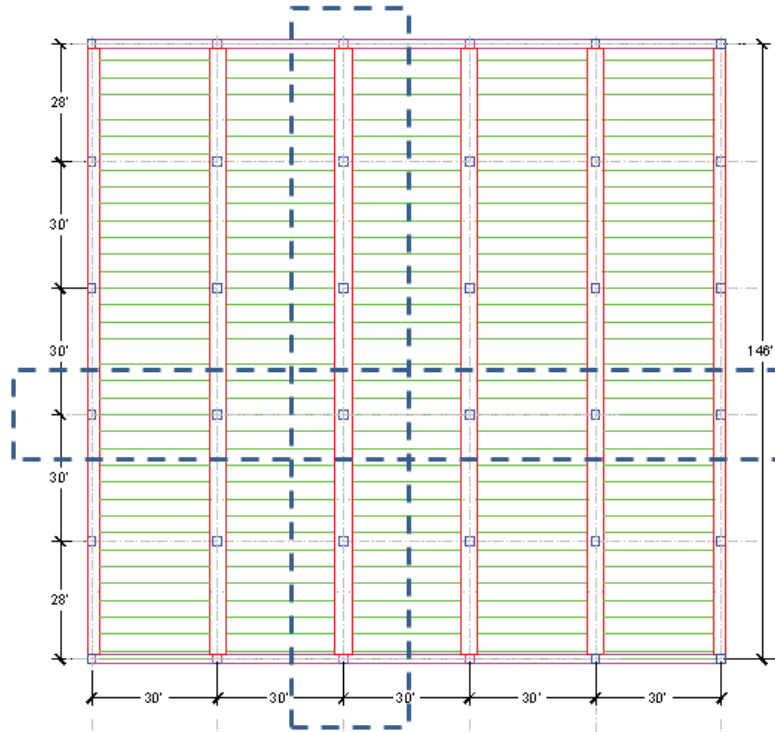
$$V_U = 16.53 \cdot \text{kip}$$

5. Design of the Column

Design of columns for the proposed floor system is similar to the design column for any conventional floor system. Columns should be designed to resist axial and bending moments according to section 10.3 of ACI 318-08.

6. Design For Lateral Loads

Lateral loads considered in the analysis of the proposed shallow floor system include the wind and seismic loads calculated according to ASCE-05. These loads were applied to the marked frames in the following for both beam and hollow core directions. two dimensional frame analysis was performed using SAP 2000 V.14.1 to determine the maximum moments due to wind and seismic loading in each direction. the following subsections present load calculations and analysis results.



TWO DIMENSIONAL FRAMES ADOPTED FOR LATERAL LOAD ANALYSIS

The following table summarizes the 2-D analysis results of the building in both beam and HC directions under wind and seismic loads.

Summary of Lateral Load Analysis Results

	Wind Load		Seismic Load	
	Moment (kip.ft)	Deflection (in)	Moment (kip.ft)	Deflection (in)
HC Direction	42.3	0.397	128	1.36
Beam Direction	41.11	0.654	104.26	1.88

To evaluate the adequacy of the proposed design to resist these loads, the following calculations have the load combinations considered in the design of the example building and compare them versus the factored resistance

6.1 FS 10 Beam Negative End-Section (Wind Case)

$$M_{\text{wind}} := -41.11 \text{ kip}\cdot\text{ft}$$

$$M_{\text{dead.load}} := M_{\text{negative.non.simple.comp.}} = -62.9 \cdot \text{kip}\cdot\text{ft}$$

$$M_{\text{live.load}} := M_{\text{negative.comp.}} = -201.28 \cdot \text{kip}\cdot\text{ft}$$

$$M_{\text{combination.wind}} := 1.2 \cdot M_{\text{dead.load}} + 1.6 \cdot M_{\text{wind}} + M_{\text{live.load}} = -342.53 \cdot \text{kip}\cdot\text{ft}$$

6.2 FS 10 Beam Negative End-section (Seismic Case)

$$M_{\text{seismic}} := -104.26 \text{ kip}\cdot\text{ft}$$

$$M_{\text{dead.load}} = -62.9 \cdot \text{kip}\cdot\text{ft}$$

$$M_{\text{live.load}} = -201.28 \cdot \text{kip}\cdot\text{ft}$$

$$M_{\text{combination.seismic}} := 1.2 \cdot M_{\text{dead.load}} + 1.0 \cdot M_{\text{seismic}} + M_{\text{live.load}} = -381.01 \cdot \text{kip}\cdot\text{ft}$$

$$\text{Factor Resistance} = \text{Negative capacity Composite end section} = -425 \text{ kip}\cdot\text{ft}$$

6.3 FS 10 Beam Positive End-Section (Wind Case)

$$M_{\text{wind.}} := 40.26 \text{ kip}\cdot\text{ft}$$

$$M_{\text{dead.load.}} := 0$$

$$M_{\text{live.load.}} := 0$$

$$M_{\text{combination.wind.}} := 1.2 \cdot M_{\text{dead.load.}} + 1.6 \cdot M_{\text{wind.}} + M_{\text{live.load.}} = 64.42 \cdot \text{kip}\cdot\text{ft}$$

6.4 FS 10 Positive End-Section (Seismic Case)

$$M_{\text{seismic.}} := 102.26 \text{ kip}\cdot\text{ft}$$

$$M_{\text{dead.load.}} = 0$$

$$M_{\text{live.load.}} = 0$$

$$M_{\text{combination.seismic.}} := 1.2 \cdot M_{\text{dead.load.}} + 1.0 \cdot M_{\text{seismic.}} + M_{\text{live.load}}$$

$$M_{\text{combination.seismic.}} = 102.26 \cdot \text{kip} \cdot \text{ft}$$

$$\text{Factored Positive.mom.capacity.composite.end.section} := \phi \cdot M_{\text{ncomp.positive.}}$$

$$\text{Factored Positive.mom.capacity.composite.end.section} = 98.94 \cdot \text{kip} \cdot \text{ft}$$

$$\text{Negative.mom.from.topping} := \frac{-M_{\text{negative.non.comp.f}}}{1.2} = 62.9 \cdot \text{kip} \cdot \text{ft}$$

$$F_{\text{.Resistance.positive.end.sec}} := \phi \cdot M_{\text{ncomp.positive.}} + 0.9 \cdot \text{Negative.mom.from.topping}$$

$$F_{\text{.Resistance.positive.end.sec}} = 155.55 \cdot \text{kip} \cdot \text{ft}$$

$$\text{Factored Resistance.positive.end.section} := F_{\text{.Resistance.positive.end.sec}}$$

6.5 HC Negative End-Section (Wind Case)

$$M_{\text{wind..}} := -42.3 \text{kip} \cdot \text{ft}$$

$$M_{\text{L.L.conti..}} := 0$$

$$M_{\text{dead.load.}} = 0$$

$$M_{\text{combination.wind..}} := 1.2 \cdot M_{\text{dead.load.}} + 1.6 \cdot M_{\text{wind..}} + M_{\text{L.L.conti..}}$$

$$M_{\text{combination.wind..}} = -67.68 \cdot \text{kip} \cdot \text{ft}$$

6.6 HC. Negative End-Section (Seismic Case)

$$M_{\text{seismic..}} := -128 \text{kip} \cdot \text{ft}$$

$$M_{\text{L.L.conti...}} := 0.$$

$$M_{\text{dead.load.}} = 0$$

$$M_{\text{combination.seismic..}} := 1.2 \cdot M_{\text{dead.load.}} + 1.0 \cdot M_{\text{seismic..}} + M_{\text{L.L.conti...}}$$

$$M_{\text{combination.seismic..}} = -128 \cdot \text{kip} \cdot \text{ft}$$

Factor Resistance = Negative capacity Composite end section = $-56.36 \cdot 4 = -225.44 \text{ kip} \cdot \text{ft}$

where 56.36 kip.ft the capacity of one HC, and 4 is number of HC in Column Strip

Appendix B

FACBRICATION OF BEAM-COLUMN CONNECTION WITHOUT CORBEL
COMPONENTS



Fabrication of the column



Fabrication of the beam



Precast beam, HC, and Column

Appendix C

ERECTION OF BEAM-COLUMN CONNECTION WITHOUT CORBEL

SPECIMEN



Placing temporary corbels



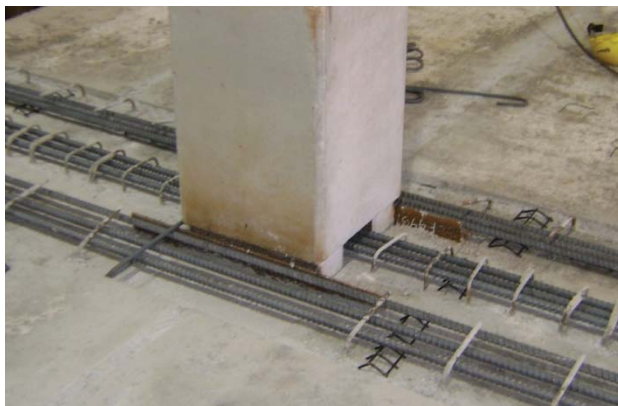
Welding the top angles to beam and column



Placing HC planks and pocket reinforcement



Grouting the H.C keys and beam pocket with SCC



Placing the topping reinforcement and C-bars



Placing the topping reinforcement



Pouring and finishing the topping concrete



Removing the temporary corbels

Appendix D

FACBRICATION OF FLAT SOFFIT BEAM



Fabrication of beam specimen

Appendix E

ERECTION OF HC-BEAM CONNECTION WITHOUT LEDGE SPECIMEN



Placing the beam on the three supports



Placing the beam steel ledge and the temporary ledges



Placing the HC



Installation of HC-beam connection reinforcement



Grouting hollow core key ways, HC opening and beam shear key



Installation of welded wire reinforcement of the topping



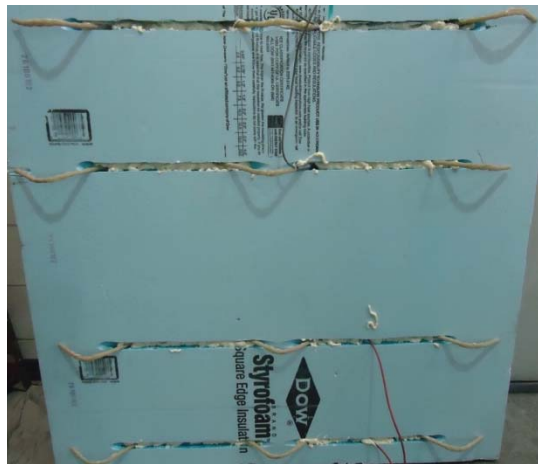
Casting the topping



Remove temporary corbels after the topping hardening

Appendix F

SANDWICH FLOOR PANEL FABRICATION



Insert GFRP tie into the XPS slot and filling the gap with expanding foam insulation



Setup the forms and tension the strands



Casting the bottom wythe, installing foam panels, and casting the top wythe



Inserting the lifting point



Place topping reinforcement



Casting and finishing the topping

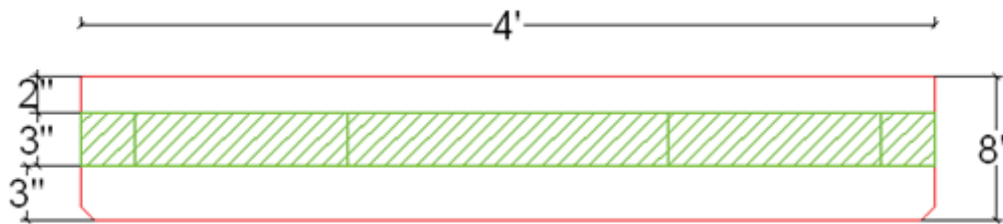
Appendix G

NU FLOOR DESIGN EXAMPLE (PANEL WITH GFRP TIES)

Span := 26ft

Width := 4ft

Topping thickness := 2.0in

 $\gamma := 0.15 \frac{\text{kip}}{\text{ft}^3}$ Lower_{layer}.thickness := 3inTop_{layer}.thickness := 2inSelf_{Weight} := $[(\text{Lower}_{\text{layer}}.\text{thickness} + \text{Top}_{\text{layer}}.\text{thickness}) \cdot \text{Width}] \cdot \gamma = 0.25 \frac{\text{kip}}{\text{ft}}$ $W_{\text{panel}} := \text{Self}_{\text{Weight}} = 0.25 \frac{\text{kip}}{\text{ft}}$ $W_{\text{topping}} := \text{Topping}_{\text{thickness}} \cdot \text{Width} \cdot \gamma = 0.1 \frac{\text{kip}}{\text{ft}}$

Construction Load := 50psf

 $W_{\text{construction.load}} := \text{Construction Load} \cdot \text{Width}$ $L_L := 0.1 \frac{\text{kip}}{\text{ft}^2}$ $W_{\text{construction.load}} = 0.2 \frac{\text{kip}}{\text{ft}}$ $W_{L.L} := L_L \cdot \text{Width} = 0.4 \frac{\text{kip}}{\text{ft}}$ $M_{\text{panel}} := W_{\text{panel}} \cdot \frac{\text{Span}^2}{8} = 21.12 \text{ kip}\cdot\text{ft}$ $M_{\text{topping}} := W_{\text{topping}} \cdot \frac{\text{Span}^2}{8} = 8.45 \text{ kip}\cdot\text{ft}$ $M_{\text{Construction}} := W_{\text{construction.load}} \cdot \frac{\text{Span}^2}{8} = 16.9 \text{ kip}\cdot\text{ft}$ $M_{L.L} := W_{L.L} \cdot \frac{\text{Span}^2}{8} = 33.8 \text{ kip}\cdot\text{ft}$ $M_{\text{Sustain.factor}} := (M_{\text{panel}} + M_{\text{topping}}) \cdot 1.2 = 35.49 \text{ kip}\cdot\text{ft}$ $M_{L.L.\text{factor}} := 1.6 \cdot M_{L.L} = 54.08 \text{ kip}\cdot\text{ft}$

1. Load

1.1 At Final Stage

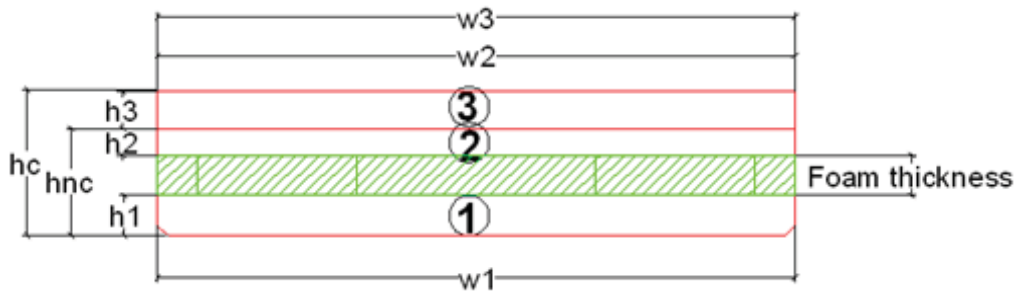
$$\text{Factor}_{\text{Load.Final}} := 1.2 \cdot (W_{\text{panel}} + W_{\text{topping}}) + 1.6 \cdot W_{\text{L.L}} = 1.06 \frac{\text{kip}}{\text{ft}}$$

$$M_u := \frac{\text{Factor}_{\text{Load.Final}} \cdot \text{Span}^2}{8} = 89.57 \text{ kip}\cdot\text{ft}$$

$$Q_u := \frac{\text{Factor}_{\text{Load.Final}} \cdot \text{Span}}{2} = 13.78 \text{ kip}$$

2. Panel Design

2.1 Section Properties



$$W_1 := 48 \text{ in} \quad h_1 := 3 \text{ in} \quad A_1 := W_1 \cdot h_1 = 144 \text{ in}^2$$

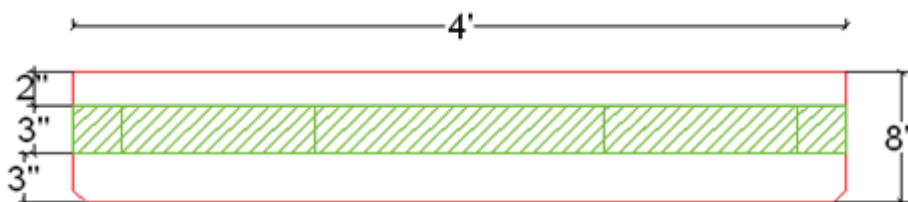
$$W_2 := 48 \text{ in} \quad h_2 := 2 \text{ in} \quad A_2 := W_2 \cdot h_2 = 96 \text{ in}^2$$

$$W_3 := 48 \text{ in} \quad h_3 := \text{Topping thickness} = 2 \text{ in} \quad A_3 := W_3 \cdot h_3 = 96 \text{ in}^2$$

$$\text{Foam}_{\text{thickness}} := 3 \text{ in}$$

$$h_{nc} := h_1 + h_2 + \text{Foam}_{\text{thickness}} = 8 \text{ in} \quad h_c := h_{nc} + h_3 = 10 \text{ in}$$

2.1.1 Non-Composite Section



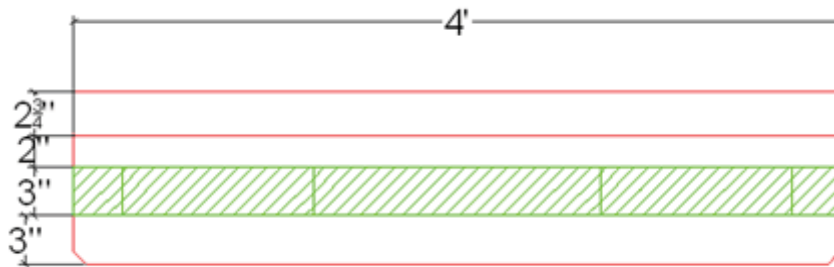
$$A_{nc} := A_1 + A_2 = 240 \text{ in}^2 \quad Y_{nc} := \frac{A_1 \cdot \frac{h_1}{2} + A_2 \cdot \left(h_1 + \text{Foam}_{\text{thickness}} + \frac{h_2}{2} \right)}{A_{nc}} = 3.7 \text{ in}$$

$$Y_{bnc} := Y_{nc} = 3.7 \text{ in} \quad Y_{tnc} := h_{nc} - Y_{nc} = 4.3 \text{ in}$$

$$I_{nc} := \left[\frac{W_1}{12} \cdot (h_1)^3 + A_1 \cdot \left(Y_{bnc} - \frac{h_1}{2} \right)^2 + \frac{W_2}{12} \cdot (h_2)^3 + A_2 \cdot \left(Y_{tnc} - \frac{h_2}{2} \right)^2 \right] = 1.88 \times 10^3 \cdot \text{in}^4$$

$$S_{bnc} := \frac{I_{nc}}{Y_{bnc}} = 508.76 \text{ in}^3 \quad S_{tnc} := \frac{I_{nc}}{Y_{tnc}} = 437.77 \text{ in}^3$$

2.1.2 Composite Section



$$F_{cbeam} := 8000 \frac{\text{lb}}{\text{in}^2} \quad F_{ctop} := 4000 \frac{\text{lb}}{\text{in}^2} \quad n := \sqrt{\left(\frac{F_{ctop}}{F_{cbeam}} \right)} = 0.71$$

$$A_c := A_{nc} + A_3 \cdot n = 307.88 \text{ in}^2$$

$$Y_c := \frac{\left[A_{nc} \cdot Y_{nc} + A_3 \cdot n \cdot \left(h_{nc} + \frac{h_3}{2} \right) \right]}{A_c} = 4.87 \text{ in}$$

$$Y_{bc} := Y_c = 4.87 \text{ in} \quad Y_{tc} := (h_{nc} + h_3) - Y_{bc} = 5.13 \text{ in}$$

$$I_{cA1} := W_1 \cdot \frac{h_1^3}{12} + A_1 \cdot \left(Y_{bc} - \frac{h_1}{2} \right)^2 = 1.74 \times 10^3 \cdot \text{in}^4$$

$$I_{cA2} := W_2 \cdot \frac{h_2^3}{12} + A_2 \cdot \left(h_1 + \text{Foam}_{\text{thickness}} + \frac{h_2}{2} - Y_{bc} \right)^2 = 468.14 \text{ in}^4$$

$$I_{cA3} := W_3 \cdot n \cdot \frac{h_3^3}{12} + A_3 \cdot n \cdot \left(h_1 + \text{Foam}_{\text{thickness}} + h_2 + \frac{h_3}{2} - Y_{bc} \right)^2 = 1.18 \times 10^3 \cdot \text{in}^4$$

$$I_c := I_{cA1} + I_{cA2} + I_{cA3} = 3.39 \times 10^3 \cdot \text{in}^4$$

3. Prestressing steel

(7)-0.5 in. Diameter 270k low-relaxation strand

$$N_{\text{strands}} := 4$$

$$A_{\text{strand}} := 0.153 \text{in}^2$$

$$A_{\text{ps}} := N_{\text{strands}} \cdot A_{\text{strand}} = 0.61 \text{in}^2$$

$$Y_{\text{ps}} := 1.5 \text{in}$$

$$e := Y_{\text{nc}} - Y_{\text{ps}} = 2.2 \text{in}$$

4. Prestress losses

Prestress loss calculations performed according to the PCI Design Handbook 6th Edition method outlined in section 4.7.

$$f_{\text{ci,panel}} := 6000 \text{psi}$$

$$f_{\text{c,panel}} := 8000 \text{psi}$$

$$N_{\text{strand}} := 4$$

$$A_{\text{one.ps}} := 0.217 \text{in}^2$$

$$A_g := A_{\text{nc}} = 240 \text{in}^2$$

$$I_g := I_{\text{nc}} = 1.88 \times 10^3 \cdot \text{in}^4$$

$$V := 1 \text{in} \cdot (A_{\text{nc}}) = 240 \text{in}^3$$

$$S := 2 \cdot (W_1 + h_{\text{nc}}) = 112 \text{in}$$

$$\frac{V}{S} = 2.14 \text{in}^2$$

$$RH := 70$$

$$A_{\text{ps}} = 0.61 \text{in}^2$$

$$e = 2.2 \text{in}$$

$$f_{\text{pu}} := 270 \text{ksi}$$

$$E_{\text{ps}} := 28500 \text{ksi}$$

$$f_{\text{pj}} := 0.75 \cdot f_{\text{pu}} = 202.5 \text{ksi}$$

$$P_i := f_{\text{pj}} \cdot A_{\text{ps}} = 123.93 \text{kip}$$

$$E_{\text{ci}} := 57000 \text{psi}^{0.5} \cdot \sqrt{f_{\text{ci,panel}}} = 4.42 \times 10^3 \cdot \text{ksi}$$

$$E_{\text{c}} := 57000 \text{psi}^{0.5} \cdot \sqrt{f_{\text{c,panel}}} = 5.1 \times 10^3 \cdot \text{ksi}$$

$$M_g := \frac{W_{\text{panel}} \text{Span}^2}{8} = 21.12 \text{kip}\cdot\text{ft}$$

$$M_{\text{dl}} := W_{\text{topping}} \cdot \frac{(\text{Span}^2)}{8} + \left(W_{\text{construction.load}} \cdot \frac{\text{Span}^2}{8} \right) = 25.35 \text{kip}\cdot\text{ft}$$

4.1 Elastic Shortening Losses

$$K_{es} := 1 \quad \text{For pretension members}$$

$$K_{cir} := 0.9 \quad \text{For pretension members}$$

$$f_{cir} := K_{cir} \left(\frac{P_i}{A_g} + P_i \frac{e^2}{I_g} \right) - M_g \frac{e}{I_g} = 0.46 \text{ ksi}$$

$$ES := K_{es} \cdot \frac{E_{ps}}{E_{ci}} \cdot f_{cir} = 2.94 \text{ ksi}$$

4.2 Creep Losses

$$K_{cr} := 2 \quad \text{For normal weight concrete}$$

$$f_{c ds} := M_{dl} \frac{e}{I_g} = 0.36 \text{ ksi}$$

$$CR := K_{cr} \cdot \frac{E_{ps}}{E_c} \cdot (f_{cir} - f_{c ds}) = 1.11 \text{ ksi}$$

4.3 Shrinkage Losses

$$K_{sh} := 1 \quad \text{For pretension members}$$

$$SH := 8.2 \cdot 10^{-6} \cdot K_{sh} \cdot E_{ps} \cdot \left[1 - 0.06 \left(\frac{1}{\text{in}^2} \cdot \frac{V}{S} \right) \right] \cdot (100 - RH) = 6.11 \text{ ksi}$$

4.4 Relaxation Losses

$$K_{re} := 5000 \text{ psi}$$

$$J := .037$$

$$C := 1$$

$$RE := [K_{re} - J \cdot (SH + CR + ES)] \cdot C = 4.62 \text{ ksi}$$

4.5 Total / Losses

$$TL := ES + CR + SH + RE = 14.79 \text{ ksi}$$

$$\text{Losses\%} := \frac{TL \cdot 100}{f_{pj}} = 7.3$$

$$f_p := f_{pj} - TL = 187.71 \text{ ksi}$$

$$P_o := (f_{pj} - ES) \cdot A_{ps} = 122.13 \text{ kip}$$

$$P := A_{ps} \cdot (f_p) = 114.88 \text{ kip}$$

6. Service Design

For serviceability design requirements
See PCI Design Handbook 6th Edition Section 4.2.2
See ACI 318-08 Section 18.4.2

Non-Composite Section

$$A_{nc} = 240 \text{ in}^2 \qquad I_{nc} = 1.88 \times 10^3 \cdot \text{in}^4$$

$$Y_{bnc} = 3.7 \text{ in} \qquad Y_{tnc} = 4.3 \text{ in}$$

Composite Section

$$A_c = 307.88 \text{ in}^2 \qquad I_c = 23.55 \text{ ft}^2 \cdot \text{in}^2$$

$$Y_{bc} = 4.87 \text{ in} \qquad Y_{tc} = 5.13 \text{ in}$$

6.1 At Release (Section at Distance = 2.5 ft from the End)

$$D_{ps} := 0.5 \text{ in} \qquad L_t := 50 \cdot D_{ps} = 2.08 \text{ ft}$$

$$M_{end} := W_{panel} \cdot \frac{\text{Span}}{2} \cdot (L_t) - W_{panel} \cdot L_t \cdot \frac{L_t}{2} = 6.23 \text{ kip-ft}$$

$$f_{top.end} := \frac{P_o}{A_g} - \left[\frac{(P_o \cdot e)}{I_g} \cdot Y_{tnc} \right] + \left(\frac{M_{end}}{I_g} \cdot Y_{tnc} \right) = 0.07 \text{ ksi} \qquad \text{Compression}$$

It should less than $6(f_{ci})^{0.5}$

$$f_{top.all.end} := -6(\text{psi}^{0.5}) \sqrt{f_{ci,panel}} = -0.46 \text{ ksi}$$

$$f_{top.end} \leq f_{top.all.end}$$

$$f_{bot.end} := \left[\frac{P_o}{A_g} + \frac{(P_o \cdot e)}{I_g} \cdot Y_{bnc} \right] - \frac{M_{end}}{I_g} \cdot Y_{bnc} = 0.89 \text{ ksi} \qquad \text{Compression}$$

It should less than $0.7f_{ci}$

$$f_{bot.all.end} := 0.7 \cdot f_{ci,panel} = 4.2 \text{ ksi}$$

6.2 At Release (Mid - Span Section)

$$f_{top.mid} := \frac{P_o}{A_g} - \left[\frac{(P_o \cdot e)}{I_g} \cdot Y_{tnc} \right] + \left(\frac{M_{panel}}{I_g} \cdot Y_{tnc} \right) = 0.47 \text{ ksi} \qquad \text{Compression}$$

It should less than $3(f_{ci})^{0.5}$

$$f_{\text{top.all.mid}} := -3\text{psi}^{0.5} \cdot \sqrt{f_{\text{ci.panel}}} = -0.23 \text{ ksi}$$

$$f_{\text{top.mid}} \leq f_{\text{top.all.mid}}$$

$$f_{\text{bot.mid}} := \frac{P_o}{A_g} + \frac{(P_o \cdot e)}{I_g} \cdot Y_{\text{bnc}} - \frac{M_{\text{panel}}}{I_g} \cdot Y_{\text{bnc}} = 0.54 \text{ ksi}$$

It should less than $0.6f_{ci}$

$$f_{\text{bot.all.mid}} := 0.6 \cdot f_{\text{ci.panel}} = 3.6 \text{ ksi}$$

$$f_{\text{bot.mid}} \leq f_{\text{bot.all.mid}}$$

6.3 During Construction (Mid-Span Section)

$$P = 114.88 \text{ kip}$$

$$f_{\text{top.con.}} := \frac{P}{A_g} - \left[\frac{(P \cdot e)}{I_g} \cdot Y_{\text{tnc}} \right] + \frac{(M_{\text{panel}} + M_{\text{Construction}} + M_{\text{topping}})}{I_g} \cdot Y_{\text{tnc}} = 1.18 \text{ ksi}$$

It should less than $0.45f_c$

$$f_{\text{top.con.all}} := 0.45 \cdot f_{\text{c.panel}} = 3.6 \text{ ksi}$$

$$f_{\text{top.con}} \leq f_{\text{top.con.all}}$$

$$f_{\text{bot.con}} := \left[\frac{P}{A_g} + \frac{(P \cdot e)}{I_g} \cdot Y_{\text{tnc}} \right] - \frac{(M_{\text{panel}} + M_{\text{topping}})}{I_g} \cdot Y_{\text{tnc}} = 0.25 \text{ ksi} \quad \text{Comp}$$

No Limit

6.4 At Final (Mid-Span Section)

$$f_{\text{int.final}} := f_{\text{top.con.}} + \frac{M_{\text{L.L.}}}{I_c} \cdot (Y_{\text{tc}} - h_c + h_{\text{nc}}) = 1.55 \text{ ksi}$$

It should less than $0.6f_c$ (beam)

$$f_{\text{int.all.final}} := 0.6 \cdot f_{\text{c.panel}} = 4.8 \text{ ksi}$$

$$f_{\text{bot.final}} := f_{\text{bot.con}} - \frac{M_{\text{L.L.}}}{I_c} \cdot (Y_{\text{bc}}) = -0.34 \text{ ksi}$$

$$f_{\text{int.final}} \leq f_{\text{int.all.final}}$$

$$\text{Class}_U := -7.5\text{psi}^{0.5} \cdot f_{\text{c.panel}}^{0.5} = -0.67 \text{ ksi}$$

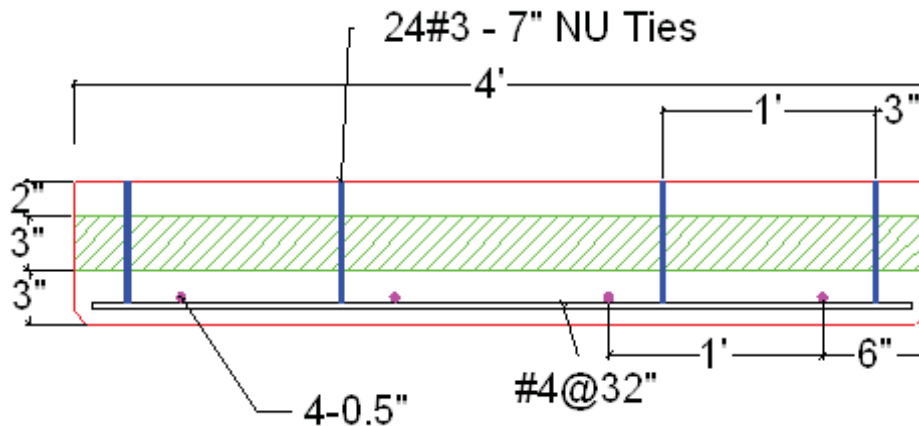
$$\text{Class}_T := -12\text{psi}^{0.5} \cdot f_{\text{c.panel}}^{0.5} = -1.07 \text{ ksi}$$

$$M_{\text{L.L.}} = 33.8 \text{ kip-ft}$$

It is Ok

7. Flexural Strength

7.1 Flexural Strength for Positive Mid-Span Section



Strain compatibility approach was used to calculate the section strength

$$A_{ps} = 0.61 \text{ in}^2$$

$$W_2 = 4 \text{ ft}$$

$$f_{cpanel} := 8 \text{ ksi}$$

$$\varepsilon_c := 0.002$$

$$\beta_{1panel} := 0.85 - \frac{(f_{cpanel} - 4 \text{ ksi})}{1 \text{ ksi}} \cdot 0.05 = 0.65$$

$$C_{non.comp.positive} := 0.78 \text{ in}$$

$$a_{non.comp.positive} := \beta_{1panel} \cdot C_{non.comp.positive} = 0.51 \text{ in}$$

$$C_{1non.comp.positive} := 0.85 \cdot a_{non.comp.positive} \cdot W_2 \cdot f_{cpanel} = 165.48 \text{ kip}$$

$$d_{1non.comp.positive} := h_{nc} - 1.5 \text{ in} = 6.5 \text{ in}$$

$$\varepsilon_{s1non.comp.positive} := \varepsilon_c \cdot \frac{(d_{1non.comp.positive} - C_{non.comp.positive})}{C_{non.comp.positive}} = 0.02$$

$$\varepsilon_{ps1non.comp.positive} := \varepsilon_{s1non.comp.positive} + \left(\frac{f_p}{E_{ps}} \right) = 0.03$$

$$Q_{ps1} := 887 + \frac{27613}{\left[1 + (112.4 \varepsilon_{ps1non.comp.positive})^{7.36} \right] \left(\frac{1}{7.36} \right)} = 9.48 \times 10^3$$

$$f_{ps1non.comp.positive} := \varepsilon_{ps1non.comp.positive} \cdot (Q_{ps1}) \cdot 1000psi = 271.02 \text{ ksi}$$

$$T_{1non.comp.positive} := f_{ps1non.comp.positive} \cdot N_{strand} \cdot A_{strand} = 165.86 \text{ kip}$$

$$\text{Tension}_{total.non.comp.positive} := T_{1non.comp.positive} = 165.86 \text{ kip}$$

$$\text{Compression}_{total.non.comp.positive} := C_{1non.comp.positive} = 165.48 \text{ kip}$$

Σ Moment at the top fibers

$$M_{Strand} := T_{1non.comp.positive} \cdot d_{1non.comp.positive} = 89.84 \text{ kip-ft}$$

$$M_{comp.block} := C_{1non.comp.positive} \cdot \frac{a_{non.comp.positive}}{2} = 3.5 \text{ kip-ft}$$

$$\Sigma M_{Ten..non.comp.positive} := M_{Strand} = 89.84 \text{ kip-ft}$$

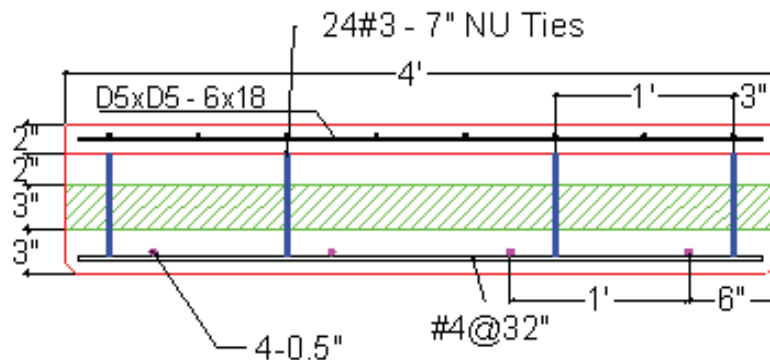
$$\Sigma M_{Comp.non.comp.positive} := M_{comp.block} = 3.5 \text{ kip-ft}$$

$$M_{n.c.positive} := \Sigma M_{Ten..non.comp.positive} - \Sigma M_{Comp.non.comp.positive} = 86.35 \text{ kip-ft}$$

$$\phi := 0.9$$

$$\phi M_{n.c.positive} := \phi \cdot M_{n.c.positive} = 77.71 \text{ kip-ft}$$

7.1.2 Composite Section



$$f_{ctopping} := 4 \text{ ksi}$$

$$f_{cpanel} = 8 \text{ ksi}$$

$$\beta_{1topping} := 0.85 - \frac{(f_{ctopping} - 4000psi)}{1000psi} \cdot 0.05 = 0.85$$

$$\beta_{1panel} = 0.65$$

$$\beta_{1average} := 0.65$$

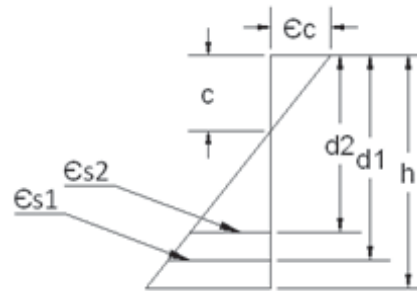
$$c_{comp.positive} := 1.52 \text{ in}$$

$$a_{comp.positive} := c_{comp.positive} \cdot \beta_{1average} = 0.99 \text{ in}$$

$$C_{1\text{comp.positive}} := 0.85 f_{c\text{topping}} \cdot W_3 \cdot a_{\text{comp.positive}} = 161.24 \text{ kip}$$

$$h := h_c = 10 \text{ in}$$

$$d_{1\text{ten.}} := h_c - 1.5 \text{ in} = 8.5 \text{ in}$$



$$\varepsilon_{s1\text{comp.positive}} := \varepsilon_c \cdot \frac{(d_{1\text{ten.}} - c_{\text{comp.positive}})}{c_{\text{comp.positive}}} = 0.01$$

$$\varepsilon_{ps1\text{comp.positive}} := \varepsilon_{s1\text{comp.positive}} + \frac{f_p}{E_{ps}} = 0.02$$

Using the Power formula

$$Q_{ps1\text{comp.positive}} := 887 + \frac{27613}{\left[1 + (112.4 \varepsilon_{ps1\text{comp.positive}})^{7.36} \right] \left(\frac{1}{7.36} \right)}$$

$$f_{ps1\text{comp.positive}} := \varepsilon_{ps1\text{comp.positive}} \cdot (Q_{ps1\text{comp.positive}}) \cdot 1000 \text{ psi} = 263.65 \text{ ksi}$$

$$T_{1\text{comp.positive}} := N_{\text{strand}} \cdot A_{\text{strand}} \cdot f_{ps1\text{comp.positive}} = 161.36 \text{ kip}$$

$$C_{\text{total}} := C_{1\text{comp.positive}} = 161.24 \text{ kip}$$

$$T_{\text{total}} := T_{1\text{comp.positive}} = 161.36 \text{ kip}$$

$$d_{3\text{comp.}} := \frac{a_{\text{comp.positive}}}{2} = 0.49 \text{ in}$$

Σ Moment at the top fiber

$$\Sigma M_{\text{comp.strand}} := T_{1\text{comp.positive}} \cdot d_{1\text{ten.}} = 114.29 \text{ kip}\cdot\text{ft}$$

$$M_{C.1\text{non.comp}} := C_{1\text{comp.positive}} \cdot d_{3\text{comp.}} = 6.64 \text{ kip}\cdot\text{ft}$$

$$\Sigma M_{\text{comp.concrete}} := M_{C.1\text{non.comp}} = 6.64 \text{ kip}\cdot\text{ft}$$

$$M_{n_{\text{comp.positive}}} := \Sigma M_{\text{comp.strand}} - \Sigma M_{\text{comp.concrete}} = 107.66 \text{ kip}\cdot\text{ft}$$

$$\phi := 0.9$$

$$\phi \cdot M_{n_{\text{comp.positive}}} = 96.89 \text{ kip}\cdot\text{ft}$$

Thus provided that the strength much higher than the required strength. OK

8. Design of GFRB Ties

NU-Ties Properties

$$A_{\text{tie.no3}} := 0.11 \text{ in}^2$$

$$C_e := 0.7$$

$$\alpha_{\text{tie.no3}} := 40$$

$$C_r := 0.65$$

$$\text{Tie}_{\text{Tensile.Strength}} := 110 \text{ ksi}$$

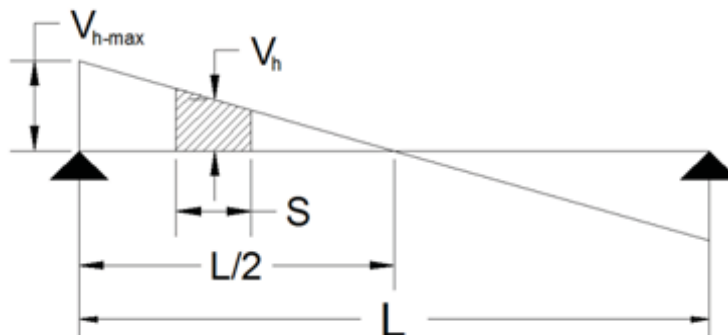
$$\text{Tie}_{\text{depth.no3}} := 7 \text{ in}$$

$$\phi_{\text{shear}} := 0.75$$

$$M_U := \text{Factor}_{\text{Load.Final}} = 1.06 \frac{\text{kip}}{\text{ft}}$$

$$\text{Span} = 26 \text{ ft}$$

$$M_u = 89.57 \text{ kip}\cdot\text{ft}$$



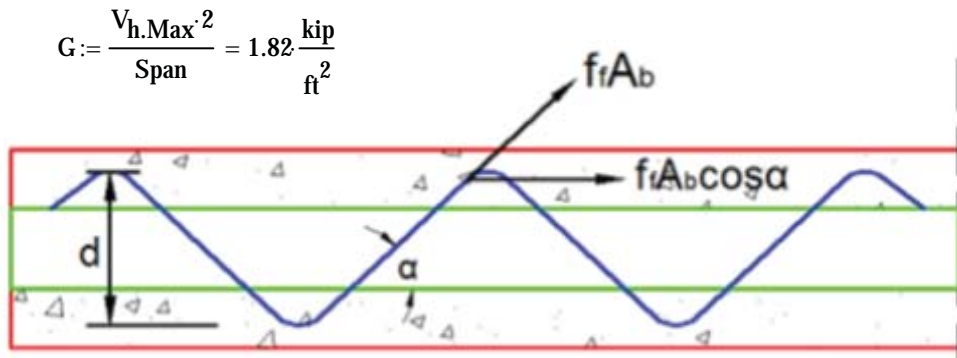
Total Horizontal Shear

$$V_{h.\text{total}} := \frac{M_u}{\text{Tie}_{\text{depth.no3}}} = 153.55 \text{ kip}$$

Maximum Horizontal Shear

$$V_{h.\text{Max}} := \frac{V_{h.\text{total}} \cdot 4}{\text{Span}} = 23.62 \frac{\text{kip}}{\text{ft}}$$

Horizontal Shear Gradient



$$F_{f.no3} := \phi_{shear} \cdot T_{ie} \cdot T_{ensile.Strength} \cdot C_e \cdot C_T = 37.54 \text{ ksi} \quad \# 3$$

$$F_{no3} := A_{tie.no3} \cdot F_{f.no3} \cdot \cos\left(\alpha_{tie.no3} \cdot \frac{\pi}{180}\right) = 3.16 \text{ kip} \quad \# 3 \text{ Leg}$$

Since the length of NU-Tie is approximately 4 ft, the panel can be divided into segments that are 4 ft in length.

First segments

$$\text{First}_{segments} := 4 \text{ ft}$$

$$\text{Area}_{segment.one} := \frac{[V_{h,Max} + (V_{h,Max} - G \cdot \text{First}_{segments})]}{2} \cdot \text{First}_{segments} = 79.95 \text{ kip}$$

$$\text{Number}_{Legs.segment1} := \frac{\text{Area}_{segment.one}}{F_{no3}} = 25.28$$

Second segments

$$\text{Second}_{segments} := 4 \text{ ft}$$

$$V_{1second} := V_{h,Max} - G \cdot \text{First}_{segments} = 16.35 \frac{kip}{ft}$$

$$V_{2.second} := V_{1second} - G \cdot \text{Second}_{segments} = 9.09 \frac{kip}{ft}$$

$$\text{Area}_{segment.second} := \frac{(V_{1second} + V_{2.second})}{2} \cdot \text{Second}_{segments} = 50.88 \text{ kip}$$

$$\text{Number}_{Legs.segment2} := \frac{\text{Area}_{segment.second}}{F_{no3}} = 16.09$$

Third segments

$$\text{Third}_{\text{segments}} := 4\text{ft} \quad V_{1\text{third}} := V_{2.\text{second}} = 2.92 \times 10^5 \frac{\text{lb}}{\text{s}^2}$$

$$V_{2.\text{third}} := V_{1\text{third}} - G_{\text{Third}_{\text{segments}}} = 1.82 \frac{\text{kip}}{\text{ft}}$$

$$\text{Area}_{\text{segment.third}} := \frac{(V_{1\text{third}} + V_{2.\text{third}})}{2} \cdot \text{Third}_{\text{segments}} = 21.81 \text{ kip}$$

$$\text{Number}_{\text{Legs.segment3.}} := \frac{\text{Area}_{\text{segment.third}}}{F_{\text{no3}}} = 6.89$$

$$\text{Total}_{\text{legs}} := \text{Number}_{\text{Legs.segment3.}} + \text{Number}_{\text{Legs.segment2.}} + \text{Number}_{\text{Legs.segment1}} = 48.26$$

$$\text{Number}_{\text{ties}} := \frac{\text{Total}_{\text{legs}}}{4} = 12.06$$

Check the stresses in the ties under sustain Load

$$M_{\text{Sustain}} := \frac{(W_{\text{topping}} + W_{\text{panel}}) \cdot \text{Span}^2 \cdot 1.2}{8} = 35.49 \text{ kip}\cdot\text{ft}$$

$$V_{\text{h.total.sustain.loads}} := \frac{M_{\text{Sustain}}}{\text{Tie}_{\text{depth.no3}}} = 60.84 \text{ kip}$$

Actual Stress in the ties due to Sustain Load

$$\text{Actual}_{\text{leg.force}} := \frac{V_{\text{h.total.sustain.loads}}}{\text{Actual}_{\text{no3.legs}}} = 1.27 \text{ kip}$$

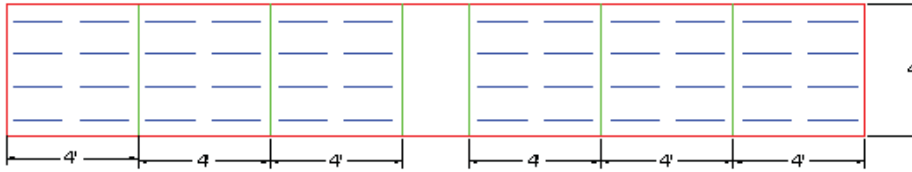
$$\text{Actual}_{\text{leg.Stress}} := \frac{\text{Actual}_{\text{leg.force}}}{A_{\text{tie.no3}} \cdot \cos\left(\alpha_{\text{tie.no3}} \cdot \frac{\pi}{180}\right)} = 15.04 \text{ ksi} \quad \text{Less than 18 ksi}$$

$$V_{\text{h.total.Live.load}} := \frac{M_{\text{L.L.factor}}}{\text{Tie}_{\text{depth.no3}}} = 92.71 \text{ kip}$$

Actual Stress in the ties due to Live Load

$$\text{Actual}_{\text{leg.force.}} := \frac{V_{\text{h.total.Live.load}}}{\text{Actual}_{\text{no3.legs}}} = 1.93 \text{ kip}$$

$$\text{Actual}_{\text{leg.Stress.}} := \frac{\text{Actual}_{\text{leg.force.}}}{A_{\text{tie.no3}} \cdot \cos\left(\alpha_{\text{tie.no3}} \cdot \frac{\pi}{180}\right)} = 22.92 \text{ ksi} \quad \text{Less than 30 ksi}$$



9. Calculation of Mu. and Pu (Demand)

For four point loads

$$W_{\text{panel}} = 0.25 \frac{\text{kip}}{\text{ft}}$$

$$M_{\text{panel}} = 21.12 \text{ kip}\cdot\text{ft}$$

$$W_{\text{topping}} = 0.1 \frac{\text{kip}}{\text{ft}}$$

$$M_{\text{topping}} = 8.45 \text{ kip}\cdot\text{ft}$$

$$W_{\text{L.L}} = 0.4 \frac{\text{kip}}{\text{ft}}$$

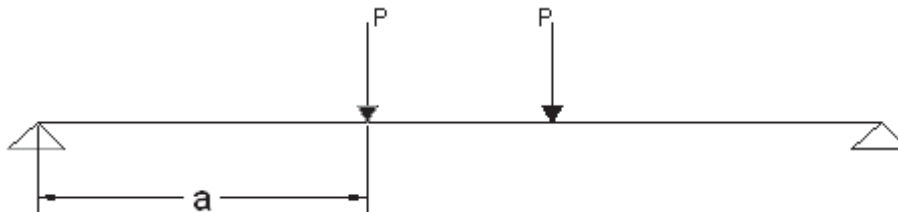
$$M_{\text{L.L}} = 33.8 \text{ kip}\cdot\text{ft}$$

$$M_u = 89.57 \text{ kip}\cdot\text{ft}$$

$$\text{Testing panel.Span} := 26\text{ft}$$

$$W_{\text{panel.and.topping}} := W_{\text{panel}} + W_{\text{topping}} = 0.35 \frac{\text{kip}}{\text{ft}}$$

$$L_{\text{eff}} := \text{Span} - 8\text{in} = 25.33\text{ft}$$



$$a := 9\text{ft}$$

$$P_u := \frac{\left(M_u - W_{\text{panel.and.topping}} \cdot L_{\text{eff}} \cdot 0.5 \cdot a + W_{\text{panel.and.topping}} \cdot a^2 \cdot 0.5 \right) \cdot 2}{a} = 14.19 \text{ kip}$$

For three point loads

$$P_u := \left(M_u - \frac{W_{\text{panel.and.topping}} \cdot L_{\text{eff}}^2}{8} \right) \cdot \frac{4}{L_{\text{eff}}} = 9.71 \text{ kip}$$

10. Calculation of Mn. and Pn (Nominal)

For four point loads

$$M_n := M_{n \text{ comp. positive}} = 107.66 \text{ kip}\cdot\text{ft}$$

$$P_n := \frac{\left(M_n - W_{\text{panel and topping}} \cdot L_{\text{eff}} \cdot 0.5 \cdot a + W_{\text{panel and topping}} \cdot a^2 \cdot 0.5 \right) \cdot 2}{a} = 18.21 \text{ kip}$$

M_n from the actual concrete compressive strength at the time of testing equal to 112 kip.ft, so $p_n = 19.2$ kip

For three point loads

$$P_{u..} := \left(M_n - \frac{W_{\text{panel and topping}} \cdot L_{\text{eff}}^2}{8} \right) \cdot \frac{4}{L_{\text{eff}}} = 12.57 \text{ kip}$$

M_n from the actual concrete compressive strength at the time of testing equal to 112 kip.ft, so $p_n = 13.25$ kip

11. Calculation of the cracking load

Assume cracking Stress at the bottom fibers = 0 instead of $0.2(f_c)^{0.5}$

$$F_r := 0 \text{ ksi}$$

$$P = 114.88 \text{ kip}$$

$$A_{nc} = 240 \text{ in}^2$$

$$I_{nc} = 1.88 \times 10^3 \cdot \text{in}^4$$

$$M_{Cr} := \frac{I_{nc}}{Y_{bnc}} \cdot \left(\frac{P_o}{A_{nc}} + \frac{P_o \cdot e \cdot Y_{bnc}}{I_{nc}} \right) = 43.97 \text{ kip}\cdot\text{ft}$$

O_1

$$S_c := S_{bnc} = 508.76 \text{ in}^3$$

$$F_r := 6 \cdot \left(\text{psi}^{0.5} \cdot \sqrt{f_{c, \text{panel}}} \right) = 536.66 \text{ psi}$$

$$F_{cpc} := \frac{P_o}{A_{nc}} + \frac{P_o \cdot e \cdot Y_{bnc}}{I_{nc}} = 1.04 \times 10^3 \text{ psi}$$

$$F_d := \frac{M_{\text{panel}}}{S_{bnc}} = 498.27 \text{ psi}$$

$$M_{Cr} := S_c \cdot (F_r + F_{cpc} - F_d) = 45.59 \text{ kip}\cdot\text{ft}$$

So

For four point loads

$$P := \frac{M_{Cr}}{a} = 5.07 \text{ kip}$$

$$P_{Cr} := 2 \cdot P = 10.13 \text{ kip}$$

For four point loads

$$P_{cr.} := 4 \cdot \frac{M_{Cr}}{L_{eff}} = 7.2 \text{ kip}$$

11. Service load

$$P_{Service1} := L_L \cdot \text{Width} \cdot L_{eff} = 10.13 \text{ kip}$$

Equivalent load

$$P_{Service2} := \frac{(W_{L.L} \cdot L_{eff}^2) \cdot 2}{8 \cdot a} = 7.13 \text{ kip}$$

In term of moment

$$P_{Service3} := \frac{2 \cdot (30 \cdot W_{L.L} \cdot L_{eff}^4)}{a^2 \cdot (3 \cdot L_{eff} - 4 \cdot a) \cdot 384} = 7.95 \text{ kip}$$

In term of deflection

12. Camber and Deflection

From PCI Design Hand book 6th Edition section 4.8

11.1 Stage I: At Release

$$f_{c,panel.test} := 11500 \text{ psi}$$

$$f_{ci,panel.at.release} := 8034 \text{ psi}$$

$$E_{ci} := 57000 \text{ psi}^{0.5} \cdot \sqrt{f_{ci,panel.at.release}} = 5.11 \times 10^3 \cdot \text{ksi}$$

$$E_c := 57000 \text{ psi}^{0.5} \cdot \sqrt{f_{c,panel.test}} = 6.11 \times 10^3 \cdot \text{ksi}$$

$$E_c = 6.11 \times 10^6 \text{ psi}$$

$$I_g = 1.88 \times 10^3 \cdot \text{in}^4$$

$$A_g = 240 \text{ in}^2$$

$$L_1 := \text{Span} = 26 \text{ ft}$$

$$e = 2.2 \text{ in}$$

$$P_0 = 122.13 \text{ kip}$$

$$P = 114.88 \text{ kip}$$

Initial Camber

From Beam model

$$\Delta_{\text{Beam.c}} := \frac{-P_0 \cdot e \cdot L_1^2}{8 \cdot E_{ci} \cdot I_g} = -0.34 \text{ in}$$

From Truss model $\Delta_{\text{Truss.c}} := -0.282\text{in}$

From the Finite Elements model $\Delta_{\text{Finite.C}} := -0.286\text{in}$

Own Weight Deflection

$$W_{\text{panel}} = 0.25 \frac{\text{kip}}{\text{ft}} \quad \Delta_{\text{Beam.D}} := \frac{(5 \cdot W_{\text{panel}} \cdot L_{\text{eff}}^4)}{384 E_c \cdot I_g} = 0.24 \text{ in}$$

From Truss model $\Delta_{\text{Truss.D}} := 0.772\text{in}$

From the Finite Elements model $\Delta_{\text{Finite.D}} := 0.770\text{in}$

$$\frac{\Delta_{\text{Beam.D}}}{\Delta_{\text{Truss.D}}} = 0.31$$

For using the Beam deflection equation

* Inertia reduction factor should be used, which equal to 0.475

Net Camber/Deflection

$$\Delta_{\text{net.camber.deflection.span1}} := \Delta_{\text{Beam.c}} + \Delta_{\text{Truss.c}} = -0.62 \text{ in}$$

11.2 Stage II: At Erection

$$W_{\text{topping}} = 0.1 \frac{\text{kip}}{\text{ft}}$$

$$\text{From Beam model} \quad \Delta_{\text{1D.due.top}} := \frac{5W_{\text{topping}} \cdot L_{\text{eff}}^4}{384 E_c \cdot I_g} = 0.1 \text{ in}$$

From Truss model $\Delta_{\text{Truss.D.top}} := 0.266\text{in}$

From the Finite Elements model $\Delta_{\text{Finite.D.top}} := 0.266\text{in}$

12 Thermal Performances

R-Value are calculated using thr Zone Method proposed by PCI Design Handbook

12.1 R-Value of Sandwich Panel with Solid Blocks at the ends

Panel Span $L := 26\text{ft}$ Panel Width $W := 4\text{ft}$

Thickness of the topping $t_{\text{cf1}} := 2\text{in}$

Thickness of the top wythe $t_{\text{cf2}} := 1\text{in}$

Thickness of insulation	$t_{in} := 4in$
Thickness of the bottom wythe	$t_{cb} := 3in$
Solid concrete block length	$L_{solid.block} := 12in$
Insulation conductivity value	$K_{in} := 0.2$
Insulation conductivity value	$K_{con} := 13.3$

$$\alpha := 1 + 2.25 \left(\frac{K_{in} - 0.26}{0.26} \right) = 0.48$$

$$\beta := 1 + 1.458 \left(\frac{K_{con} - 12.05}{12.05} \right) = 1.15$$

$$E_z := 1.4in - 0.1 \cdot t_{in} \cdot \alpha + \left[0.4(t_{cf1} + t_{cf2}) + 0.1[t_{cb} - (t_{cf1} + t_{cf2})] \right] \cdot \beta = 2.59in$$

$$A_t := L \cdot W = 1.5 \times 10^4 \cdot in^2$$

$$A_s := 2 \cdot [W \cdot (L_{solid.block} + E_z)] = 1.4 \times 10^3 \cdot in^2$$

$$A_p := A_t - A_s = 1.36 \times 10^4 \cdot in^2$$

$$R_{value.summer} := 0.25 + \left[\frac{1}{\left[\frac{K_{con}}{(t_{cf1} + t_{cf2})} \right]} \cdot in^{-1} + \left[\frac{1}{\left(\frac{K_{in}}{t_{in}} \right)} \cdot in^{-1} \right] + \frac{1}{\left(\frac{K_{con}}{t_{cb}} \right)} \cdot in^{-1} \right] + 0.68$$

$$R_{value.summer} = 21.38 \quad \text{For insulated path}$$

$$R_{value.summer.solid.path} := 0.25 + \left[\frac{1}{\left[\frac{K_{con}}{(t_{cf1} + t_{cf2} + t_{cb} + t_{in})} \right]} \cdot in^{-1} \right] + 0.68 = 1.68$$

$$A'_s := \frac{A_s}{A_t} = 0.09$$

$$A'_p := \frac{A_p}{A_t} = 0.91$$

$$Final R_{.Value} := \frac{1}{\left(\frac{A'_s}{R_{value.summer.solid.path}} + \frac{A'_p}{R_{value.summer}} \right)} = 10.2$$